

AD A103579

LEVEL ^{II}

2

UTSI REPORT 81-1
A FLIGHT TEST EVALUATION
OF THE
BALL-BARTOE JETWING
PROPULSIVE LIFT CONCEPT

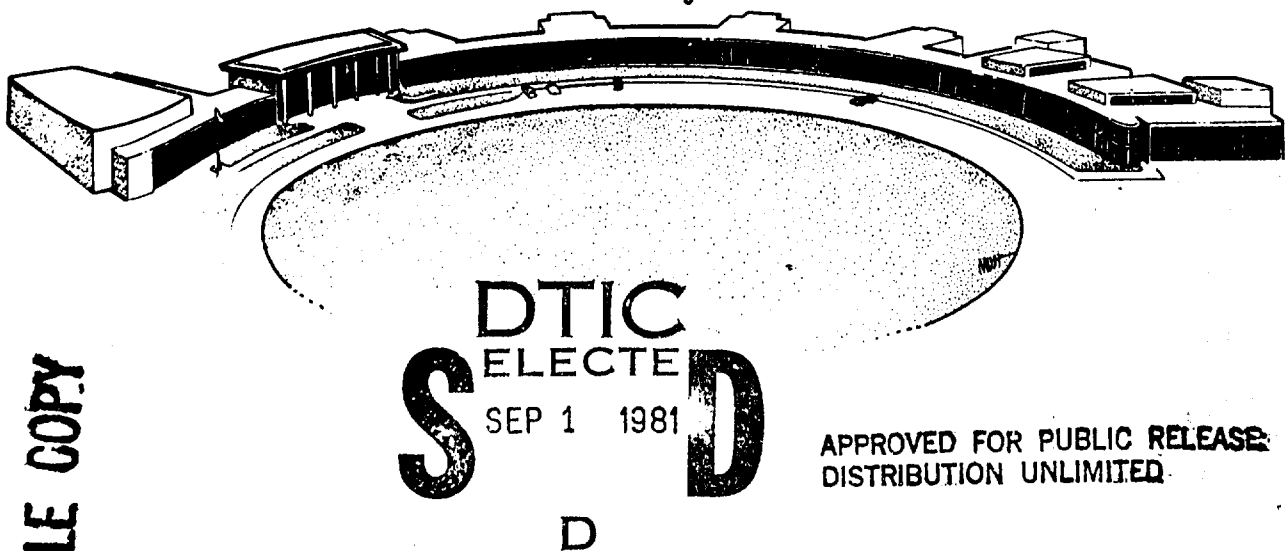
Completed For
NAVAL AIR SYSTEMS COMMAND
(AIR-03PA)

Under Contract
N00019-80-C-0126
19 Feb 80

by
Ralph D. Kimberlin
Associate Professor
The University of Tennessee
Space Institute



1 July 1981



DTIC FILE COPY

THE UNIVERSITY of TENNESSEE
SPACE INSTITUTE

Knoxville, Tennessee

81 9 01 138

6
A FLIGHT TEST EVALUATION
OF THE
BALL-BARTOE JETWING
PROPELLIVE LIFT CONCEPT

TE NO. 13-79-2-0261

64/30712-87-1

BY

John D. Kimberlin

10 RALPH D. KIMBERLIN

ASSOCIATE PROFESSOR

THE UNIVERSITY OF TENNESSEE

SPACE INSTITUTE

Accession For	
NTIS CRA&I	<input checked="" type="checkbox"/>
DTIC TAB	<input type="checkbox"/>
Unannounced	<input type="checkbox"/>
Justification	
By	
Distribution/	
Availability Codes	
Avail and/or	
Dist	Special
A	

APPROVED FOR PUBLIC RELEASE
DISTRIBUTION UNLIMITED

1 JULY 1981

12/1891

DTIC
SELECTED
SEP 1 1981
S D
D

FOREWARD

This program was performed by The University of Tennessee Space Institute for the Naval Air Systems Command Advanced Aircraft Development and Systems Objectives Office (AIR-03PA) under Naval Air Systems Command Contract N00019-80-C-126, dated 19 Feb. 1980. Active testing began on 18 April 1980 and was completed on 17 April 1981.

A total of 59.5 hours of flying time were flown in the performance of this task along with 108.2 hours of aircraft ground test operation.

The following key personnel were primarily responsible for the conduct of this test and/or the preparation of this report.

UTSI

Principal Investigator
and Project Test Pilot

Ralph D. Kimberlin
Associate Professor

Research Assistants

Kenny A. Rooke
Uwe P. Solies
A. K. Sinha
John M. Trimbach

Instrumentation Engineer

Robert Jones

Aircraft Maintenance

Donald D. Freeman

Support Groups

UTSI Gas Diagnostics
Division

NAVAL AIR SYSTEMS COMMAND

Contract Monitor

Mr. W. T. Sparrow
AIR-03PA3

TABLE OF CONTENTS

<u>ITEM</u>	<u>PAGE</u>
EXECUTIVE SUMMARY	1
LIST OF FIGURES	iii
LIST OF TABLES	xii
LIST OF SYMBOLS AND ABBREVIATIONS	xiii
SECTION I. INTRODUCTION	1
SECTION II. DESCRIPTION AND BACKGROUND OF THE TEST ARTICLE	3
DESCRIPTION	3
BACKGROUND	14
SECTION III. POTENTIAL APPLICATIONS OF JETWING CONCEPT	15
SECTION IV. TEST PROCEDURES	24
1. Taxi Test	24
2. Familiarization Flights	25
3. Airspeed Calibration	25
4. Thrust Calibration	26
5. Performance Flight Tests including C_L vs. α Determination	28
6. Control Friction	29
7. Lateral Control Power	29
8. Lateral-Directional Stability	30
9. Longitudinal Stability	32
10. Flight Path Stability	33
11. Longitudinal Trim Changes	33
12. Maneuvering Stability	34
13. Approach Handling Qualities	35

<u>ITEM</u>	<u>PAGE</u>
14. Takeoff and Landing Tests	36
15. Laser Velocimeter Thrust Measurement	39
SECTION V INSTRUMENTATION	43
1. Air Data Instrumentation	43
2. Engine Thrust Instrumentation	45
3. Stability and Control Instrumentation	45
4. Takeoff and Landing Instrumentation	55
5. Laser Velocimeter Instrumentation	55
SECTION VI RESULTS AND DISCUSSION	62
1. Familiarization Flying	62
2. Airspeed Calibration	63
3. Thrust Calibration	63
4. Inflight Performance	66
5. C_L Capabilities	79
6. Control System Friction Measurement	86
7. Lateral Control Power	86
8. Lateral-Directional Stability	90
9. Longitudinal Stability and Control	91
a. Static Longitudinal Stability, Stick Fixed and Stick Free	97
b. Maneuvering Stability	105
c. Flight Path Stability	115
d. Longitudinal Dynamic Stability	115
e. Longitudinal Control and Trim	118

<u>ITEM</u>	<u>PAGE</u>
10. Approach Handling Qualities Evaluation	118
11. Takeoff and Landing Tests	121
12. Laser Velocimeter Thrust Measurement	122
REFERENCES	140
SECTION VII CONCLUSIONS	142
SECTION VIII RECOMMENDATIONS	144
APPENDIX I EJECTOR GEOMETRY	I-1
APPENDIX II PERFORMANCE DATA REDUCTION METHODS	II-1
APPENDIX III ESTIMATED WEIGHTS AND MOMENTS OF INERTIA FOR JETWING	III-1
DISTRIBUTION LIST	

EXECUTIVE SUMMARY

The need for military aircraft that will operate from short unimproved airfields, and the decks of smaller aircraft carriers has increased in recent years due to a changing world situation and the shrinking of the dollar. Such aircraft need to be fuel efficient, quiet, maneuverable, have low infrared signature, and carry a large useful load.

The Ball-Bartoe "Jetwing" is a single engine upper surface blowing concept which offers the possibility of achieving these objectives. The "Jetwing" concept achieves supercirculation lift and STOL performance by ducting all engine air through the leading edge of the wing and ejecting it over the top surface of the wing through a slot nozzle. This nozzle extends along approximately 70% of the wing span. A Coanda flap is mounted at the trailing edge of the blown portion of the wing. In addition to the main wing, a smaller wing panel is mounted above the slot nozzle. The air passage between the main wing and the smaller upper wing acts as an ejector to reduce installed thrust losses. For high speed applications the concept may be used without this upper wing. A thrust reversing method is also incorporated into the concept. The thrust is reversed by rotating the top of the slot nozzle so as to close the nozzle and open a reverse flow path.

The "Jetwing" concept has been incorporated into a research aircraft. The Jetwing research aircraft is a single seat, jet aircraft of conventional design powered by a Pratt and Whitney of Canada JT15D-1 turbofan engine of 2200 pounds static thrust. The aircraft has a wingspan of 21.75 feet, a wing area of 105.6 square feet and a maximum gross weight of 3750 pounds.

This report covers the flight test program of the Jetwing research airplane, which was conducted for Naval Air Systems Command by the University of Tennessee Space Institute. The purpose of the flight test program was to validate NASA Ames Research Center 40 x 80 foot wind tunnel data on the aircraft by flight test, and to obtain performance, stability, and control data sufficient to evaluate the Jetwing concept for future application to other flight vehicles.

The Jetwing research aircraft has flown in level flight at an equivalent airspeed of 53 knots. However, at that speed it has sufficient excess power to climb at a four degree climb angle. The 53 knots airspeed corresponds to a lift coefficient of approximately 3.5. This lift coefficient is achieved with a 30° deflection of the Coanda flap and without leading edge devices. The blowing coefficient at the lift coefficient of 3.5 was approximately 1.0. The minimum speed capabilities of the Jetwing research aircraft are limited in free flight by horizontal tail stall. However full scale data from the NASA Ames Research Center 40 x 80 foot wind tunnel have shown the aircraft to be capable of lift coefficients in excess of 5.0. Where not prohibited by the tail stall, the flight test results agree well with the tunnel data.

In addition to the horizontal tail stall, the research aircraft is longitudinally unstable. However, it is felt that both problems can be corrected by a properly designed horizontal tail, and such tail redesign is recommended.

In spite of the longitudinal stability problem the aircraft has acceptable handling qualities in both 3° and 6° glideslope approaches. These acceptable handling qualities are the result of small longitudinal trim changes and excellent flight path stability. Due to the powered lift, the flight path angle is nearly a direct function of power setting, and large changes in approach speed have little effect on the glide path. This fact reduces the pilot workload during an approach considerably.

In conclusion the Jetwing concept shows promise as a single engine, upper surface blowing, short takeoff and landing concept for application to several military aircraft categories. Its further development is recommended.

LIST OF FIGURES

<u>FIGURE NO.</u>	<u>TITLE</u>	<u>PAGE</u>
Figure 1.	Side View of Jetwing Research Aircraft	4
Figure 2.	Three Quarter Front View of Jetwing Research Aircraft	4
Figure 3.	General Arrangement Drawing Jetwing Research Aircraft	9
Figure 4.	Jetwing Ducting Arrangement	10
Figure 5.	Two Dimensional Sketch of Jetwing Concept	10
Figure 6.	Wind Tunnel Data with Upper Wing Installed	11
Figure 7.	Wind Tunnel Data with Upper Wing Removed	12
Figure 8.	Two Dimensional View of Jetwing Concept with Thrust Reverser Deployed	13
Figure 9.	Fighter/Attack Aircraft using Jetwing Concept	16
Figure 10.	Fighter/Attack Aircraft with afterburning turbofan engine using Modified Jetwing Concept with only Fan By-Pass Air ducted over the wing	17
Figure 11.	Jetwing Supersonic Fighter using Supercritical Airfoil-Supersonic Flight Configuration	18
Figure 12.	Jetwing Supersonic Fighter using Supercritical Airfoil-Subsonic Flight Configuration	19
Figure 13.	Jetwing Supersonic Fighter using Circular Arc Airfoil-Supersonic Flight Configuration	20

<u>FIGURE NO.</u>	<u>TITLE</u>	<u>PAGE</u>
Figure 14.	Jetwing Supersonic Fighter using Circular Arc Airfoil-Subsonic Flight Configuration	21
Figure 15.	Transport or Carrier on Board Delivery Aircraft Using Jetwing Concept	23
Figure 16.	Thrust Calibration Test Setup	27
Figure 17.	Sketch of Takeoff and Landing Test Site	37
Figure 18.	Sketch of Engine Inlet showing location of velocity measurements	41
Figure 19.	Sketch of Wing Profile and Exhaust Nozzle showing location of velocity measurements	41
Figure 20.	Sketch of Right Wing showing location of points on the Nozzle where vertical profiles of velocity were taken	42
Figure 21.	Sketch of Right Wing showing chordwise and spanwise location of vertical velocity profiles	42
Figure 22.	Photograph of Pilots Instrument Panel showing Air Data and Engine Thrust Instrumentation	44
Figure 23.	Full Swivel Pitot-Static Boom	44
Figure 24.	Photograph of Dillon Dynamometer as installed in Thrust Measuring Apparatus	46
Figure 25.	Miliampmeter used for readout of Stability and Control Parameters	48
Figure 26a.	Elevator Position Potentiometer	49
26b.	Aileron Position Potentiometer	49
26c.	Rudder Position Potentiometer	50
26d.	Stabilizer Position Potentiometer	51
Figure 27.	Wingtips Boom with Angle of attack and Sideslip Sensors.	52

<u>FIGURE NO.</u>	<u>TITLE</u>	<u>PAGE</u>
Figure 28.	Mounting Arrangements of Vertical Gyro	53
Figure 29.	Mounting Arrangement of the Rate Gyros and their Power Supply	53
Figure 30.	Instrumentation Amplifier and Signal Conditioner	54
Figure 31.	Liftoff and Landing Distance Indicator shown mounted in Jetwing Cockpit (Center)	56
Figure 32.	Takeoff and Landing Distance and Height Measuring Theodolite with operator	57
Figure 33.	Height Strings and Horizontal Distance Pointer of Takeoff and Landing Distance Theodolite	57
Figure 34.	Laboratory Thermometer, Hand Held Wind Direction Indicator, and Hand Held Wind Speed Indicator used for Takeoff and Landing Tests	58
Figure 35.	Schematic diagram of UTSI Afocal Scan Laser Velocimeter System	60
Figure 36.	Laser Velocimeter Test Setup	61
Figure 37.	Jetwing Airspeed Calibration Data Plot	64
Figure 38.	Jetwing Static Thrust Calibration Data Plots Upper Wing Installed	65
Figure 39.	Jetwing Static Thrust Calibration Data Plots Upper Wing Removed	65
Figure 40.	Plot of Jetwing Installed "Referred" Thrust versus "Referred" Engine Speed for various True Airspeed with Upper Wing Installed	67
Figure 41.	Comparison of Jetwing Installed Gross Thrust predicted from Nozzle Pressure Ratio and predicted from Main Rotor Speed	68

<u>FIGURE NO.</u>	<u>TITLE</u>	<u>PAGE</u>
Figure 42.	Jetwing V-γ Performance Map for the Clean Configuration	69
Figure 43.	Jetwing V-γ Performance Map for the Gear Down, 15° Flaps Configuration	70
Figure 44.	Jetwing V-γ Performance Map for the Gear Down, 30° Flaps Configuration	71
Figure 45.	Plot of C_L versus C_{FEX} for the Jetwing in Clean Configuration	72
Figure 46.	Plot of C_L versus C_{FEX} for the Jetwing in the Gear Down, 15° Flaps Configuration	73
Figure 47.	Plot of C_L versus C_{FEX} for the Jetwing in the Gear Down, 30° Flaps Configuration	74
Figure 48.	Plot Comparing Wind Tunnel and Flight Test Results of C_L versus C_{FEX} of the Jetwing in the Clean Configuration at $C_J = 0.43$	76
Figure 49.	Plot Comparing Wind Tunnel and Flight Test Results of C_L versus C_{FEX} of the Jetwing in the Gear Down, 15° Flaps Configuration at $C_J = 0.75$	77
Figure 50.	Plot Comparing Wind Tunnel and Flight Test Results of C_L versus C_{FEX} of the Jetwing in the Gear Down, 30° Flaps Configuration at $C_J = 0.75$	78
Figure 51.	Plot of C_L versus C_J for the Jetwing in the Clean Configuration	80
Figure 52.	Plot of C_L versus C_J for the Jetwing in the Gear Down, 15° Flaps Configuration	81

<u>FIGURE NO.</u>	<u>TITLE</u>	<u>PAGE</u>
Figure 53.	Plot of C_L versus C_J for the Jetwing in the Gear Down, 30° Flaps Configuration	82
Figure 54.	Plot Comparing Wind Tunnel and Flight Test C_L versus α or α' of the Jetwing in the Clean Configuration at $C_J = 0.43$	83
Figure 55.	Plot Comparing Wind Tunnel and Flight Test C_L versus α or α' of the Jetwing in the Gear Down, 15° Flaps Configuration at $C_J = 0.75$	84
Figure 56.	Plot Comparing Wind Tunnel and Flight Test C_L versus α or α' of the Jetwing in the Gear Down, 30° Flaps Configuration at $C_J = 0.75$	85
Figure 57.	Elevator Control System Static Friction Measurement Plot	87
Figure 58.	Aileron Control System Static Friction Measurement Plot	88
Figure 59.	Rudder Control System Static Friction Measurement Plot	89
Figure 60.	Power Approach Lateral-Directional Static Stability Plots - 3° Approach at 70 KIAS	92
Figure 61.	Power Approach Lateral-Directional Static Stability Plots - 3° Approach at 90 KIAS	93
Figure 62.	Low Cruise Lateral-Directional Static Stability Plots - 110 KIAS	94
Figure 63.	Cruise Lateral-Directional Static Stability Plots - 150 KIAS	95
Figure 64.	Jetwing Spiral Stability, Cruise and Power Approach	96
Figure 65.	Plots of F_S and δ_e versus V_c for the Jetwing in the Climb Configuration with the c. g. at 31.93% M.A.C.	98

<u>FIGURE NO.</u>	<u>TITLE</u>	<u>PAGE</u>
Figure 66.	Plots of F_S and δ_e versus V_c for the Jetwing in the Climb Configuration with the c.g. at 33.63% M.A.C.	99
Figure 67.	Plots of F_S and δ_e versus V_c for the Jetwing in the Climb Configuration with the c.g. at 35.37% M.A.C.	100
Figure 68.	Plots of F_S and δ_e versus V_c for the Jetwing in the Power Approach Configuration with the c.g. at 31.93% M.A.C.	101
Figure 69.	Plots of F_S and δ_e versus V_c for the Jetwing in the Power Approach Configuration with the c.g. at 33.63% M.A.C.	102
Figure 70.	Plots of F_S and δ_e versus V_c for the Jetwing in the Power Approach Configuration with the c.g. at 35.63% M.A.C.	103
Figure 71.	Plots of F_S and δ_e versus n_z for the Jetwing in the Cruise Configuration with the c.g. at 31.93% M.A.C.	106
Figure 72.	Plots of F_S and δ_e versus n_z for the Jetwing in the Cruise Configuration with the c.g. at 33.63% M.A.C.	107
Figure 73.	Plots of F_S and δ_e versus n_z for the Jetwing in the Cruise Configuration with the c.g. at 35.37% M.A.C.	108
Figure 74a.	Plot of F_S versus n_z for the Jetwing in the Power Approach Configuration with the c.g. at 31.93% M.A.C.	109

<u>FIGURE NO.</u>	<u>TITLE</u>	<u>PAGE</u>
Figure 74b.	Plots of δ_e versus n_z for the Jetwing in the Power Approach Configuration with the c.g. at 31.93% M.A.C.	110
Figure 75a.	Plot of F_S versus n_z for the Jetwing in the Power Approach Configuration with the c.g. at 33.93% M.A.C.	111
Figure 75b.	Plot of δ_e versus n_z for the Jetwing in the Power Approach Configuration with the c.g. at 33.63% M.A.C.	112
Figure 76.	Plot of F_S and δ_e versus n_z for the Jetwing in the Power Approach Configuration with the c.g. at 35.37% M.A.C.	113
Figure 77.	Plots of C_Y , C_N and C_R versus C_L for the Jetwing taken in the NASA Ames 40 x 80 foot Wind Tunnel	114
Figure 78.	Plot of Longitudinal Phugoid in the Climb Configuration at a c.g. of 31.93% M.A.C.	116
Figure 79.	Plot of Longitudinal Phugoid in the Climb Configuration at a c.g. of 35.37% M.A.C.	117
Figure 80.	Control Movement Time Histories for 3° and 6° Approaches	120
Figure 81.	Jetwing Sea Level Standard Takeoff Distances as a function of Headwind Velocity	123
Figure 82.	Jetwing Sea Level Standard Landing Distances as a function of Headwind Velocity	124
Figure 83.	Jetwing Engine Intake Air Velocity Profile - Vertical Scan at 55% N_1	126

<u>FIGURE NO.</u>	<u>TITLE</u>	<u>PAGE</u>
Figure 84.	Jetwing Engine Intake Air Velocity Profile - Horizontal Scan at 55% N_1	127
Figure 85.	Jetwing Engine Exhaust Velocity Profile at Right Wing Hot Duct - Horizontal Scan at 55% N_1	129
Figure 86.	Jetwing Engine Exhaust Velocity Profile at Right Wing Hot Duct - Vertical Scan 8 inches from fuselage at 55% N_1	130
Figure 87.	Jetwing Engine Exhaust Velocity Profile at Right Wing Inner Cold Duct - Horizontal Scan at 55% N_1	131
Figure 88.	Jetwing Engine Exhaust Velocity Profile at Right Wing Inner Cold Duct - Vertical Scan 17 inches from Inner Wing Strut at 55% N_1	132
Figure 89.	Jetwing Engine Exhaust Velocity Profile at Right Wing Outer Cold Duct - Horizontal Scan at 55% N_1	133
Figure 90.	Jetwing Engine Exhaust Velocity Profile at Right Wing Outer Cold Duct - Vertical Scan 7 inches from Outer Wing Strut at 55% N_1	134
Figure 91.	Jetwing Ejector Exhaust Velocity Profile behind Right Inner Cold Nozzle at Upper Wing Trailing Edge - Vertical Scan at 55% N_1	135
Figure 92.	Jetwing Ejector Exhaust Velocity Profile behind Right Outer Cold Nozzle at Upper Wing Trailing Edge - Vertical Scan at 55% N_1	136
Figure 93.	Jetwing Ejector Inlet Velocity Profile in front of Right Hot Exhaust Duct at Leading Edge of Upper Wing - Vertical Scan at 55% N_1	137

<u>FIGURE NO.</u>	<u>TITLE</u>	<u>PAGE</u>
Figure 94.	Jetwing Ejector Inlet Velocity Profile in front of Right Inner Cold Duct at Leading Edge of Upper wing - Vertical Scan at 55% N_1	138
Figure I-1	Locations of Ejector Area Measurements	I-2
Figure II-1	Sample Plot of H_{pI} Versus Time	II-3
Figure II-2	Sample Plot of F_{GS} Versus γ	II-6

LIST OF TABLES

<u>TABLE NO.</u>	<u>TITLE</u>	<u>PAGE</u>
Table 1	Jetwing Physical Description	5
Table 2	Longitudinal Trim Change Conditions	34
Table 3	Rolling Performance Summary	90
Table 4	Summary of Dutch Roll Parameters	91
Table 5	Summary of Static Longitudinal Stability Neutral Points	97
Table 6	Horizontal Tail Volume Coefficient Comparison	104
Table 7	Summary of Maneuver Point Locations	105
Table 8	Jetwing Power Approach Phugoid Summary	115
Table 9	Approach Handling Qualities Pilot Rating Summary	119
Table 10	Jetwing JW-1, Sea Level, Standard Day, No Wind, Takeoff and Landing Distances	121
Table 11	Jetwing Engine Mass Flow Summary	128
Table II-1	Sample Data Reduction	II-7
Table III-1	Component Weight and Moment of Inertia Summary	III-2

LIST OF SYMBOLS AND ABBREVIATIONS

<u>SYMBOL OR ABBREVIATION</u>	<u>DEFINITION</u>
A	Aspect ratio
APP	Approach angle
a_t	Lift curve slope of the horizontal tail
a_w	Lift curve slope of the wing
b	Wing span
$^{\circ}\text{C}$	Degrees Centigrade
$C_{1/2}$	The number of cycles required to damp to one half Amplitude
C_D	Coefficient of drag
C_{D0}	Zero lift coefficient of drag
C_{FEX}	Coefficient of excess thrust
C_J	Three dimensional blowing Coefficient
C_L	Coefficient of lift
C_{LMAX}	The maximum lift coefficient
C_M	Pitching moment coefficient
C_N	Yawing moment coefficient
C_R	Rolling moment coefficient
C_Y	Sideforce coefficient
c.g.	Aircraft center of gravity
CTOL	Conventional takeoff and landing
e	Oswald's efficiency factor

<u>SYMBOL OR ABBREVIATION</u>	<u>DEFINITION</u>
F_a	Aileron control force
F_G	Gross thrust
F_{GS}	Standardized or weight corrected gross thrust
F_r	Rudder control force
F_S	Elevator control force or stick force
G	Acceleration due to gravity
H_2O	Water expressed in its chemical composition
H_p	Pressure altitude
H_{pI}	Indicated pressure altitude
H_{pI}	Indicated pressure altitude corrected for instrument error
H_{pc}	Calibrated pressure altitude or Indicated pressure altitude corrected for instrument and position error.
ITT	Interstage turbine temperature of the Turbofan engine
JT15D-1	The Pratt and Whitney of Canada Designation for the turbofan engine installed in the Jetwing aircraft
K	Williams' Induced Drag Correction Factor
KIAS	Knots indicated airspeed
KCAS	Knots calibrated airspeed
KTAS	Knots true airspeed
M.A.C.	Mean aerodynamic chord
M R P	Maximum recommended power
M S L	Mean Sea Level
NASA	National Aeronautics and Space Administration
NBS	National Bureau of Standards

<u>SYMBOL OR ABBREVIATION</u>	<u>DEFINITION</u>
N_1	Main rotor speed of the turbofan engine
N_2	Gas generator rotor speed of the turbofan engine
n_z	Normal acceleration
O.A.T.;	Indicated ambient air temperature
p	Roll Rate
P_a	Ambient Static Pressure
PLF	Power for level flight
P_{ss}	Steady state roll rate
P_{t5}	Total pressure at the engine exhaust nozzle
Δp	Differential pressure
q	Dynamic pressure
QSRA	NASA Quiet Shorthaul Research Aircraft
r	A correction factor which accounts for blowing losses due to nozzle boundary layer growth and scrubbing losses due to blowing over a flap
R.O.C.	Rate of climb
S	Wing area
S_{ao}	The observed takeoff, or landing air distance
S_{at}	The observed takeoff, or landing, air distance corrected for winds.
S_{as}	The takeoff, or landing, air distance corrected to sea level standard conditions
S_{go}	The observed takeoff, or landing, ground roll distance
S_{gt}	The observed takeoff, or landing, ground roll distance corrected for winds

<u>SYMBOL OR ABBREVIATION</u>	<u>DEFINITION</u>
s_{gs}	The takeoff, or landing ground roll distance corrected to sea level standard conditions.
STOL	Short takeoff and landing
t	Time
T_a	Observed ambient air temperature
T_{aI}	Observed ambient air temperature corrected for instrument error
T_s	The standard temperature at the test pressure altitude
T.E.D.	Trailing edge down
T.E.U.	Trailing edge up
USB	Upper surface blowing
UTSI	The University of Tennessee Space Institute
V	Airspeed
VASI	Visual Approach Slope Indicator
V_i	Indicated Airspeed
V_I	Indicated airspeed corrected for instrument error
ΔV_{pc}	Position error correction, or the correction for the error created by the location of the static source on the aircraft
V_c	Calibrated airspeed, or the indicated airspeed corrected for instrument and position error
V_E	Equivalent airspeed - the calibrated airspeed corrected for compressibility
V_{EW}	The equivalent airspeed corrected for non-standard aircraft weight
V_T	True Airspeed - the equivalent airspeed corrected for air density

<u>SYMBOL OR ABBREVIATION</u>	<u>DEFINITION</u>
V_{TD}	The airspeed at landing touchdown
V_{TOW}	The true groundspeed at takeoff
$V_{R/C}$	The airspeed for best rate of climb
V_W	The atmospheric wind velocity
V_H	the horizontal tail volume coefficient
V_V	The vertical tail volume coefficient
W	Aircraft weight
W_E	The Aircraft empty weight
W_S	The aircraft standard weight ~ 3600 lbs. for the Jetwing.
W_T	The aircraft weight at the time of the test data point
YC-14	Boeing Prototype Advanced Medium Shorthaul Transport Aircraft
YC-15	McDonnell-Douglas Prototype Advanced Medium Shorthaul Transport Aircraft
α	The geometric angle of attack
α'	The total angle of attack-geometric angle of attack plus upwash
α'_I	The indicated angle of attack (includes upwash)
α''_I	The indicated angle of attack corrected for instrument error
β	Sideslip Angle
δ	The atmospheric pressure ratio
δ_a	The aileron deflection angle
δ_f	The flap deflection angle

<u>SYMBOL OR ABBREVIATION</u>	<u>DEFINITION</u>
δ_s	The horizontal stabilizer deflection angle
δ_r	Rudder deflection angle
δ_{rev}	The thrust reverser deflection angle
ϵ	Downwash angle
η_t	Horizontal tail efficiency factor q_t/q_∞
γ	Flight path angle, or angle of climb or descent
γ_s	Flight path, angle Corrected to Sea Leval Standard weight Conditions
ζ_D	The Dutch Roll damping factor
ζ_{sp}	The longitudinal short period damping factor
θ	The atmospheric temperature ratio
τ_R	The roll mode time constant, or the time required to reach 63.2% of a steady state roll rate
π	3.1416
ρ	The atmospheric density
ρ_0	The atmospheric density at sea level
σ	The atmospheric density ratio
σ_T	The atmospheric density ratio at the test conditions
σ_s	The standard density ratio at the test pressure altitude
ϕ	Bank angle
ω_{nD}	The Dutch Roll natural frequency
ω_{hsp}	The longitudinal short period natural frequency

SECTION I

INTRODUCTION

This report covers a flight and ground test evaluation of the Ball-Bartoe "Jetwing" Short Takeoff and Landing (STOL) Research Aircraft. These tests were conducted by the University of Tennessee Space Institute, Tullahoma, Tennessee for the Advanced Aircraft Development and Systems Objectives Office (AIR-03PA) of Naval Air Systems Command under contract Number N00019-80-C-0126. This evaluation was conducted as a part of Naval Air Systems Command continuing evaluation of new technology which may have application to future Naval aircraft.

The purpose of the evaluation was to validate data obtained on the test aircraft in the NASA Ames Research Center 40 x 80 ft. wind tunnel by flight test, and to obtain performance, stability, and control data sufficient to evaluate the Jetwing concept for future application to other flight vehicles.

The specific objectives were:

1. Aircraft checkout and pilot familiarization.
2. Airspeed calibration encompassing both high and low speed ranges.
3. Measurement of aircraft performance including takeoff and landing performances.
4. Determination of aircraft lifting capability, including lift variation with angle of attack.
5. Measurement of longitudinal stability to include neutral point determination, short period and long period dynamic stability characteristics, and flight path stability.
6. Measurement of maneuvering stability, including location of the maneuver points.
7. Determination of aileron effectiveness throughout the speed range, and with several flap positions.
8. Measurement of lateral-directional stability to include both static and dynamic stability characteristics.
9. Evaluation of the landing approach characteristics, with particular emphasis on the STOL mode of operation.
10. A static determination of net thrust available using laser velocimeter measurements.

With exception of item 10 all test objectives were met. However, it should be pointed out that the test methodology and technical approach were constrained by program budget, and the physical size of the test vehicle. As a result, some of the test methods used may not be considered "state of the art." They are, however, reliable methods which provide valid data.

Although an attempt was made, and considerable useful data collected, it was not possible to obtain an accurate measurement of static thrust using the laser velocimeter. The reasons for this failure, and the changes in method and equipment to prevent it on future attempts are discussed in the body of the report.

SECTION II
DESCRIPTION AND BACKGROUND
OF THE TEST ARTICLE

DESCRIPTION

The Jetwing STOL research aircraft is a single engine, single seat, upper surface blowing (USB) powered lift, jet aircraft with conventional landing gear. (Figures 1 & 2). Figure 3 is a three view drawing of the aircraft showing its general arrangement. Table 1 lists other pertinent design features and dimensions.

The powered lift concept used on the Jetwing aircraft allows upper surface blowing (USB) from a single jet engine. Upper surface blowing has previously been limited to multi-engine configurations such as the Boeing YC-14 and NASA Quiet Shorthaul Research Aircraft (QSRA). In the "Jetwing" concept USB is achieved from a single engine by ducting all engine air (both from by-pass and core exhaust) to a slot nozzle on the upper surface of the wing. The nozzle is located at approximately 30-40% of the wing chord and extends along approximately 70% of the wing span. The fan by-pass air is ducted to the outboard portion of the wing while the core exhaust is ducted to the inboard portion of the wing as is shown in Figure 4. Located above the nozzle is a separate, and much smaller wing surface. The purpose of this surface is to act as an ejector or thrust augmentor. A Coanda type, single element flap is located at the trailing edge of the wing along the portion of the wing span covered by the nozzle. A two dimensional sketch of the arrangement is shown in Figure 5.

The concept may be used with, or without, the smaller upper wing surface which wind tunnel tests have shown to have negligible effect on powered lift capabilities (See Figures 6 and 7). However, all testing reported herein was conducted with the upper wing installed. A follow on effort will evaluate the inflight performance of the concept with the upper wing removed.

Incorporated into the fan by-pass air nozzle is a thrust reverser which is operated as is shown in Figure 8.

Since the USB covers such a large portion of the wingspan, a separate bleed air system for the ailerons is not required.

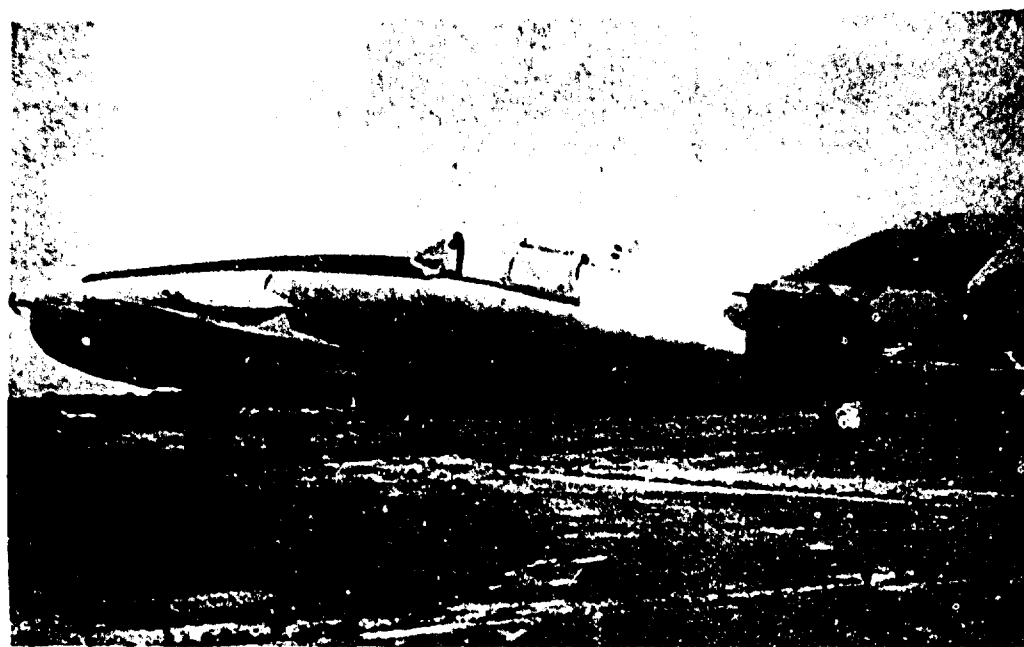


FIGURE 1

FRONT VIEW JETWING RESEARCH AIRCRAFT

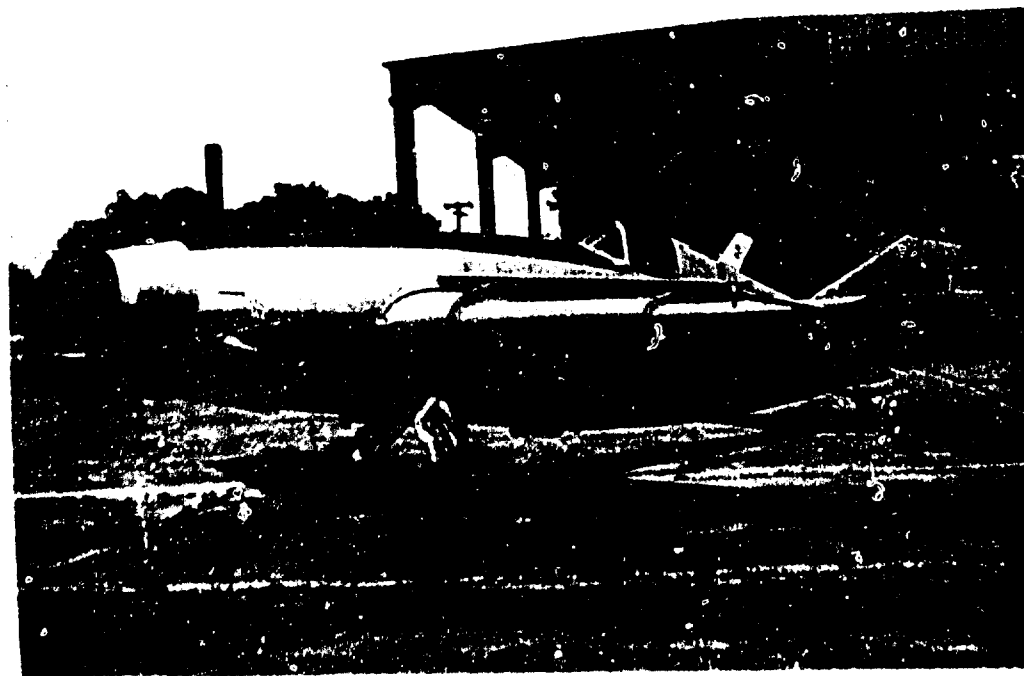


FIGURE 2

SIDE VIEW JETWING RESEARCH AIRCRAFT

TABLE I
JETWING PHYSICAL DESCRIPTION

Powerplant	Pratt & Whitney JT15D-1 Turbofan
Rated Takeoff Thrust	2200 LB. Static Thrust @ Sea Level Standard Conditions (Uninstalled)
Rated Maximum Continuous Thrust	2050 LB. Static Thrust @ Sea Level Standard Conditions (Uninstalled)
Maximum Continuous Thrust as Installed in Jetwing Aircraft	1750 LB. Static Thrust @ Sea Level Standard Conditions
Fuel Capacity	106 Gal.
Maximum Takeoff Gross Weight	3750 LB.
Empty Weight	2330 LB. Without Ballast
Ballast	412 LB.
Center of Gravity Location with Ballast, Pilot and Full Fuel	35.5% M.A.C.
Wing Airfoil Section	NACA 23020 Modified at Root NACA 23015 at Tip
Wing Span	21.75 FT
Wing Area	105.6 FT ²
Aspect Ratio	4.48
Mean Aerodynamic Chord	5.08 FT
Taper Ratio	0.46
Wing Incidence	0° Root 0° Tip

Upper Wing Airfoil Section	Clark Y-12% Thickness
Upper Wing Span	15.1 FT
Upper Wing Area	23.16 FT ²
*Upper Wing Position Measured at Trailing Edge of Upper Wing at the Inboard Support Fairing	
**Position #1	5.437 IN
Position #2	7.625 IN
Position #3	6.531 IN
Incidence Angle With Lower Wing Chord	Approximately 5°
Aileron Type	Setback Hinge
Aileron Span	35.75 IN Each
Aileron Area	3.44 FT ² Each
Aileron Deflection	± 25°
Flap Type	Coanda Single Element
Flap Span	69 IN Each
Flap Area	10.6 FT ² Each
Flap Deflection	0° to 55°
Horizontal Tail Airfoil Section	8% Thick Symmetrical
Horizontal Tail Span	9.33 FT

*See Appendix 1 for Internal Dimension of Ejector and Area Ratios

**Position Used for Flight Tests

Horizontal Tail Area	27.5 FT ²
Horizontal Tail Aspect Ratio	3.16
Horizontal Tail Volume (\bar{V}_H)	0.74
Elevator Area	13.25 FT ²
Elevator Deflection	+29° to -25°
Horizontal Stabilizer Trim Deflection	+20° to -2°
Vertical Tail Airfoil Section	8% Thick Symmetrical
Vertical Tail Span	5.67 FT
Vertical Tail Area	18.33 FT ²
Vertical Tail Aspect Ratio	1.75
Vertical Tail Volume (\bar{V}_V)	0.115
Rudder Area	8.06 FT ²
Rudder Deflection	± 20°
Engine Exhaust Nozzle Area (at top surface of wing)	
Fan Duct Total	156.2 IN ²
Gas Generator Duct Total	96.3 IN ²
Aircraft Length	28.6 FT
Aircraft Height	6.1 FT
Construction	
Fuselage	Welded Steel Tube Truss Covered With Titanium and Aluminum
Wing	Built up Aluminum and Titanium
Tail	Built up Aluminum

Landing Gear	Conventional, Retractable
Egress System	None
Longitudinal Control System	Reversible With Pushrod Linkage to Elevator
Longitudinal Trim	Electrically Actuated Trimmable Stabilizer
Directional Control System	Reversible With Cable Linkage to Rudder
Lateral Control System	Reversible With Pushrod Linkage to Ailerons
Moments of Inertia and Component Weights	See Appendix III

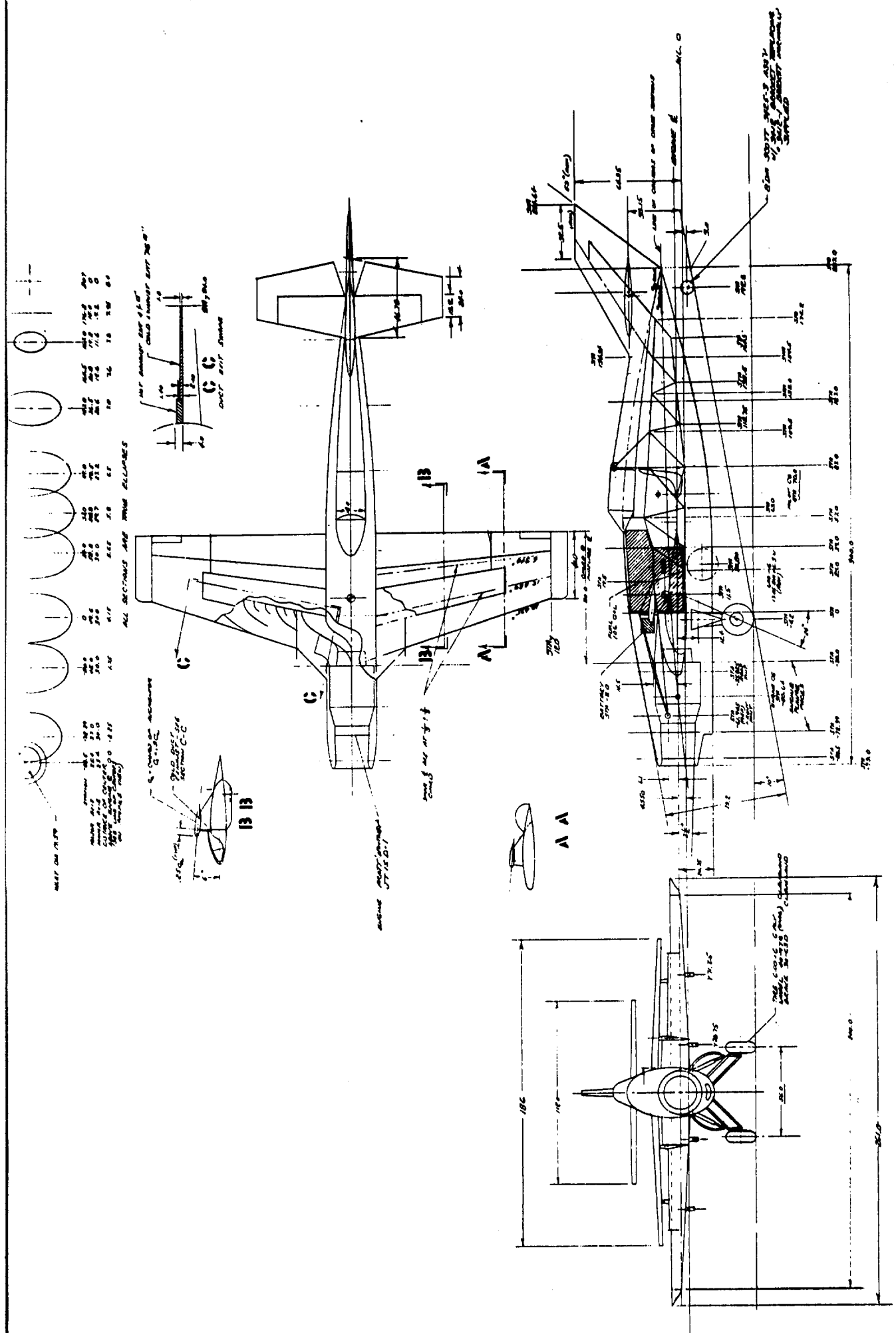
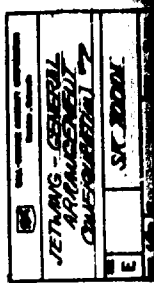


FIGURE 3 GENERAL ARRANGEMENT DRAWING OF JETWING RESEARCH AIRPLANE



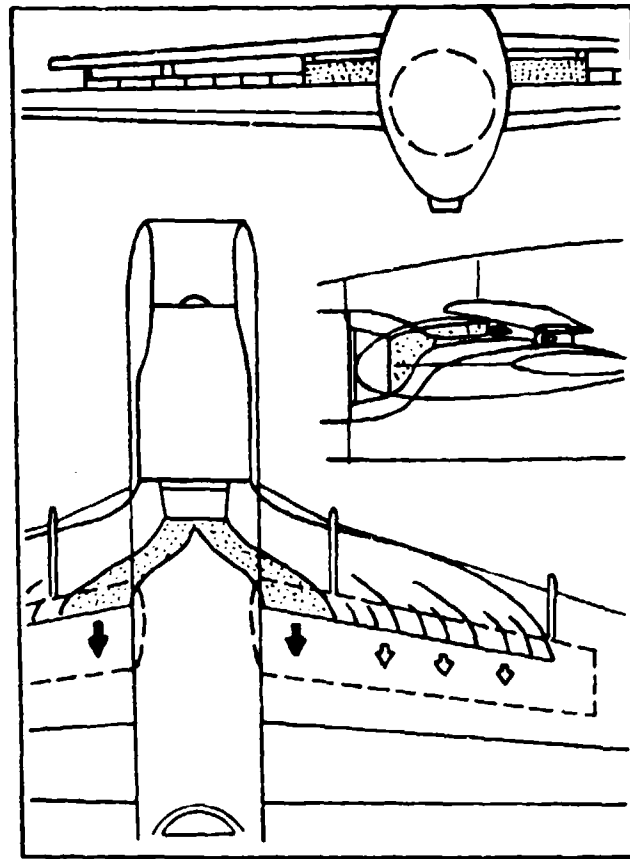


FIGURE 4 JETWING DUCTING ARRANGEMENT
(FROM REFERENCE 1)

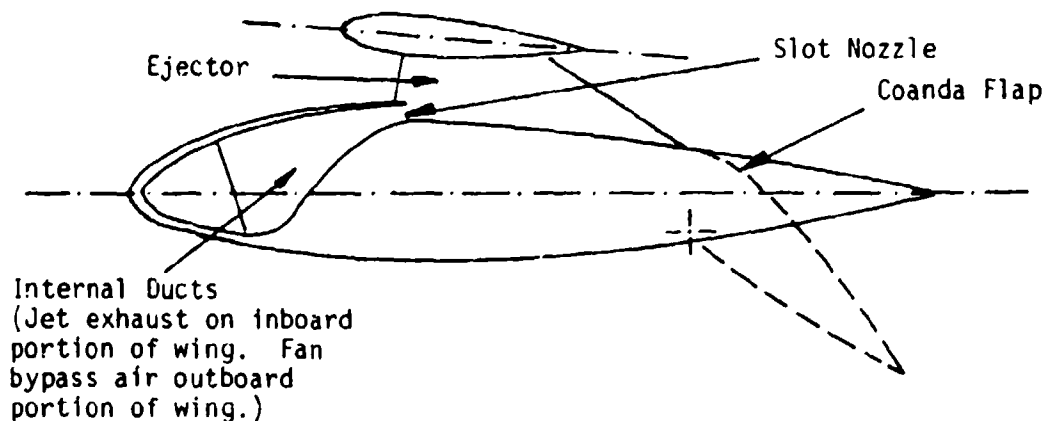


FIGURE 5 TWO DIMENSIONAL VIEW OF JETWING CONCEPT

T-495
 Gear Down/ δ_f = 30/ δ_a = 0/ δ_2 = 0/ δ_s = 0
 δ_r = 0/Upper Wing @ #1/ δ_{rev} = 0/c.g. @ .33c

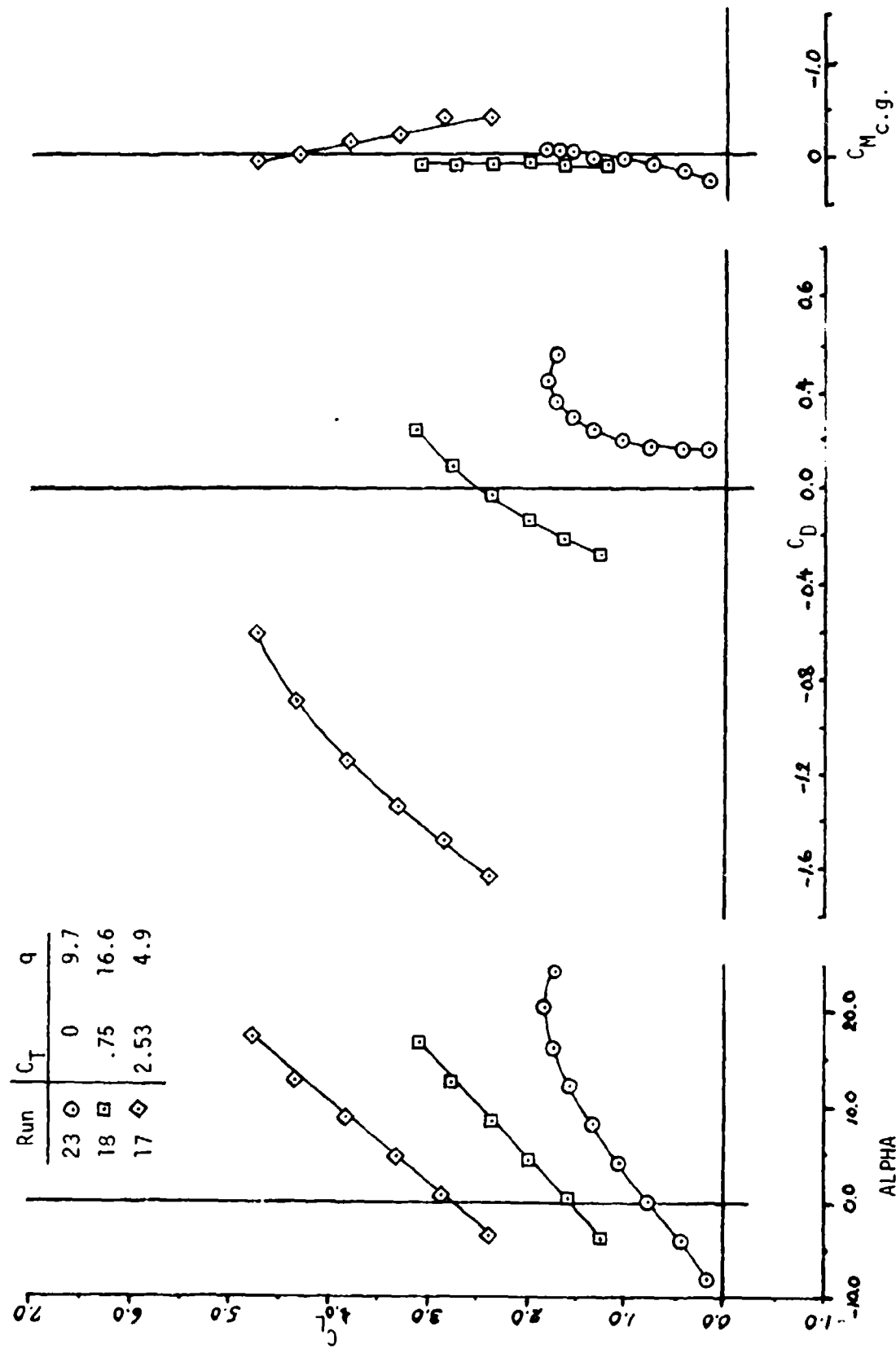


FIGURE 6
 WIND TUNNEL DATA WITH UPPER WING INSTALLED

T-496
 Gear Down/ δ_f = 30/ δ_a = \pm 15/ δ_e = 0/ δ_s = 0
 δ_r = 0/Upper wing off/ δ_{rev} = 0/cg @ .41c

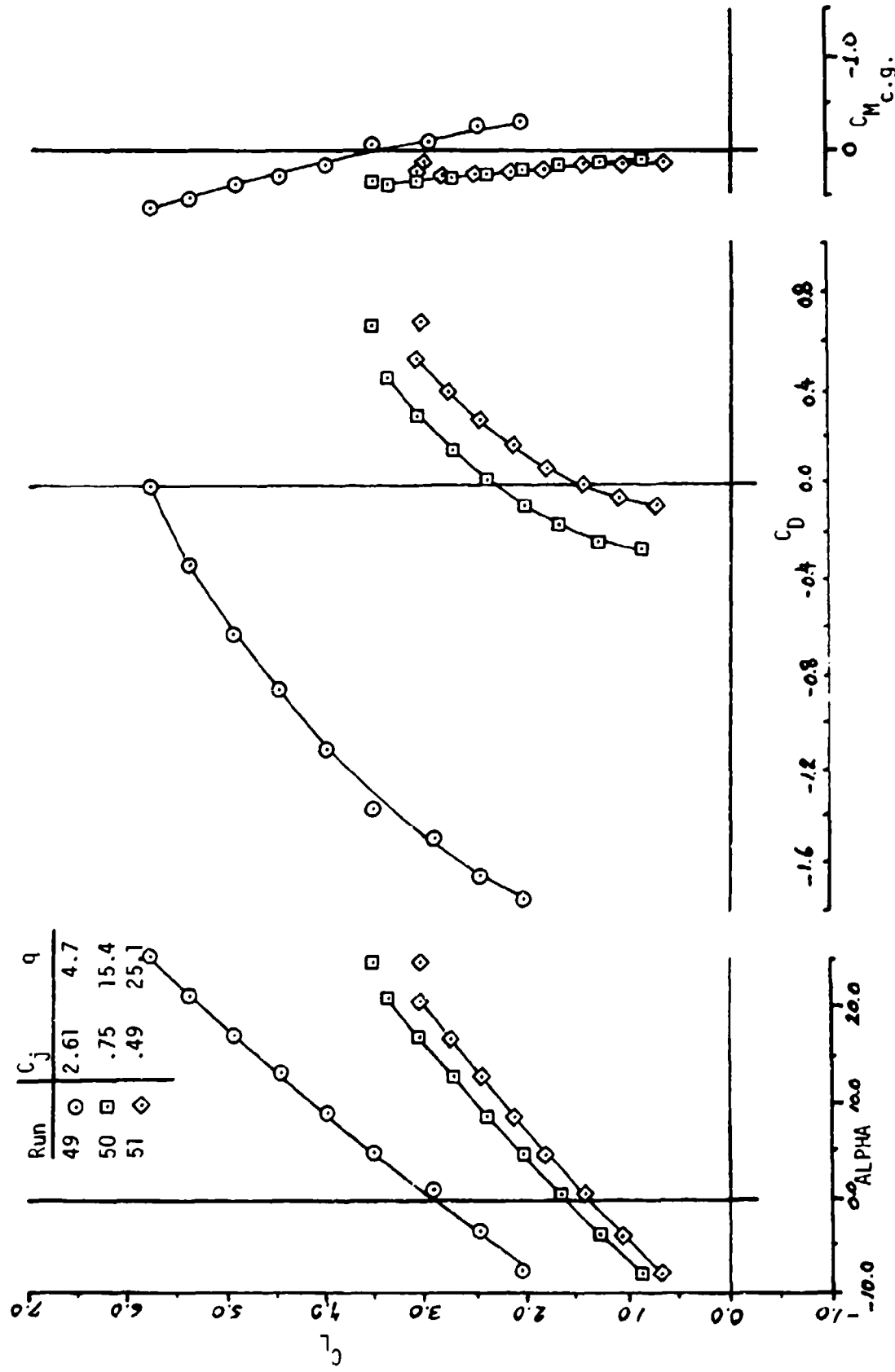


FIGURE 7
 WIND TUNNEL DATA WITH UPPER WING REMOVED

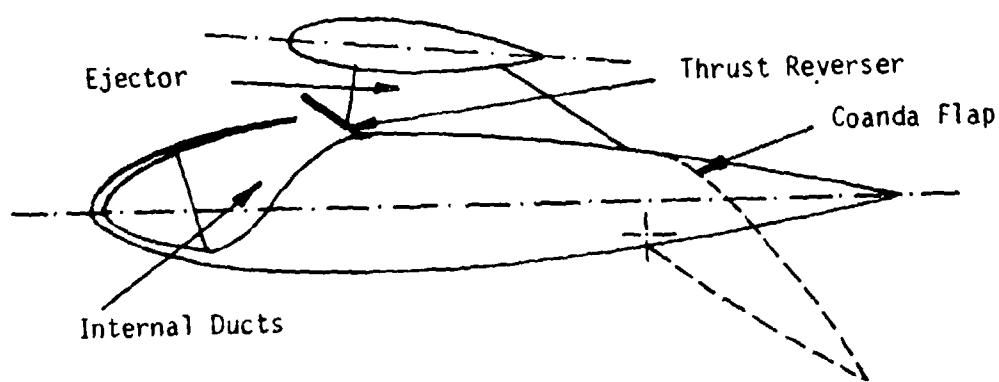


FIGURE 8 TWO DIMENSIONAL VIEW OF JETWING CONCEPT
WITH THRUST REVERSER DEPLOYED

BACKGROUND

The "Jetwing" concept was conceived by Mr. O. E. Bartoe while he was Vice President and General Manager of Ball Brothers Research, a division of the Ball Corporation. Mr. Bartoe felt so strongly about his ideas that he was able to convince the management of Ball Corporation that they were worth spending corporate funds to develop. This led to the formation of a separate company, called Ball-Bartoe Aircraft Company (with Mr. Bartoe as its President), to develop the "Jetwing" ideas into a proof of concept research aircraft.

Development started on the Jetwing research airplane in 1973. The airplane was completed and ready for testing by December of 1976.

Full scale testing started in December of 1976 in the NASA Ames Research Center 40' x 80' wind tunnel. A large matrix of aircraft configurations were tested in the full scale wind tunnel of which figures 6 and 7 are examples. Other data from these tests are also available for comparison with flight test data and with data from other USB concepts. An evaluation of the wind tunnel data revealed that the aircraft was neutrally stable to unstable longitudinally at the centers of gravity where it was likely to be flown. As a result about 300 pounds of lead ballast was added to the nose of the aircraft prior to the start of flight testing.

The first flight was conducted at Mojave, California on July 11, 1977, by Mr. H. R. Salmon. This flight confirmed the instability, and as a result an additional 100 pounds of lead ballast was added. Forty seven flights were flown at Mojave for a total of 34 hours. During this testing it was discovered that the horizontal tail would stall whenever the flaps were lowered to angles in excess of 40° in combination with flight speeds of about 50 knots indicated airspeed. As a result a safe flap deflection of 35° was established. (Testing reported in this report did not use flap deflections in excess of 30°). A certain amount of quantitative performance data were gathered during the Mojave testing, but its usefulness is limited due to the lack of calibrations on instruments and airspeed system.

Upon completion of testing at Mojave, the aircraft was ferried to the Ball-Bartoe Aircraft Company facility at Boulder, Colorado, where some testing and demonstration flying continued. An additional 44 flights and 32 flight hours were accumulated upon the aircraft during the ferry trip and test flying at Boulder.

In December of 1978, the Jetwing research aircraft and its conceptual patents were donated to the University of Tennessee. On February 19, 1980, the University of Tennessee received Contract N00019-80-C-0126 for the flight and ground testing which is described in the remainder of this report.

SECTION III

POTENTIAL APPLICATIONS

OF JETWING CONCEPT

The Jetwing concept offers a number of items useful on military aircraft. The primary item being STOL performance for single engine designs through application of USB. Other items are:

1. Increased Payload when STOL performance is not required. In such cases, the additional lift due to USB can be used to carry a greater load.
2. Enhanced Maneuvering by use of a Coanda flap programmed to deflect with increasing load factor. Such a flap system will provide increased lift through both deflected thrust and supercirculation lift.
3. Thrust Augmentation or Minimum Installed Thrust Losses, if the ejector portion of the concept is also used.
4. Low Infrared Signature due to ambient air mixing and shielding. This could be improved by mixing the cold and hot ducts upstream of the nozzle.
5. Low Noise Signature due to the slot nozzle, ambient air mixing, and shielding by the wing.
6. Simple Low Cost Design when compared to other powered lift STOL approaches.

Potential applications for the concept include:

1. Subsonic Fighter/Attack aircraft such as those shown in Figures 9 and 10. Figures 10 shows a modification of the concept in which only the fan by-pass air is ducted over the wing. In such a design an after-burning turbofan engine could be used. As was mentioned in a previous section the upper wing surface could be omitted without adverse effects.
2. Supersonic Fighter Aircraft such as those shown in Figure 11 thru 14. These designs use a conventional jet nozzle during supersonic operation and convert to the Jetwing concept during takeoff, landing and subsonic and transonic maneuvering. Figures 11 and 12 show the arrangement using a supercritical airfoil for a fighter of moderate speed capability. Figures 13 and 14 show a similar arrangement for a very high speed fighter using a circular arc airfoil.

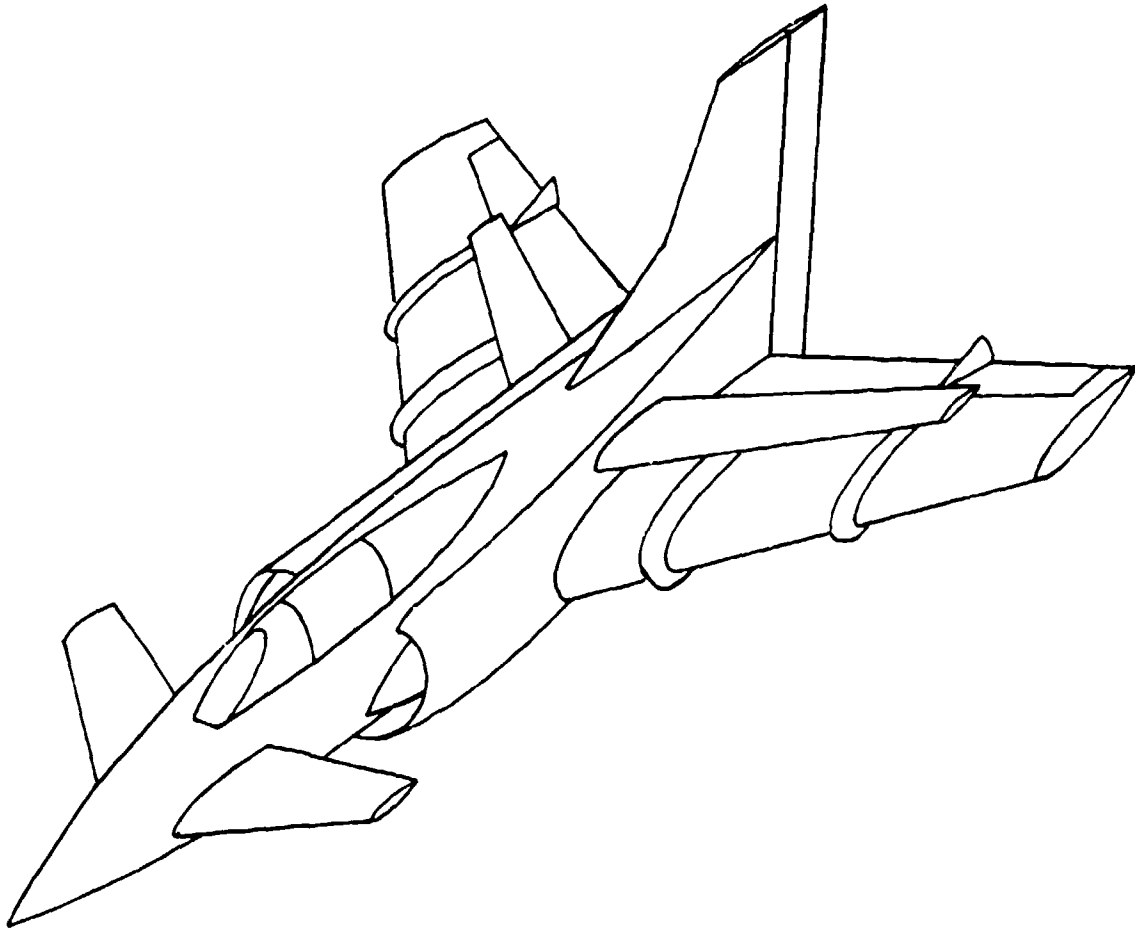


FIGURE 9
FIGHTER/ATTACK AIRCRAFT USING JETWING CONCEPT

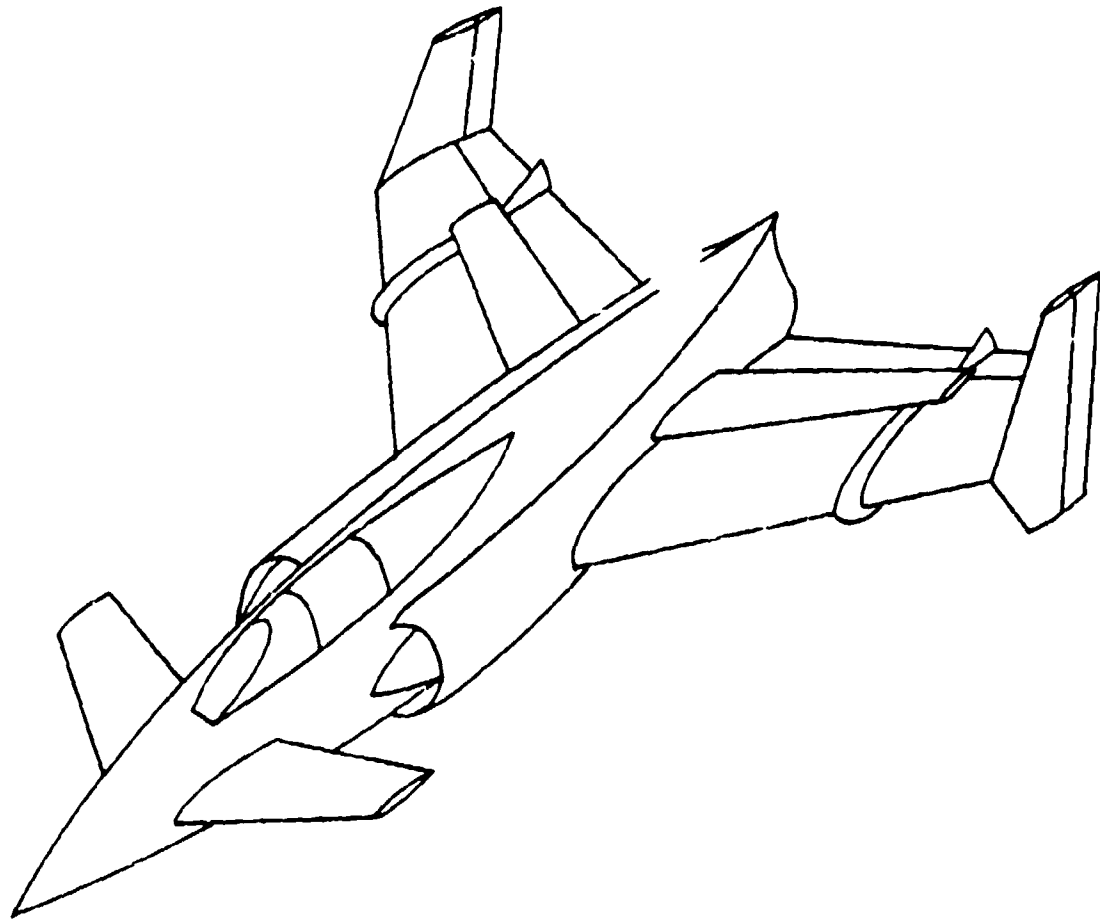


FIGURE 10

FIGHTER/ATTACK AIRCRAFT WITH AFTERBURNING TURBOFAN ENGINE
USING MODIFIED JETWING CONCEPT WITH ONLY FAN BY-PASS AIR
DUCTED OVER THE WING

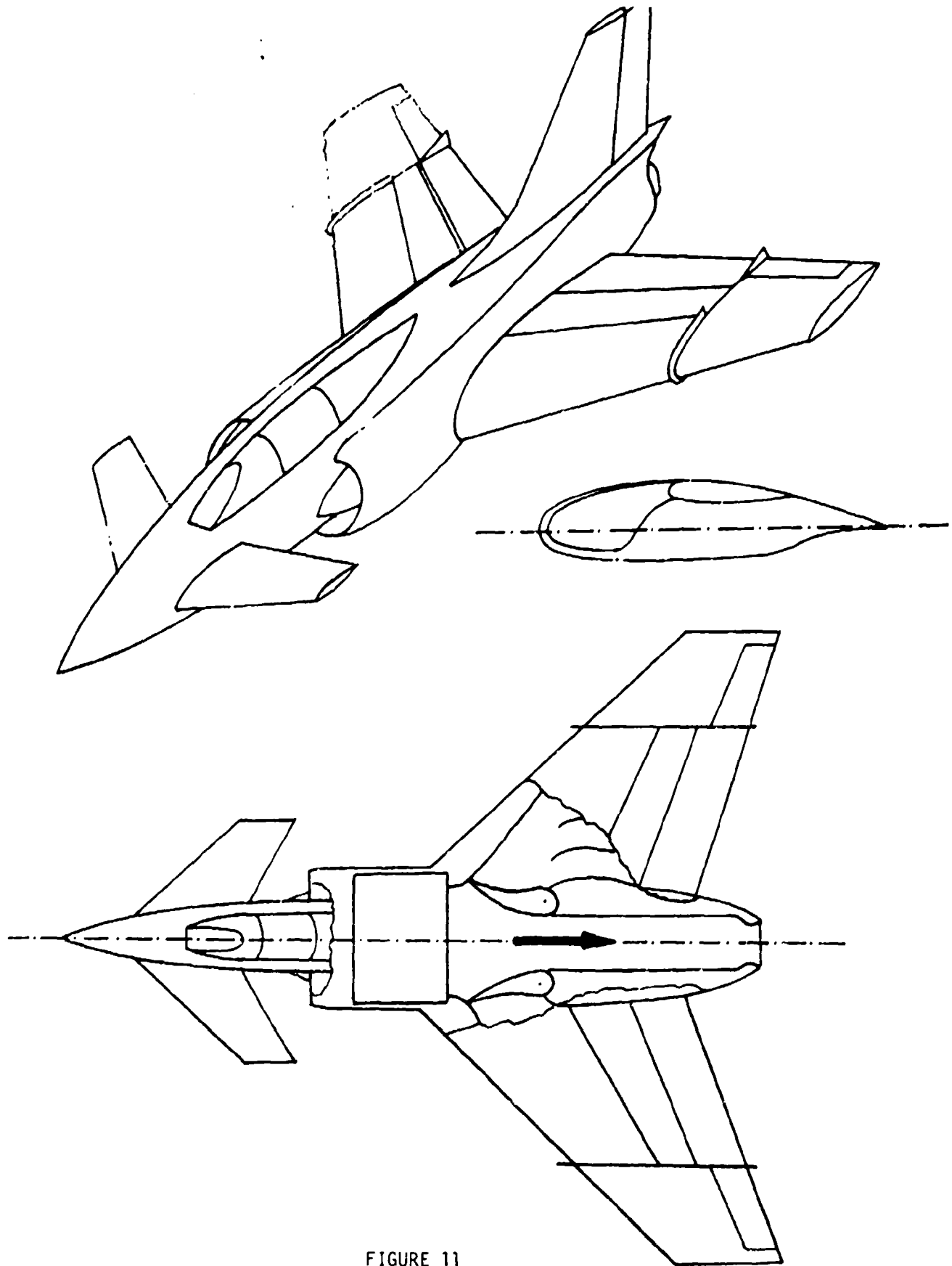


FIGURE 11

JETWING SUPERSONIC FIGHTER USING SUPERCRITICAL AIRFOIL
-SUPERSONIC FLIGHT CONFIGURATION

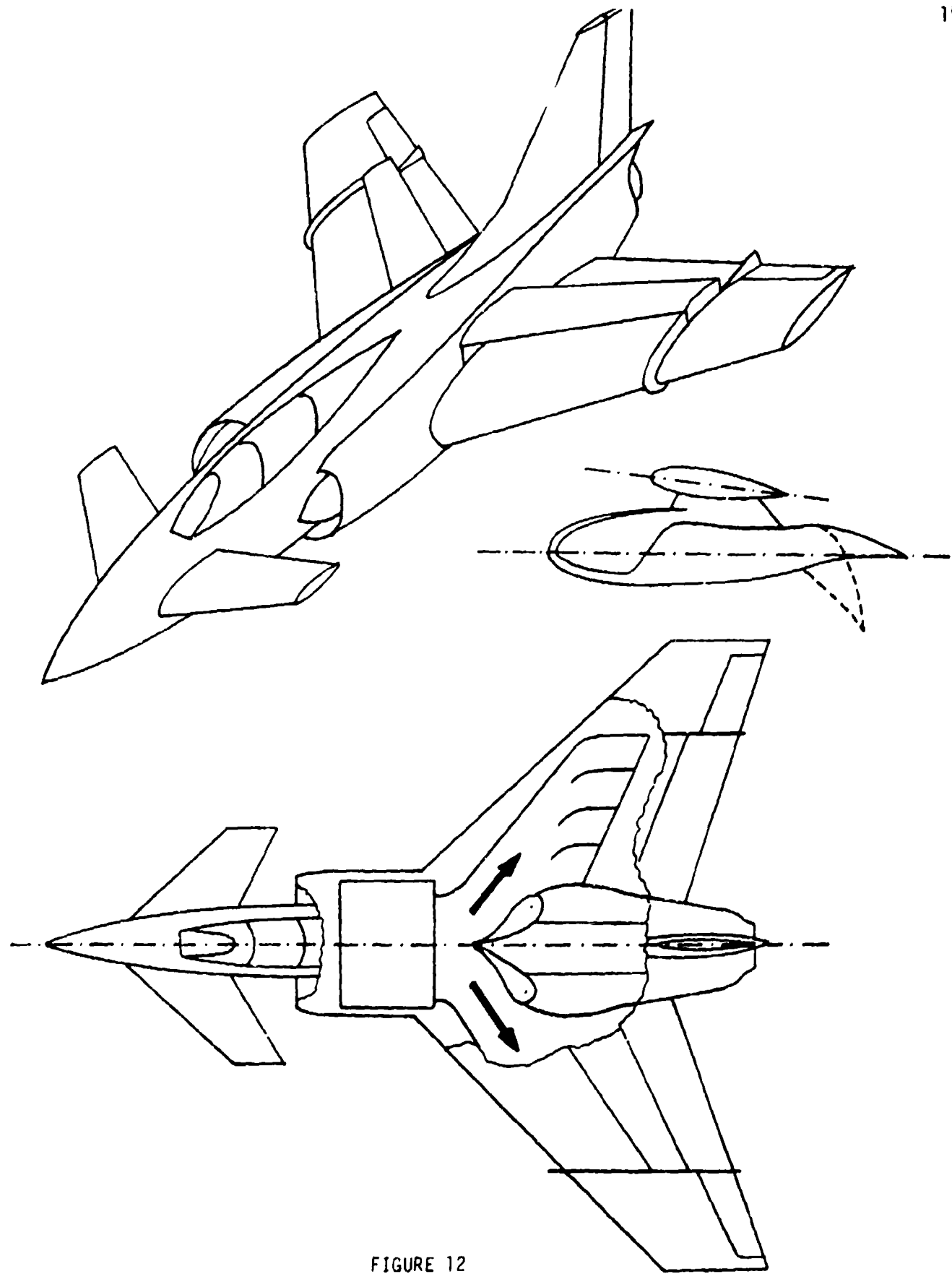


FIGURE 12

JETWING SUPERSONIC FIGHTER USING SUPERCRITICAL AIRFOIL
-SUBSONIC FLIGHT CONFIGURATION

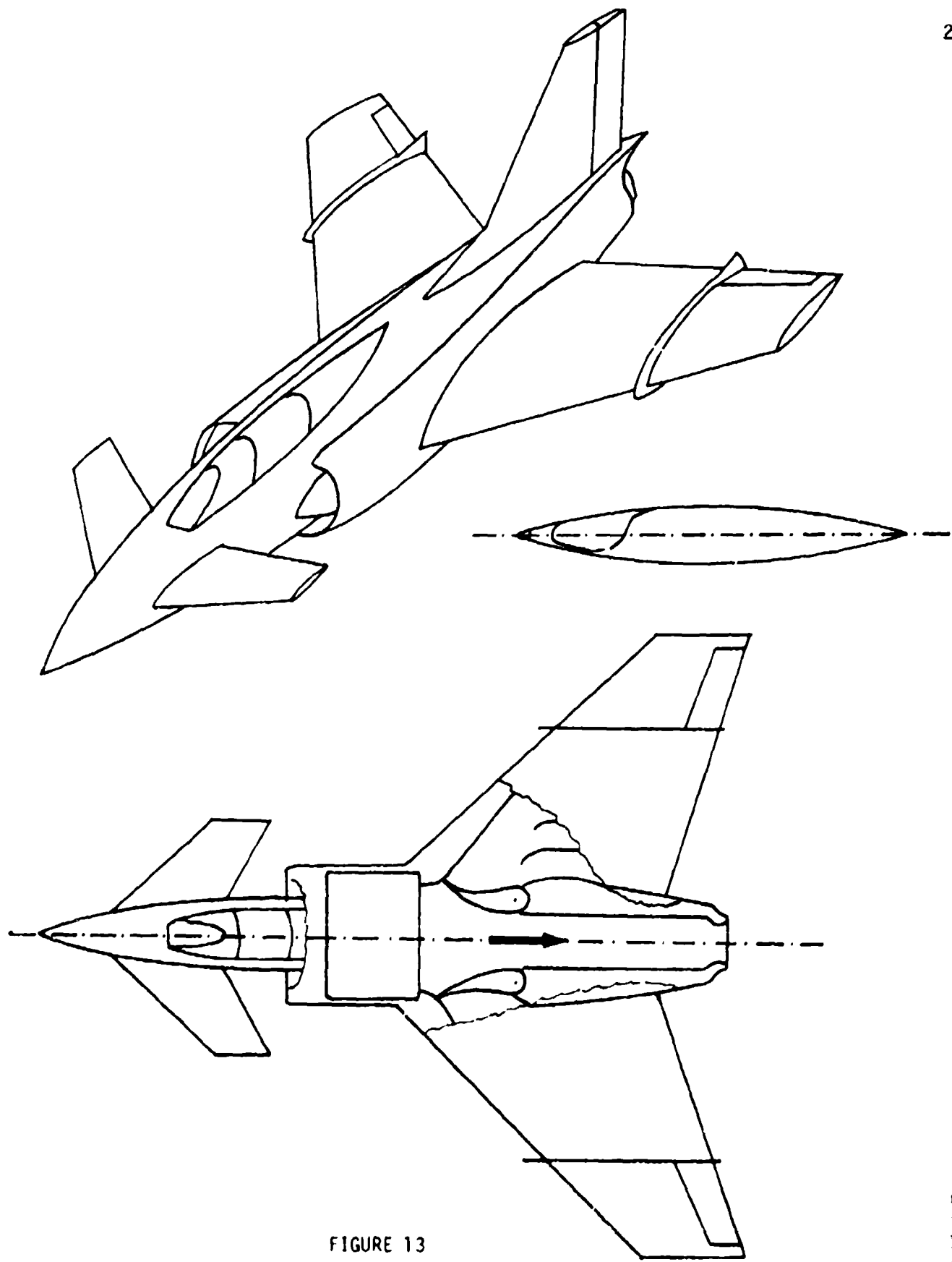


FIGURE 13

JETWING SUPERSONIC FIGHTER USING CIRCULAR ARC AIRFOIL -
SUPERSONIC FLIGHT CONFIGURATION

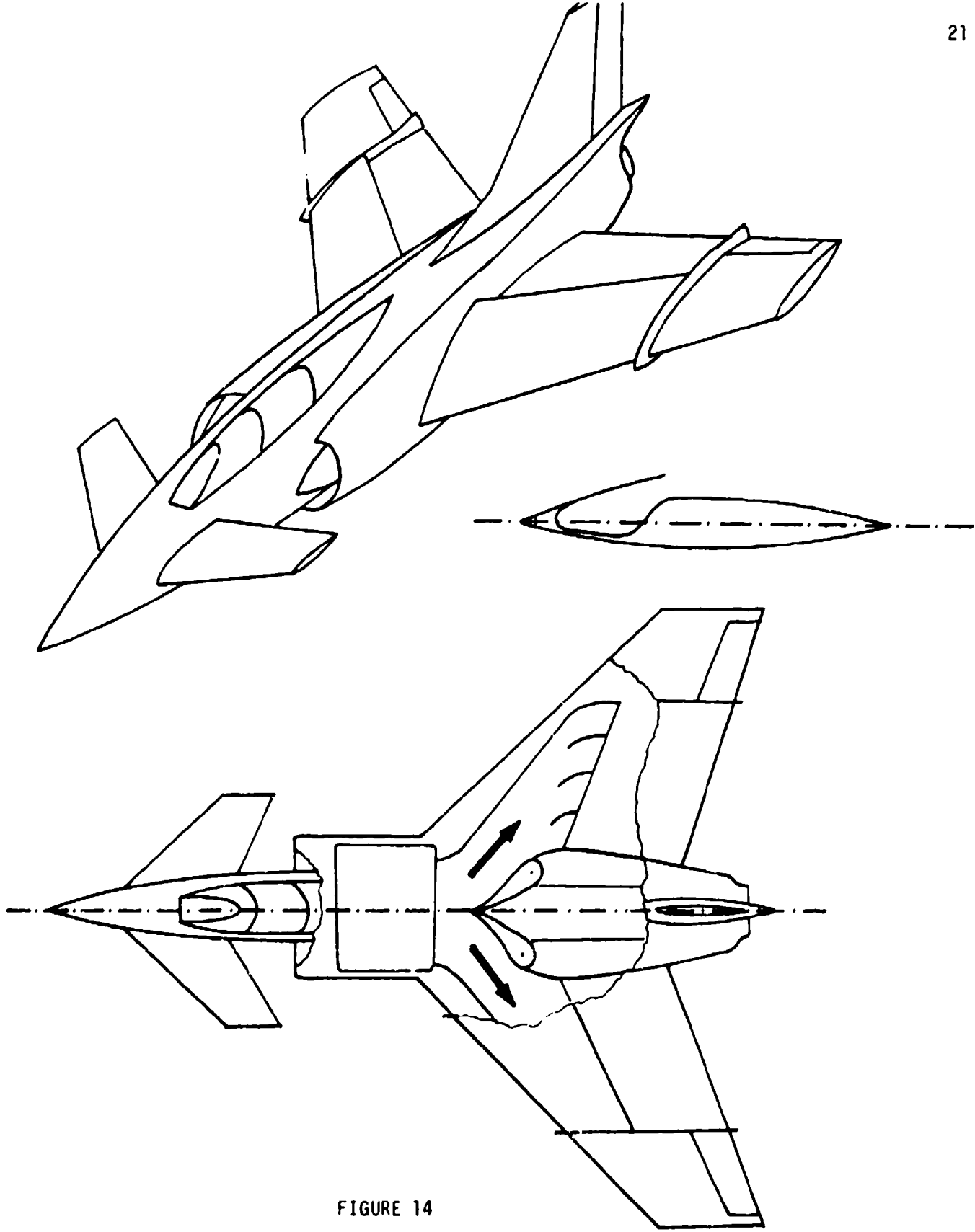


FIGURE 14

JETWING SUPersonic FIGHTER USING CIRCULAR ARC AIRFOIL -
SUBSONIC FLIGHT CONFIGURATION

3. Transport or Carrier Onboard Delivery Aircraft such as is shown in Figure 15. In such an arrangement all engines would exhaust into a common plenum for ducting to the top surface of the wing. This design would minimize engine out problems, and not require the cross ducting or differential flap arrangements of current USB multi-engine designs.

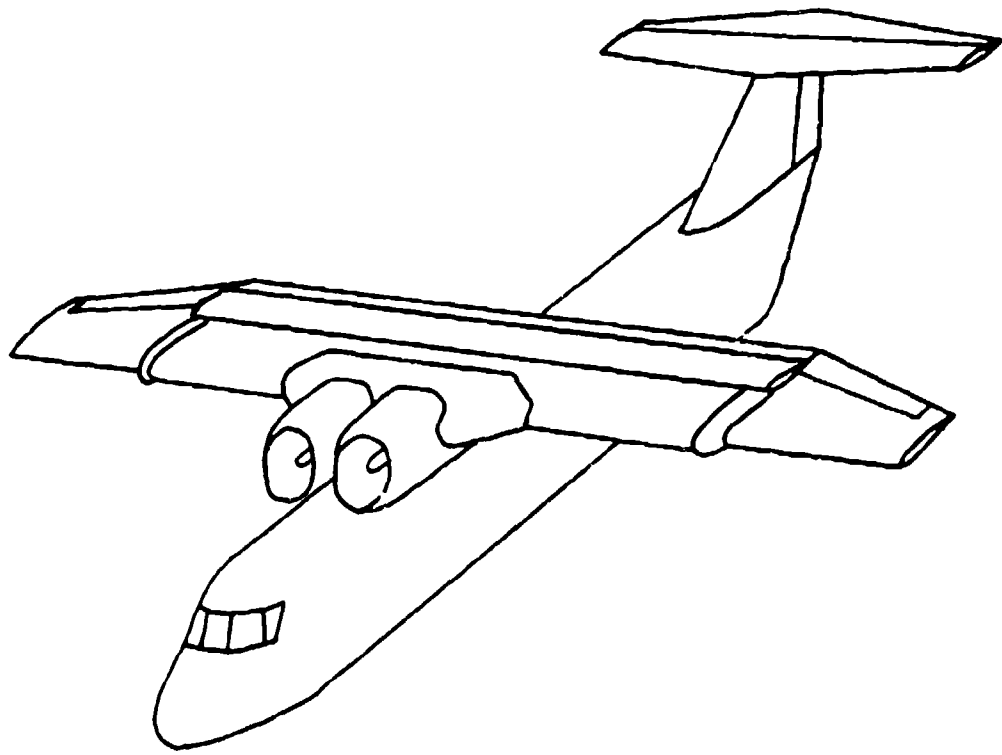


FIGURE 15

TRANSPORT OR CARRIER ON BOARD DELIVERY
AIRCRAFT USING JETWING CONCEPT

SECTION IV

TEST PROCEDURES

The test procedures used to accomplish this effort followed standard and accepted flight test practice to the extent practical considering test vehicle and program constraints. Constraints which were a factor in designing the test methods included:

1. Test vehicle size
2. Stability levels of the test vehicle
3. Emergency egress method
4. Flutter and structural clearances
5. Program budget

The size of the test vehicle proved to be a rather severe constraint. As can be seen from Figures 1 and 2 and Table I the aircraft is very small. This small size along with a limited program budget severely constrained the type of instrumentation package which could be installed. The level of static longitudinal stability also prohibited installation of all but necessary instrumentation aft of the cockpit. This resulted in the type and amount of instrumentation dictating the use of certain test methods.

The test aircraft is not equipped with an ejection seat. As a result, low altitude operation at airspeeds below power off stalling speed were avoided where possible. The egress limitation along with the absence of a flutter clearance also limited maximum speeds to less than 200 knots. These limitations also played an important role in design of the test methods.

Although, designed for a +6 and -3G normal load factor, the aircraft had not been structurally tested. As a result, all testing requiring maneuvering was limited to a +2 or -1G normal load factor. In spite of these limitations, all testing was completed safely and successfully. In most instances, it was possible to work around the limitations by changing test methods or procedures.

The procedures used to accomplish the specific test objective in the order in which they were performed follows:

1. TAXI TESTS: Prior to familiarization flying, a series of taxi tests were conducted at high and low taxi speeds to determine ground handling and control feel. In addition, these tests were used to check out ship's instrumentation and systems prior to flight. The aircraft was loaded with the same loading as used for the familiarization flying.

2. FAMILIARIZATION FLIGHTS: These flights consisted of a qualitative evaluation and familiarization with the aircraft. The operating envelope was gradually expanded until an envelope of 50 to 180 KIAS had been explored. Items that received a preliminary evaluation during this phase included:

1. Basic Static and Dynamic Stability (longitudinal, lateral, and directional).
2. Low speed handling qualities particularly in roll and pitch.
3. Landing and takeoff techniques, CTOL and STOL.
4. Effects of configuration changes on trim etc.
5. Effects of Power on Airspeed Calibration.
6. Basic flight trim (wing heaviness etc.)

Aircraft loading during familiarization flying was 3608.5 lb. gross weight with center of gravity at 35.3% M.A.C. The configuration and instrumentation during this phase was as received from Ball Corporation.

3. AIRSPEED CALIBRATION: The wing boom pitot-static system was calibrated at the following indicated airspeeds:

<u>GEAR AND FLAPS UP</u>	<u>GEAR DOWN, FLAPS UP</u>
70 - 120 knots	70 - 130 knots
IN 5 knot increments	IN 5 knot increments
120 - 170 knots	
IN 10 knot increments	
<u>GEAR DOWN, FLAPS 15°</u>	<u>GEAR DOWN FLAPS 30°</u>
60 - 120 knots	50 - 100 knots
IN 5 knot increments	IN 5 knot increments

This was accomplished by pacing the aircraft with a Cessna 310 in the speed range from 90 - 170 knots, and a DHC-3 Otter in the 50 - 100 knot range. The airspeed systems of both the Cessna 310 and DHC-3 Otter were previously calibrated by use of the speed course method. Particular attention was paid to a comparison of data with the gear down and gear up. It was hoped that these data would show if there were significant power effects to the airspeed calibration.

During the airspeed calibration a position error calibration of the altimeter was obtained along with determining the correction factor for the outside air temperature indicator.

Calibrated instrumentation required for this tests included:

1. Airspeed Indicator
2. Altimeter
3. Outside Air Temperature Indicator

The pace aircraft also required the same calibrated instruments.

4. THRUST CALIBRATION: Prior to the start of performance testing a static calibration of the in-flight thrust measuring instrumentation, and a measurement of the installed thrust, was performed. This was accomplished, as shown in Figure 16, by attaching a dynamometer between the aircraft and an immovable object. The connection between the aircraft and the immovable object (through the dynamometer) was along the thrust line, which required installing blocks under the aircraft tailwheel. The aircraft was placed on a small incline of sufficient slope to overcome the static friction of the wheels. A zero reading of the dynamometer was taken prior to starting the engine, and at the completion of the test. After the zero reading of the dynamometer was taken, the engine was started and the thrust increased in even increments. At each increment of thrust sufficient time was allowed for the engine parameters to stabilize before data were taken. Data were taken at both increasing and decreasing valves of thrust to determine hysteresis.

At each increment of thrust the following data were recorded:

1. Actual Thrust (dynamometer reading)
2. Main Rotor Speed (N_1)
3. Bypass Exhaust Duct Pressure Ratio (P_{t5}/P_a)
4. Gas Generator Speed (N_2)
5. Core Exhaust Duct Pressure Ratio (P_{t5}/P_a)
6. Interstage Turbine temperature (ITT)
7. Outside Air Temperature (T_a)
8. Pressure Altitude (H_p)

All of the above instruments were calibrated with the duct total pressure being referenced to ambient static through the airspeed static source.



FIGURE 16 THRUST CALIBRATION TEST SETUP

Best Available Copy

Data were corrected to standard conditions and thrust plotted versus various parameters in order to compare with wind tunnel data, and to determine the best parameter for in-flight reference. This calibration was conducted both with and without the upper wing surface.

5. PERFORMANCE FLIGHT TESTS, INCLUDING C_L VS α DETERMINATION:
On a powered lift airplane it becomes very difficult to separate thrust and drag, and the lift is also a function of thrust. As a result constant W/ δ data from the technique normally used for jet aircraft will not reduce to a single curve good for all altitudes.

A simpler approach which works well for powered lift aircraft is the Airspeed vs Flight Path Angle (V- γ) Map. The theory behind this technique is covered in Appendix II. In essence, it is a plot of Flight Path Angle, γ , versus Airspeed for various thrust settings from idle to maximum available. Angle of attack information was also collected and reduced to C_L vs α and C_D or C_{FEX} vs C_L by the methods shown in the Results and Discussion section.

The raw data for this approach may be obtained by:

1. Level Acceleration
2. Sawtooth Climb
3. Power Idle Descents

The sawtooth climb and power idle descent were selected for use on the Jetwing testing for the following reasons: First, the use of these techniques provides a more stable value of thrust. Secondly, they are easier to fly. This second reason is especially important on the Jetwing because of its lack of longitudinal stability. Sawtooth climbs or descents were performed in 10 knot increments in the following speed range and configuration.

<u>SPEED RANGE</u>	<u>CONFIGURATION</u>
1. 80 - 180 knots	Gear and Flaps up
2. 70 - 120 knots	Gear down, Flaps 15°
3. 50 - 120 knots	Gear down, Flaps 30°

Each speed range was repeated at four gross thrust settings.

1. Maximum Available
2. 1000 lbs.
3. 500 lbs.
4. Idle Thrust

Test altitude was varied depending upon the thrust level required. Maximum available thrust testing occurred at approximately 1000 ft. pressure altitude. Since the data reduction method reduces all data to a sea level standard condition, test altitude is not critical except for obtaining maximum thrust.

Two climbs or power idle descents were done crosswind in opposite directions for each data point. An average of the two climbs was used in determining the data point to reduce errors created by wind. During each climb, the following data were recorded at 30 second time intervals:

1. Fuel Remaining for determination of test weight (W_T)
2. Indicated Airspeed (V_i)
3. Gross Thrust indication (N_1 , Fan & Core Pt5/ P_a , N_2 , ITT).
4. Angle of attack (α)
5. Pressure altitude (H_p)
6. Time (t)
7. Outside air temperature (T_a)
8. Aircraft configuration

6. CONTROL FRICTION: Prior to beginning stability and control testing the control system friction and breakout forces were measured. This was accomplished by recording control force and control surface position simultaneously, for both increasing and decreasing values of control surface deflection, throughout the travel of the control surface.

Plots of control force versus control surface position were made, and the breakout forces and friction determined from these plots.

7. LATERAL CONTROL POWER: The roll acceleration and steady state roll rate were measured in the following trim conditions.

<u>CONDITION</u>	<u>GEAR</u>	<u>FLAPS</u>	<u>POWER</u>	<u>TRIM SPEED</u>
Cruise	Up	Up	PLF	150 KIAS
Low Cruise	Up	Up	PLF	110 KIAS
Power Approach	Down	30°	3° APP	90 KIAS
Power Approach	Down	30°	3° APP	70 KIAS
Power Approach	Down	30°	6° APP	90 KIAS
Power Approach	Down	30°	6° APP	70 KIAS

The aircraft was loaded at a center of gravity of approximately 35% MAC and a gross weight of 3600 pounds.

The tests were conducted in the following manner,

1. The aircraft was stabilized at the trim condition.
2. The aircraft was then rolled into a 45° bank opposite the intended direction of roll, and the instrumentation turned on.
3. An aileron only roll was started in the direction opposite the bank and the roll continued for at least 90° roll. During this roll the aileron deflection was held constant and the rudder held at the trim position.
4. Rolls were performed both left and right at each trim condition.
5. Three different aileron deflections up to maximum deflection were used in each direction.

The following data were collected for each roll:

1. Trim Conditions
2. Power Settings
3. Roll Rate
4. Aileron Deflection
5. Bank Angle
6. Pressure Altitude
7. Fuel Remaining (for weight calculation)

8. LATERAL-DIRECTIONAL STABILITY: Control position and control force static lateral-directional stability was measured in straight steady sideslips in the following trim conditions:

<u>CONDITION</u>	<u>GEAR</u>	<u>FLAPS</u>	<u>POWER</u>	<u>TRIM SPEED</u>
Cruise	Up	Up	PLF	150 KIAS
Cruise	Up	Up	PLF	110 KIAS
Power Approach	Down	30°	3° APP	90 KIAS
Power Approach	Down	30°	3° APP	70 KIAS

Data were taken in at least three steady state sideslips in each direction (left and right) at each trim condition.

The following data were recorded for each steady state sideslip:

1. Trim Conditions
2. Power Setting
3. Fuel Remaining (for weight calculation)
4. Pressure Altitude
5. Angle of Sideslip (β)
6. Aileron Position (δ_a)
7. Aileron Force (F_a)
8. Rudder Position (δ_r)
9. Rudder Force (F_r)
10. Bank Angle (ϕ)

Spiral Stability was evaluated at two trim conditions as follows:

<u>CONDITION</u>	<u>GEAR</u>	<u>FLAPS</u>	<u>POWER</u>	<u>TRIM SPEED</u>
Cruise	Up	Up	PLF	130 KIAS
Power Approach	Down	30°	3° APP	65 KIAS

These tests were performed by trimming the aircraft to the desired trim condition, and then banking the aircraft five degrees with the rudder while the ailerons were held neutral. Once five degrees of bank was reached the rudder was returned to trim, and the aileron and rudder were released.

Data recorded during the spiral stability tests included:

1. Trim Conditions
2. Power Setting
3. Pressure Altitude
4. Fuel Remaining
5. Bank Angle (ϕ) versus Time
6. Rudder and Aileron Float Position

Lateral-Directional Dynamic Stability and Control were evaluated at the same trim condition used for static lateral-directional stability. The Dutch Roll motion was excited by a rudder doublet input and the resulting oscillation versus time was recorded on magnetic tape.

Data parameters collected included:

1. Trim Conditions
2. Power Setting
3. Pressure Altitude
4. Rudder Positions (δ_r), Sideslip Angle, (β) and Bank Angle (ϕ) versus time
9. LONDITUDINAL STABILITY: The stick fixed and stick free neutral points were determined by conventional methods in two trim conditions. These trim conditions were:

CONDITION	GEAR	FLAPS	POWER	TRIM SPEED	EVALUATION RANGE
Climb	Up	Up	93°N ₁	V _{R/C}	.85 V _{R/C} -1.3 V _{R/C}
Power Approach	Down	30°	3°APP	70 KIAS	55 - 120 KIAS

Data were collected in approximately 5 knot increments both above and below the trim speed to the limits of the evaluation range. Three center of gravity positions were tested with 2.5% M.A.C. spread in their locations.

Data collected at each trim condition included:

1. Trim Condition
2. Power Setting
3. Pressure Altitude
4. Elevator Position
5. Elevator Force
6. Stabilizer Position
7. Angle of Attack
8. Outside Air Temperature

At each data point in the evaluation range the following data were collected.

1. Indicated Airspeed
2. Elevator Position
3. Elevator Force
4. Angle of Attack

The test runs were conducted between 2000 and 8000 feet pressure altitude with all data collected while the airspeed was stabilized. In addition to determining neutral points, several additional longitudinal flight characteristics were examined during this phase of testing.

The long period dynamic longitudinal stability, or phugoid, was also evaluated during this phase. The same centers of gravity and trim conditions as for static longitudinal stability were evaluated. The test procedure was to displace the aircraft from trim with the elevator, return the elevator to the trimmed position, and record the resultant aircraft motion. The amount of displacement from the trimmed airspeed used was dependent upon the stability level, but did not exceed 10 knots.

The following data were recorded versus time:

1. On magnetic tape:
 - (a) Elevator position
 - (b) Pitch attitude
 - (c) Pitch rate
2. On movie film, or by hand at 5 second intervals:
 - (a) Indicated airspeed
 - (b) Pressure altitude
 - (c) Angle of Attack

10. FLIGHT PATH STABILITY: A separate test was not required for flight path stability since these data are readily available from the V-Y performance information.

11. LONGITUDINAL TRIM CHANGES: Longitudinal trim changes were evaluated at the most forward and most aft centers of gravity for the sets of test conditions listed in Table 2.

Data recorded during these tests were maximum, and steady state, out of trim longitudinal control forces, and pilot comments on the difficulty of control during each trim change.

TABLE 2
LONGITUDINAL TRIM CHANGE CONDITIONS

CONDITION NO.	ALTITUDE	INITIAL TRIM CONDITION				CONFIGURATION CHANGE	PARAMETER HELD CONSTANT
		SPEED	GEAR	FLAPS	POWER		
1	LOW	120 KIAS	UP	UP	PFL	GEAR DOWN	ALTITUDE
2	LOW	120 KIAS	DOWN	UP	PFL	FLAPS DOWN	ALTITUDE
3	LOW	75 KIAS	DOWN	30°	PFL	IDLE POWER	AIR SPEED
4	LOW	60 KIAS	DOWN	30°	PFL	TAKEOFF POWER	ALTITUDE
5	LOW	90 KIAS	DOWN	15°	TAKEOFF	GEAR UP	RATE OF CLIMB
6	LOW	110 KIAS	UP	15°	TAKEOFF	FLAPS UP	RATE OF CLIMB
7	MEDIUM HIGH	LEVEL FLIGHT	UP	UP	MRP	IDLE POWER	ALTITUDE

DEFINITIONS:

LOW: 2000 - 4000 FT MSL MEDIUM: 8000 - 10,000 FT MSL

HIGH: 12,000 - 14,000 FT MSL PLF: Power for level flight

MRP: Maximum recommended power

12. MANEUVERING STABILITY: Longitudinal Maneuvering Stability was measured at each center of gravity position tested using the following trim conditions:

CONDITION	GEAR	FLAPS	POWER	TRIM SPEED
Cruise	Up	Up	PLF	130 KIAS
Power Approach	Down	30°	3°APP	70 KIAS

The test method was the steady pull up or push over method with the range of normal accelerations being from 0 - 2G's. Data points were obtained in approximately 0.25G increments with the following data being recorded:

1. At the trim condition:

- (a) Trim Condition
- (b) Power Setting

- (c) Pressure Altitude
- (d) Stabilizer Position
- (e) Elevator Position
- (f) Angle of Attack

2. At each stabilized load factor:

- (a) Load Factor
- (b) Elevator Position
- (c) Elevator Force
- (d) Angle of Attack

During the maneuvering stability phase of testing the airplane and elevator short period responses were evaluated. These tests were accomplished at the trim conditions used for maneuvering stability. Test procedure was to use a doublet input to the longitudinal control and then record the airplane response as a function of time.

The following data were recorded on magnetic tape for each trim condition and doublet input.

1. Elevator Position
2. Load Factor
3. Angle of Attack

13. APPROACH HANDLING QUALITIES EVALUATION: Approach handling qualities were evaluated at approach angles of 3° and 6°. The Tullahoma Municipal Airport Visual Approach Slope Indicator (VASI) was adjusted to obtain the desired approach angles, and the approaches were flown at the airport. A minimum of 10 approaches were evaluated at each approach angle. The trim conditions for these approaches were as follows:

<u>CONDITION</u>	<u>GEAR</u>	<u>FLAPS</u>	<u>POWER</u>	<u>TRIM SPEED</u>
Power Approach	Down	30°	3° APP.	70 KIAS
Power Approach	Down	30°	6° APP.	70 KIAS

Approaches were conducted in both smooth and turbulent air to determine the effects of turbulence.

The Aircrafts center of gravity location was a nominal one of approximately 35% M.A.C.

Data for this evaluation were collected in three ways. First, the pilot rated each approach using the Cooper-Harper pilot rating system for aircraft handling qualities. Secondly, the VASI lights and runway was filmed from the test aircraft to determine deviations from the approach path and runway centerline. Thirdly, time histories of elevator, aileron, rudder and throttle movement were obtained during the approaches to evaluate pilot workload. All three forms of data were correlated for an overall evaluation of each approach.

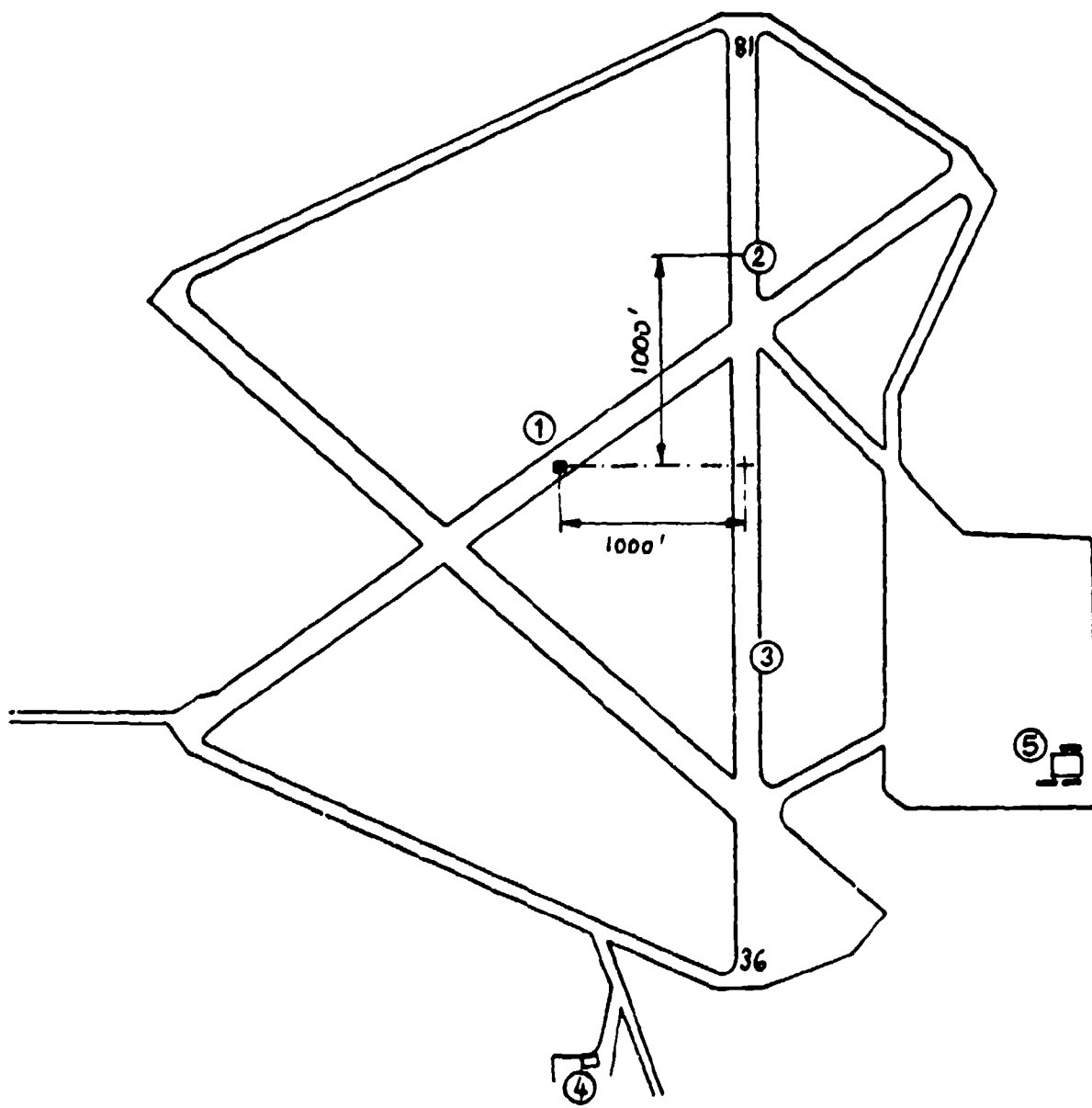
14. TAKEOFF AND LANDING TESTS: Takeoff and landing tests were conducted using a surveyed test site at the Tullahoma Municipal Airport. Figure 17 shows a sketch of that test site. Since takeoff and landing tests are quite complicated, a complete rehearsal was conducted prior to performing the actual tests.

The method of measuring the takeoff or landing distances consisted of two elements, ground roll distance and air distance. Ground roll distance was measured by an instrument installed on the test aircraft which counted revolutions of the landing gear tire. As a backup method, the point of liftoff or touch down, on the runway was marked by a runway observer and the ground roll distance measured. The air distance was determined by use of a simple theodolite located 1000 feet from the runway centerline. By tracking the aircraft on the theodolite it was possible to determine at what distance down the runway the aircraft passed through the 50 foot obstacle height. By knowing this point, the ground roll distance, and the start (or stop) point for the takeoff (or landing) run it was possible to calculate the air distance. A description of the theodolite and other instrumentation used for these tests is included in the instrumentation section of this report.

In addition to the pilot of the test aircraft, the following other personnel were required for the tests:

1. Theodolite Operator
2. Data Recorder (Theodolite)
3. Takeoff Runway Observer
4. Liftoff or Touchdown Runway Observer
5. Landing Runway Observer
6. Tower Observer

The theodolite operator was responsible for tracking the aircraft and determining the distance down the runway at which the aircraft passed through 50 feet of altitude. He was also responsible for measuring the time required for the total run (brake release to 50 ft. altitude, or 50 ft altitude to full stop).



- ① Theodolite Site and Radio (2 Observers)
- ② Take-Off Observer
- ③ Landing Observer
- ④ Tower Observer
- ⑤ UTSI Flight Operations Facilities

FIGURE 17 SKETCH OF TAKE-OFF AND LANDING TEST SITE

The data recorder, who was located at the theodolite site, was responsible for recording the data obtained by the theodolite operator and the pilot in the test aircraft. The pilots data were communicated to him via radio. In addition, he was responsible to communicate to the pilot any discrepancies in getting the takeoff or landing event within the limited range of the theodolite. Data recorded by this individual included:

1. Total distance to or from the 50 foot altitude in feet.
2. Time in seconds required for the total event listed in Item 1.
3. Ground roll distance (from pilot)
4. Liftoff or touchdown airspeed (from Pilot)
5. Climb or Approach airspeed (from Pilot)
6. Engine Power Setting for the event (from Pilot)

The takeoff runway observer was responsible for assisting the pilot in lining the aircraft up at the start point. In addition, he recorded the following data:

1. Wind direction and velocity at 6 ft. altitude for both takeoff and landing runs.
2. Outside air temperature at 6 ft. altitude for both takeoff and landing runs.
3. Time in seconds from brake release to liftoff for takeoff runs.

The liftoff or touchdown observers duties were to observe, mark and record the point on the runway where the aircraft lifted off or touched down. Since the information gathered by this observer was only backup information, he was used only when sufficient manpower was available.

The landing runway observer was responsible for inspection of the aircraft at the end of each landing run and for collecting the following data:

1. Distance down the runway at which the aircraft came to a complete stop.
2. Time in seconds from touchdown to complete stop.

The tower observer, located in a tower near the runway, collected the following data on atmospheric conditions at an altitude of 50 feet:

1. Wind direction and velocity at 50 feet.
2. Outside air temperature at 50 feet.

These data were collected during each test run.

In addition, to collecting and transmitting (to the data recorder) the data previously given, the pilot was also responsible for transmitting to the data recorder the time of brake release on takeoff, and when the aircraft came to a complete stop on landing. This was done so that the total time for the events might be obtained.

Aircraft configurations, speeds, and power settings used for the tests were as follows:

TAKEOFF

1. Gear Down, Flaps 15°
2. Power Setting - 95% N_1
3. Liftoff Speed - 60 - 65 KIAS
4. Climb Speed - 70 KIAS (target)

LANDING

1. Gear Down, Flaps 30°
2. Power Setting - 74% N_1
3. Approach Speed - 70 KIAS (target)
4. Touchdown Speed - 65 - 55 KIAS
5. Thrust Reverser - Deployed after touchdown
6. Braking - Maximum after touchdown

The takeoff weight and center of gravity for these tests was 3608 lb. at 35.5% M.A.C. The aircraft was refueled after a maximum of three test runs in order to keep weight and center of gravity excursions small.

Since takeoff and landing tests are prone to have large data scatter due to pilot technique, sufficient number of runs were made in order to have a reasonable statistical sample. Thrust reversing was used on each run since the thrust reverser is an integral part of the Jetwing concept.

15. LASER VELOCIMETER THRUST MEASUREMENT: In addition to the thrust measurement described previously, data were taken with a laser velocimeter to measure the velocities of the engine inlet and exhaust air during static ground runs. In addition to the inlet and exhaust velocities other data recorded during these test runs included:

1. Ambient air temperature
2. Wind direction and velocity
3. Engine main rotor speed (N_1)

4. Engine gas generator rotor speed (N_2)
5. Fuel Flow
6. Cold Duct differential pressure ($P_{t5} - P_a$)
7. Hot duct differential pressure ($P_{t5} - P_a$)
8. Interstage turbine temperature (ITT)
9. Pressure altitude

The first series of tests were conducted with the upper wing removed. Test runs were made at 40, 55, and 70% N_1 . These runs were later repeated with the upper wing installed to determine if there was any thrust augmentation due to the ejector. In addition to the inlet and exhaust nozzles, velocity profiles were made at several other locations during the runs to determine how the ambient air and ejector air were mixing with the exhaust flows from the nozzles.

A majority of the measurements were made on the right wing. However, a limited number of measurements were made on the left wing to verify that the flows from the right and left nozzles were symmetrical. These runs were only conducted at 55% N_1 .

During each test run velocity measurements were made at the following locations:

1. Engine Inlet - One vertical and one horizontal profile through the center of the inlet plane at each test power setting as shown in Figure 18.
2. Exhaust Duct Exit Nozzles - One spanwise profile through the centerline of the nozzle, was taken along both hot and cold nozzles of the right wing as shown in Figure 19. This measurement was repeated on the left wing at 55% N_1 .
3. Exhaust Duct Exit Nozzles - Vertical profiles of velocity were taken at the three nozzle locations on the right wing as is shown in Figure 20.
4. On Upper Surface of Right Wing - Vertical profiles of velocity were taken at three chordwise locations on the wing. This was done at one spanwise location for both hot and cold ducts as shown in Figure 21. These measurements were repeated with the upper wing installed.

Velocity readings were taken at one inch intervals for item 1, at two inch intervals for item 2, and at 1/8 to 1/4 inch intervals for items 3 and 4. While velocity readings were being taken, other test data were collected at five minute intervals. When possible, tests were conducted in no wind conditions, and were stopped when the wind speeds exceeded 10 mph. In addition, testing in direct headwinds or tailwinds was avoided.

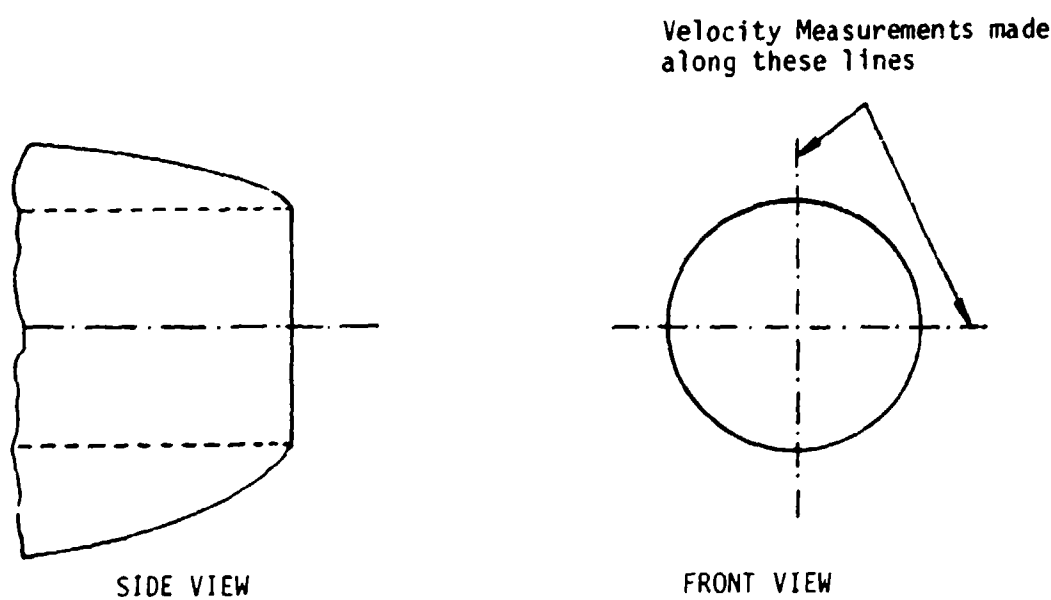


FIGURE 18

SKETCH OF ENGINE INLET SHOWING
LOCATION OF VELOCITY MEASUREMENTS

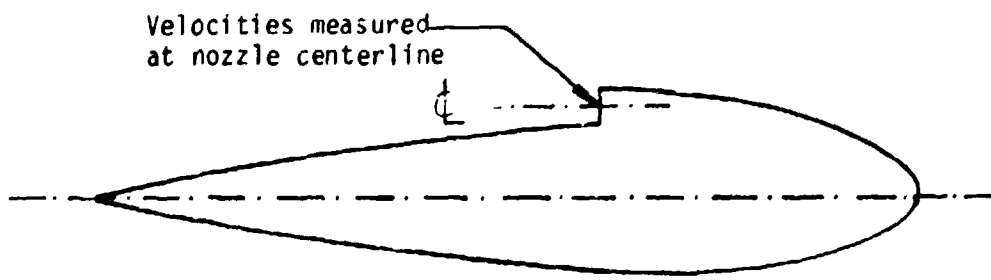
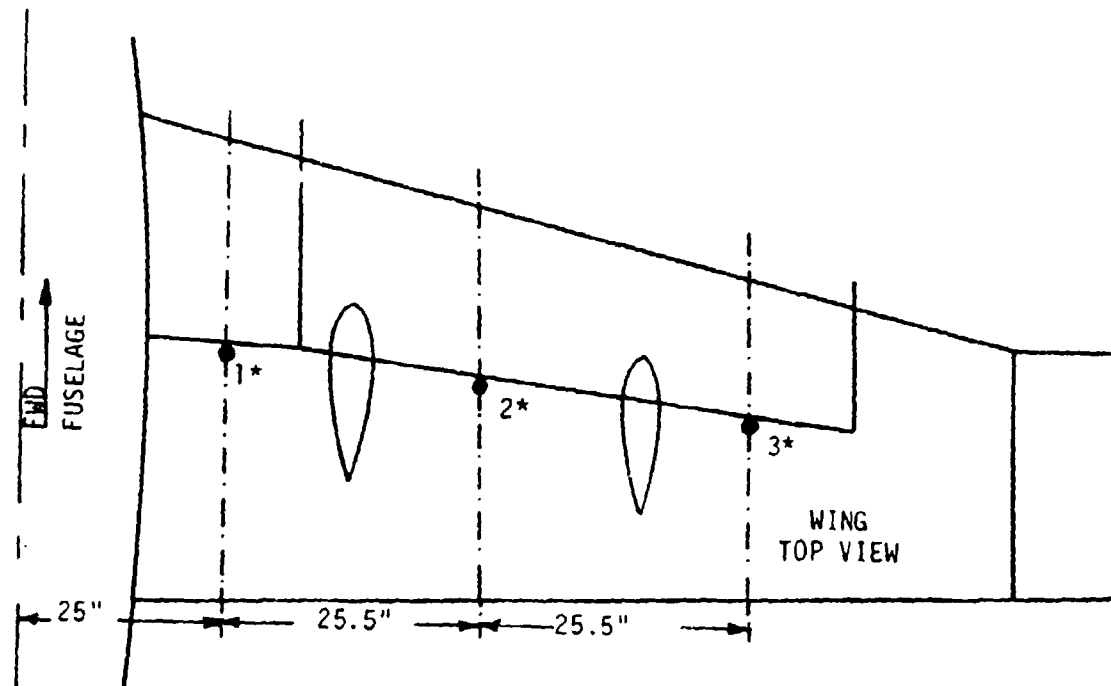


FIG 19

SKETCH OF WING PROFILE AND EXHAUST
NOZZLE SHOWING LOCATION OF VELOCITY
MEASUREMENTS



*SPANWISE LOCATIONS FOR VERTICAL PROFILES

FIGURE 20

SKETCH OF RIGHT WING SHOWING LOCATION OF POINTS
POINTS ON THE NOZZLE WHERE VERTICAL PROFILES OF
VELOCITY WERE TAKEN

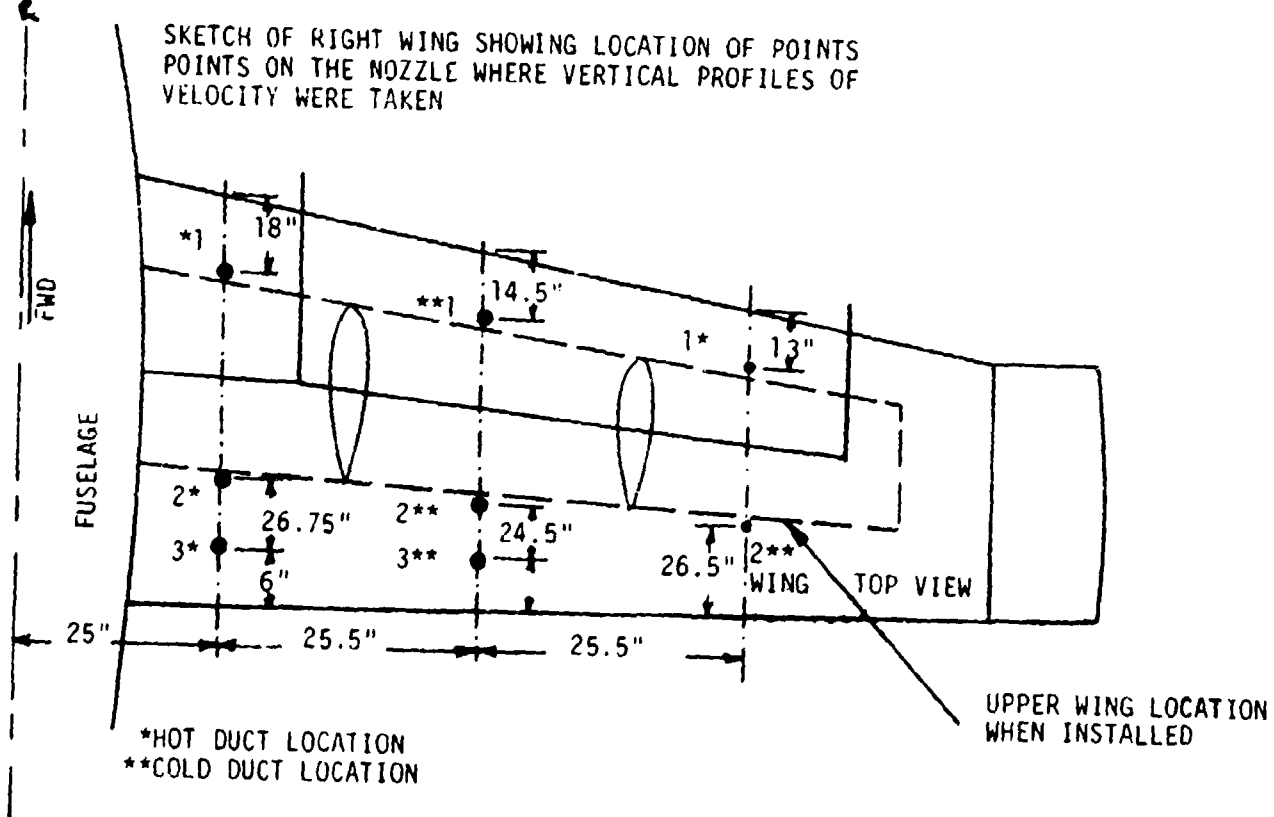


FIGURE 21

SKETCH OF RIGHT WING SHOWING CHORDWISE AND
SPANWISE LOCATION OF VERTICAL VELOCITY
PROFILES

SECTION V

INSTRUMENTATION

As was discussed previously under test procedures, the type and design of instrumentation installed in the test aircraft was constrained by its size, weight and location in the aircraft. The type and design of all test instrumentation was constrained by the program budget. These constraints led to simple and reliable instrumentation approaches. Although some loss of accuracy is incurred by taking simple instrumentation approaches, the payoff was that data were lost on only four flights, due to instrumentation failure, in a 90 flight test program.

The types of instrumentation required for this program may be placed in groups which relate to the type of data being collected. These groups of instrumentation are:

1. Air Data Instrumentation
2. Engine Thrust Instrumentation
3. Stability and Control Instrumentation
4. Takeoff and Landing Instrumentation
5. Laser Velocimeter Instrumentation

1. AIR DATA INSTRUMENTATION. The instrumentation installed on the test aircraft which collected air data included:

1. Sensitive Airspeed Indicator calibrated in knots.
2. Sensitive Altimeter calibrated in feet.
3. Ambient Air Temperature Gauge calibrated in degrees Centigrade.

The airspeed indicator and altimeter were panel mounted as shown in Figure 22 and connected to a wingtip mounted, swivel pitot static boom shown in Figure 23. These instruments were calibrated through the airspeed and altitude ranges of interest using water and mercury manometers with traceability to the National Bureau of Standards (NBS).

The ambient air temperature gauge was calibrated from 0-40°C in a water bath using a laboratory thermometer which was also traceable to NBS.

Similar calibrated instrumentation was installed on the Cessna 310 and DHC-3 Otter which were used as pace aircraft during the Airspeed Calibration portion of the flight test program.



FIGURE 22
PICTURE OF PILOTS INSTRUMENT PANEL SHOWING
AIR DATA AND ENGINE THRUST INSTRUMENTATION



FIGURE 23 FULL SWIVEL PITOT-STATIC BOOM

2. ENGINE THRUST INSTRUMENTATION. Instrumentation installed in the test aircraft which gave an indication of engine thrust included:

1. Main Rotor Speed Tachometer (N_1) calibrated in percent RPM.
2. Gas Generator Speed Tachometer (N_2) calibrated in percent RPM.
3. Interstage Turbine Temperature gauge (ITT) calibrated in °F.
4. Pressure Gauge calibrated in inches H_2O which measured the differential pressure between the total pressure in the hot or cold duct and the outside ambient static pressure. This was a single gauge which operated through a pressure switch in order to read hot or cold duct differential pressure.
5. SDI Huskins Fuel Flow and Fuel Quantity Instrumentation which consists of two panel mounted instruments which contain an integral computer. Fuel flow calibration is in either gallons or pounds per hour.

All of the engine instrumentation and air data instrumentation was panel mounted for visual readout by the pilot as is shown in figure 22.

All of the engine instrumentation listed above except for the fuel flow instrumentation was calibrated using standards traceable to NBS. The fuel flow instrumentation was calibrated at the manufacturer and guaranteed to maintain two percent accuracy in normal use. Periodic spot checks during the test program confirmed this level of accuracy.

In addition to the engine related thrust instrumentation one other piece of instrumentation was required during the thrust calibration. This instrument, A Dillon Dynamometer is shown in figure 24 as it was installed in the thrust measuring apparatus. This instrument readout in pounds of force and has received a traceable calibration by its manufacturer.

3. STABILITY AND CONTROL INSTRUMENTATION. The instrumentation required in the test aircraft for stability and control testing consisted of:

1. Control Force Instrumentation
2. Control Surface Position Instrumentation
3. Angle of Attack Instrumentation
4. Angle of Sideslip Instrumentation
5. Accelerometer for Normal Acceleration
6. Vertical Gyro for Pitch and Bank Angle
7. Rate Gyro's for Pitch, Roll, and Yaw Rates



FIGURE 24
PICTURE OF DILLON DYNAMOMETER AS INSTALLED
IN THRUST MEASURING APPARATUS

Aileron and elevator control forces were obtained by use of a hand held force gauge (AMES GAUGE). Rudder forces were obtained from load cells mounted on the rudder pedals. These load cells were connected electrically, through a rotary switch, to a milliammeter which could be read by the pilot (See Figure 25). Control force instruments were calibrated by measuring the force created by standard weights of various sizes.

Control surface position information was obtained by attaching linear potentiometers to the control surface or control pushrods as shown in Figure 26a, b, c and d. These potentiometers were also connected to the milliammeter of Figure 25. Calibration of these instruments was accomplished by measuring control surface deflection angles and obtaining corresponding milliammeter readings.

Angle of attack and angle of sideslip information was obtained from the sensors shown in Figure 27. The angle of attack and sideslip vanes drive rotary potentiometers which are also connected electrically through the 12 position rotary switch to the milliammeter of Figure 25. Calibration was accomplished in a manner similar to the control surface position instrumentation. Zero reference was the aircraft waterline for angle of attack and the aircraft centerline for angle of sideslip.

An accelerometer with a range of 0-5G was installed so as to be located at a nominal aircraft center of gravity. The output of this accelerometer could also be read out on the milliammeter. In addition, the pilot also had available a panel mounted accelerometer which could be used as a reference.

A vertical gyro mounted, near the center of gravity, above the exhaust ducting, as shown in Figure 28, was used to determine pitch and bank angles. Prior to installation this device was calibrated with the instrumentation package on a calibration bench. This device was also wired to provide a visual readout through the milliammeter.

Rate gyros for the determination of pitch, roll, and yaw rates were mounted at the aircraft's nominal center of gravity position in the manner shown in Figure 29. These gyros were also bench calibrated with the instrumentation package. Readout of the output of these instruments was also through the milliammeter.

All instrument readings which could be displayed on the milliammeter could also be recorded, three at a time versus a time base, on a cassette magnetic tape recorder. These data could then be played back on an oscilloscope or strip recorder after the flight. The cassette recorder was located just aft of the pilot's seat.

Before being displayed on the milliammeter or recorded on the cassette recorder all data signals were amplified and conditioned in an instrumentation amplifier and signal conditioner located near the vertical gyro as is shown in Figure 30. Power for the electrical instrumentation was controlled through an instrumentation master switch located next to the rotary selector switch.



FIGURE 25

MILLIAMMETER USED FOR READOUT OF STABILITY
AND CONTROL PARAMETERS (CENTER)



FIGURE 26 a

ELEVATOR POSITION POTENTIOMETER (A1010)
ATTACHED TO ELEVATOR PUSHROD IN AIRCRAFT FUSELAGE

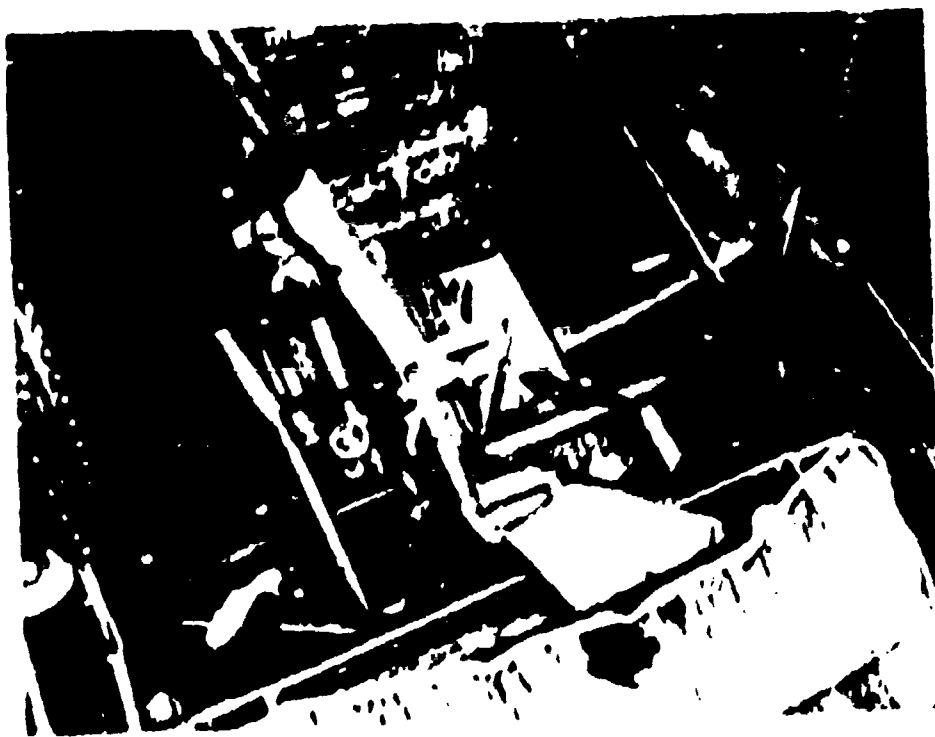


FIGURE 26 b

ELEVATOR POSITION POTENTIOMETER (A1010)
ATTACHED TO BOTTOM OF CONTROL STICK



FIGURE 26 C

RUDDER POSITION POTENTIOMETER (ARROW)
ATTACHED TO RUDDER CONTROL CABLE IN
AFT FUSELAGE

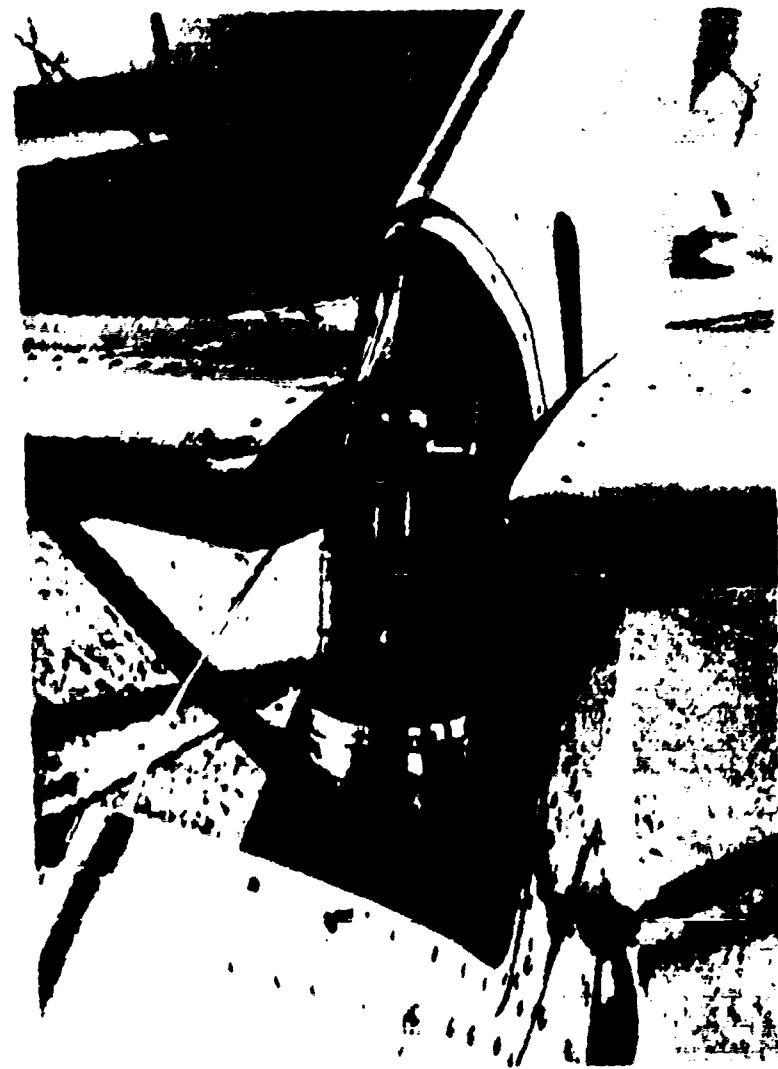


FIGURE 26 d

STABILIZER POSITION POTENTIOMETER (ARROW)
ATTACHED TO STABILIZER FRONT SPAR

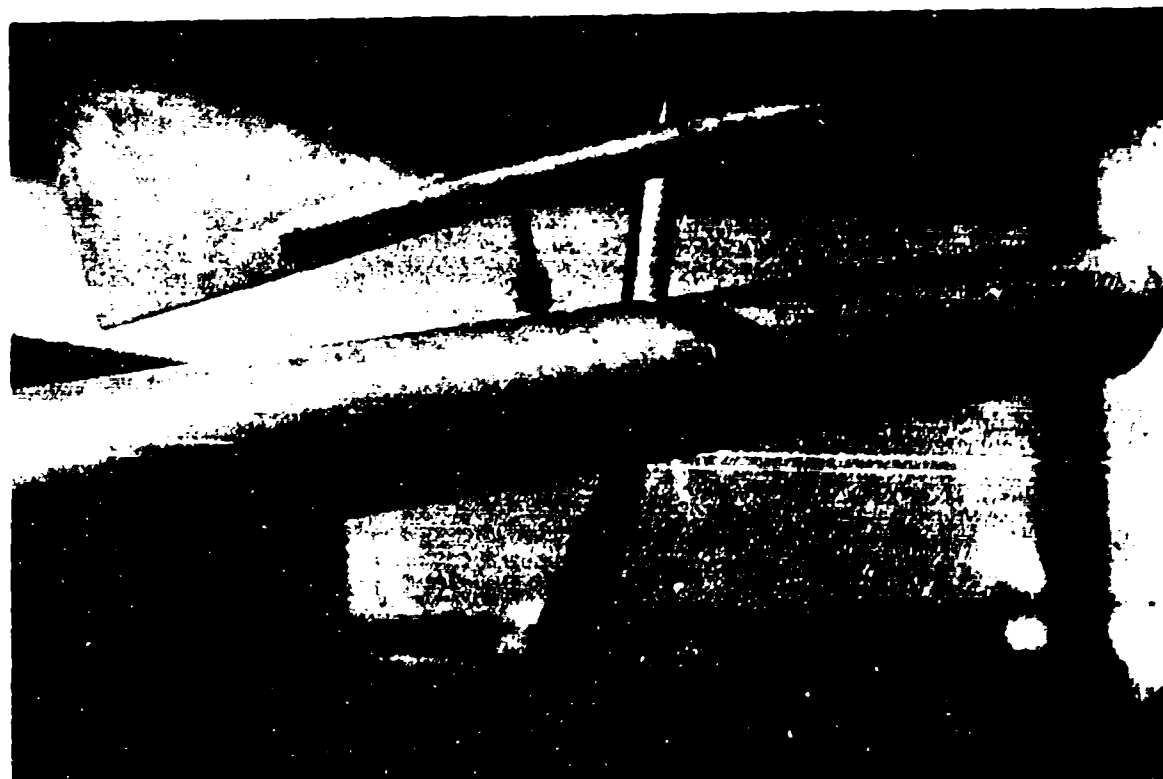


FIGURE 27

WINGTIP BOOM WITH ANGLE OF ATTACK AND SIDESLIP SENSORS
MOUNTED ON RIGHT WING TIP 52 INCHES FORWARD OF THE
WING LEADING EDGE

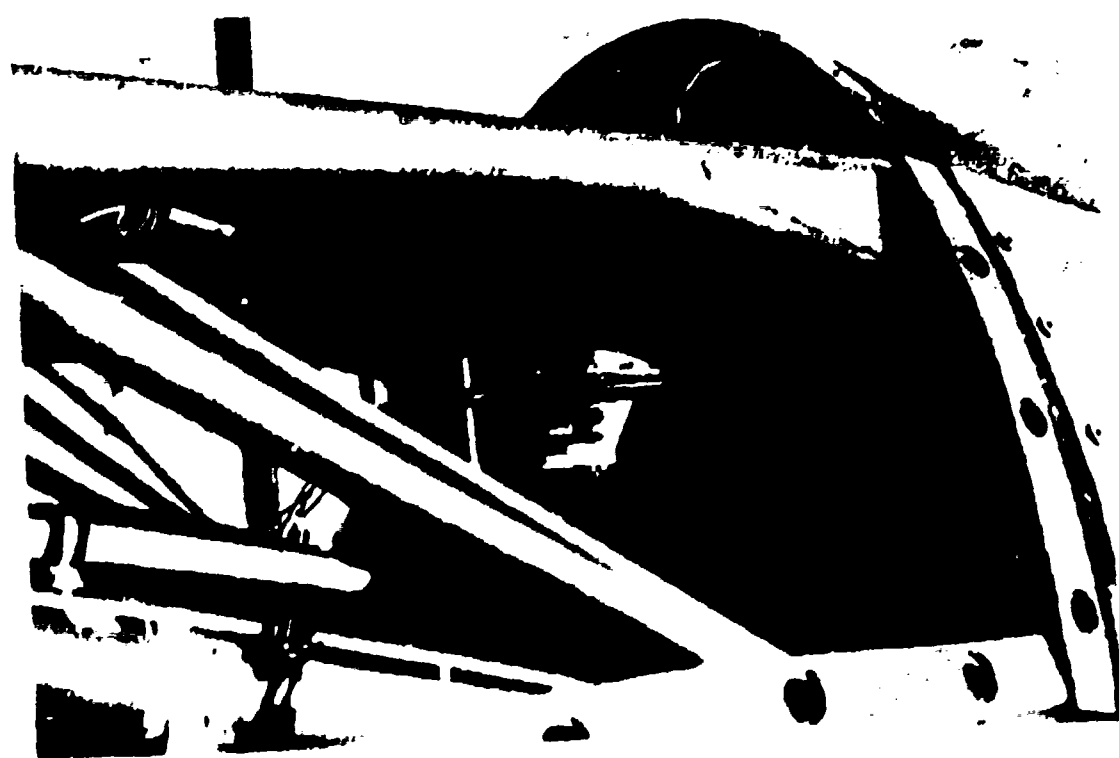


FIGURE 28

MECHANICAL ARRANGEMENT OF VERTICAL GYRO

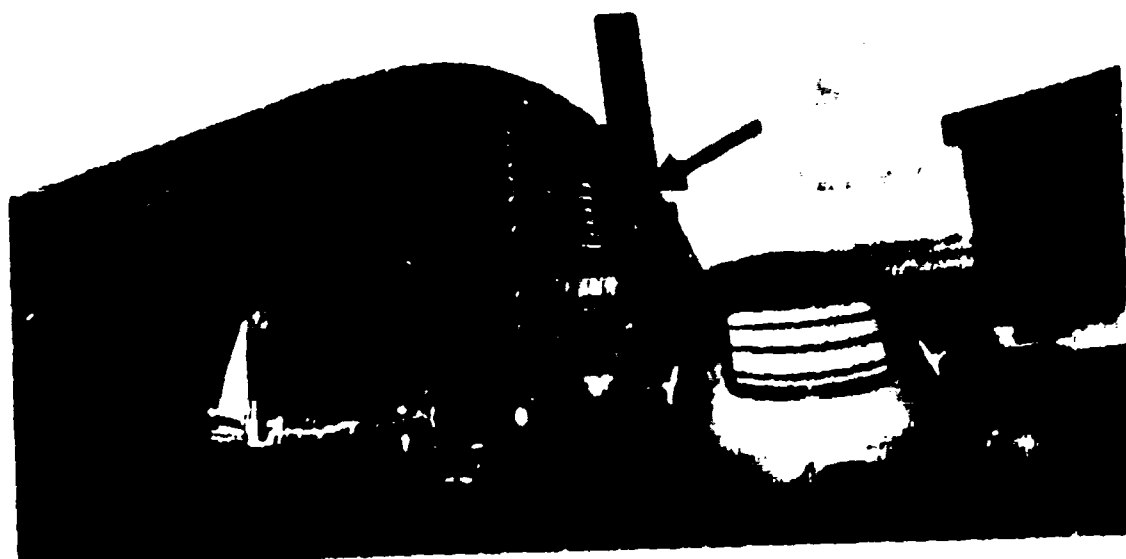


FIGURE 29

MECHANICAL ARRANGEMENT OF THE VERTICAL GYRO
WITH POWER SUPPLY (ARROW)

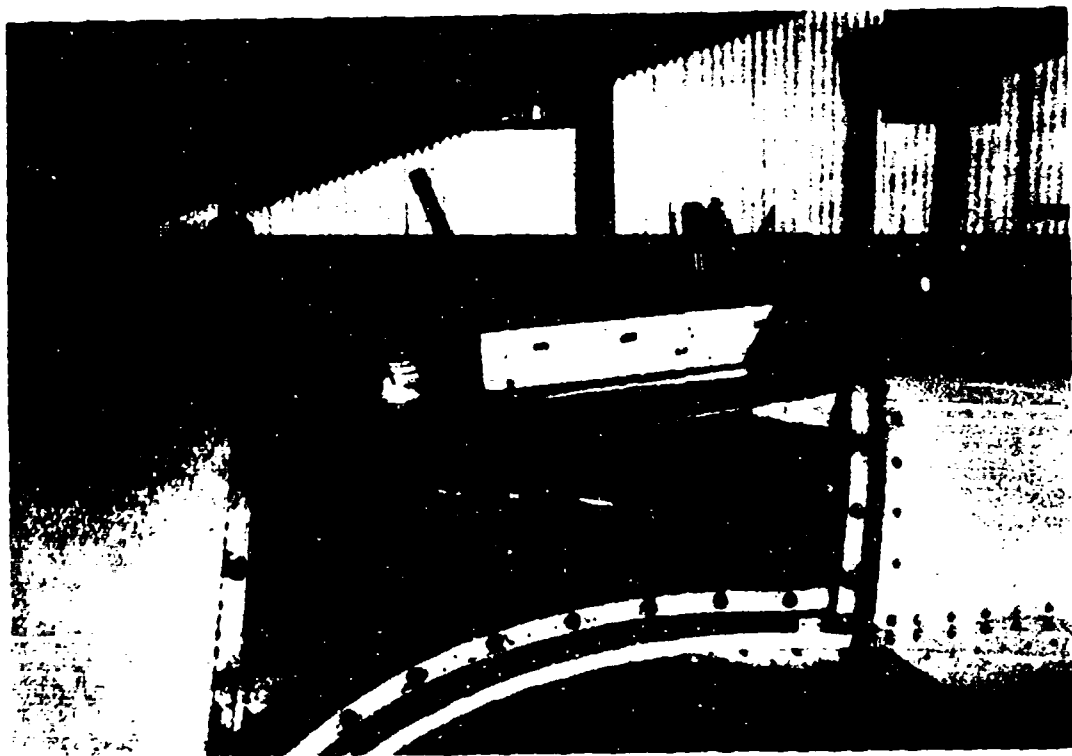


FIGURE 30
INSTRUMENTATION AMPLIFIER AND SIGNAL CONDITIONER (ARROW)

4. TAKEOFF AND LANDING INSTRUMENTATION. Takeoff and landing instrumentation consisted of three types:

1. Onboard Aircraft Instrumentation
2. Distance and Height Measuring Instrumentation
3. Instrumentation for atmospheric measurements

The onboard aircraft instrumentation included the air data and engine thrust instrumentation mentioned previously plus the Liftoff and Landing Distance Indicator TM shown in Figure 31. This instrument measures ground roll distance by counting revolutions of one of the main landing gear tires by means of a magnetic pickup mounted near the brake drum. This pickup senses the magnetic disturbance of small holes drilled in the brake drum. By having the size of the wheel in its program, the Liftoff and Landing Distance Indicator TM may then calculate the ground roll distance. Special circuitry is provided in the indicator to detect when the wheel rotation stops accelerating at liftoff. When the wheel stops accelerating the counter stops counting.

Distance and height measuring instrumentation consisted of the simple theodolite shown being operated in Figure 32. This device was located at a surveyed site 1000 feet from the runway centerline. By sighting through the eyepiece and aligning the bottom of the two height strings on the runway by adjusting the board, the top string then indicates a 50 foot height above the runway. By tracking the aircraft with a pointer (which could be moved horizontally with a hand crank) and stopping the pointer at the point where the aircraft passed through 50 feet, it was possible to determine the horizontal distance the aircraft required to clear a 50 foot height. This was accomplished by reading the distance value to which the pointer pointed on a scale located on the theodolite. The distance scale has previously been obtained by observing the measurement of actual distance on the runway through the instrument and marking those distances on the scale. Figure 33 shows the height strings and horizontal distance pointer.

Atmospheric measurements were made with the instruments shown in Figure 34. These consisted of a laboratory thermometer, a hand held wind direction indicator, and a hand held wind speed indicator as shown from left to right in the figure.

5. LASER VELOCIMETER INSTRUMENTATION. For the Laser Velocimeter thrust measurement the following instrumentation was used:

1. Air Data instrumentation
2. Engine Thrust Instrumentation
3. UTSI 2D Laser Velocimeter and Afocal Scan System

The Air Data Instrumentation and Engine Thrust Instrumentation have been previously described.



FIGURE 31

LIFTOFF AND LANDING DISTANCE INDICATOR
SHOWN MOUNTED IN JETWING COCKPIT. (CENTER)

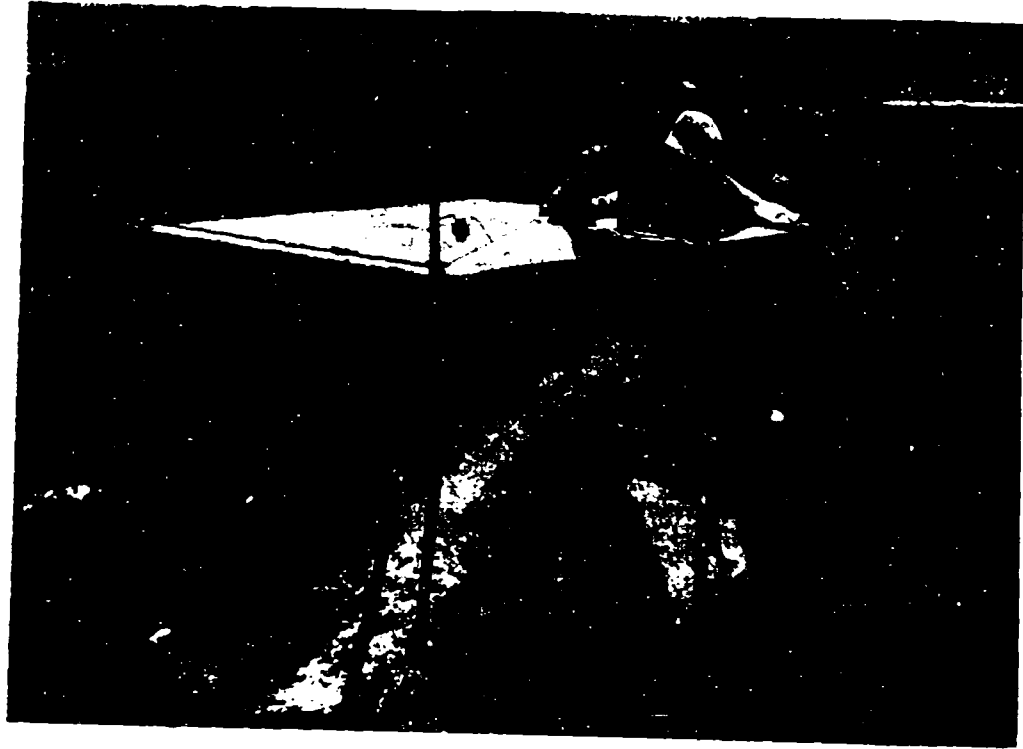


FIGURE 32

TAKEOFF AND LANDING DISTANCE AND HEIGHT
MEASURING THEODOLITE WITH OPERATOR



FIGURE 33

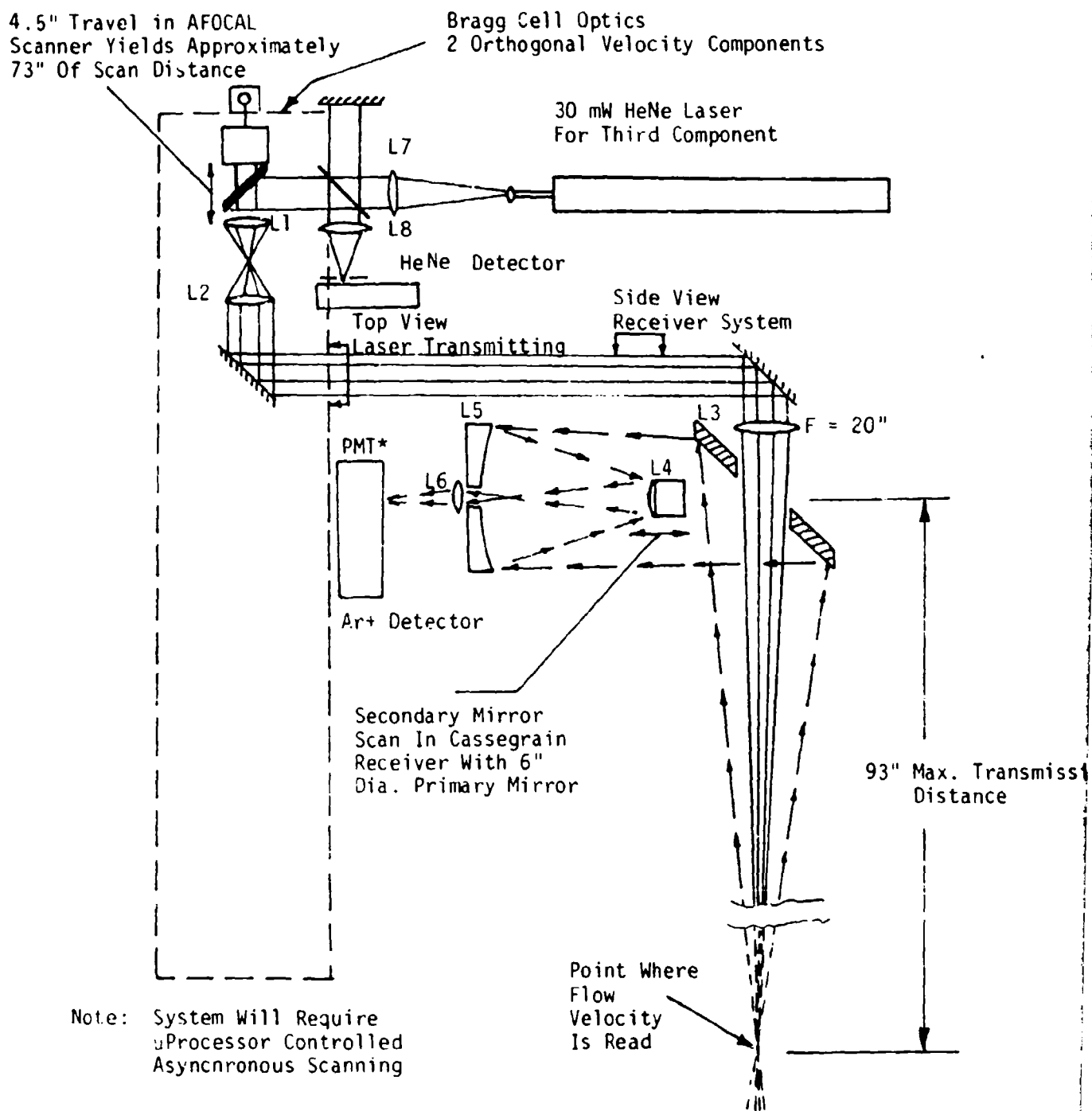
HEIGHT STRINGS (SHORT ARROW) AND HORIZONTAL DISTANCE POINTER
(LONG ARROW) OF TAKEOFF AND LANDING DISTANCE THEODOLITE



FIGURE 34

LABORATORY THERMOMETER, HAND HELD WIND DIRECTION INDICATOR,
AND HAND HELD WIND SPEED INDICATOR USED FOR TAKEOFF AND
LANDING TESTS

The UTSI 2D Laser Velocimeter and Afocal Scan System is an in house developed Laser Doppler Velocimeter. It is capable of measuring particle velocities and turbulent correlations up to 2 km/sec. A schematic diagram of the system is shown in Figure 35. Flow velocities are measured by the device by its measuring the Doppler phase shift in the frequency of light fringes reflected from microscopic particles in the flow which pass through the point where the two beams of laser light cross. The system is capable of measuring two components of velocity. However, for the tests described in this report only one component of velocity was measured. For these tests the system shown in Figure 35 was mounted upon a milling machine bed so that accurate pointing of the laser could be accomplished. This arrangement is shown in Figure 36.



UTSC AFOCAL SCAN SYSTEM

FIGURE 35

SCHEMATIC DIAGRAM OF UTSC AFOCAL SCAN LASER VELOCIMETER SYSTEM

* Photo Multiplier Tube

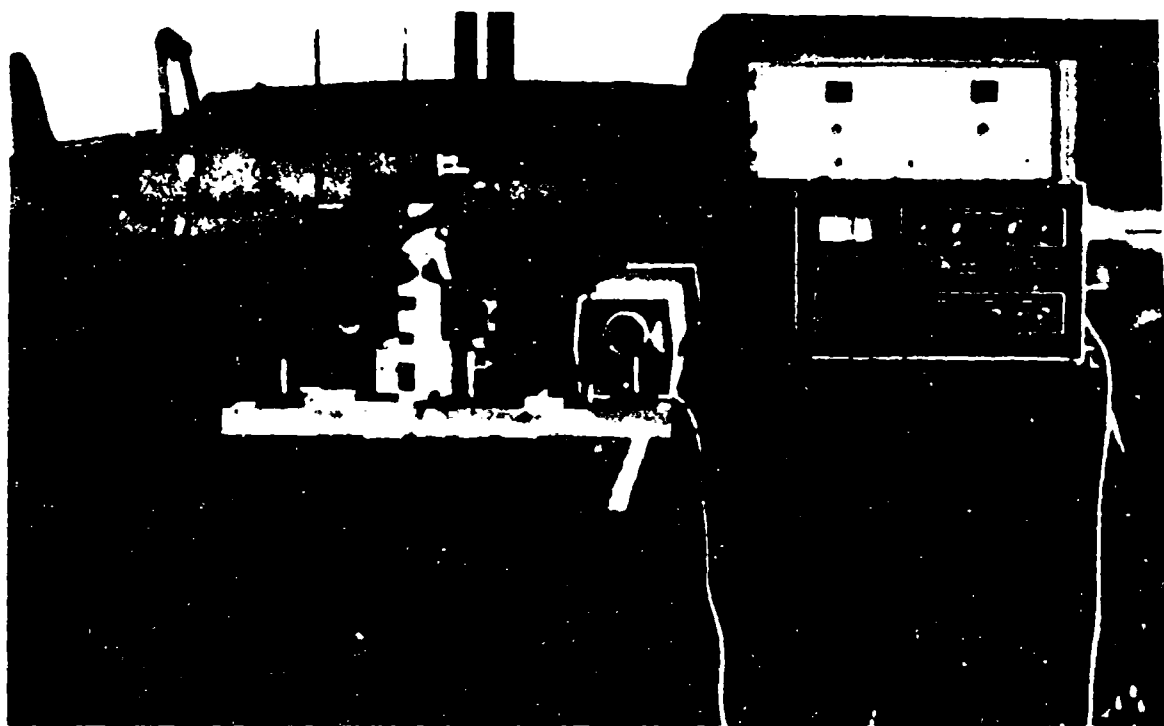


FIGURE 36
LASER VELOCIMETER TEST SETUP

SECTION VI

RESULTS AND DISCUSSION

1. FAMILIARIZATION FLYING. A total of six familiarization flights were flown for a total of 2 hours and 55 minutes flying time. Flight durations were kept to 30 minutes or less in order to be back in the traffic pattern with at least one half of the fuel remaining. These flights confirmed reports from the Ball-Bartoe Company flight tests that the airplane was unstable longitudinally in all configurations. The best configuration with regard to longitudinal stability was power approach with 30° flap extension and gear down.

Landings were attempted using flap settings of 15° to 30°, and approach speeds from 65 to 90 knots indicated airspeed (KIAS). Power settings for these varied between 76% N₁ and 68% N₁ with the higher settings corresponding to the lower airspeeds. The airplane was found to be quite difficult to land. The longitudinal instability, coupled with a "tail wheel" landing gear, and the forward center of pressure shift of a powered lift wing in ground effect combine to make some unconventional landing characteristics. For instance, if the power setting is only a few percent above idle, the main gear will not remain on the runway during landing. However, the longitudinal instability, and the wing forward center of pressure shift in ground effect, make it quite easy to get the tail down. As a result, it is possible to have the airplane going down the runway with the tailwheel on the ground and the main gear two to six feet in the air. If wheel landings are attempted, the stiffness of the main landing gear oleo make the airplane easy to bounce. This tendency coupled with the other landing problems make the airplane difficult to land. These problems with landing appear to be more of a problem with the configuration and design of the Jetwing research airplane than with the Jetwing powered lift concept. It is the opinion of the test pilot that most of these problems would disappear if the aircraft has a tricycle landing gear with large oleo deflection, and more positive longitudinal stability.

Other flight characteristics, including power effects, were found to be easy to adapt to in spite of the test pilot's lack of experience with powered lift aircraft.

Ground handling was found to be very good with no tendency to ground loop.

The familiarization flying confirmed the decision to use the sawtooth climb method for performance testing rather than the level acceleration method. The level acceleration method proved to be much more difficult to fly than sawtooth climb method primarily because of the aircraft's longitudinal instability.

2. AIRSPEED CALIBRATION. The airspeed calibration required 10 flights for a total of 6 hours and 40 minutes of flying time. The calibration was accomplished using the pace method as discussed in Section IV. Normally, the pace method would not require so much flying time. However, in this test three flights required reflying due to leaks developing in the pitot-static system. In one instance the plastic static line touched the hot wing skin behind the engine exhaust and burned through. All pitot-static lines in this area were changed from plastic to stainless steel and the problem did not reappear. A second reason for the amount of flying time was the time consumed in obtaining stabilized formation on the pace airplane. This problem in stabilizing on the pace airplane was caused by the longitudinal instability of the test aircraft. A third problem which increased test time was the short endurance of the test aircraft. With a relatively short endurance the useable time at the test altitude is small and a great deal of time is spent climbing and descending.

The results of the airspeed calibration, plotted as total position correction (ΔV_{pc}) versus instrument corrected indicated airspeed (V_I), is shown in Figure 37 for three configurations. The scatter of data generally falls within 2% of the faired curves. Those points near 100 KIAS which exceed this value may be explained by an anomaly in the airspeed instrument of the Cessna 310 pace aircraft. The calibration of the Cessna 310's airspeed instrument shows a large friction bump at this airspeed.

Prior to the start of testing it was felt that there would be large power effects in the airspeed calibration of the Jetwing due to the wing pressure field change with change in power. As a result, the airspeed calibration test was designed to determine if these effects existed by repeating several calibration points with the landing gear in a different position from the one primarily tested. It was felt that this large change in aircraft drag would provide a power change large enough to show power effects in the calibration if such existed. In spite of the use of this procedure, power effects were not discernable in the data. Some scatter did exist between the points taken at different power settings, but this scatter was random. It did not show patterns which could be attributed to power effects.

3. THRUST CALIBRATION. Figure 38 shows the results of the static thrust calibration conducted with the upper wing removed. Plotted along with that data are results from similar calibration tests conducted in the NASA Ames Research Centers 40' x 80' wind tunnel. The NASA Ames calibration was also conducted with the upper wing removed. As may be seen from this comparison, the simple thrust calibration method used during the flight tests provides good agreement with the wind tunnel calibration data. This good correlation of data increases the confidence in data obtained by the method when the upper wing was installed. Static thrust data with the upper wing installed is shown in Figure 39. These data were used as a basis for thrust determination during the flight tests.

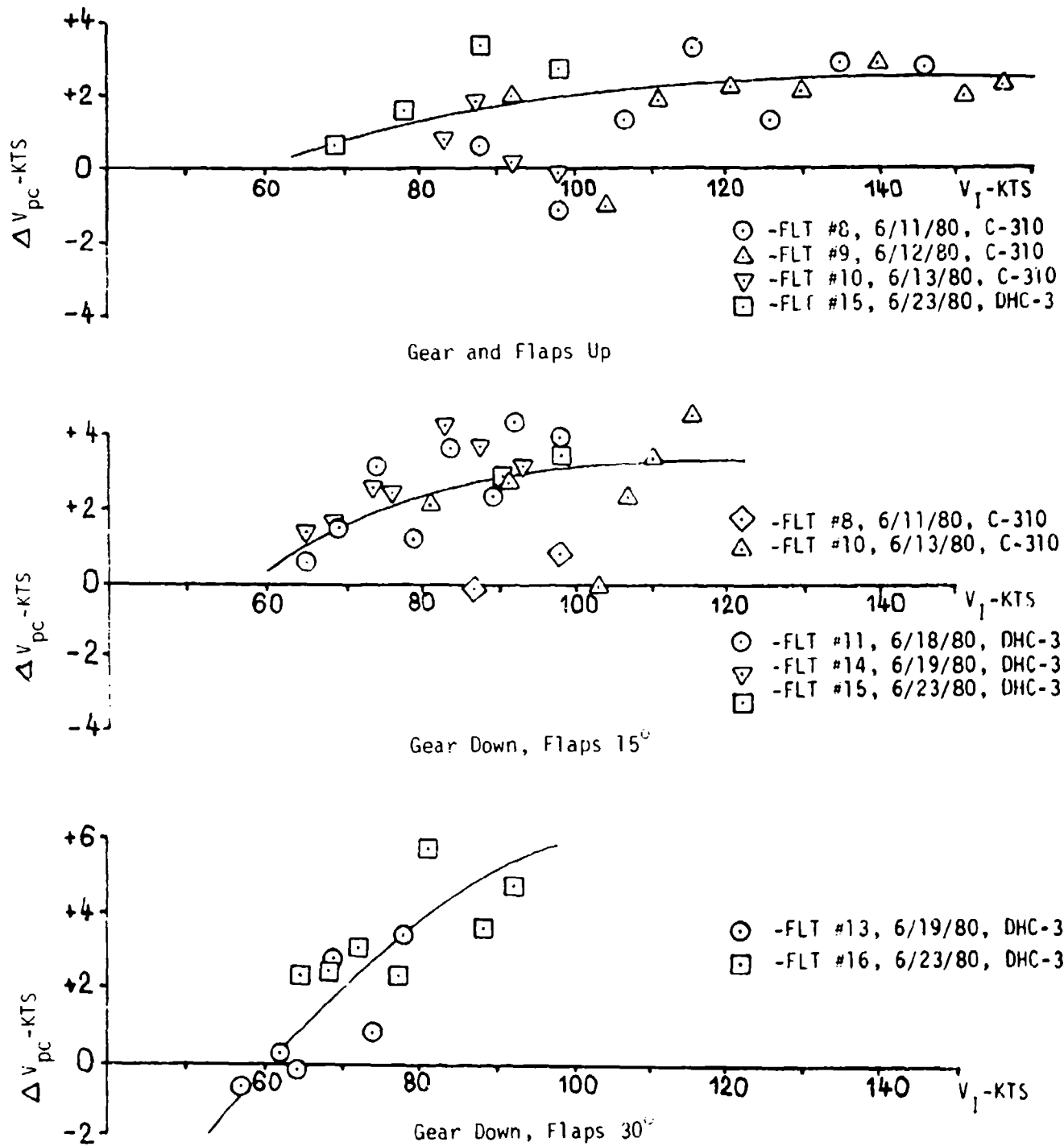


FIGURE 3/
JETWING AIRSPEED CALIBRATION

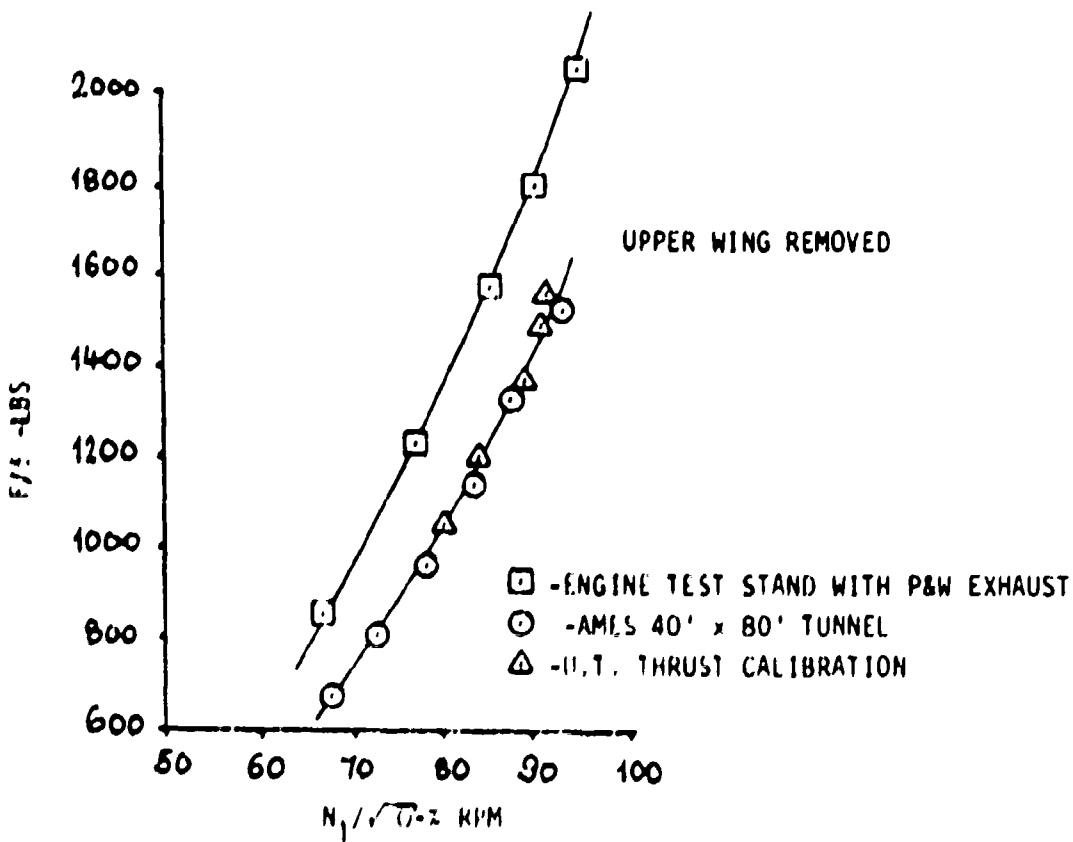


FIGURE 38

J11WING JW-1 STATIC THRUST CALIBRATION

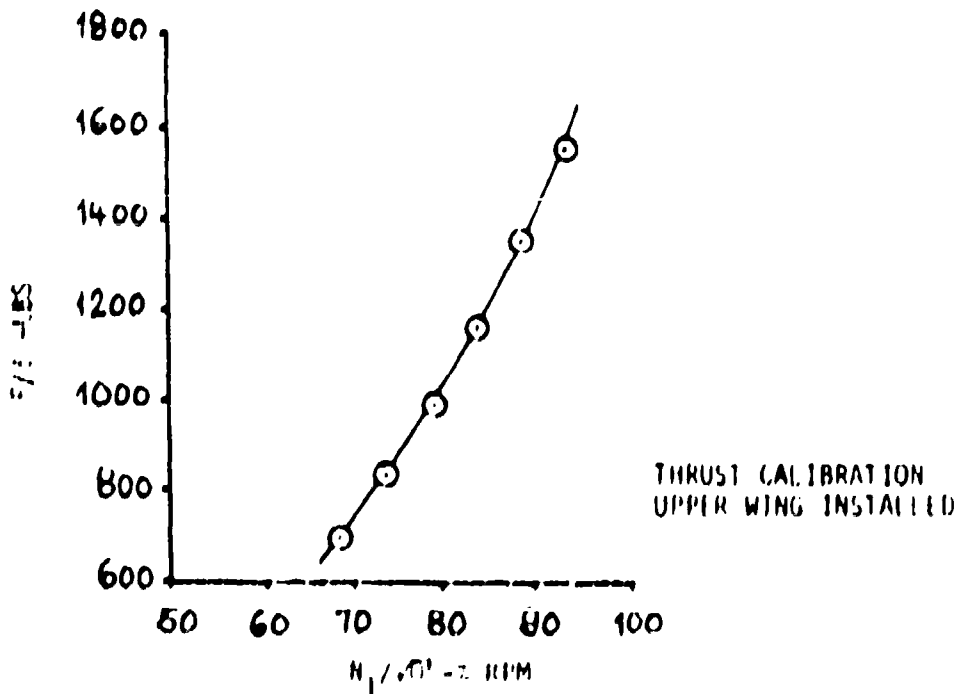


FIGURE 39

The effects of airspeed upon gross thrust were accounted for by adding thrust increments to the data shown in Figure 39. The thrust increments due to airspeed were obtained using Pratt and Whitney's engine performance computer program for the JT15D-1. The program had been modified by Pratt and Whitney to account for the Jetwings installed losses. The resultant family of curves obtained by using this approach is shown in Figure 40. As a verification for this approach inflight comparisons were made between thrust determined in this manner, and thrust determined using pressure ratios measured in the hot and cold exhaust ducts. The results of this comparison are shown in Figure 41. As may be seen from this figure reasonably good agreement exists between the two methods.

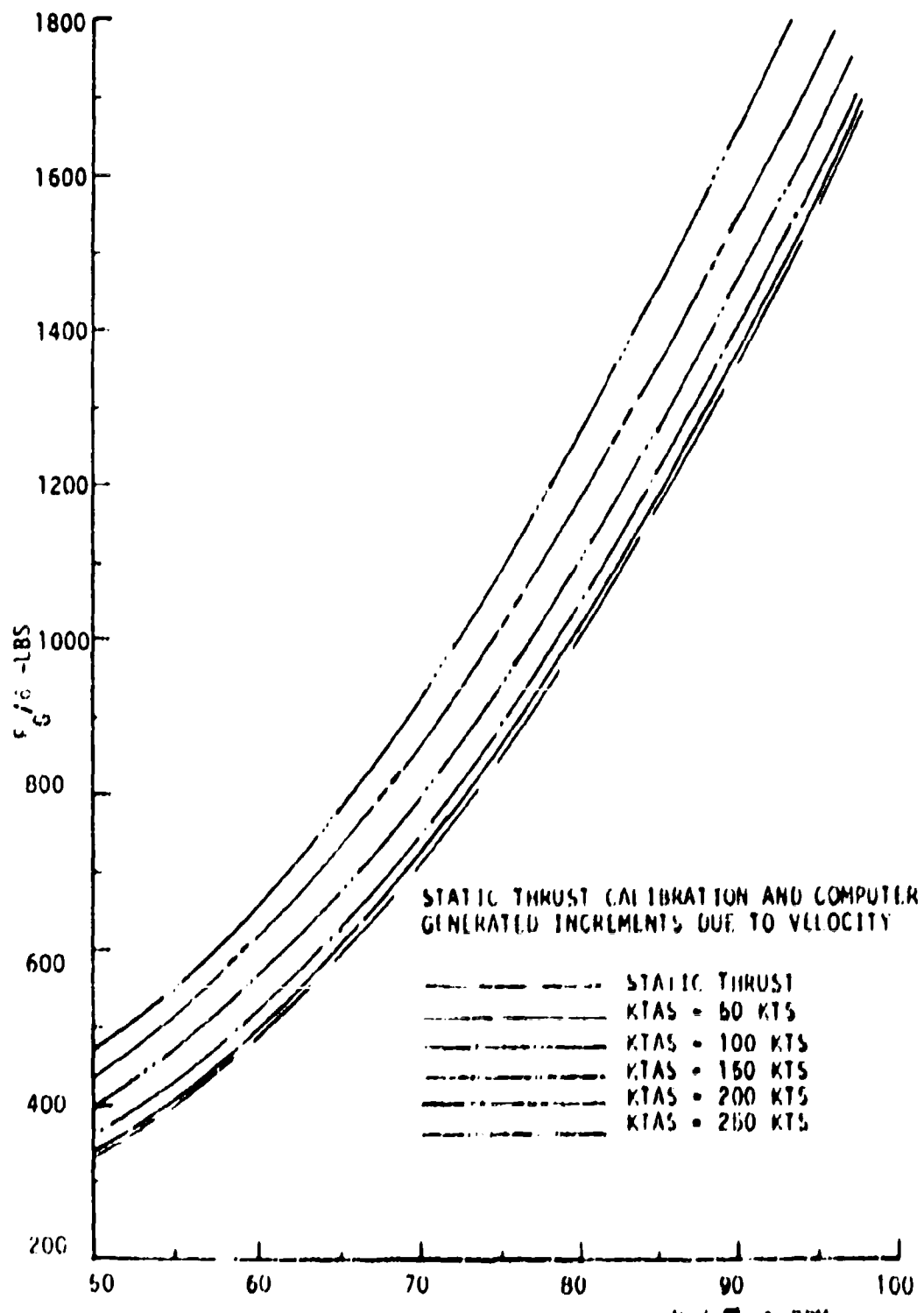
Exhaust Pressure Ratio was not used as a primary thrust reference because of considerable scatter in the pressure ratio data.

A further check on the thrust calibration was conducted late in the program using a laser velocimeter to measure exhaust velocities. Results of this check are discussed later in this report.

4. INFLIGHT PERFORMANCE. As discussed in the section on test procedures, inflight performance was determined in three configurations:

1. Gear and Flaps Up
2. Gear Down and 15° Flap Extension
3. Gear Down and 30° Flap Extension

Results of performance tests in these configurations are shown as $V-\gamma$ Maps in Figures 42, 43, and 44, and as Excess Thrust (C_{FEX}), or drag, versus lift coefficient (C_L) in Figures 45, 46, and 47. As may be seen in Figures 42, 43, and 44, the extreme low speed end of the performance envelope was not investigated. There were two reasons for not investigating the performance at these very low speeds. One reason was that a horizontal tail stall was encountered at a calibrated airspeed of 53 knots when the flaps were extended to 30° extension. The second reason was that for smaller flap deflections the longitudinal instability became quite pronounced, especially when a combination of low airspeed and high power existed. It is believed that both of these problems could be significantly reduced if the horizontal tail was redesigned. They are not considered insurmountable problems in applying the Jetwing concept to other flight vehicles. Further discussion of these problems occurs in the longitudinal stability section of this report.



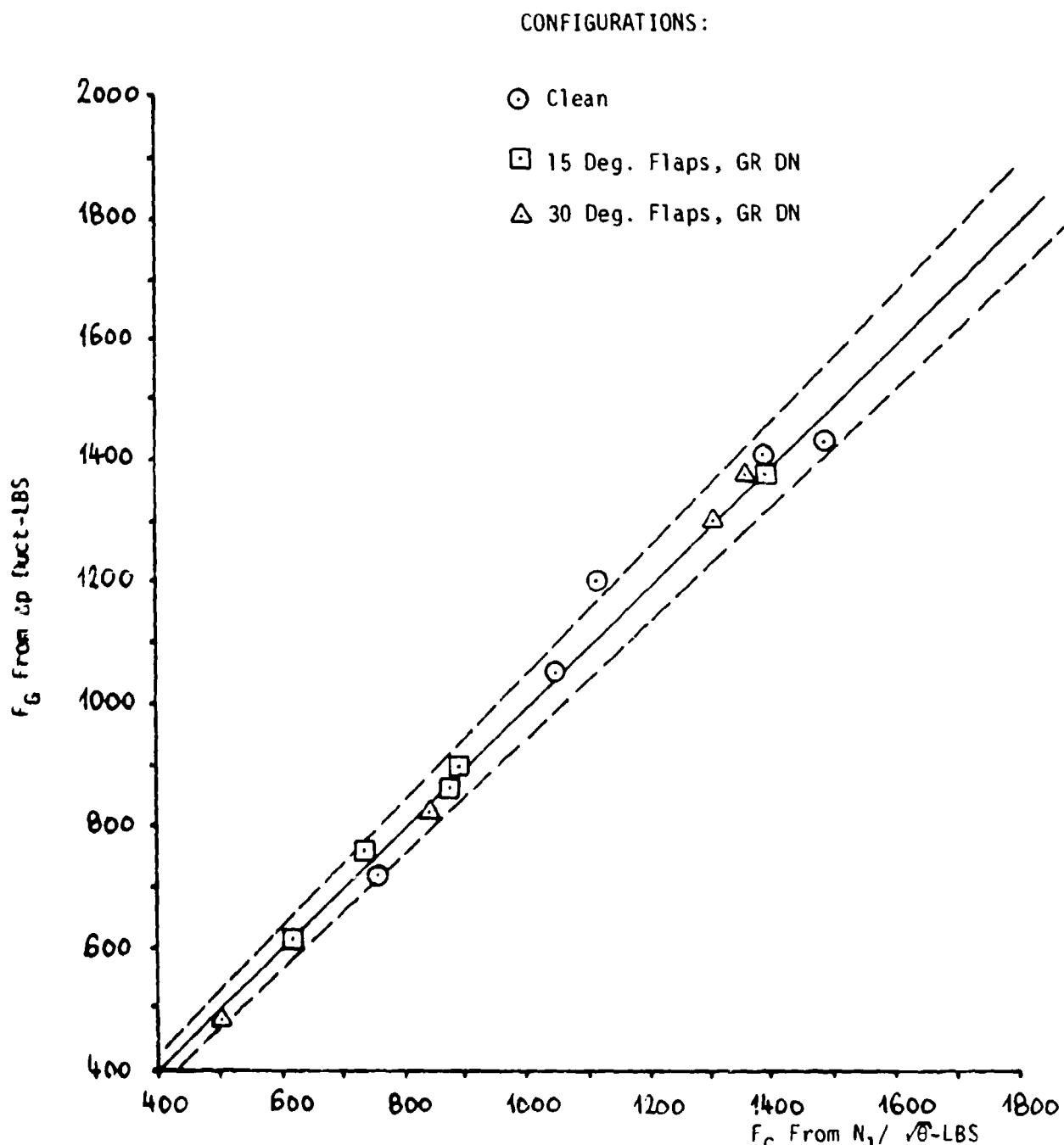


FIGURE 41

IN FLIGHT GROSS THRUST PREDICTED FROM DUCT PRESSURE
VERSUS THRUST PREDICTED FROM FAN SPEED

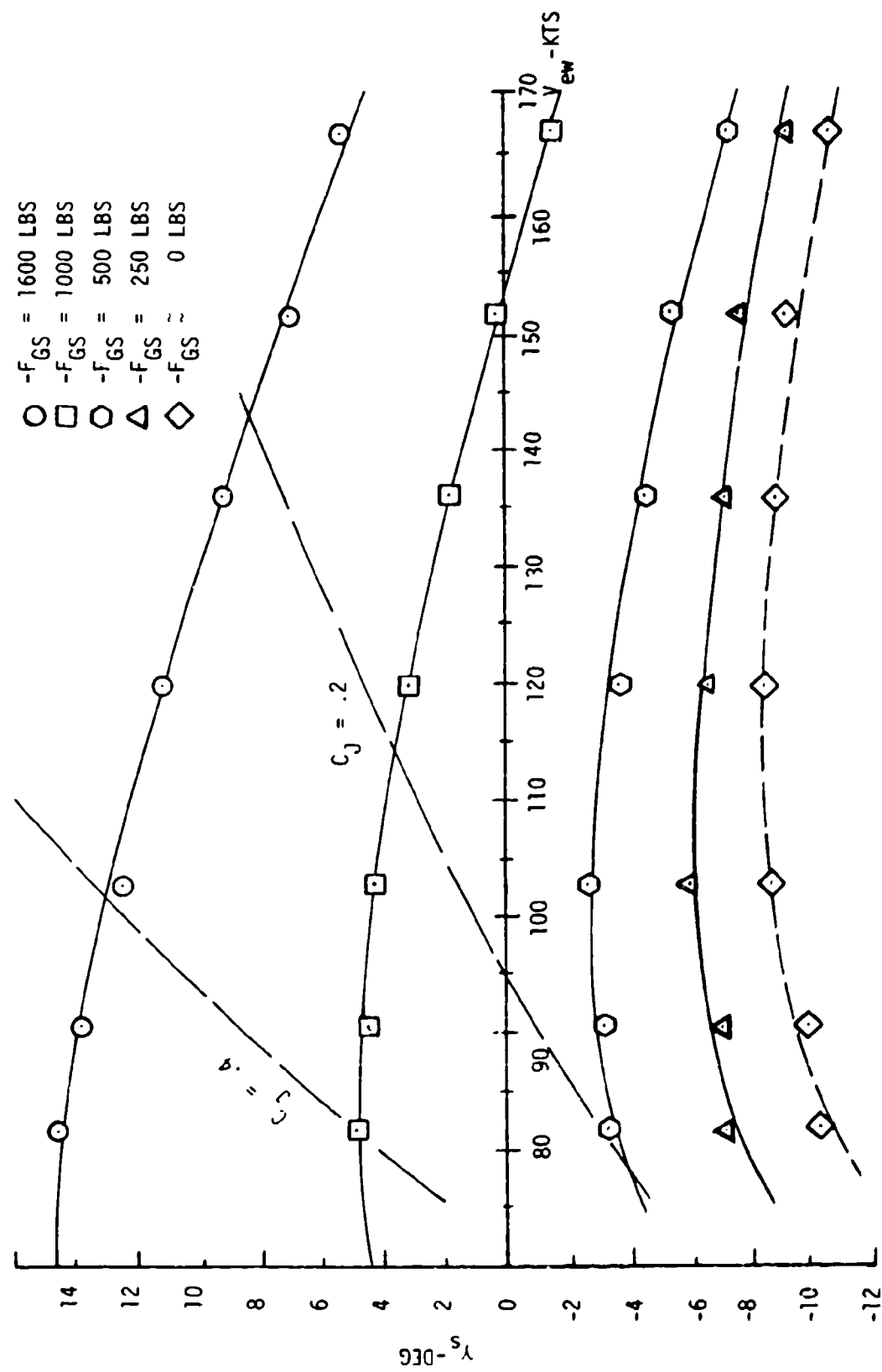
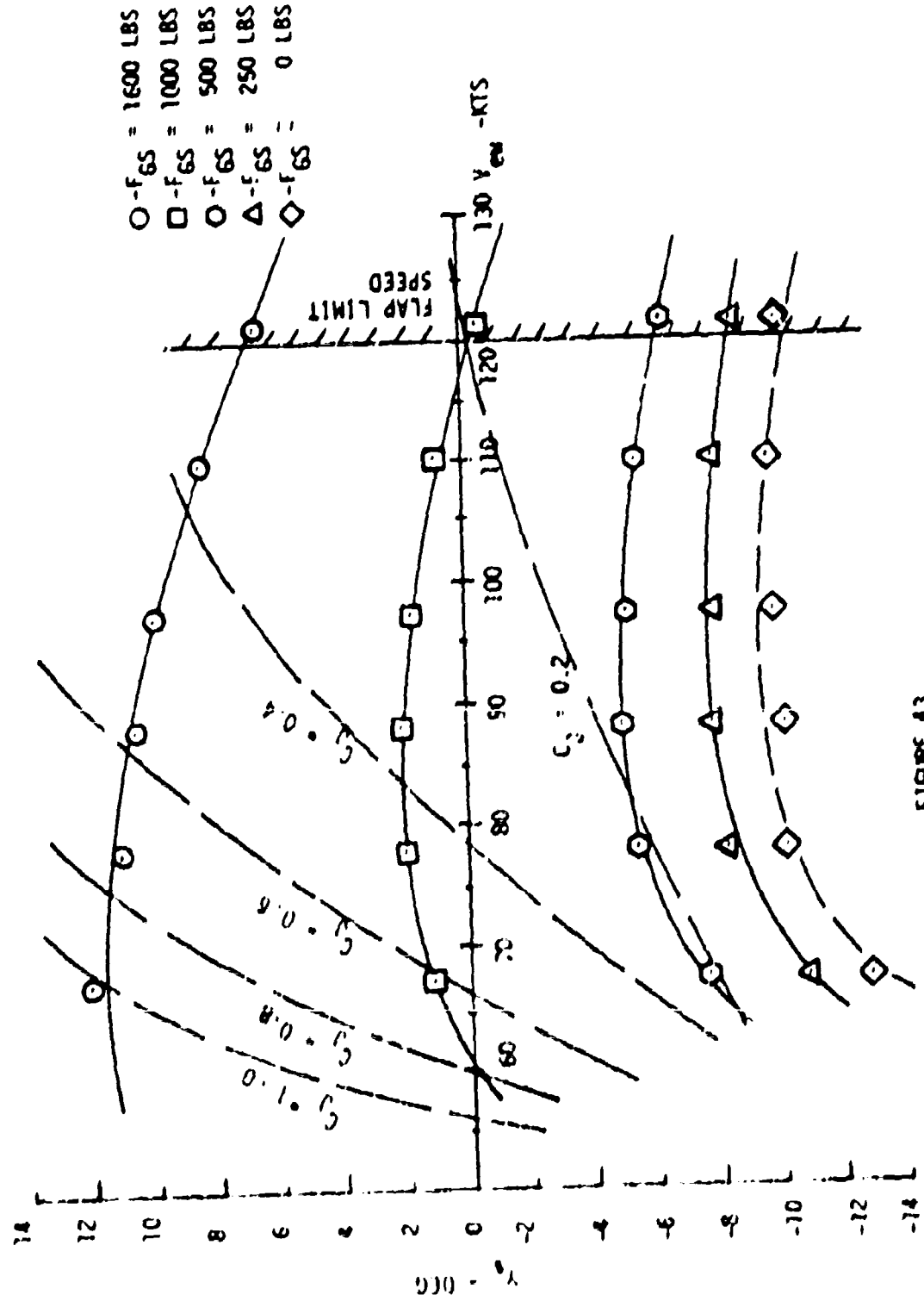


FIGURE 42
JETMING JN-1 y_s vs v_w
 $f_{GS} = 1600$ LBS

FIGURE 43
EFFECTS OF WIND SHEARS IN
TURBULENT FLOW



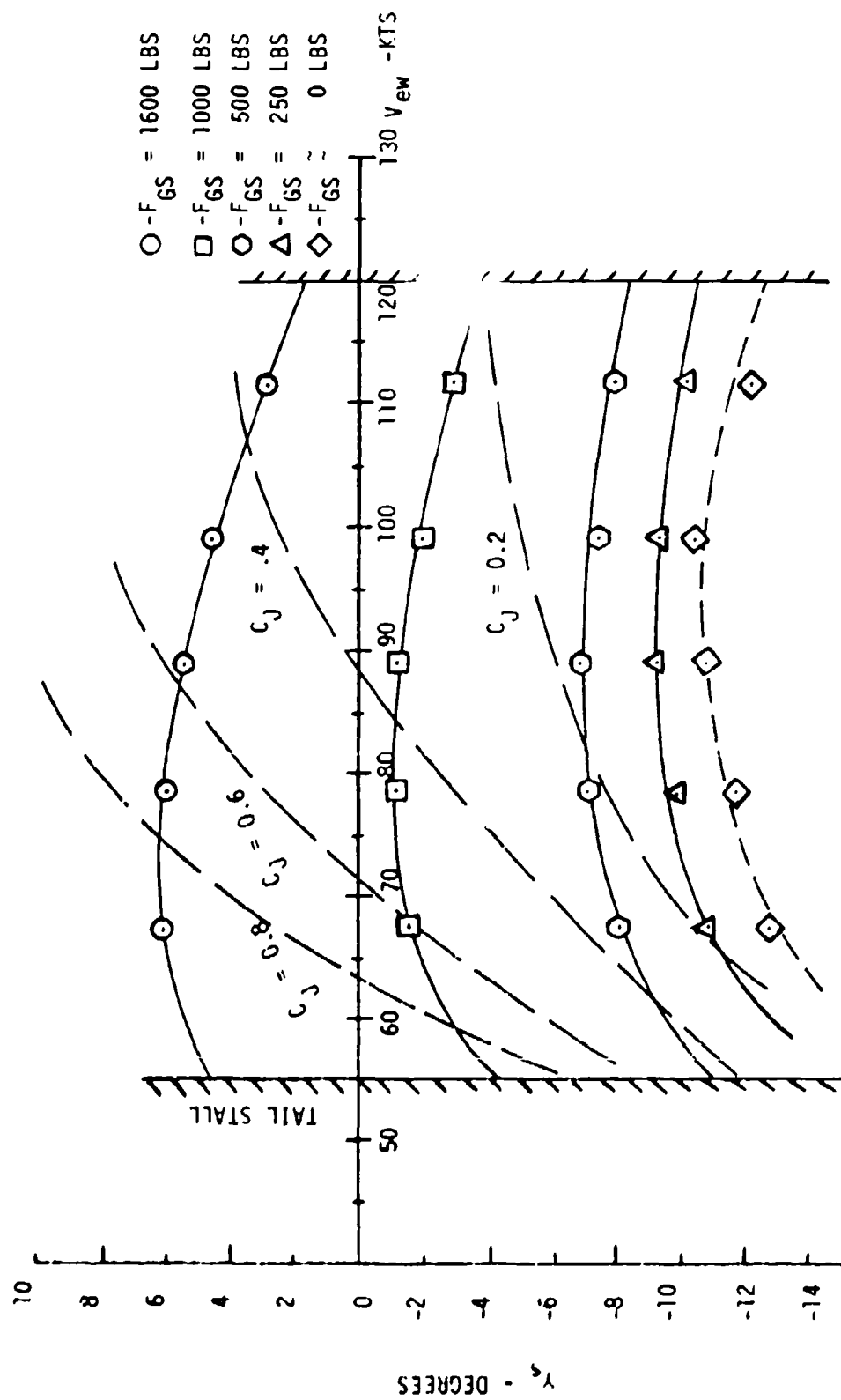
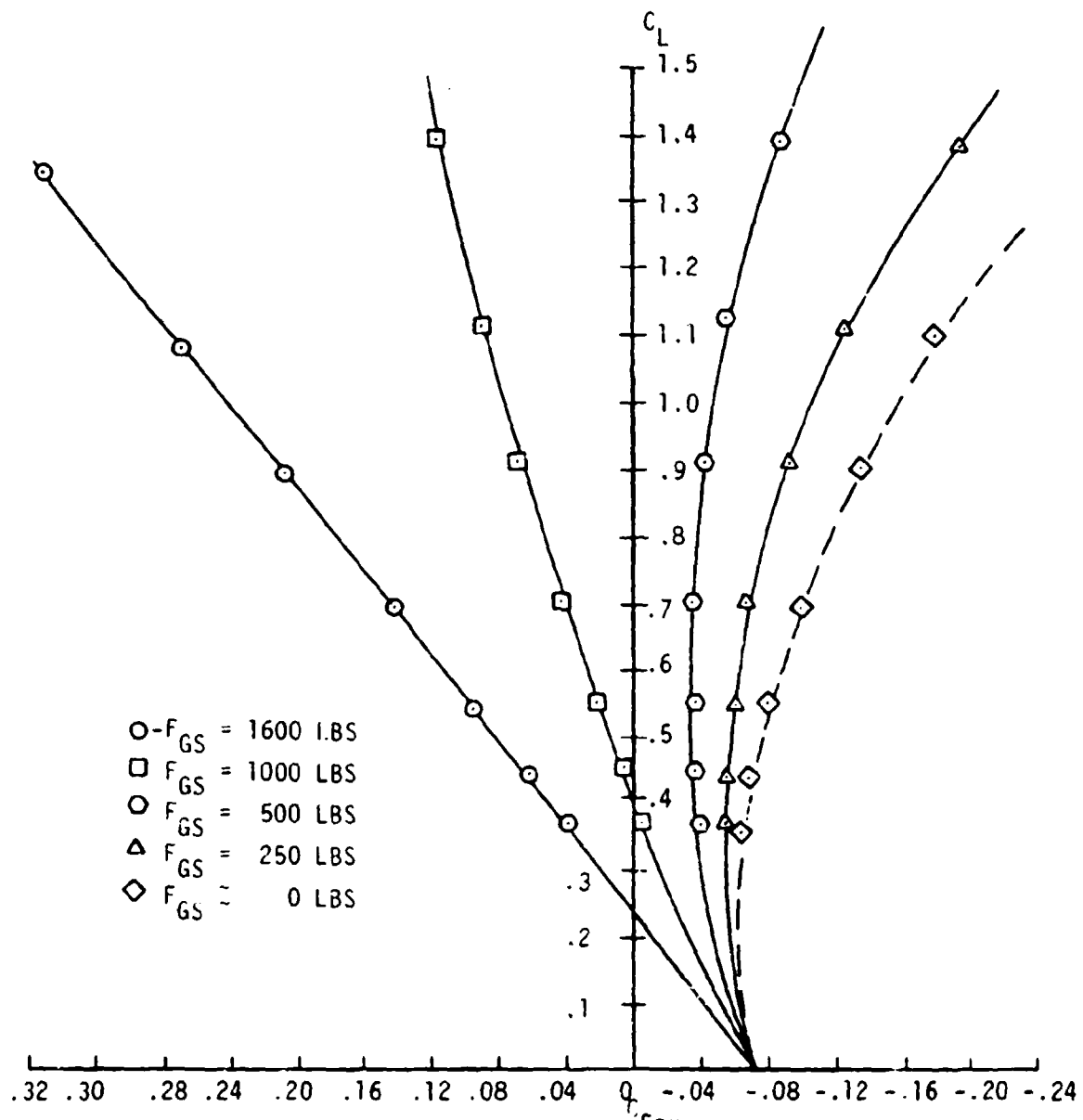


FIGURE 44
 JETWING JW-1
 Y_s vs V_{ew}
 GEAR DOWN, FLAPS 30°
 $W_s = 3600$ LBS



JETWING JW-1
 C_L vs C_{Fex}
 Clean Configuration
 $W_S = 3600$ LBS

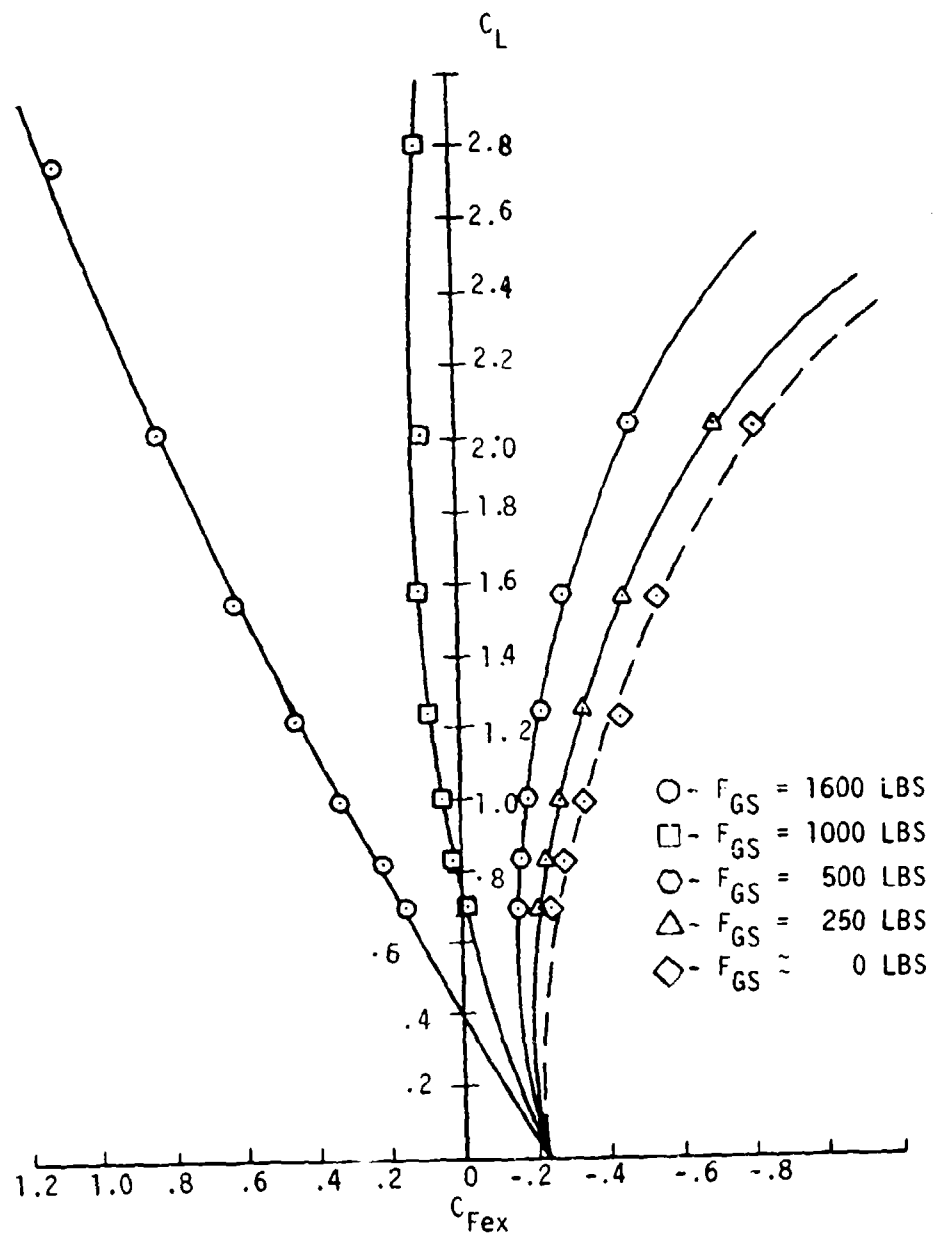


FIGURE 46

JETWING JW-1
 C_L VS C_{Fex}
 GEAR DOWN, FLAPS 15°
 $W_s = 3600$ LBS

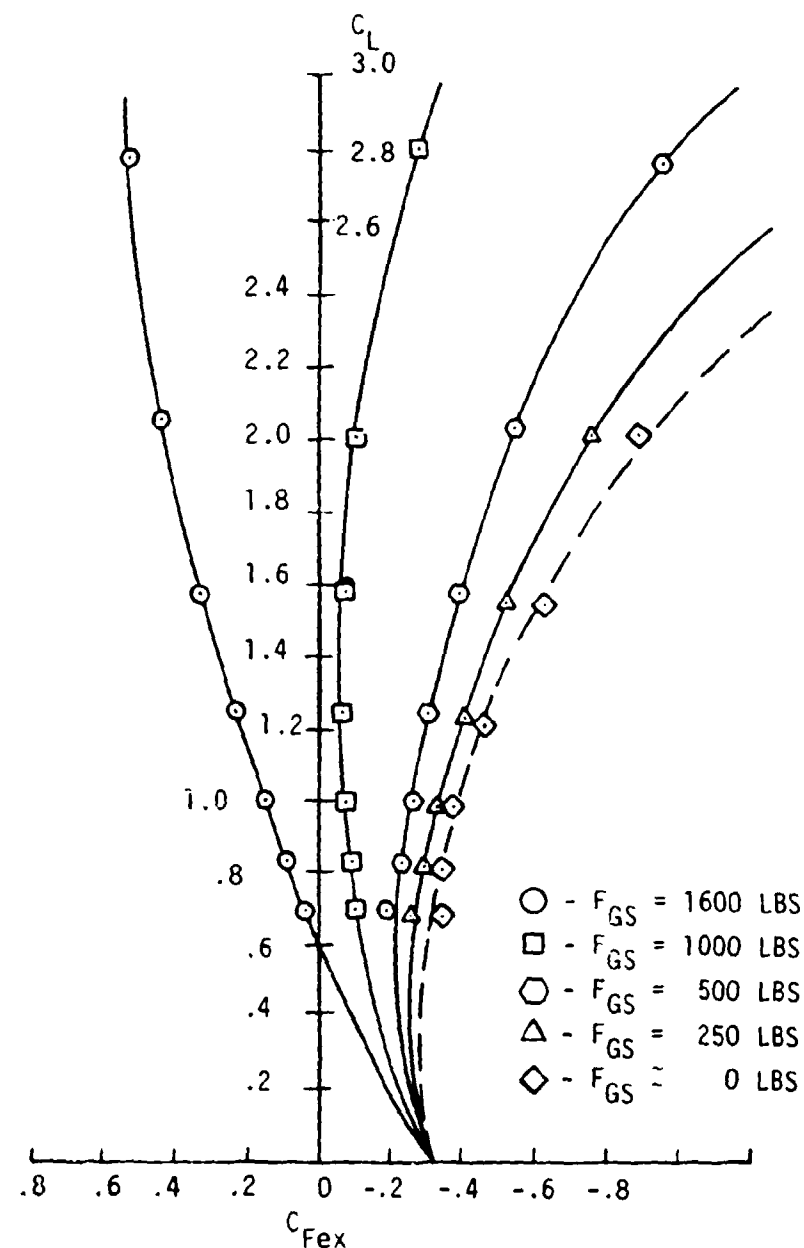


FIGURE 47
 JETWING JW-1
 C_L VS C_{Fex}
 GEAR DOWN, FLAPS 30°
 $W_s = 3600$ LBS

Figures 45, 46, and 47 demonstrate graphically why drag coefficient is no longer a meaningful variable when applied to powered lift airplanes. The right hand curve ($C_J = 0$) in each of these figures would be the same as a conventional drag polar. However, when thrust is applied to airplane ($C_J > 0$) the polar shifts to the left. If enough thrust (blowing) is applied the curves become negative. It is interesting to note that this shift to the left only occurs for lift coefficients in excess of zero ($C_L > 0$). The reason for these unusual characteristics is easily seen when one examines the drag equation for a powered lift airplane.

$$C_D = C_{D0} + \frac{K C_L^2}{\pi A + 2C_J} \quad (1)$$

This equation developed by Maskell and Spence in Reference 2 for jet flapped airfoils shows that the induced drag term of the drag equation contains the thrust related term C_J . C_J the blowing coefficient may be defined for the Jetwing airplane as:

$$C_J = \frac{F_q}{qS} \quad (2)$$

Since this intermingling of thrust with drag invalidates the conventional meaning of drag, equation 1 is generally expressed as the excess thrust coefficient C_{FEX} .

$$C_{FEX} = rC_J - C_{D0} - \frac{K C_L^2}{\pi A + 2C_J} \quad (3)$$

It may be seen from equation 3 that for the special case of zero thrust ($C_J = 0$), the equation reduces to:

$$C_{FEX} = -C_D \quad (4)$$

Therefore, when comparing performance of powered lift airplanes one must always be sure to compare at equal values of C_J .

Sufficient performance data were obtained to make comparisons with the NASA-Ames Research Center 40' x 80' wind tunnel data at blowing coefficients of $C_J = 0.43$ for the gear and flaps up configuration, and at $C_J = 0.75$ for the other two configurations. These comparisons are shown in Figures 48, 49, and 50. These figures show good correlation between the flight test and wind tunnel data. The correlation should be even better if an accounting is made of the trim drag difference between the flight and wind tunnel tests. The reason for the trim drag

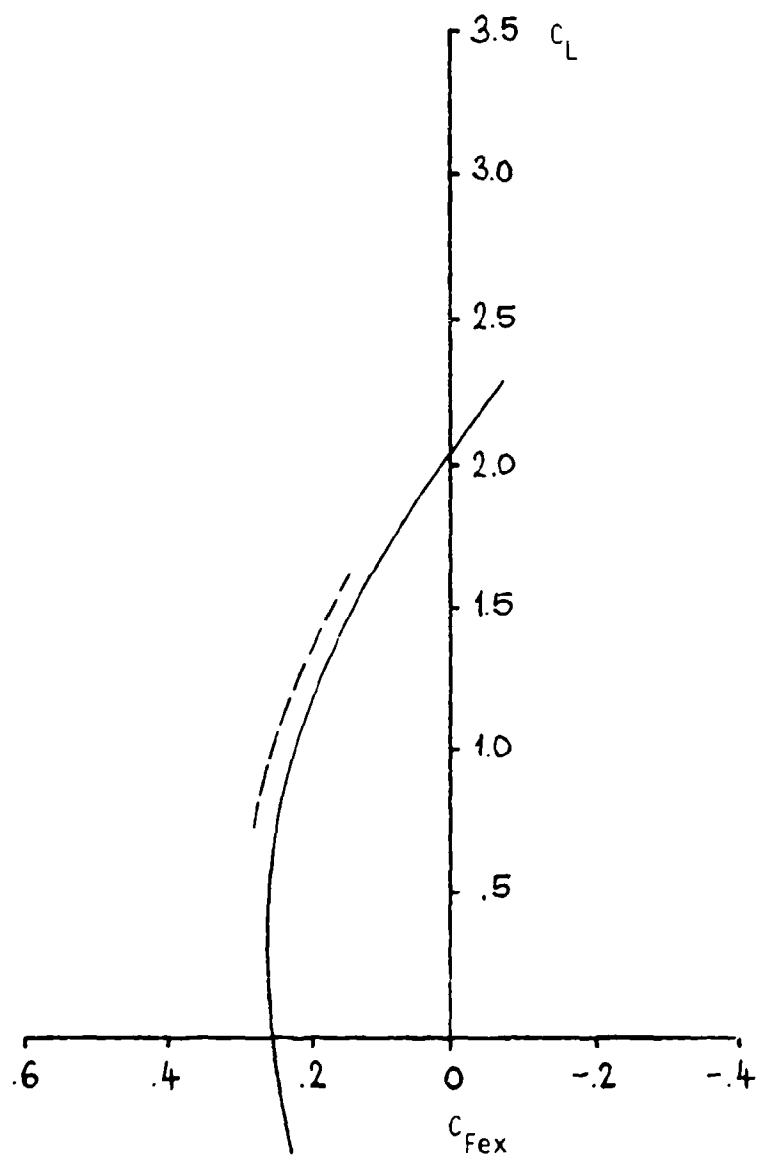


FIGURE 48

Jetwing JW-1
Wind Tunnel VS
Flight Test Comparison
 C_L VS C_{Fex}

Clean Configuration
 $C_J = .43$

Wind Tunnel —————
Flight Test - - - - -

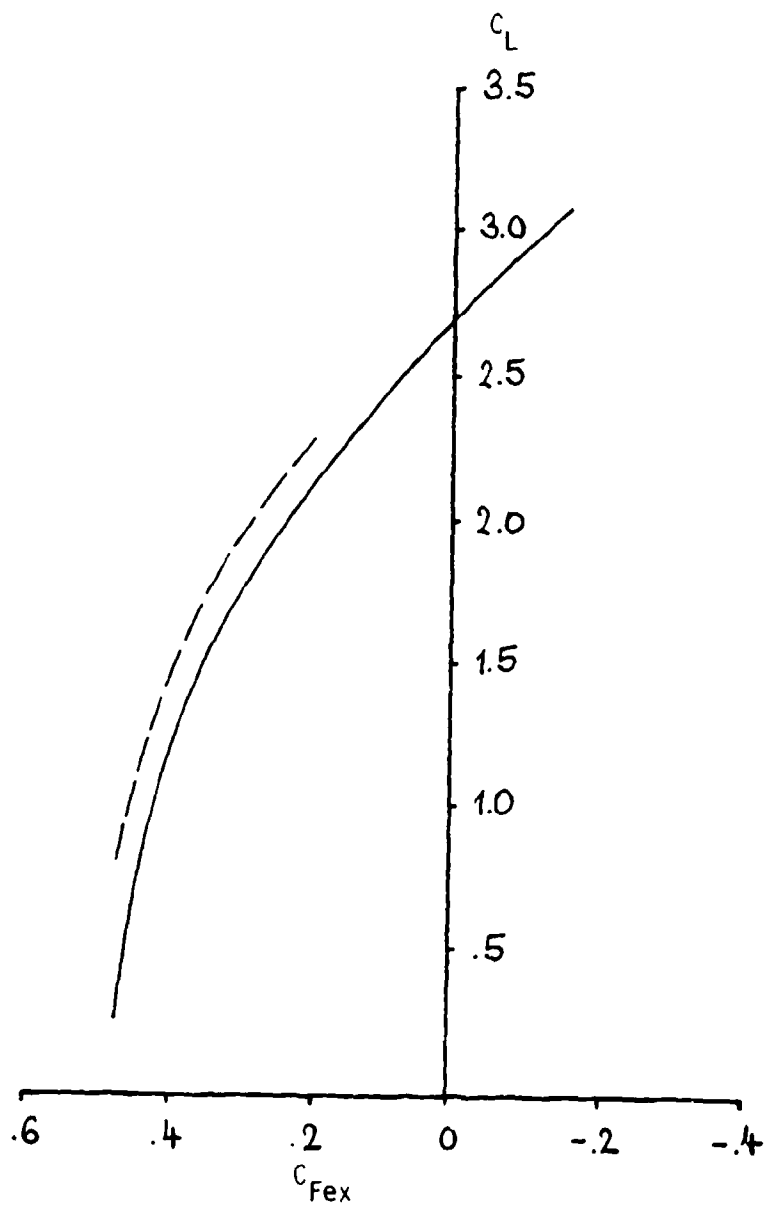


FIGURE 49

Jetwing JW-1
Wind Tunnel Verses Flight Test Comparison
 C_L VS C_{Fex}
Gear Down, Flaps 15°
Wind Tunnel —
Flight Test - - -
 $C_J = .75$

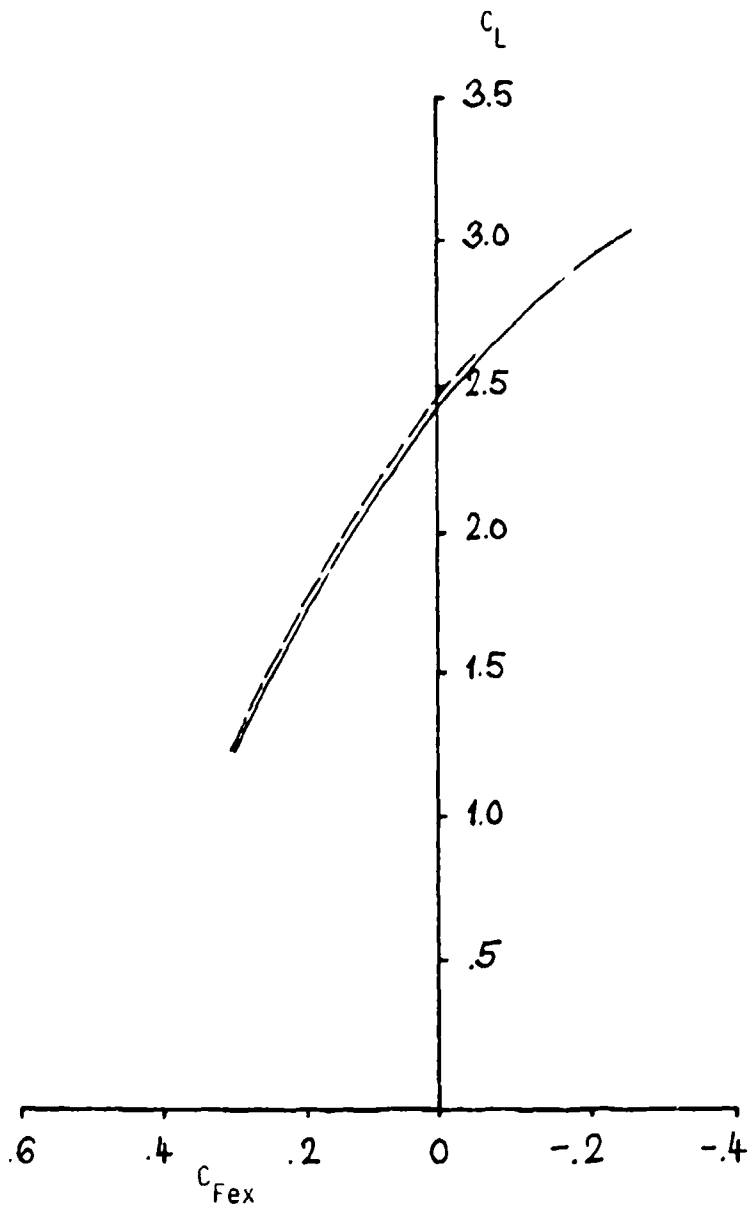


FIGURE 50

Jetwing JW-1
Wind Tunnel-Flight
Test Comparison
Gear Down, Flaps 30°
 $C_J = .75$
Wind Tunnel ———
Flight Test - - - -

difference is that the flight tests were conducted at a center of gravity position which was 2.5% M.A.C. further aft than the center of gravity position during the wind tunnel tests. Data comparisons at blowing coefficients in excess of $C_j = 0.75$ were not possible due to the stability and control considerations discussed earlier.

In summary the flight test performance results can be said to confirm the results obtained in the 40' x 80' wind tunnel.

5. C_L CAPABILITIES. For powered lift aircraft the lift coefficient (C_L) is a function of blowing coefficient (C_j) as well as the angle of attack (α).

$$C_L = f(\alpha, C_j) \quad (5)$$

As a result of this relation it is very difficult to obtain classic C_L vs. α curves at constant C_j from direct flight test methods. To obtain such data by direct methods would require that a unique combination of aircraft weight, power setting, and airspeed be established for each data point. To avoid such a difficult task the following approach was used. Angle of attack data were collected along with the other data required to measure performance during the sawtooth climbs and descents. From these data plots of C_L vs. C_j were made with α' cross plotted over them. These plots are shown in Figures 51, 52, and 53. From these plots cross plots of C_L vs α' at a constant C_j may be obtained. Such plots are shown in Figures 54, 55, and 56 where they are compared with the 40' x 80' wind tunnel data taken at similar blowing coefficients. The lift curve slope ($dC_L/d\alpha$) compares well between the tunnel and flight test at the 30° flap setting, but not as well at other settings. This difference in ($dC_L/d\alpha$) and C_L vs α may be accounted for by the fact that the flight test angle of attack data includes upwash while the corresponding wind tunnel data does not. In addition, both the method of obtaining the data, and the method of reducing it have some inaccuracy. It may be possible to remove such differences from the flight test data if flight path angle and pitch attitude angle are measured at the same time as angle of attack. This measurement was not accomplished during these tests because a sufficiently accurate attitude gyro was not installed at the time of the tests. It is hoped that the differences shown can be resolved during follow on testing.

In spite of these problems the correlation of $dC_L/d\alpha$ between wind tunnel and flight tests is sufficient to confirm the validity of the wind tunnel tests.

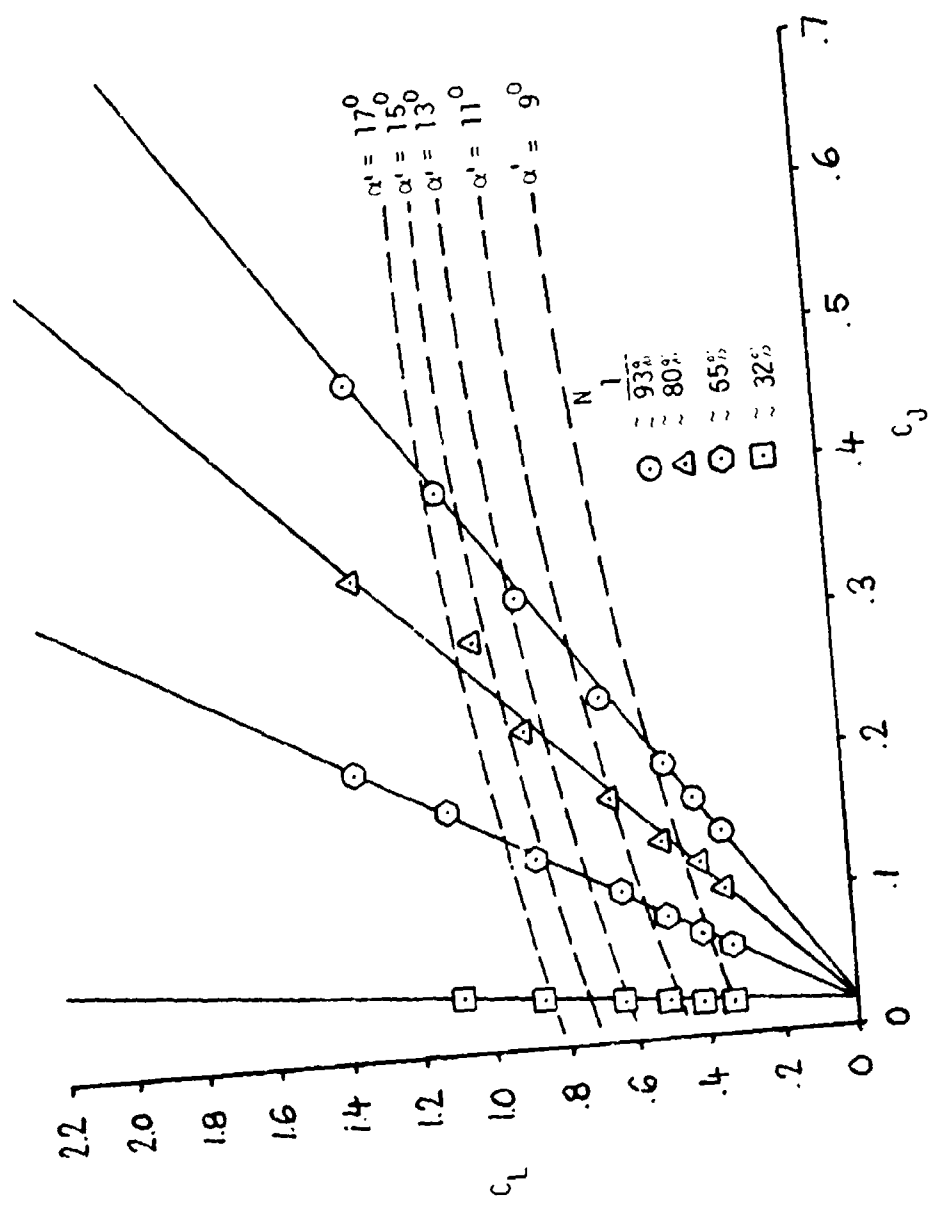


FIGURE 51
 C_L vs C_J
JETWING JW-1
GEAR UP, FLAPS UP

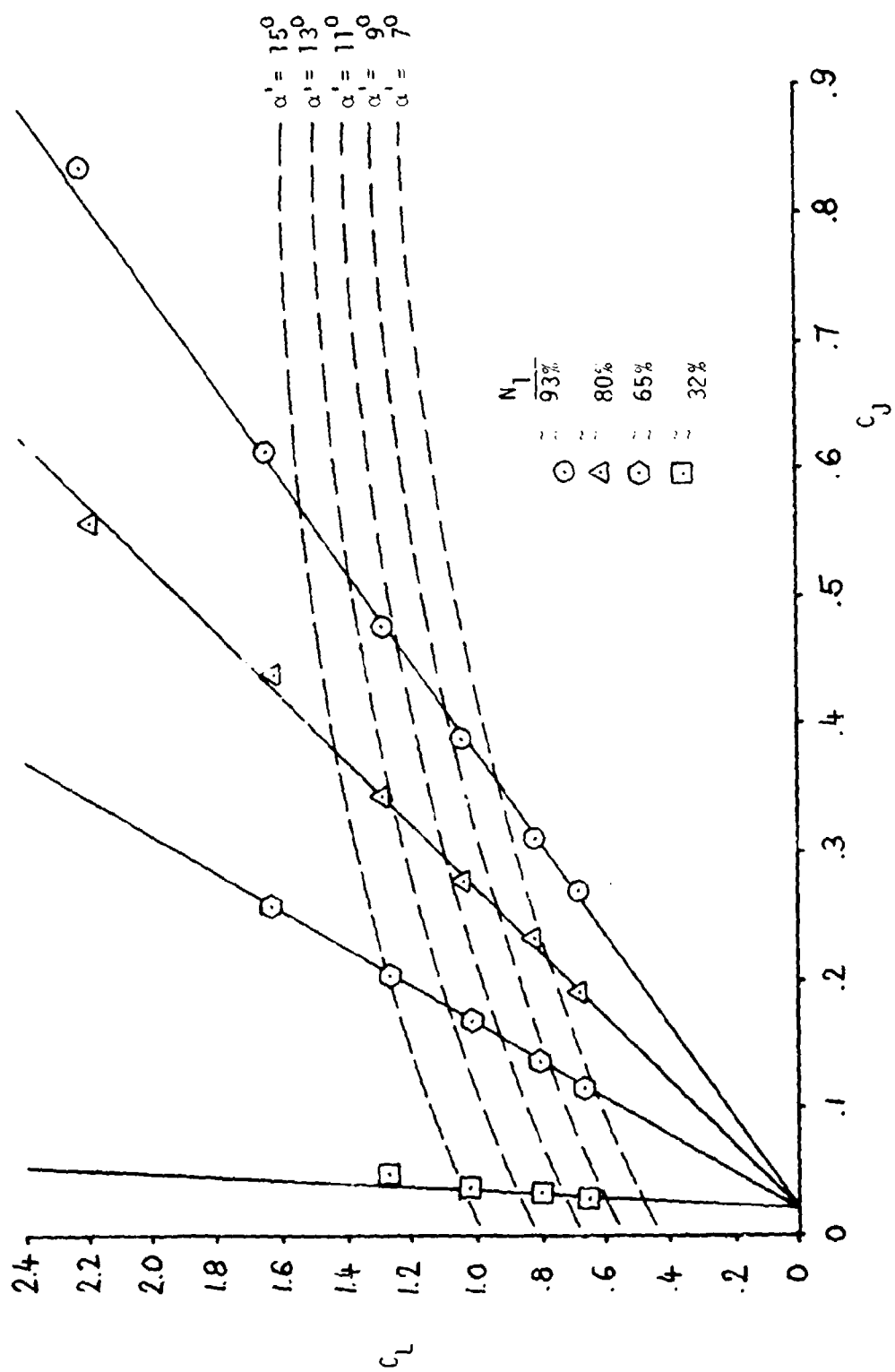


FIGURE 52
 c_L vs c_J
 JETWING JW-1
 GEAR DOWN, FLAPS 15°

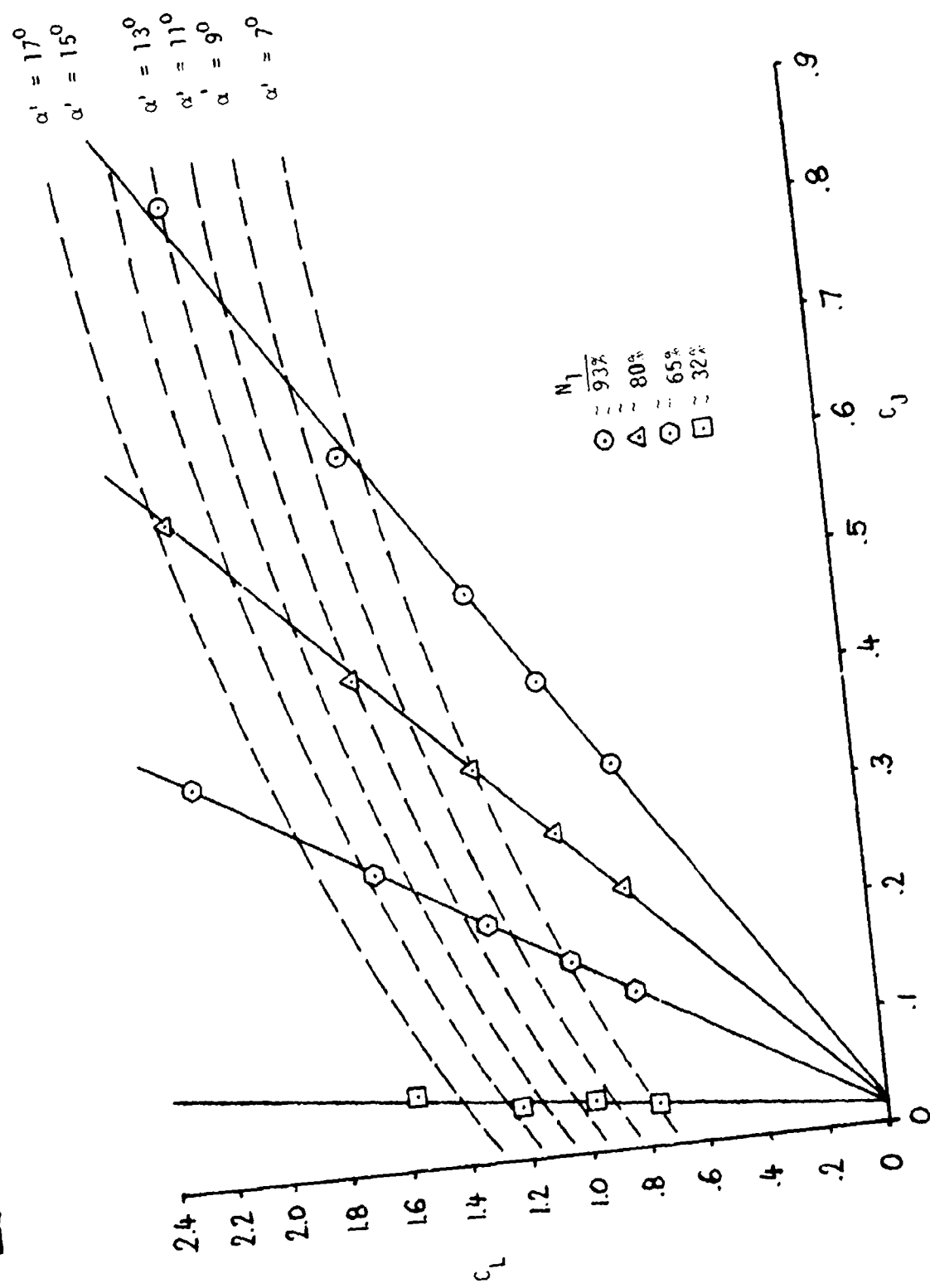


FIGURE 53
 C_L vs C_J
 JETWING JW-1
 GEAR DOWN, FLAPS 30°

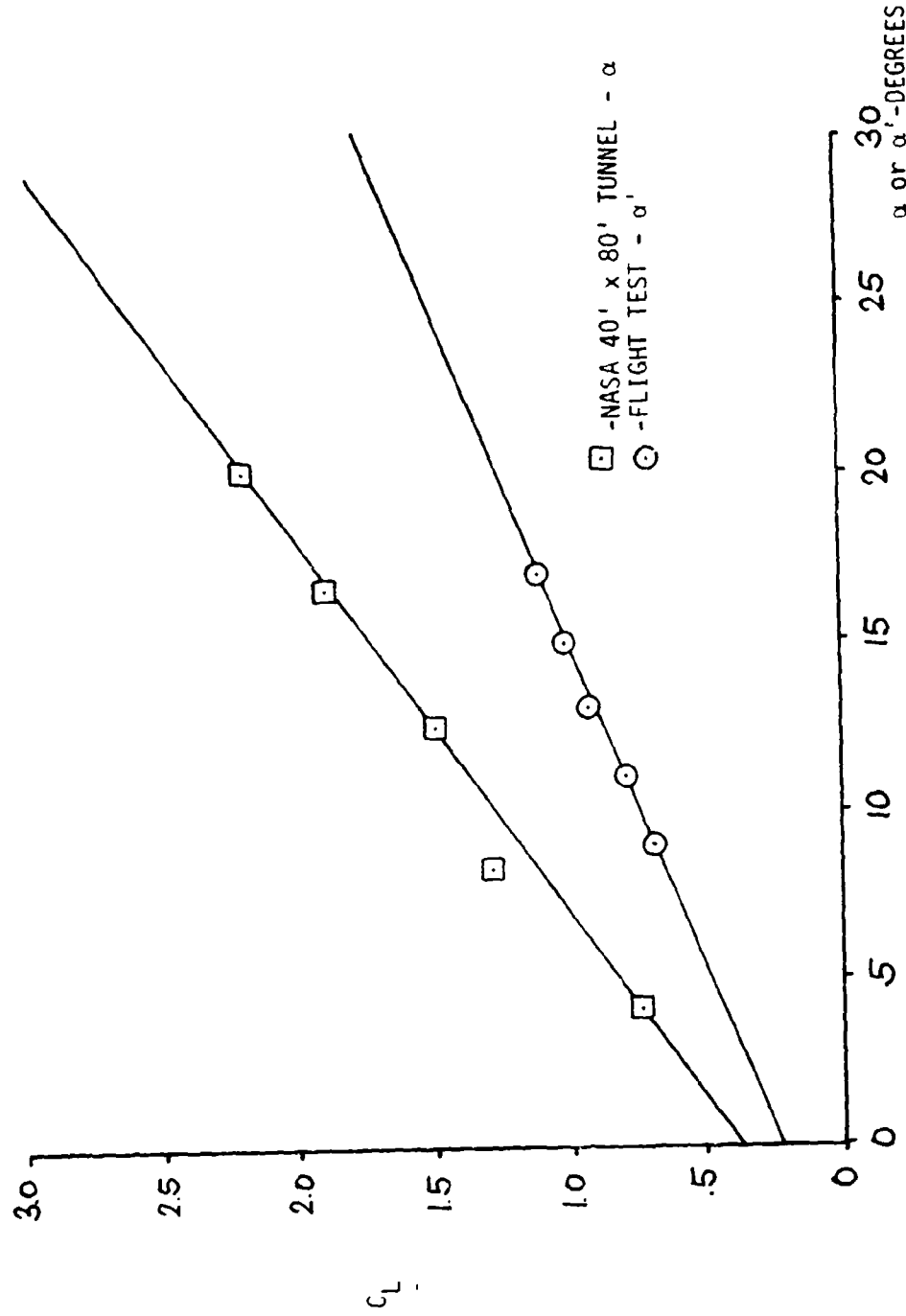


FIGURE 54

C_L vs α or α'
 WIND TUNNEL AND FLIGHT TEST RESULTS
 GEAR UP, FLAPS UP
 $C_J = 0.43$

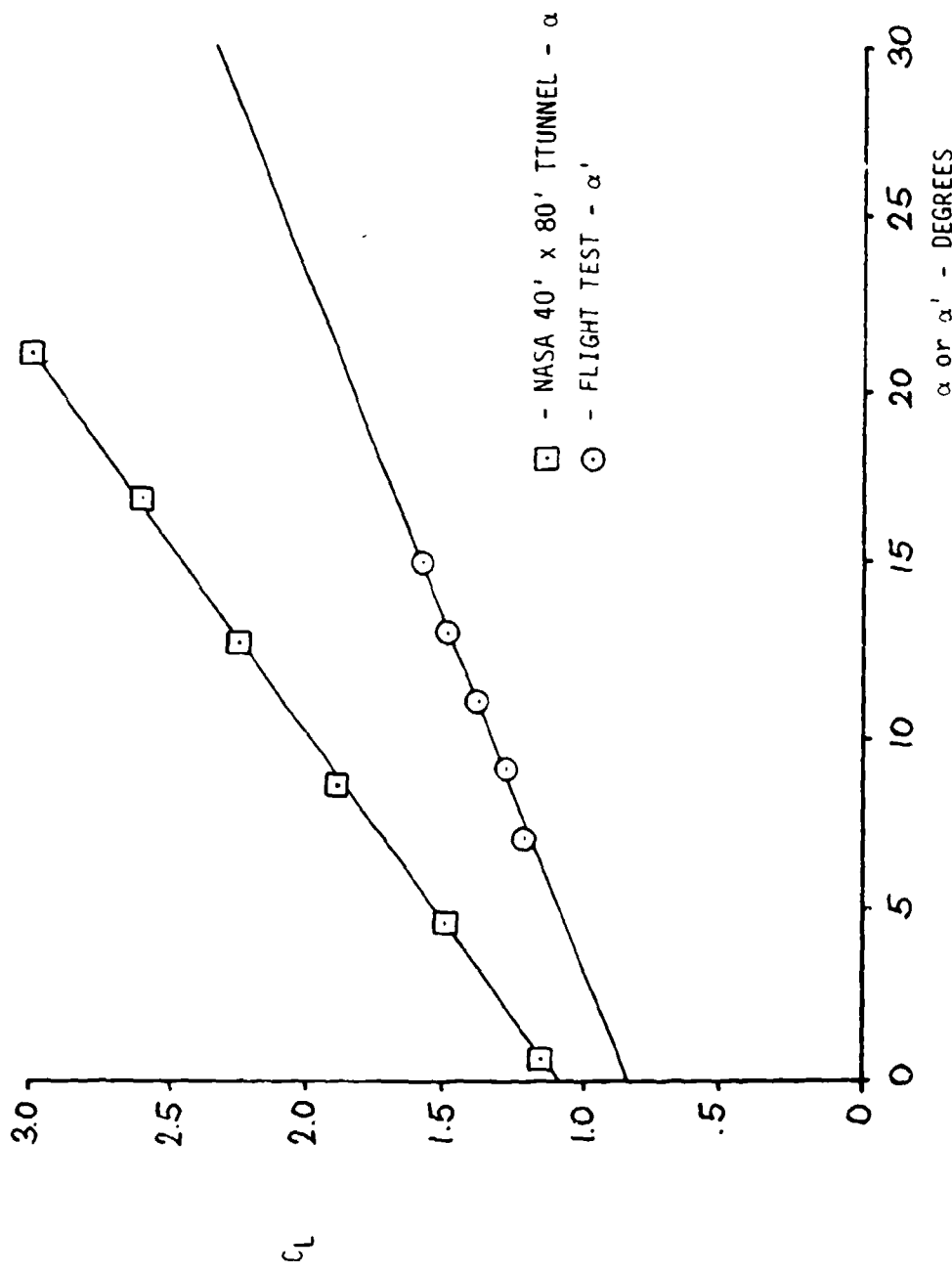


FIGURE 55

JETWING JW-1, N27BB
 C_L vs α or α'
 WIND TUNNEL AND FLIGHT TEST RESULTS
 GEAR DOWN, 15° FLAPS
 $C_J = .75$

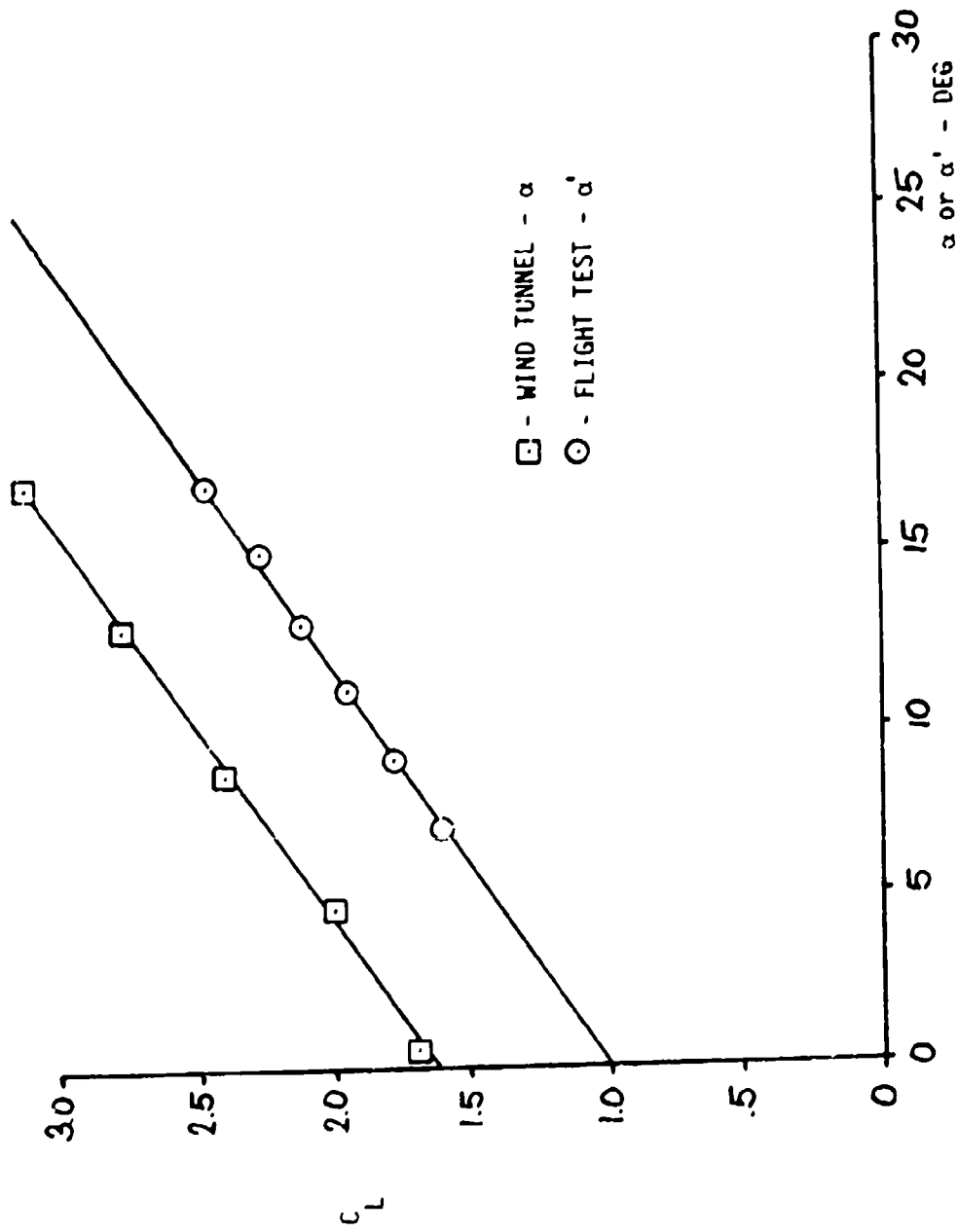


FIGURE 56

JETWING JW-1, N2788
 C_L vs α or α'
 WIND TUNNEL AND FLIGHT TEST RESULTS
 GEAR DOWN, 30° FLAPS
 $C_J = .75$

An intentional investigation of $C_{L\text{MAX}}$ capability was not attempted due to a lack of an emergency egress system. However, an inadvertent $C_{L\text{MAX}}$ point was obtained during Maneuvering Stability testing. This single point compared well with wind tunnel test data for similar configuration and blowing coefficient. This data point and the aircraft reaction will be discussed further in the Maneuvering Stability section of this report.

6. CONTROL SYSTEM FRICTION MEASUREMENT. The results of static ground measurements of control system friction are shown in Figures 57, 58, and 59. These figures show that very low system friction levels exist for the elevator and aileron control systems, but that the rudder control system has very high friction levels. In addition, the rudder control system has high breakout forces. The high friction and large forces shown for the rudder control system can primarily be attributed to the tailwheel anti-shimmy mechanism and the tailwheel steering springs. The anti-shimmy mechanism creates considerable friction while the tailwheel steering springs contribute to the control forces at the rudder. All testing conducted which involved the rudder was done with the tailwheel locked in the center position. The friction measurements shown in Figure 59 were also conducted with the tailwheel locked in center position.

7. LATERAL CONTROL POWER. Lateral control power was evaluated by measuring steady state roll rate ($\dot{\phi}_{ss}$) and roll mode time constant in the following configurations and airspeeds.

<u>CONFIGURATION</u>	<u>AIRSPEED</u>
1. Gear and Flaps up	150 KIAS
2. Gear and Flaps up	120 KIAS
3. Gear down, Flaps 30°	90 KIAS
4. Gear down, Flaps 30°	70 KIAS

In addition, configurations 3 and 4 were conducted in 3° and 6° descents. Three degrees and 6° descents were used to evaluate the effects of blowing (C_J) upon lateral control power, since different power settings are required to maintain the different glide paths.

In performing the test, the aircraft was rolled through 90° of the bank by rolling from one 45° bank to the opposite 45° of the bank using aileron only and keeping the rudder centered. Data were recorded on magnetic tape.

Table 3 presents a summary of the data for all of the configurations and airspeeds tested.

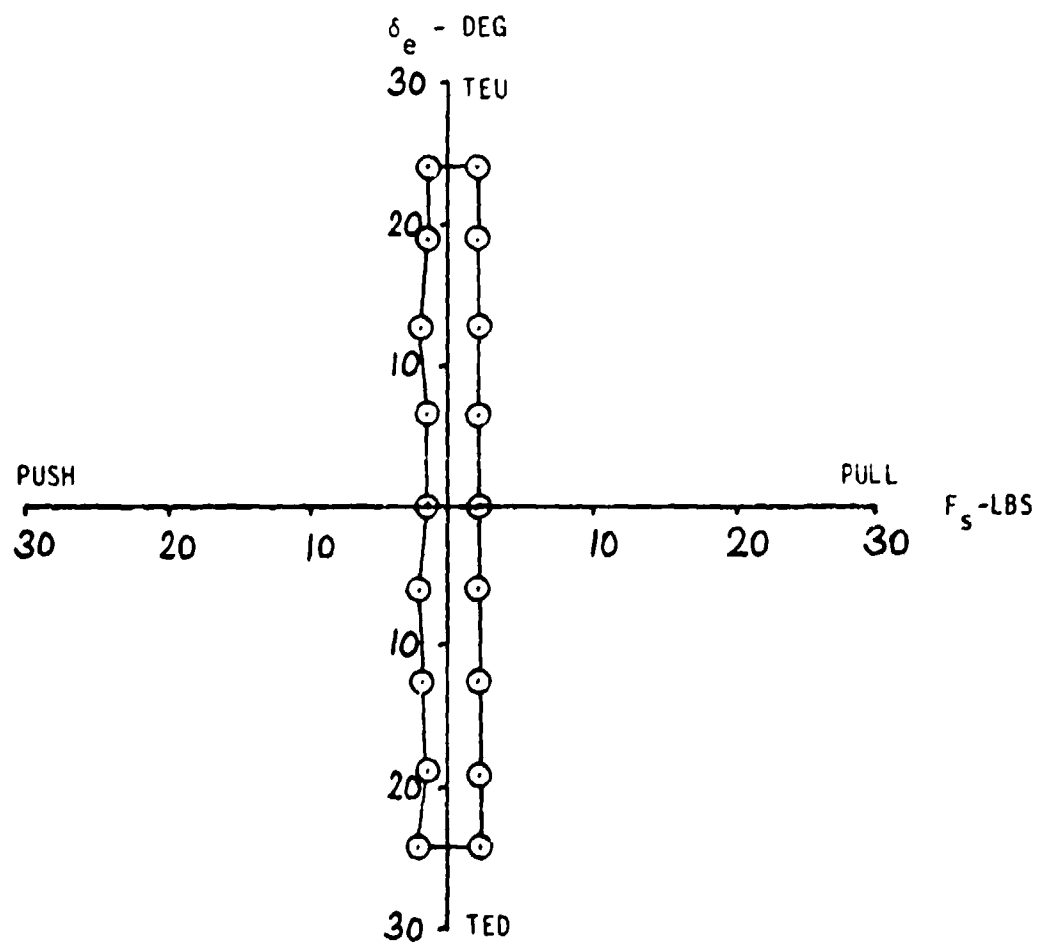


FIGURE 57

JETWING JW-1, N2788
ELEVATOR CONTROL SYSTEM STATIC FRICTION MEASUREMENT

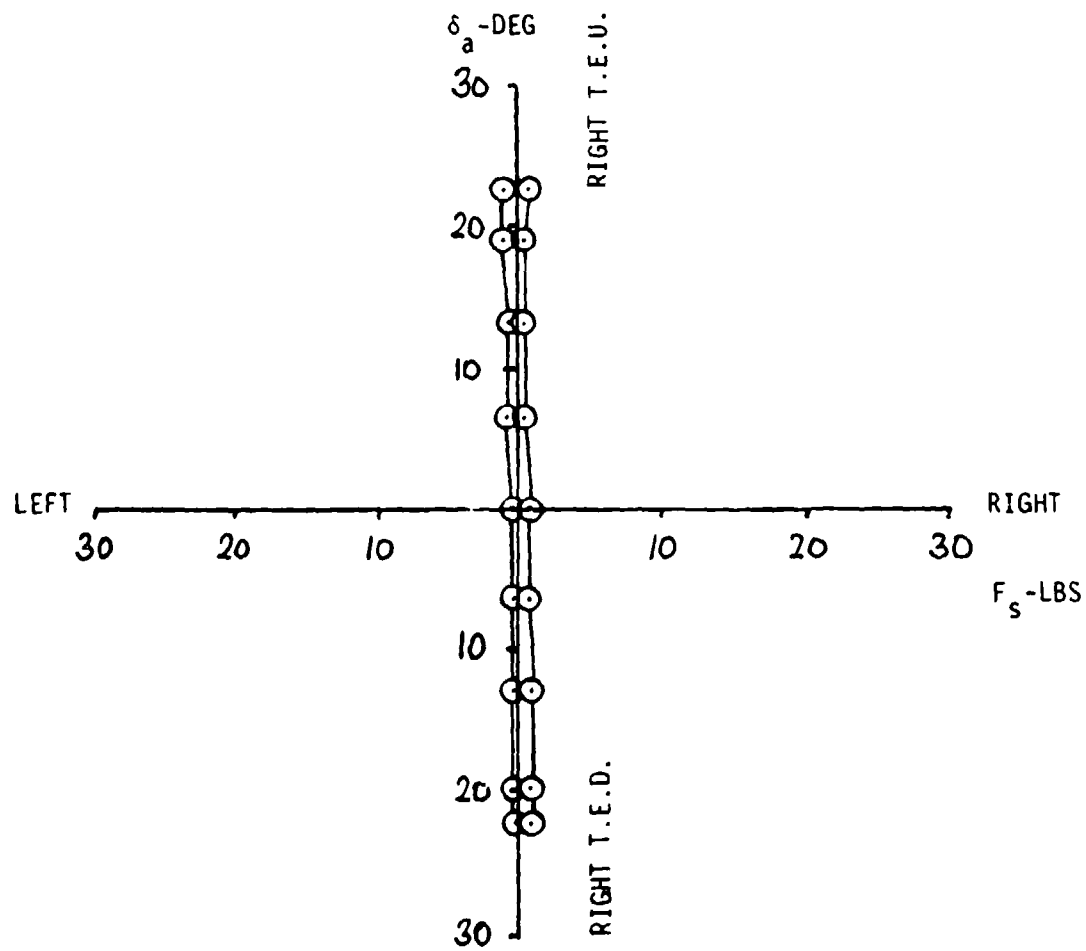


FIGURE 58

JETWING JW-1, N2788
AILERON CONTROL SYSTEM STATIC FRICTION MEASUREMENT

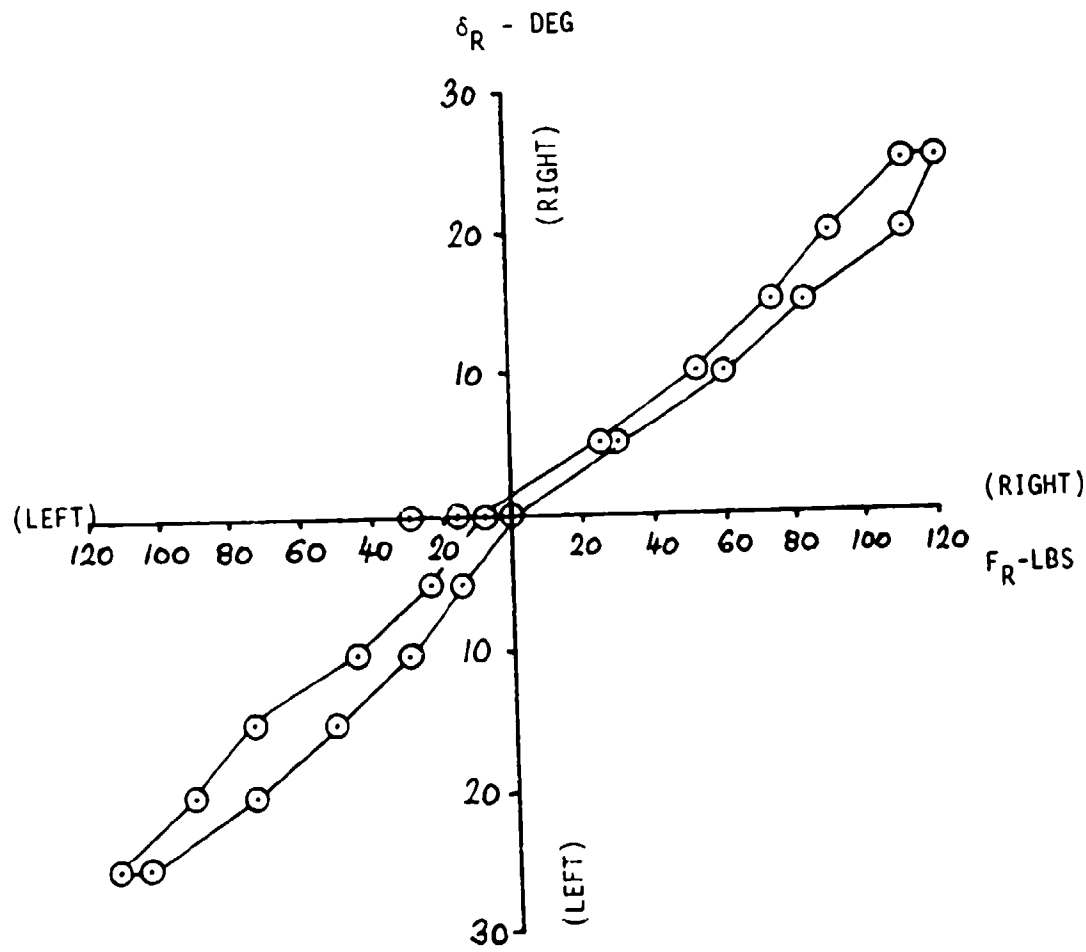


FIGURE 59

JETWING JW-1, N27BB
RUDDER CONTROL SYSTEM STATIC FRICTION MEASUREMENT

TABLE 3
ROLLING PERFORMANCE SUMMARY

CONFIGURATION	V_c	V_T	C_J	$P_{ss\ max}$	$\frac{P_b}{2V_T\ MAX}$	R
GEAR & FLAPS UP	111 KT	118.5 KT	0.15	36.5°/sec	0.035	0.44sec
GEAR & FLAPS UP	152.5 KT	170 KT	0.12	74°/sec	0.049	0.43sec
GEAR DOWN FLAPS 30; 3° APPROACH	71.5 KT	73.7 KT	0.15	30°/sec	0.046	0.48sec
GEAR DOWN FLAPS 30° 3° APPROACH	92 KT	100 KT	0.35	48°/sec	0.053	0.48sec
GEAR DOWN FLAPS 30° 6° APPROACH	71.5 KT	75 KT	0.38	32.5°/sec	0.049	0.48sec
GEAR DOWN FLAPS 30° 6° APPROACH	92 KT	100 KT	0.23	44°/sec	0.049	0.48sec

In examining this table it may be seen that the aircraft responds readily to lateral control input, since the roll mode time constant (τ_R) is less than one half second for all the configurations tested. The roll mode time constant is the time required for the aircraft to reach 63.2% of its steady state roll rate and is an indication of roll acceleration. The values for this parameter are well within the 1.0 seconds allowed by MIL-F-87858 (ASG), Reference 3.

With the rudder free the steady state roll rate will only meet MIL-F-87858 Level 1 requirements in Classes I, II, and III and drops to Level 2 for Class IV. However, if rudder were used to reduce sideslip the aircraft would meet Level 1 requirements in all Classes since the rudder has a powerful effect on roll. If rudder is not used, the aircraft will accelerate to an initially higher roll rate than the steady state rate. If rudder is used, this higher rate will be sustained.

The rolling performance of the Jetwing speaks well for this powered lift approach since no separate bleed air system is required for the ailerons in order to achieve the roll rates shown. However, the data does not show an increase in roll rate with an increase in blowing coefficient, even though the ailerons remain effective to much lower airspeeds than would normally be expected.

8. LATERAL-DIRECTIONAL STABILITY. Static lateral-directional stability was evaluated at two airspeeds in both the cruise and power approach configurations using the steady sideslip technique.

Figures 60 through 63 show the results of these evaluations. As may be seen from these figures, the aircraft has strong positive static lateral-directional stability in all configurations. This was surprising in the case of lateral stability since the aircraft has small dihedral.

The Dutch Roll dynamic lateral-directional stability mode was evaluated in the same configurations and airspeeds as the static lateral-directional stability. The Dutch Roll motion was excited by rudder doublets. Data were collected on magnetic tape and evaluated by the methods of Reference 4. The results of these evaluations are shown in Table 4.

TABLE 4
SUMMARY OF DUTCH ROLL PARAMETERS

CONFIGURATION	GEAR AND FLAPS UP		GEAR DOWN, FLAPS 30°	
AIRSPEED	111 KCAS	152.5 KCAS	71.5 KCAS	92 KCAS
DAMPING FACTOR ζ_D	0.21	0.2	0.16	0.16
NATURAL FREQUENCY ω_n	1.69 Rad/sec	1.83 Rad/sec	1.87 Rad/sec	2.18 Rad/sec
$C_{1/2}$	0.52	0.55	0.69	0.69
ϕ / β	1.1	0.97	0.87	0.73
$\zeta_D \omega_n$	0.355	0.366	0.299	0.348

All of these parameters meet or exceed the minimum Dutch Roll Frequency and Damping requirements of Level 1 for aircraft Classes I through IV as specified in MIL-F-8785B.

The spiral stability was evaluated in cruise at 130 knots indicated airspeed and in power approach at 65 knots indicated airspeed. The results of these tests are shown in Figure 64. The power approach spiral mode is mildly divergent requiring about 35 seconds to achieve a 20° of bank. The spiral would only meet level 3 requirements of MIL-F-8785B in cruise. Power approach is slightly better, and will meet the Level 2 requirements. The rather poor characteristics in the spiral mode could be expected, since the aircraft has rather strong directional stability while having small dihedral.

9. LONGITUDINAL STABILITY AND CONTROL. Since the longitudinal static, dynamic and maneuvering stabilities all play an important part in the pilot's perception of an airplane's longitudinal handling qualities, they will all be discussed in this section.

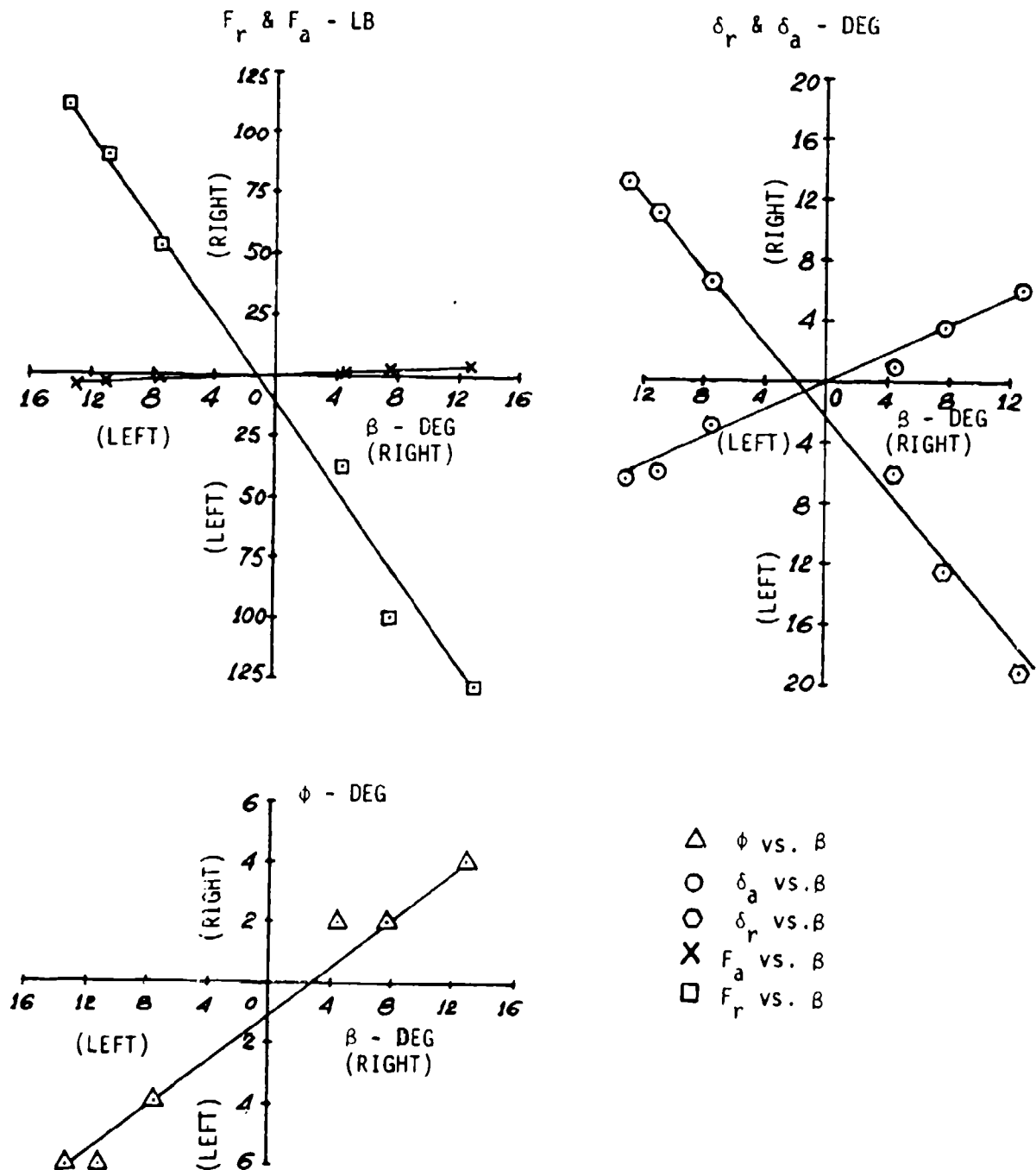


FIGURE 60

JETWING JW-1
N27BB
LATERAL-DIRECTIONAL
STABILITY
POWER APPROACH
3° APPROACH
70 KIAS

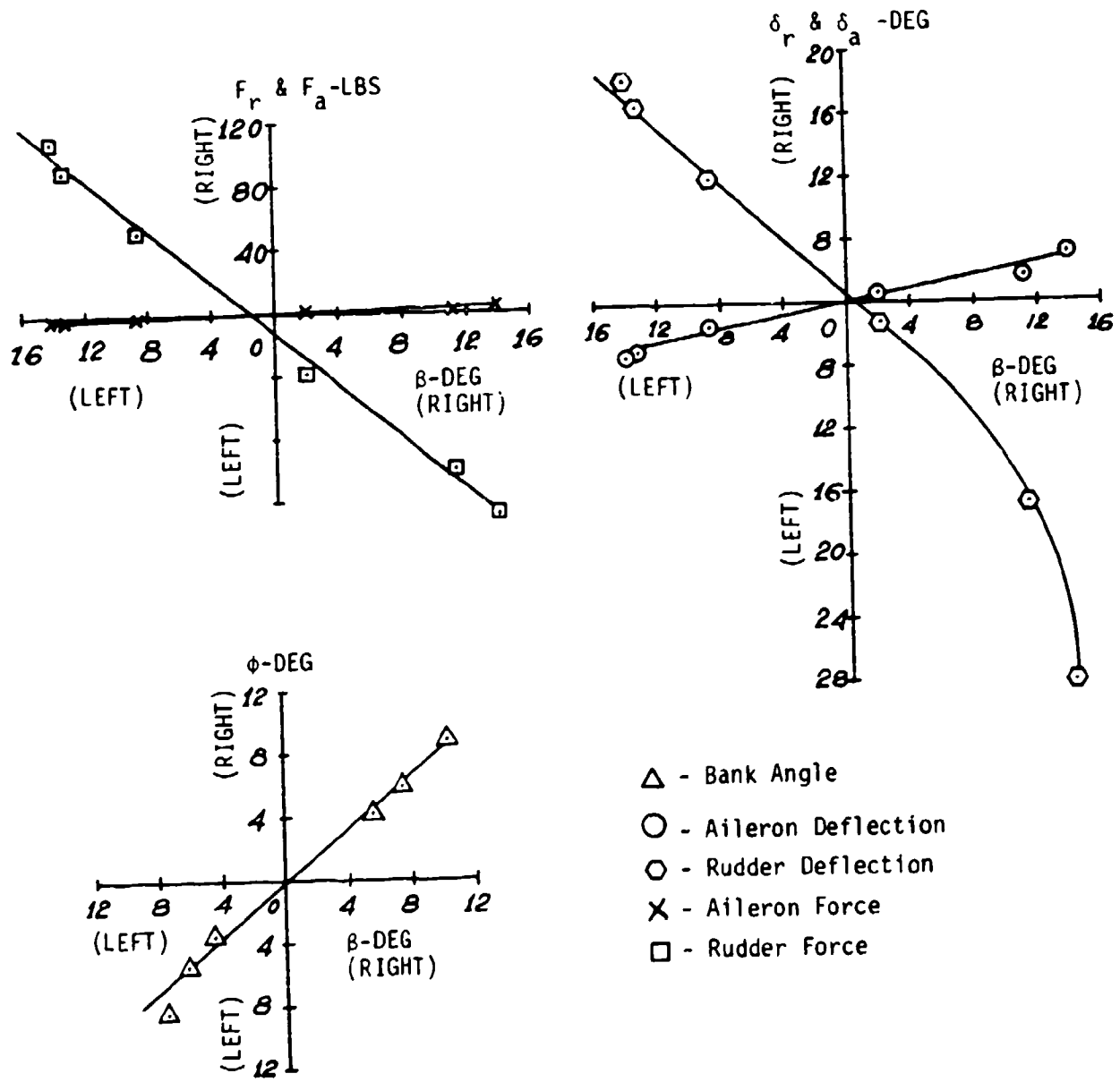


FIGURE 61

JETWING JW-1, N27BB
 LATERAL-DIRECTIONAL STABILITY
 POWER APPROACH
 3° APPROACH
 90 KIAS

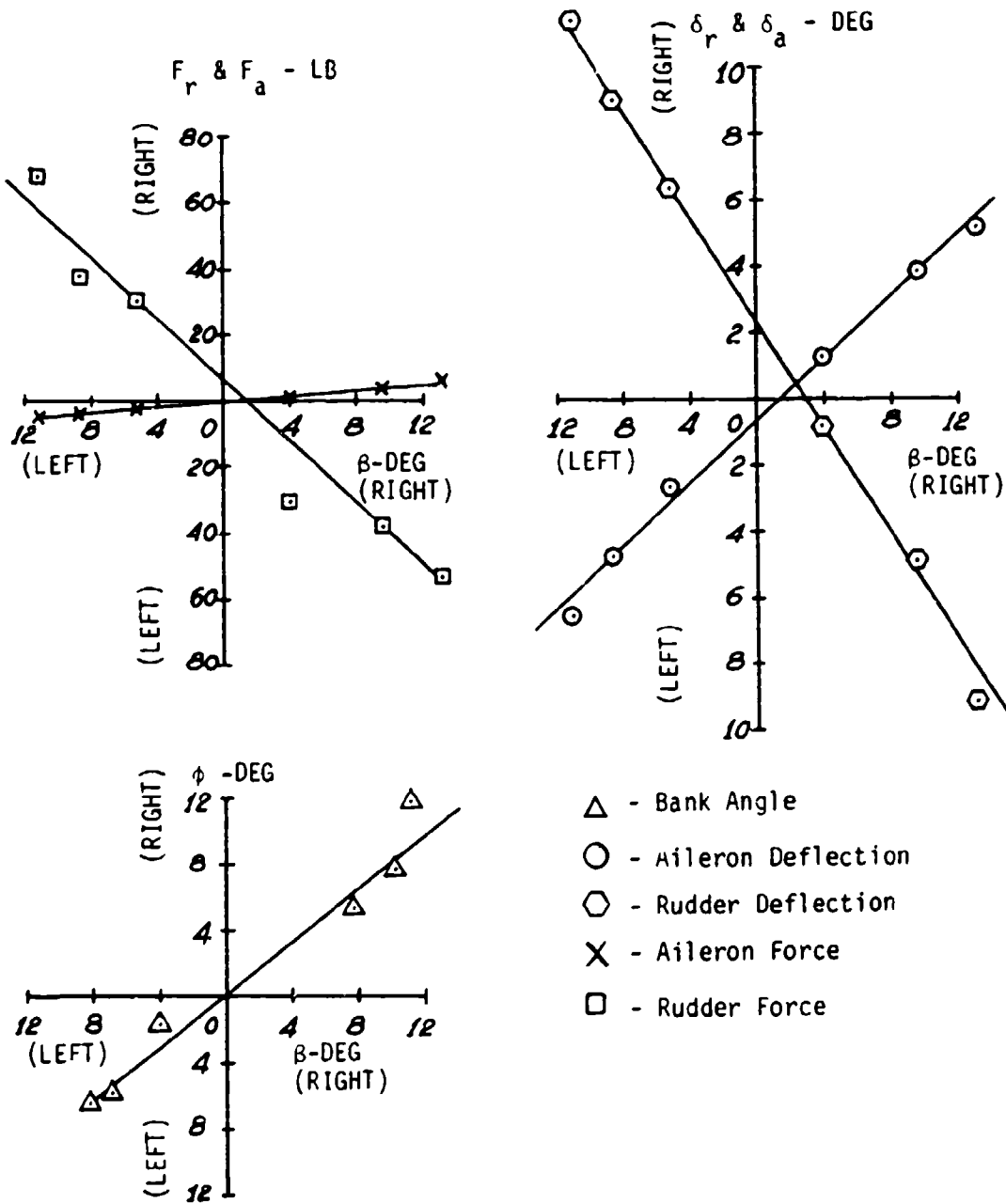


FIGURE 62

JETWING JW-1, N27BB
 LATERAL-DIRECTIONAL STABILITY
 LOW CRUISE
 110 KIAS

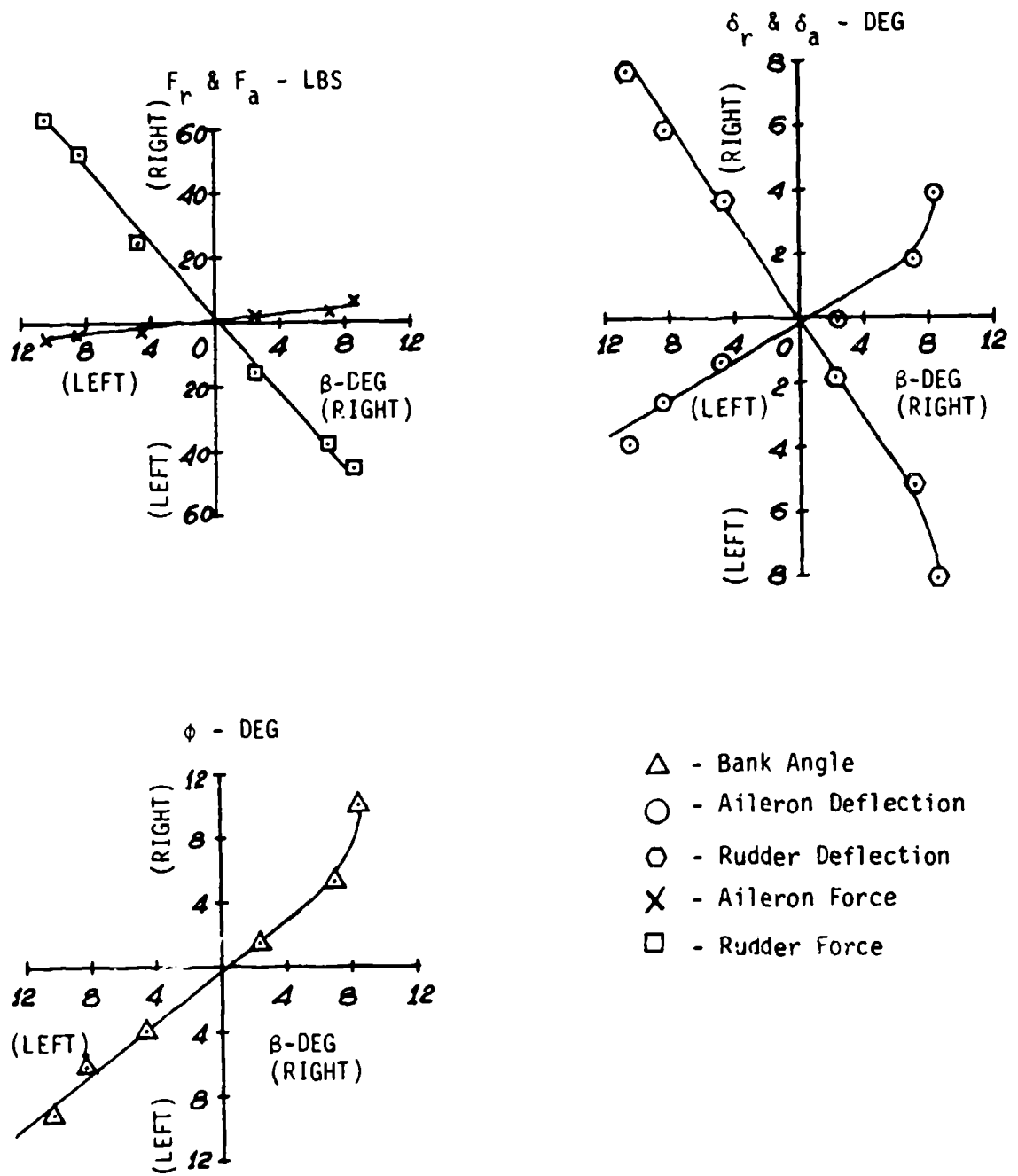


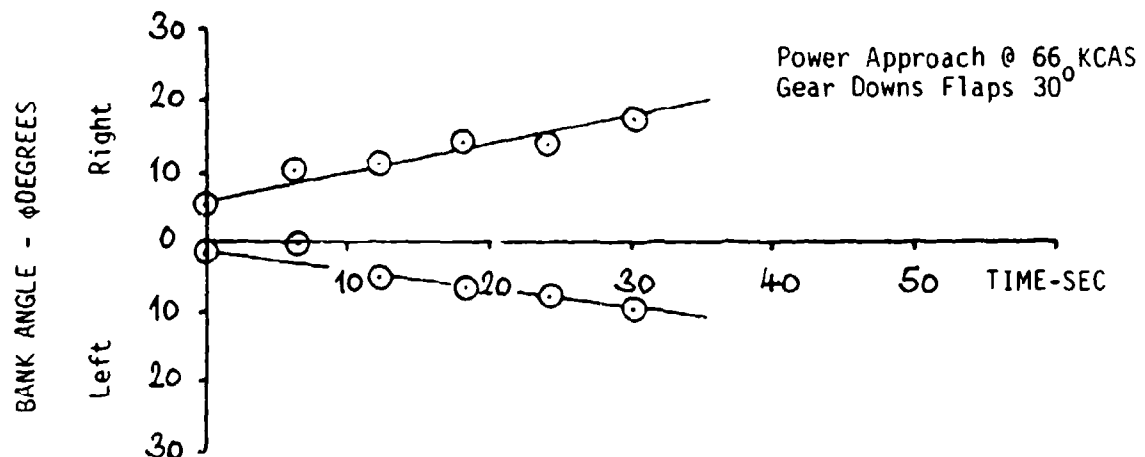
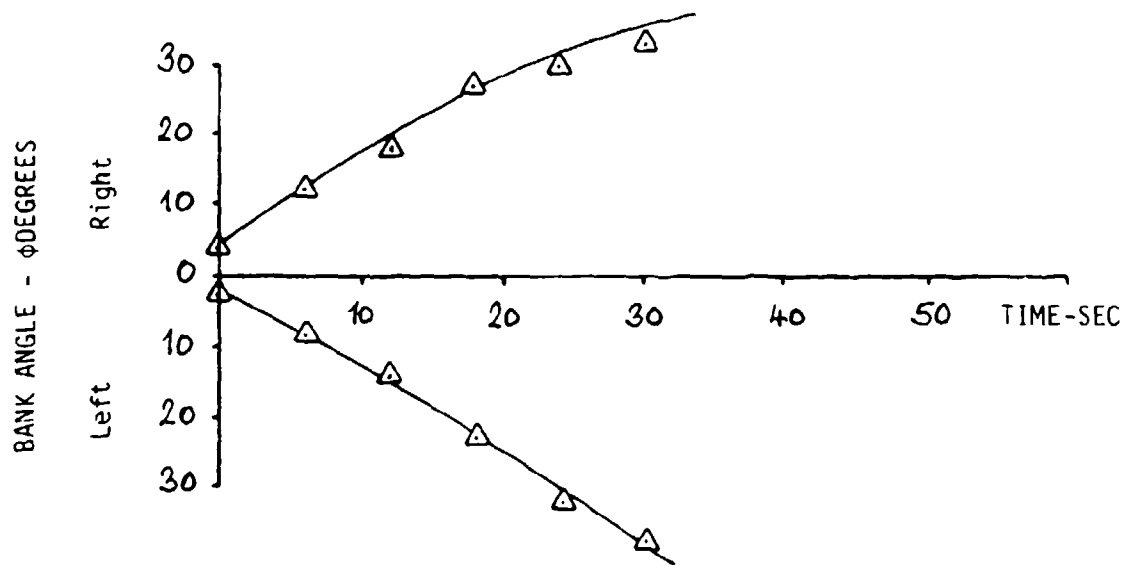
FIGURE 63

JETWING JW-1, N27BB
LATERAL-DIRECTIONAL STABILITY
CRUISE, 150 KIAS

FIGURE 64

JETWING JW-1
N27BB
SPIRAL STABILITY
3667 LB @ 35.37% M.A.C.

Cruise @ 132.5 KCAS
Gear & Flaps Up



Static and long period (Phugoid) dynamic longitudinal stability were measured in the climb and power approach configurations at three center of gravity positions. Longitudinal maneuvering stability and the longitudinal short period oscillation were measured in the low cruise and power approach configurations at the same three center of gravity positions. Longitudinal control and trim were evaluated at the most forward and most aft of these three positions. The three positions were:

1. 31.93% M.A.C. - Most Forward
2. 33.63% M.A.C. - Intermediate
3. 35.37% M.A.C. - Most Aft

This is not a very large center of gravity envelope. However, the ability to ballast the aircraft to more forward locations was limited by structural considerations, and for aft locations by flying safety. The most aft center of gravity shown represents the aircraft with full fuel, pilot, and test equipment.

a. STATIC LONGITUDINAL STABILITY, STICK FIXED AND STICK FREE. In the climb configuration the aircraft was unstable stick free at all of the centers of gravity tested as is shown by the slopes of stick force (F_s) versus calibrated airspeed (V_c) plots in Figures 65, 66, and 67. The aircraft was also unstable stick fixed in climb at all centers of gravity tested except for the most forward where it exhibited neutral stick fixed stability. These stability levels are shown by the plots of elevator position (δ_e) versus calibrated airspeed (V_c) in figures 65, 66, and 67.

The Power Approach configuration was slightly more well behaved than was climb. Power approach exhibits positive stick free and stick fixed stability at the most forward center of gravity as is shown in Figure 68. The stick fixed Power Approach stability was near neutral at other centers of gravity as may be seen from the δ_e versus V_c plots of figures 69 and 70.

The stick fixed and stick free longitudinal stability neutral points were determined using figures 65 through 70 and the extrapolation methods of Reference 4. The locations of these neutral points are summarized in Table 5.

TABLE 5
SUMMARY OF STATIC LONGITUDINAL
STABILITY NEUTRAL POINTS

CONFIGURATION	STICK FREE NEUTRAL POINT No'	STICK FIXED NEUTRAL POINT No
CLIMB	30% M.A.C.	32% M.A.C.
POWER APPROACH	32.5% M.A.C.	34.75% M.A.C.

FIGURE 65

JETWING JW-1, N27BB
 F_s and δ_e vs V_c
 CLIMB, GEAR AND FLAPS UP
 POWER - 93% N₁
 T.O. WEIGHT 3757 LB
 C.G. at 31.93% M.A.C.
 $\delta_s = 2.3^\circ$ L.E.D.

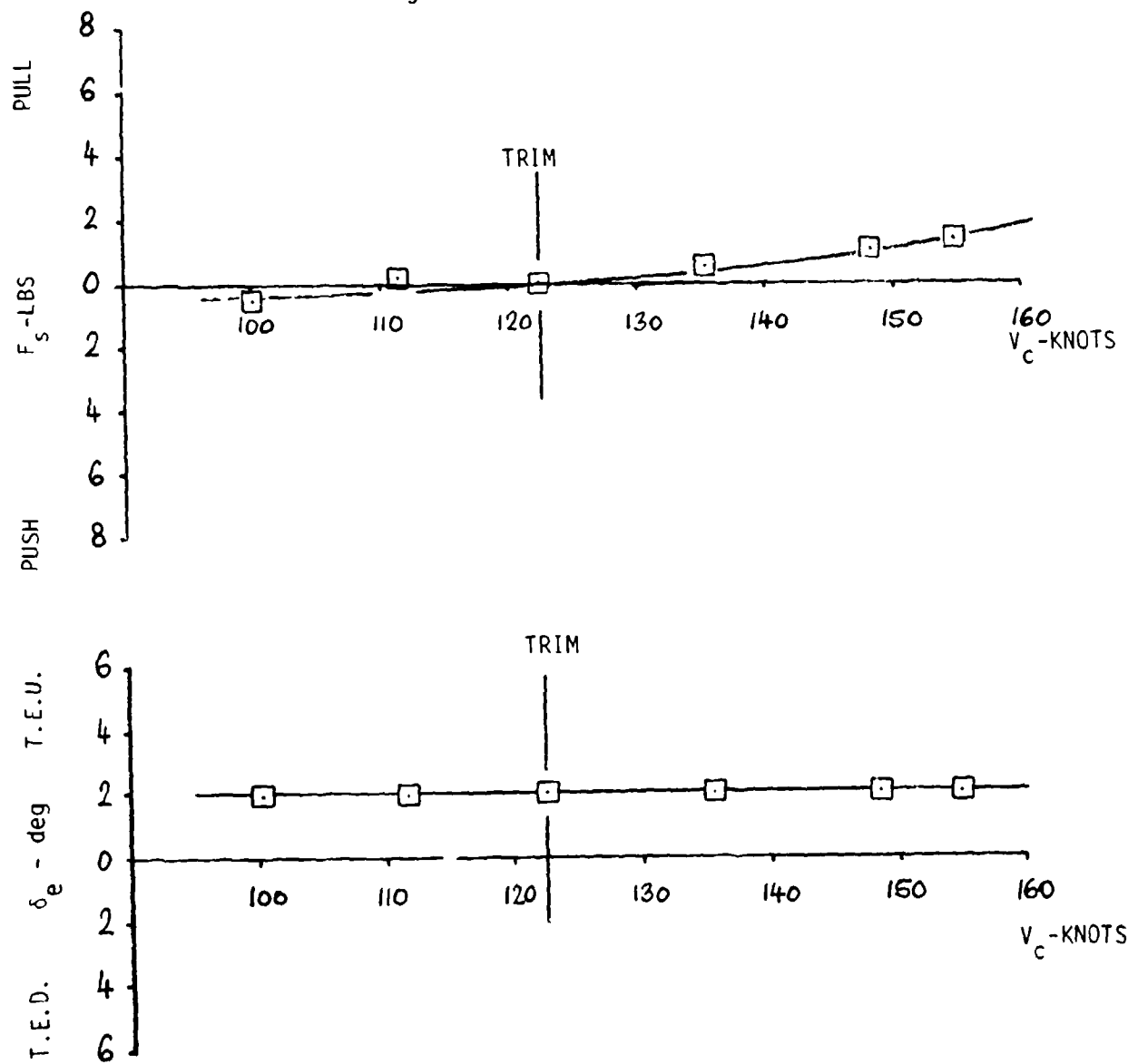


FIGURE 66

JETWING JW-1, N27BB
 F_s and δ_e vs V_c
 CLIMB, GEAR AND FLAPS UP
 POWER 93% N₁
 T.O. WEIGHT 3707 LB
 C.G. AT 33.63% M.A.C.
 $\delta_s = 1.95^\circ$ L.E.D.

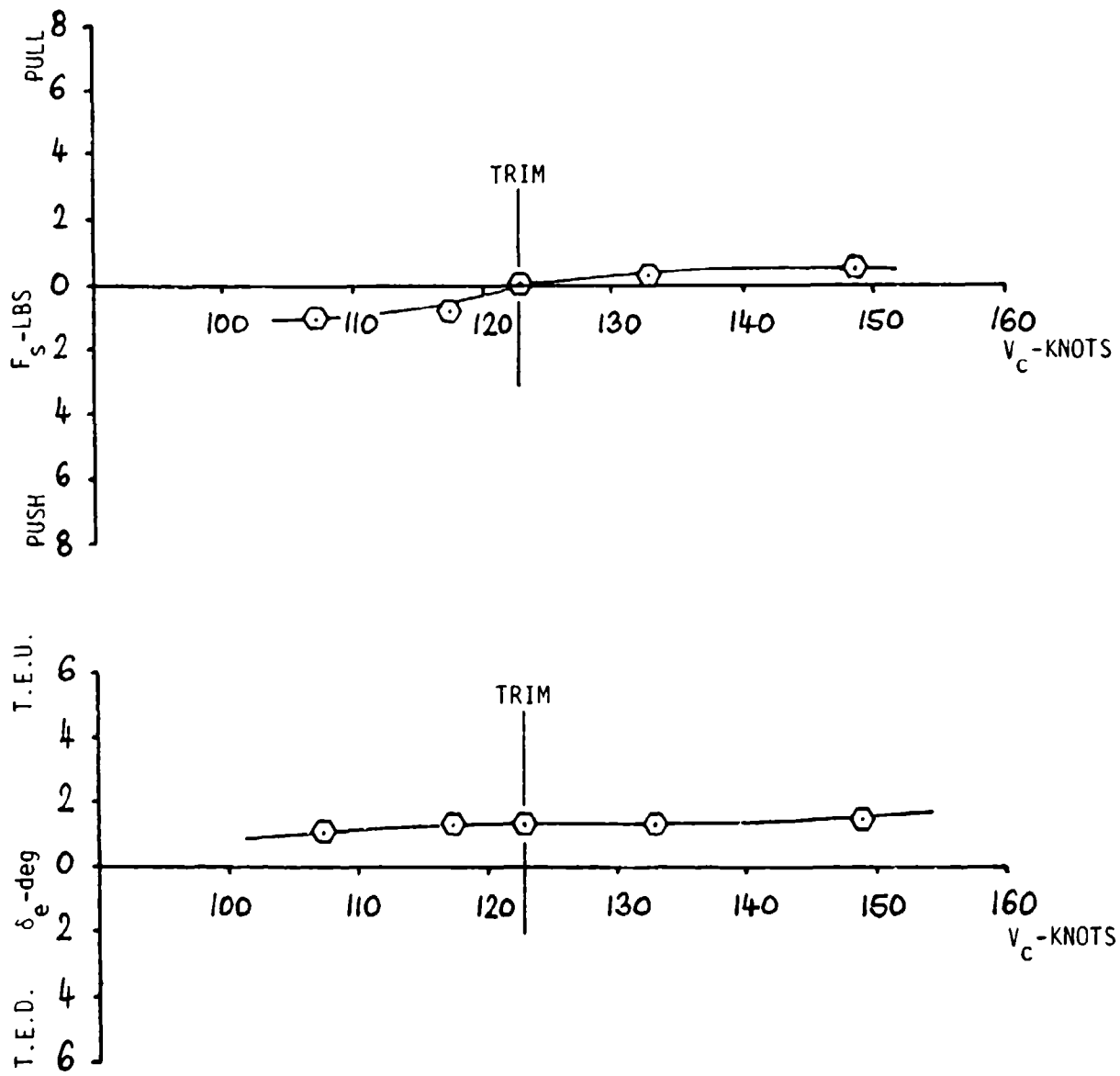


FIGURE 67

JETWING JW-1, N27BB
 F_s and δ_e vs V_c
CLIMB, GEAR AND FLAPS UP
POWER 93% N₁
T.O. WEIGHT 3657 LB
C.G. AT 35.37%, M.A.C.
 $\delta_s = 1.43^\circ$ L.E.D.

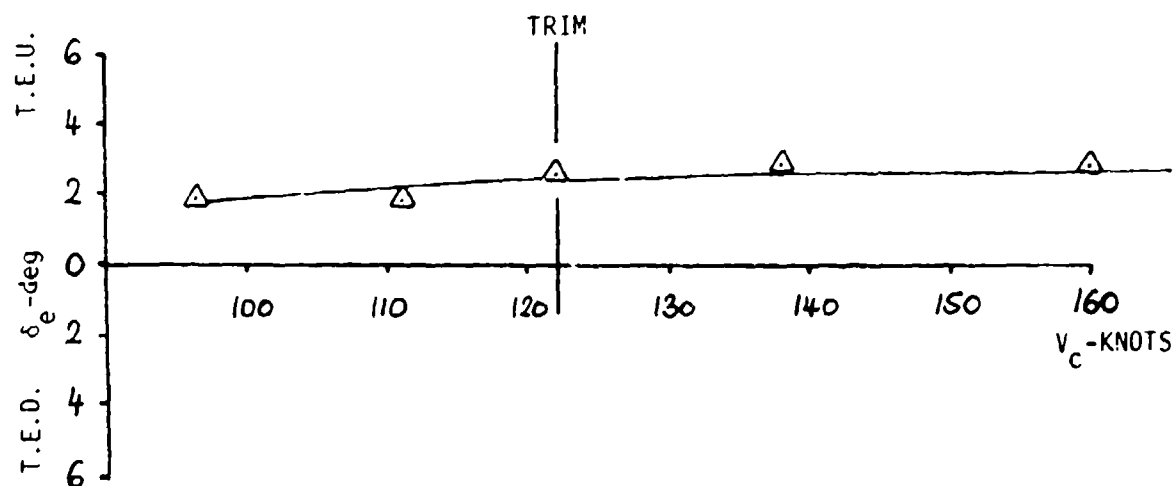
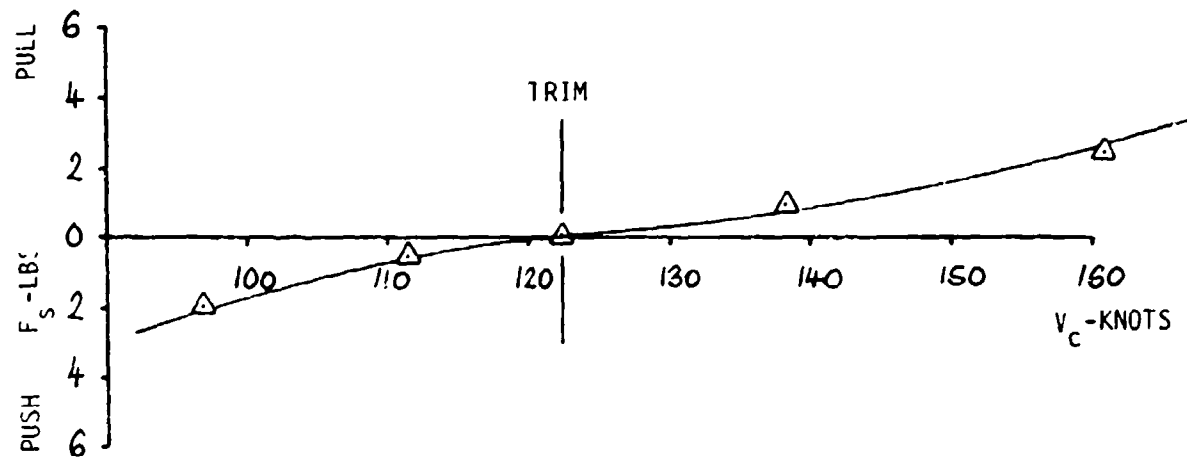


FIGURE 68

JETWING JW-1, N27BB
 F_s and δ_e vs V_c
 POWER APPROACH, GEAR DOWN
 FLAPS 30°, POWER FOR 30° DESCENT
 T.O. WEIGHT 3757 LB
 C.G. AT 31.93% M.A.C.
 $\delta_s = 2.93^\circ$ L.E.D.

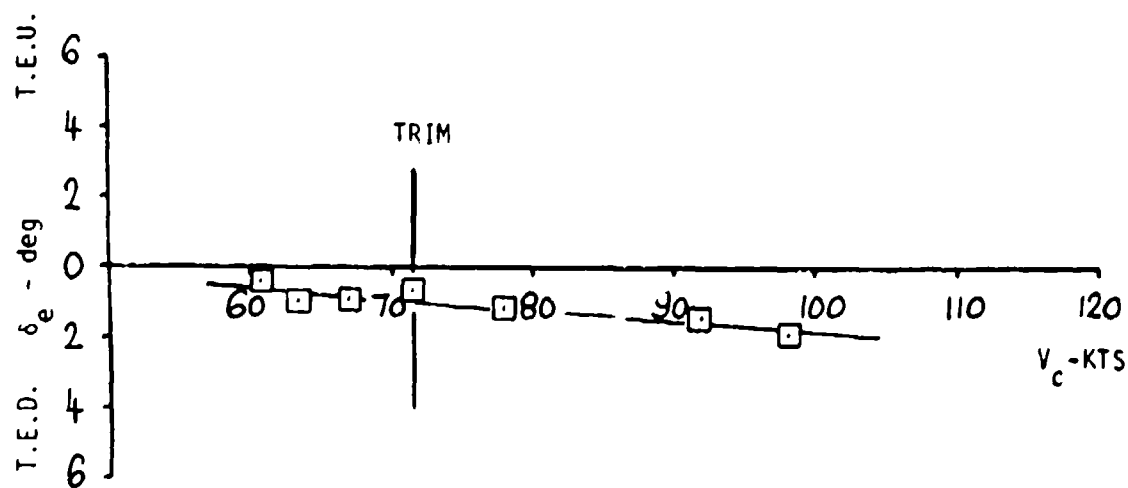
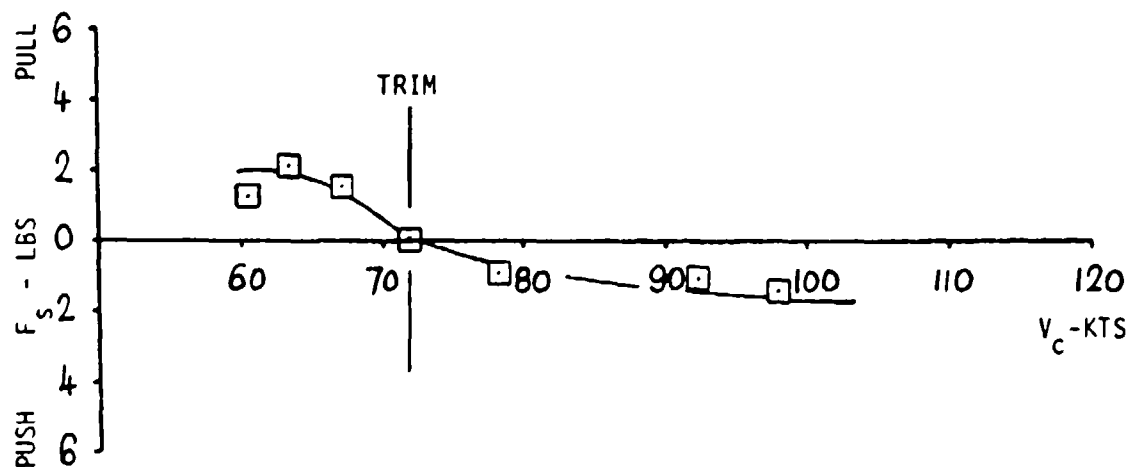


FIGURE 69

JETWING JW-1, N27B8
 F_s and δ_e vs V_c
 POWER APPROACH, GEAR DOWN
 FLAPS 30°, POWER FOR 3° DESCENT
 T.O. WEIGHT 3707 LB
 C.G. AT 33.63% M.A.C.
 $\delta_s = 0.98^\circ$ L.E.D.

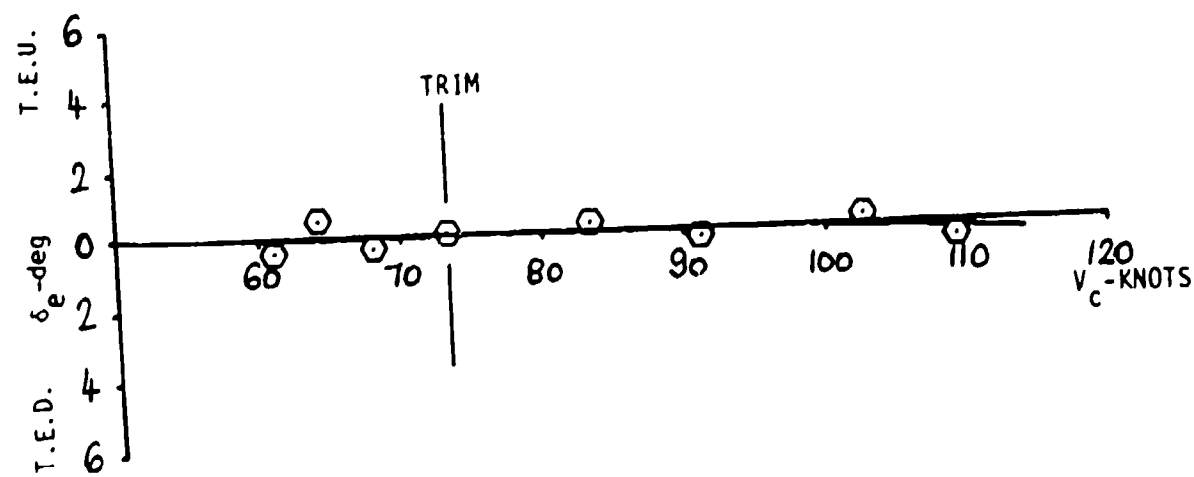
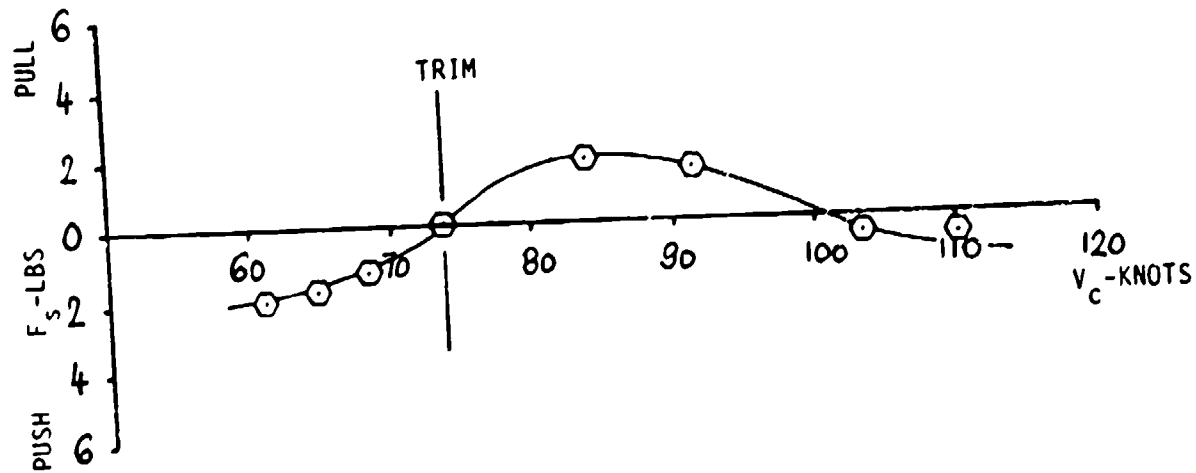
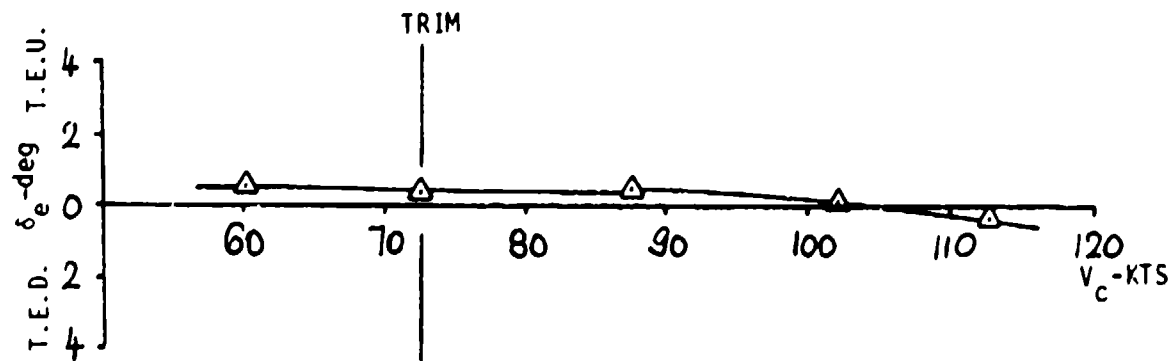
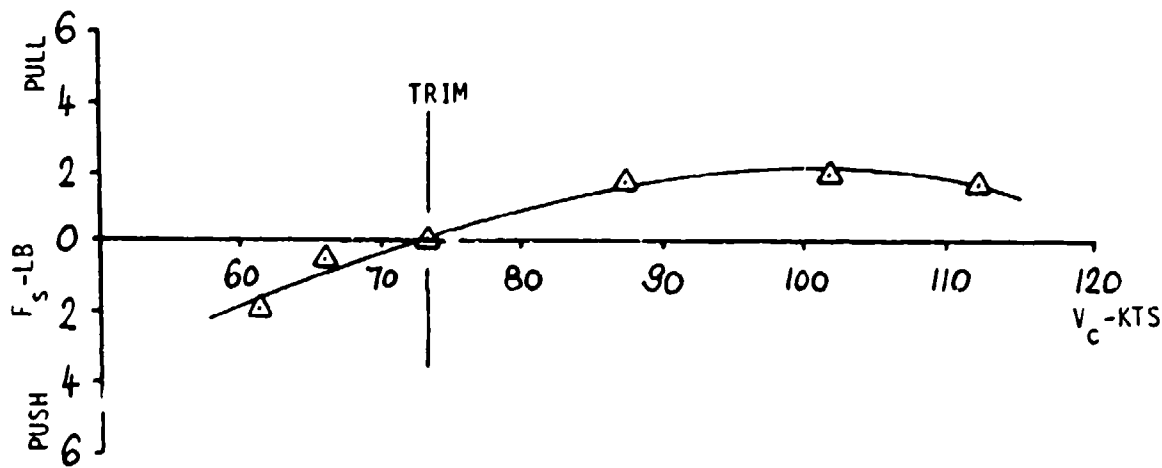


FIGURE 70
JETWING JW-1, N27BB
 F_s and δ_e VS V_c
POWER APPROACH, GEAR DOWN
FLAPS 30°, POWER FOR 3° DESCENT
T.O. WEIGHT 3657 LB
C.G. AT 35.37% M.A.C.
 $\delta_s = .2^\circ$ L.E.D.



There are two primary reasons for the static longitudinal instability of the Jetwing research aircraft. One reason is the high downwash created by the upper surface blowing. This high downwash tends to reduce the contribution of the horizontal tail to static longitudinal stability. This may be seen when one examines the horizontal tail term in the longitudinal stability equation.

The tail term is expressed by:

$$\frac{dC_M}{dC_L}_{\text{Tail}} = -\frac{a_t}{a_w} (\bar{V}_H) n_t (1 - \frac{d\varepsilon}{da}) \quad (6)$$

from Reference 5.

When the change in downwash with change in angle of attack term ($d\varepsilon/da$) approaches one, the tail's contribution to stability approaches zero. This relation seems to indicate that upper surface blowing concepts, such as that employed on the Jetwing, may be better adapted to Canard configurations which only depend upon the horizontal surface for balance and control, and not for longitudinal stability.

The high downwash may not be the prime cause for the instability of the Jetwing, however. If one compares the tail volume coefficient (\bar{V}_H) of the Jetwing with that of other recent powered lift aircraft one may discover another potential cause. Table 6 makes this comparison.

TABLE 6

HORIZONTAL TAIL VOLUME
COEFFICIENT COMPARISON

AIRCRAFT	\bar{V}_H
JETWING JW-1	0.74
YC-15	1.323*
YC-14	1.60*
NASA QSRA**	1.898†

* APPROXIMATE CALCULATION FROM SCALE DRAWINGS

** QUIET SHORHAUL RESEARCH AIRCRAFT

† FROM REFERENCE 6

This table shows that the Jetwing has only one half the tail volume coefficient of other recent powered lift aircraft, and may explain much of the reason for the poor longitudinal stability characteristics.

b. MANEUVERING STABILITY. Results of maneuvering stability tests in the low cruise configuration, as plots of stick force (F_s) and elevator position (δ_e), are shown in Figures 71, 72, and 73. These plots show low values of maneuvering stability as might be expected from an airplane with its center of gravity located aft of its longitudinal stability neutral point. Figures 74, 75, and 76 are similar plots for the power approach configuration. These plots show a somewhat better level of maneuvering stability and may partially account for the significant improvement in handling qualities when the aircraft is in the approach configuration. Maneuver points were extrapolated using the methods of Reference 4 and are summarized in Table 7.

TABLE 7

SUMMARY OF
MANEUVER POINT LOCATIONS

CONFIGURATION	STICK FORCE MANEUVER POINT	ELEVATOR POSITION MANEUVER POINT
LOW CRUISE	37.5% M.A.C.	42% M.A.C.
POWER APPROACH	41.5% M.A.C.	45% M.A.C.

The location of these maneuver points with respect to the longitudinal stability neutral points shows that the pitch damping is not significantly affected by the upper surface blowing concept used on the Jetwing.

During maneuvering stability tests in the power approach configuration at the most forward center of gravity the right outboard wing panel was apparently stalled. This occurred at a load factor of 1.65G which corresponds to a lift coefficient of $C_L = 3.24$ and at a C_j of 0.48. The aircraft rolled 90° right rather rapidly, but recovered from the maneuver by a normal stall recovery control application. Upon comparing the data from the event with the rolling moment (C_p) data from the NASA-AMES 40 x 80 foot wind tunnel, it was discovered that the flight test data correlated well with the wind tunnel data since the tunnel data shows large rolling moments developing at near the same lift coefficient. This tunnel data is shown in Figure 77. It is also interesting to note that at higher blowing coefficients the tunnel data shows that this rolling moment change does not develop. This data indicates that higher blowing will prevent the stall.

FIGURE 71

JETWING JW-1, N27BB
 F_s and δ_e VS n_z
CRUISE, GEAR AND FLAPS UP
133 KCAS, POWER FOR LEVEL FLIGHT
T.O. WEIGHT 3757 LBS
C.G. AT 31.93% M.A.C.
 $\delta_s = 2.6^\circ$ L.E.D.

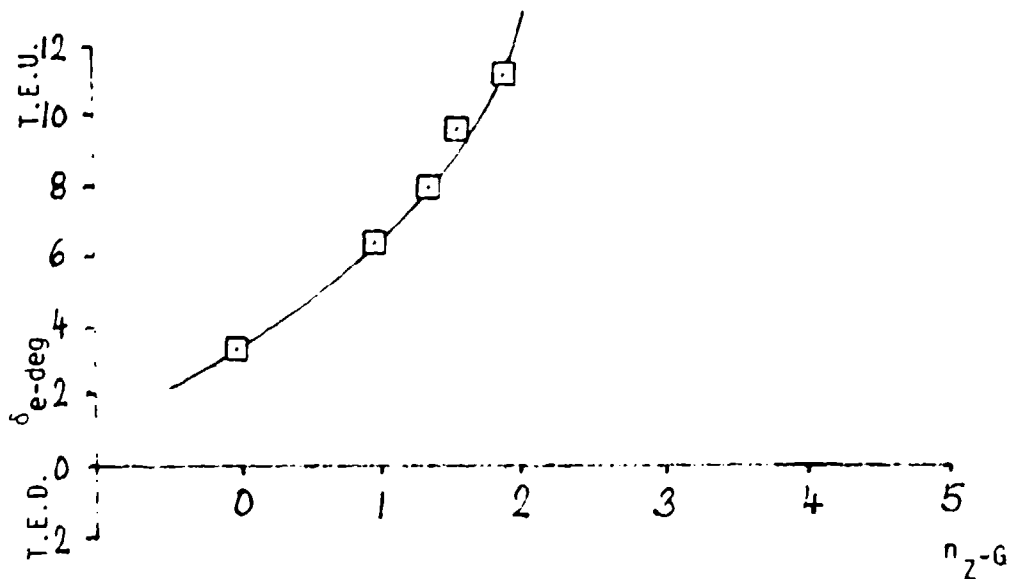
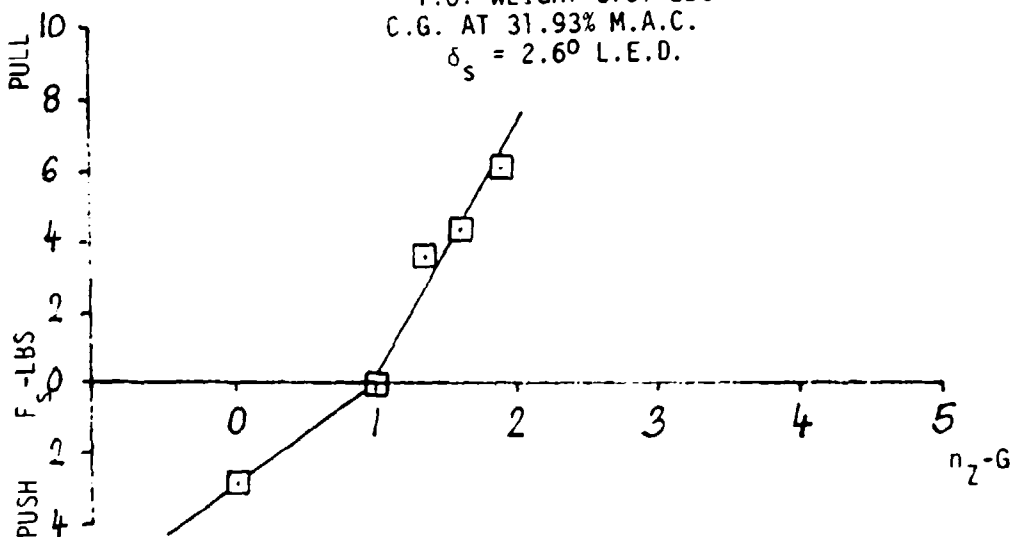


FIGURE 72

JETWING JW-1, N27BB
 F_s and δ_e vs n_z
CRUISE, GEAR AND FLAPS UP
133 KCAS, POWER FOR LEVEL FLIGHT
T.O. WEIGHT 3707 LBS
C.G. AT 33.63% M.A.C.
 $\delta_s = 1.82^\circ$ L.E.D.

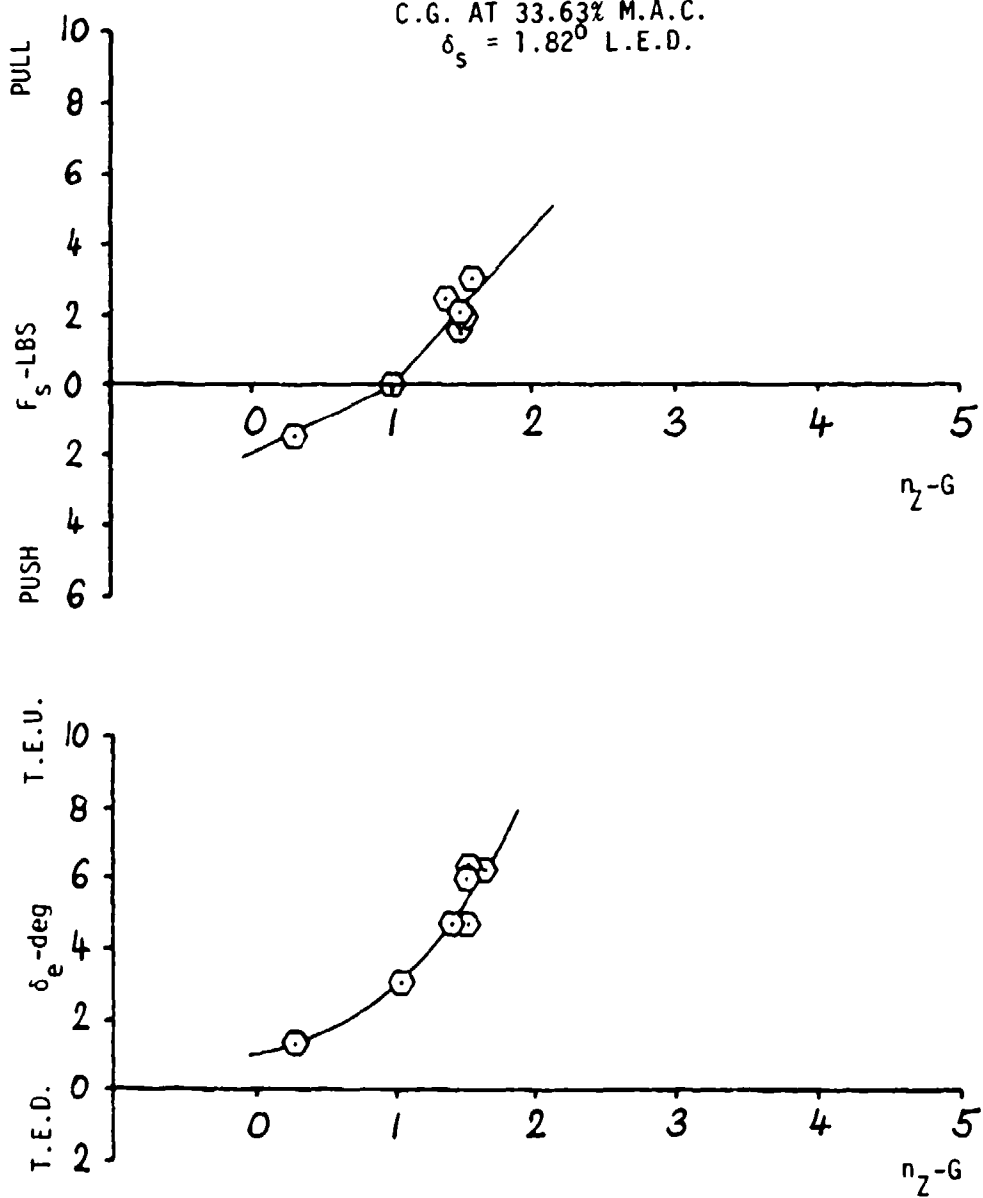


FIGURE 73

JETWING JW-1, N27BB
 F_s and δ_e vs n_z
CRUISE, GEAR AND FLAPS UP
133 KCAS, POWER FOR LVL. FLT.
T.O. WEIGHT 3657 LBS
C.G. AT 35.37% M.A.C.
 $\delta_s = 1.82^\circ$ L.E.D.

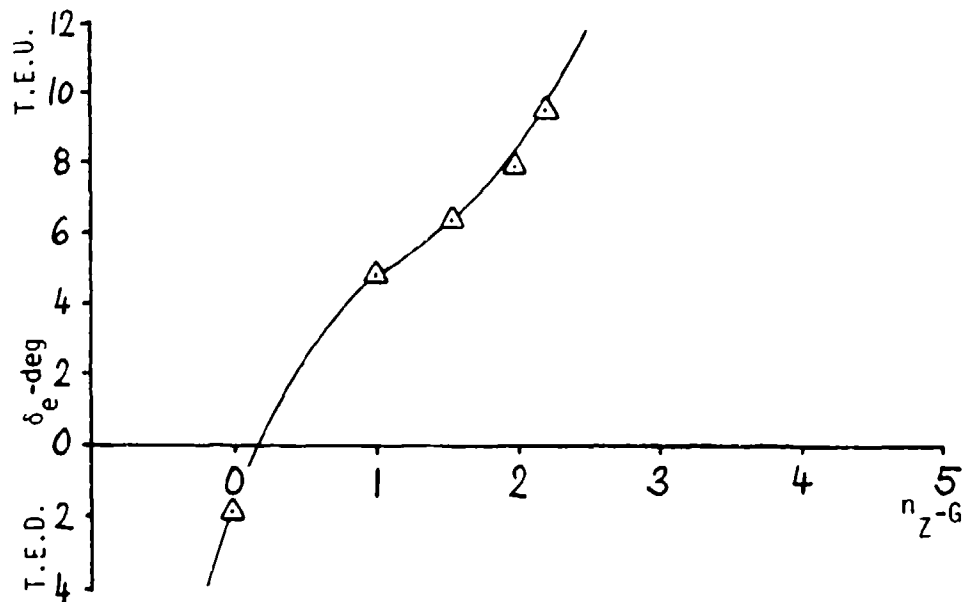
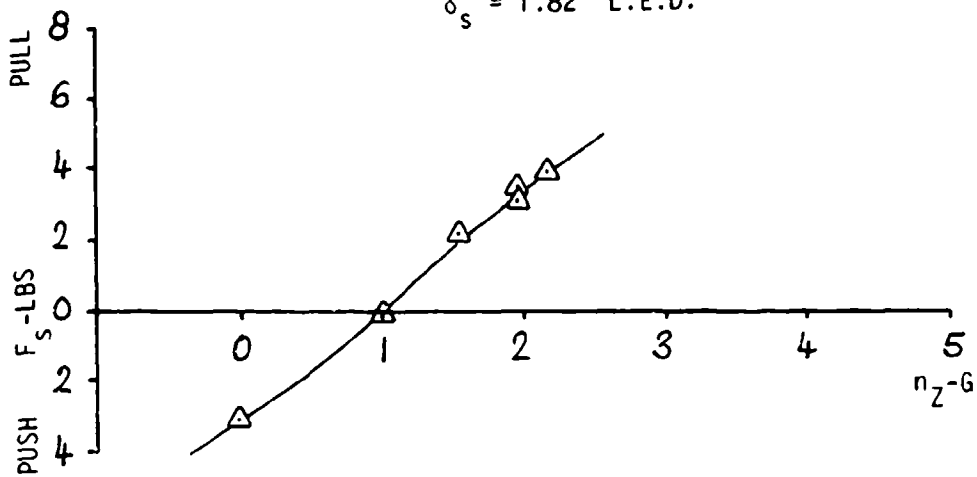


FIGURE 74a

JETWING JW-1, N27BB
 F_s vs n_z
POWER APPROACH, GEAR DOWN
FLAPS 30°, 71 KCAS
POWER FOR 3°, DESCENT
T.O. WEIGHT 3757 LB
C.G. AT 31.93% M.A.C.
 $\delta_s = 2.3^\circ$ L.E.D.

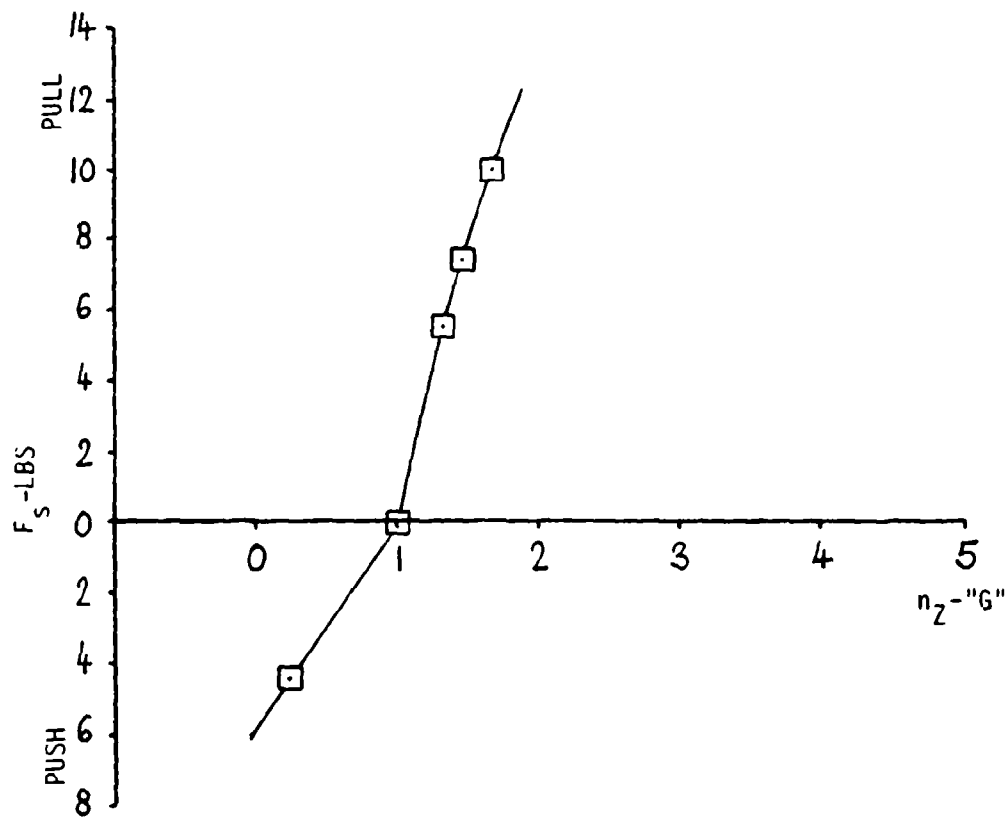


FIGURE 74b

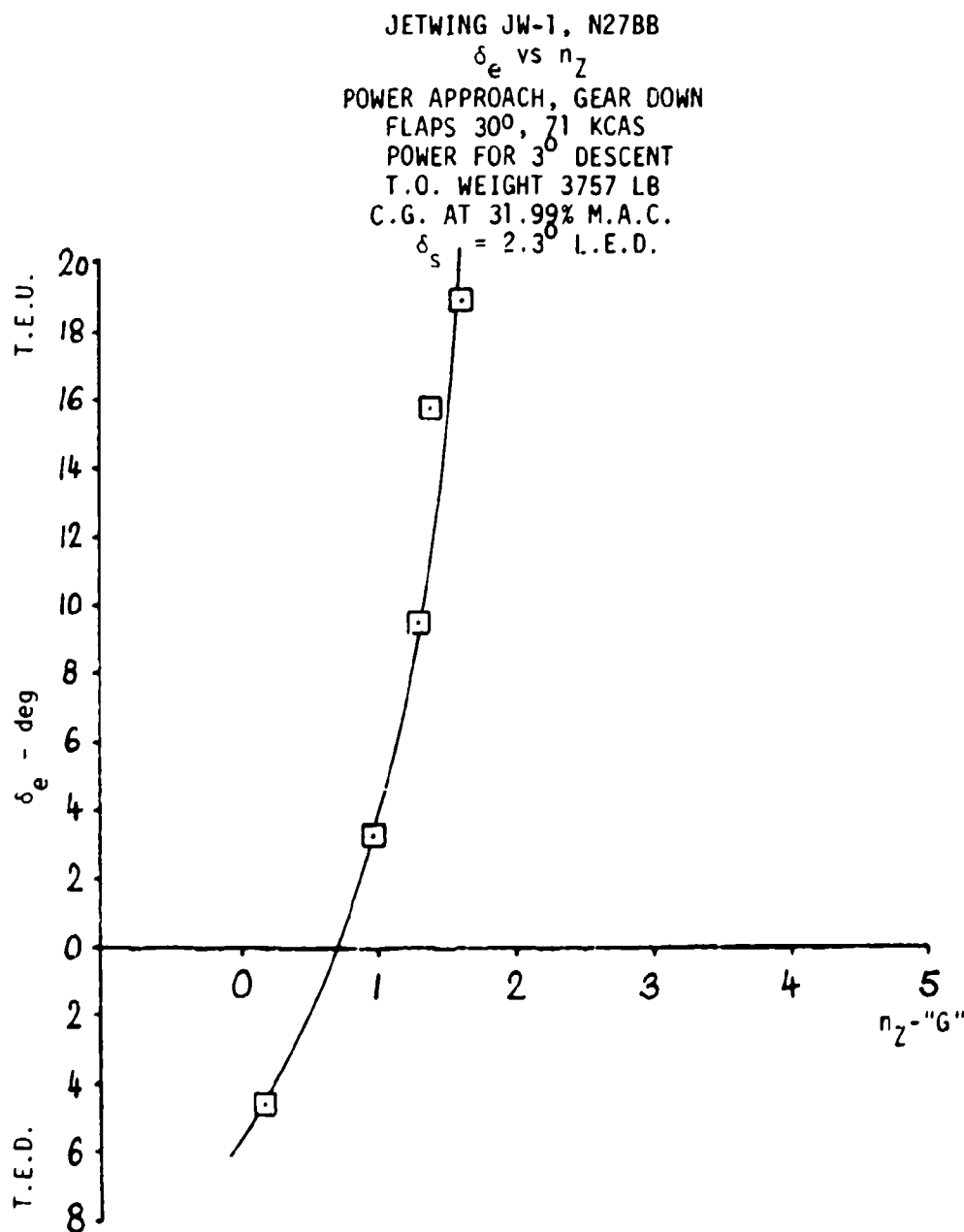


Figure 75a

JETWING JW-1, N27BB
 F_s vs n_z
FLAPS 30°, 71 KCAS
POWER FOR 30° DESCENT
T.O. WEIGHT 3707 LBS
C.G. AT 33.63% M.A.C.
 $\delta_s = 1.3^\circ$ L.E.D.

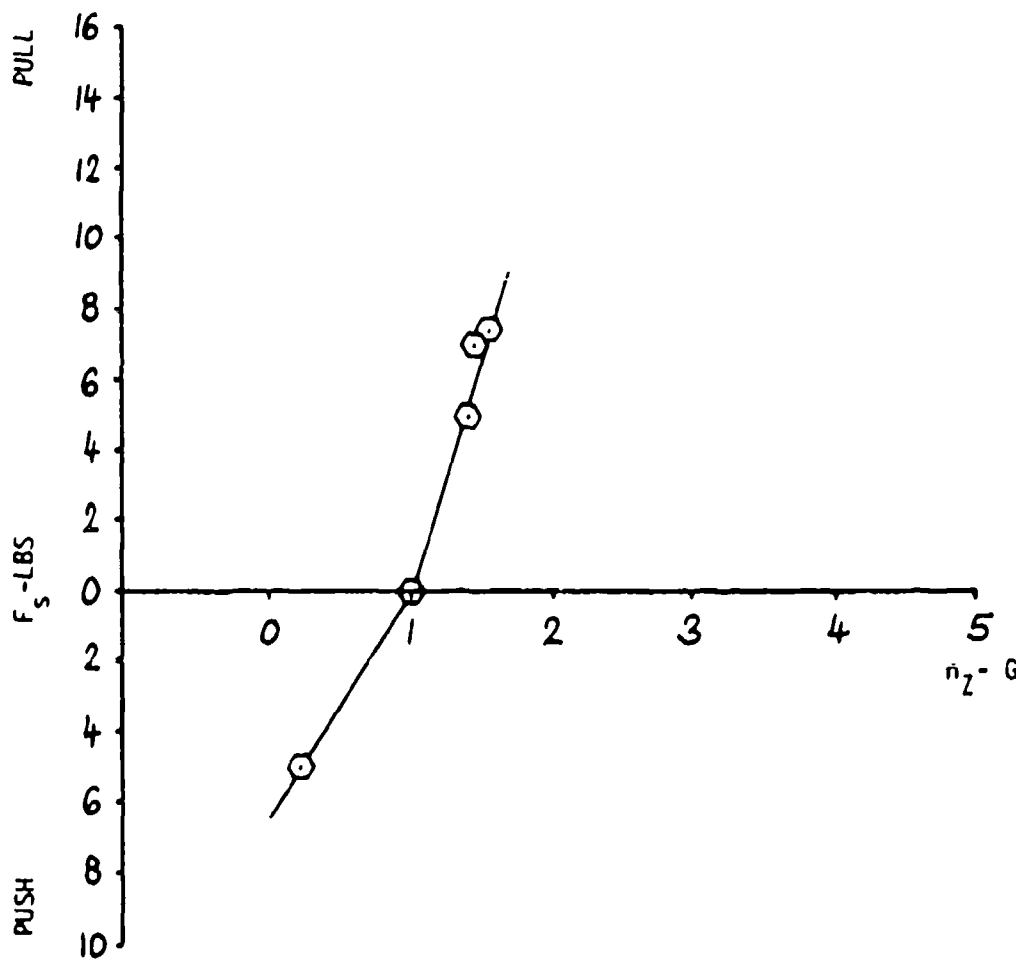


FIGURE 75b

JETWING JW-1, N27BB

 δ_e VS n_2

POWER APPROACH, GEAR DOWN

FLAPS 30°, 71 KCAS

POWER FOR 3° DESCENT

T.O. WEIGHT 3707 LBS

C.G. AT 33.63% M.A.C.

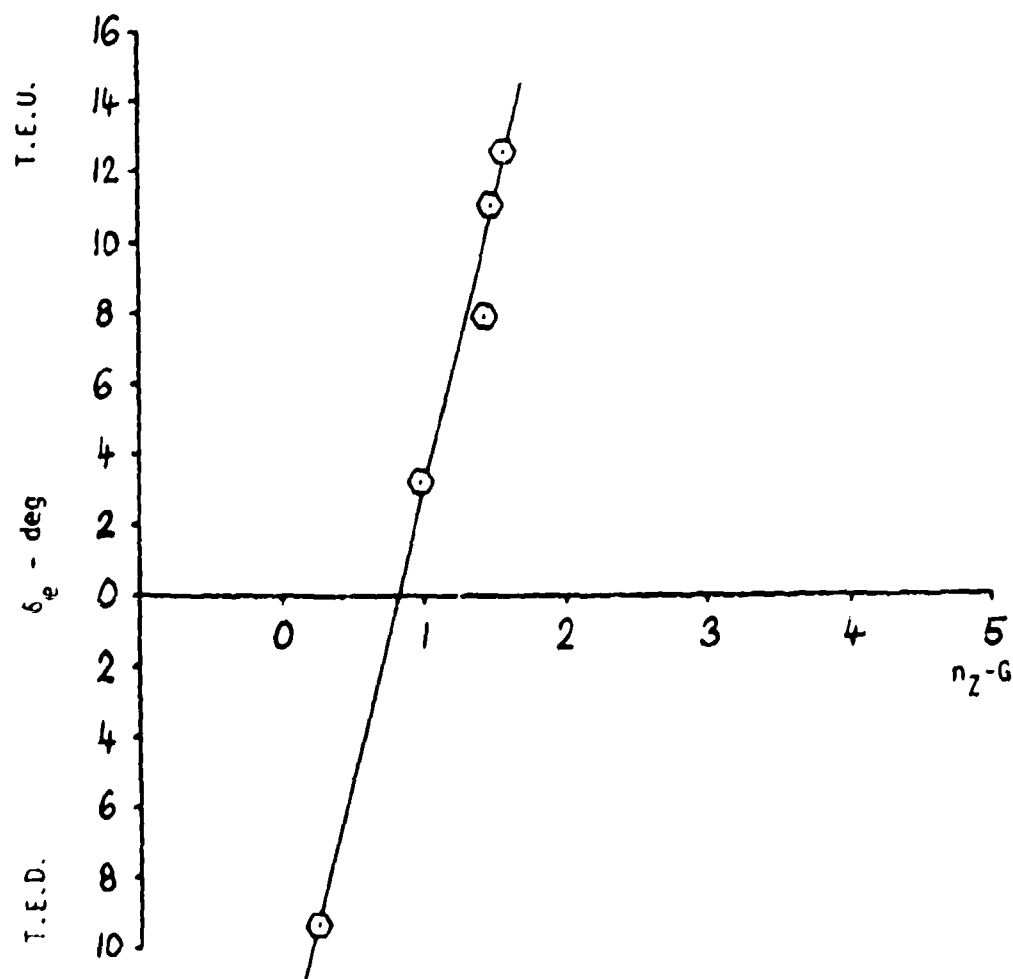
 $\delta_s = 1.3^\circ$ L.E.D.

FIGURE 76

JETWING JW-1, N27BB
 F_s and δ_e vs N_z
POWER APPROACH, GEAR DOWN
FLAPS 30° 71 KCAS
POWER FOR 3° DESCENT
T.O. WEIGHT 3657 LB
C.G. at 35.37%

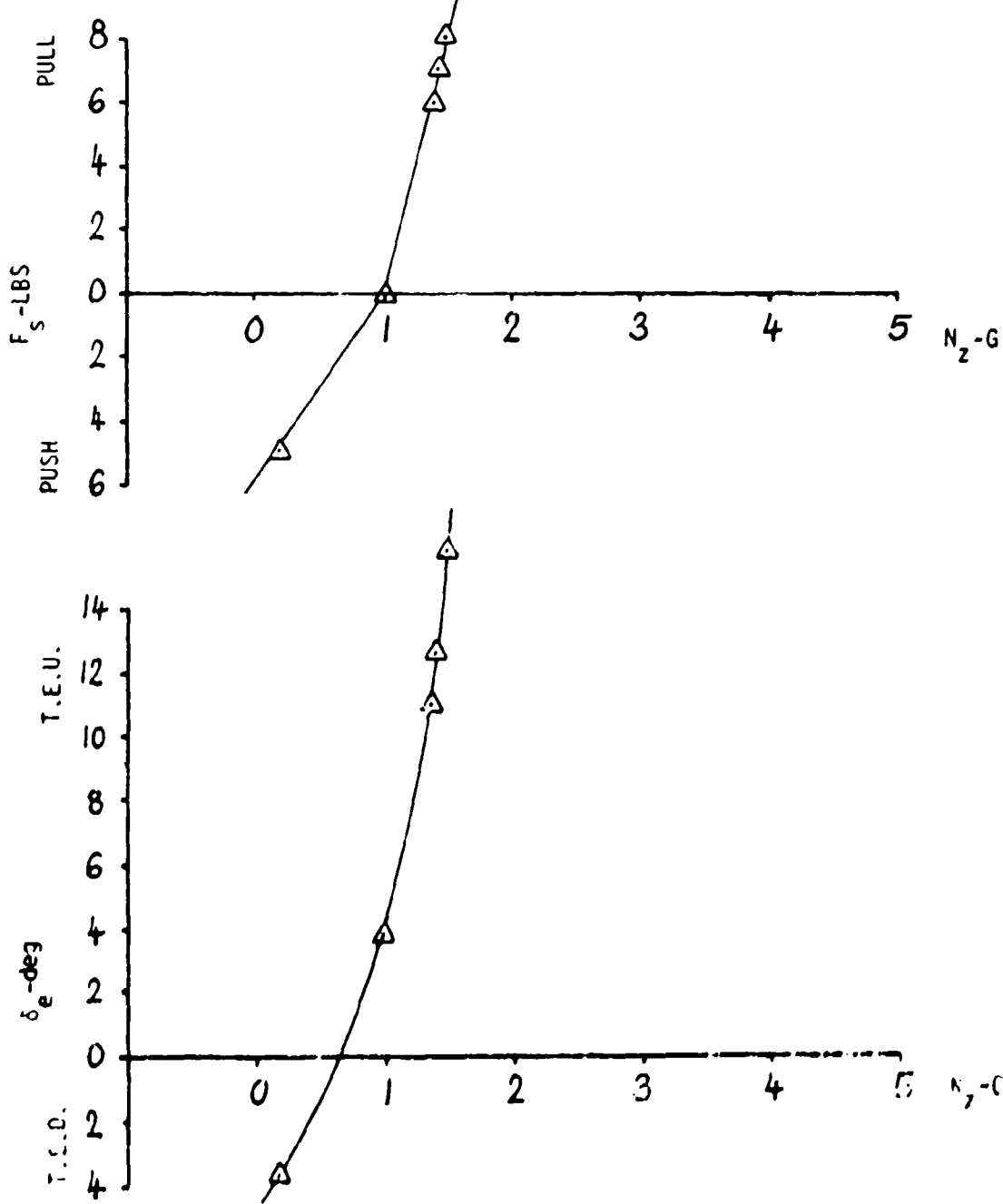
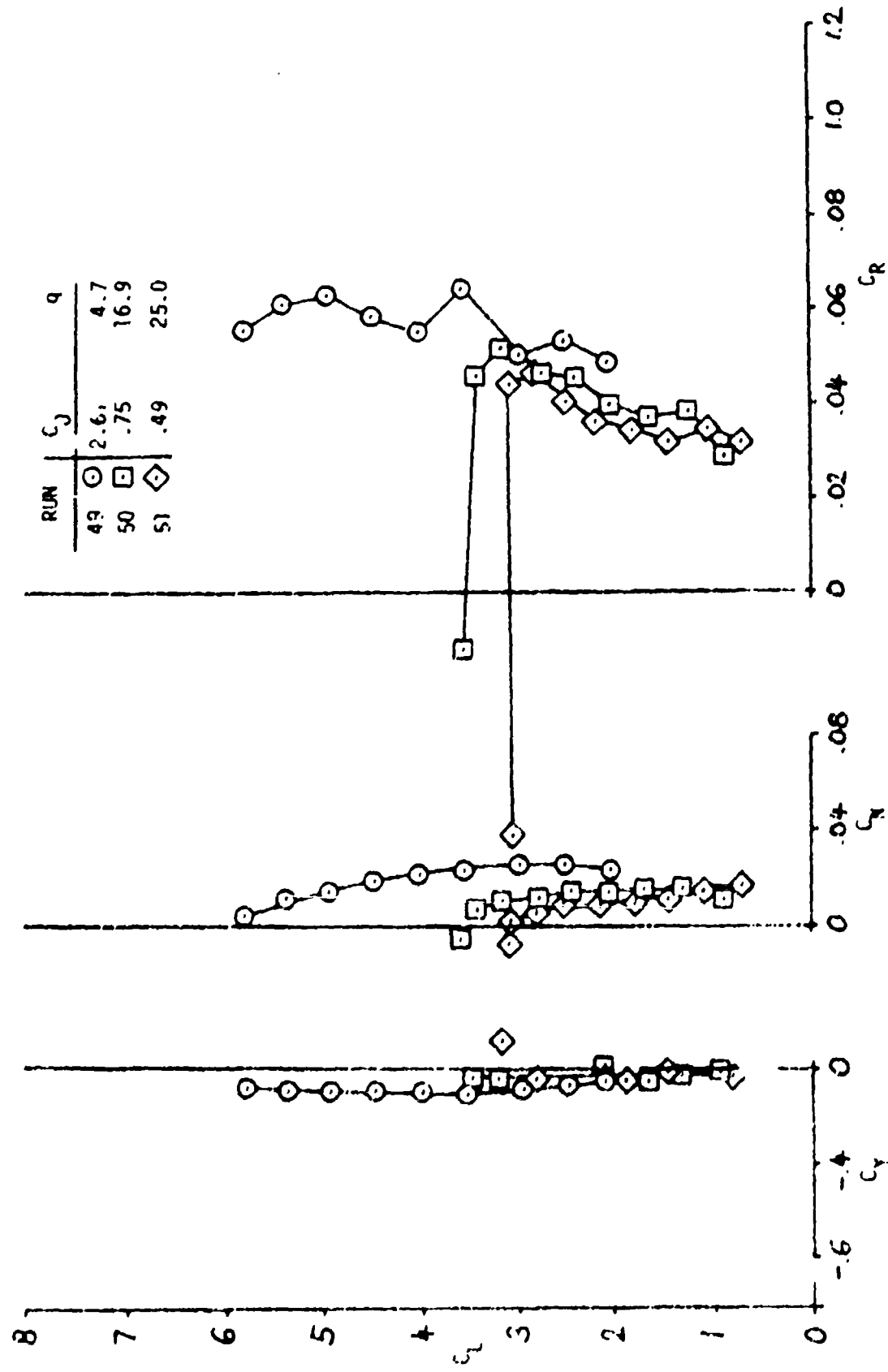


FIGURE 77

T-498
 GEAR DOWN/ δ_f = 30/ δ_a = + 15/ δ_e = 0/ δ_s = 0
 δ_r = 0/UPPER WING OFF/ δ_{rev} = 0/c.g. 0.41c



C. FLIGHT PATH STABILITY. The flight path stability of the Jetwing is excellent, with little change occurring in the slope of the flight path angle (γ) versus airspeed curve through a wide range of approach airspeeds. This level of flight path stability is reflected in the plot of flight path angle versus equivalent airspeed in the power approach configuration shown in figure 44. The aircraft will meet the flight path stability requirements of MIL-F-8785B for Level 1, having a slope of flight path angle versus airspeed of .0667 degrees/knot at its 70 knot approach speed. At five knots below this speed the slope has changed only .033 degrees/knot. This good level of flight path stability reduces pilot workload during the approach and allows him to concentrate his efforts upon overcoming the longitudinal instability. Excellent flight path stability appears to be one of the handling qualities pluses for powered lift aircraft.

D. LONGITUDINAL DYNAMIC STABILITY. The long period dynamic longitudinal stability, or Phugoid oscillation was evaluated in the same configurations and centers of gravity as was the static longitudinal stability. In the climb configuration the aircraft displayed an aperiodic divergence at all centers of gravity tested. Results at the most forward and most aft centers of gravity tested are shown in Figures 78 and 79. Such results might be expected from an aircraft which is at, or behind, its stick fixed neutral point.

In power approach the aircraft was somewhat better behaved. Phugoid oscillations did occur at the most forward and intermediate centers of gravity, but did not occur at the aft center of gravity. Table 8 summarizes the results in this configuration.

TABLE 8
JETWING POWER APPROACH
PHUGOID SUMMARY

C.G. POSITION	PERIOD	DAMPING FACTOR	NATURAL FREQUENCY
31.93% M.A.C.	21.2 sec	-.1	0.298 Rad/sec
33.63% M.A.C.	21 sec	-.05	0.3 Rad/sec
34.4% M.A.C.	No oscillation	---	---

Results did not vary significantly between controls free and controls fixed.

The longitudinal short period motion was evaluated in the same configurations as was the maneuvering stability. In the low cruise configuration the short period has a half cycle time of approximately 0.4 seconds with a damping factor (ζ_{sp}) in excess of 0.5. The natural frequency (ω_{nsp}) was approximately 5 Rad/sec.

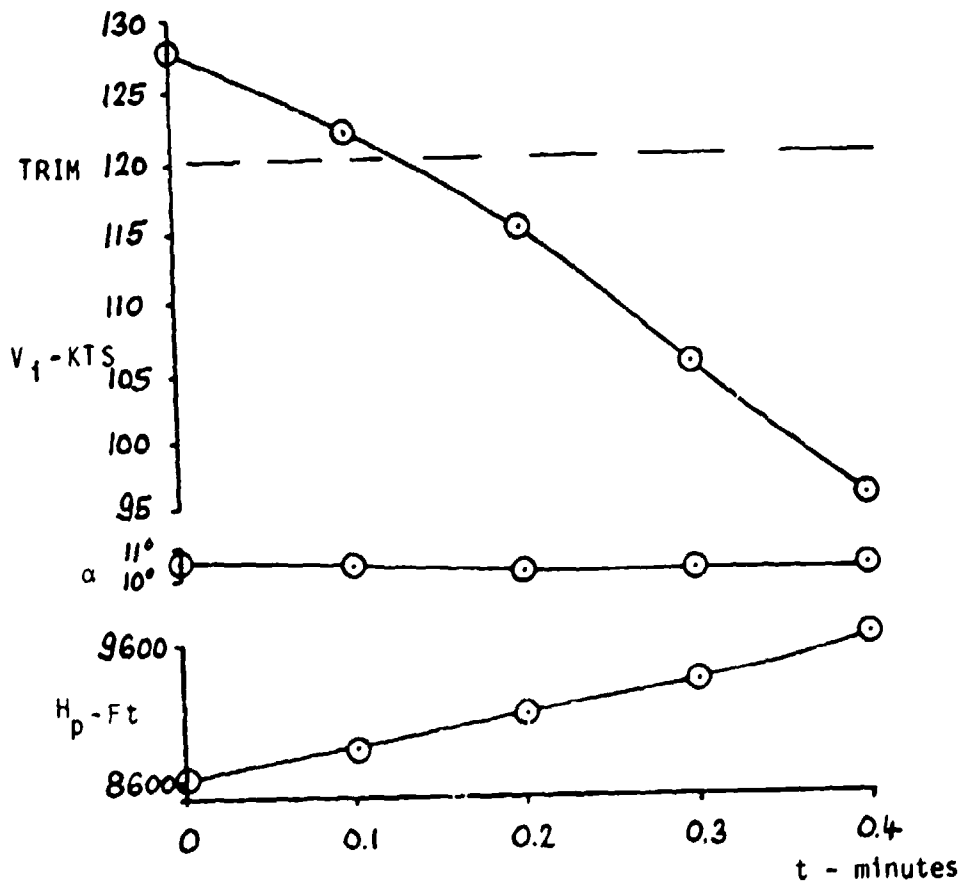


FIGURE 78
JETWING JW-1, N27BB
CLIMB PHUGOID
3757 LB @ 31.93% M.A.C.
TRIM AIRSPEED - 120 KIAS
CLEAN CONFIGURATION

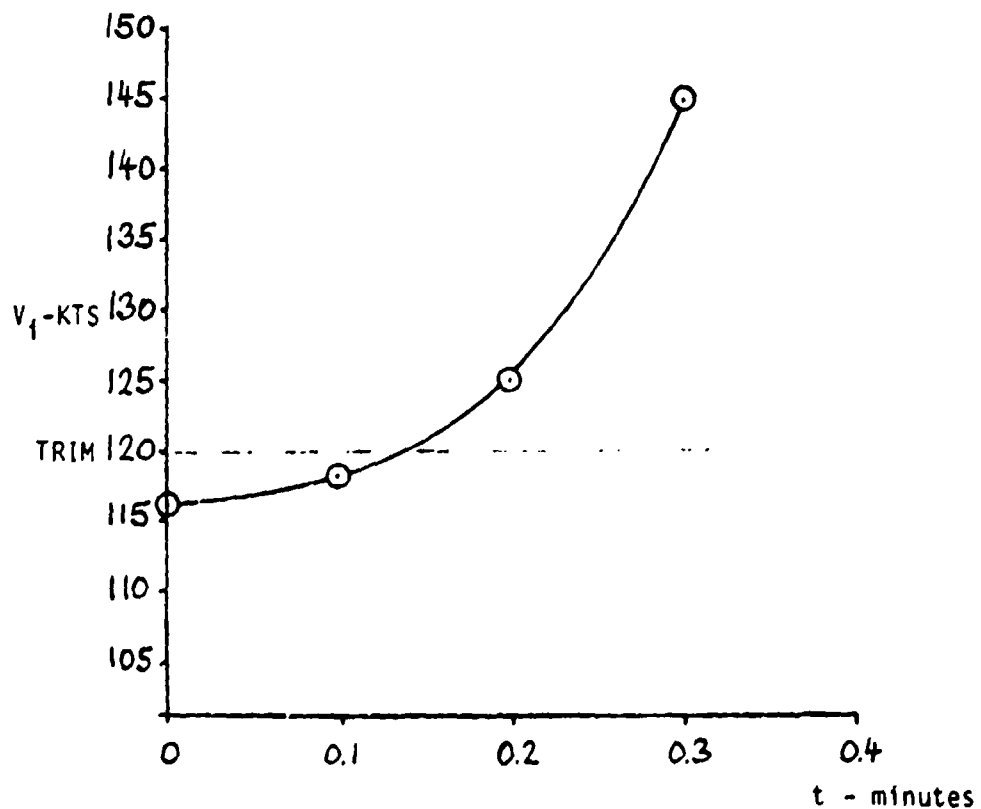


FIGURE 79

JETWING JW-1, N27BB
CLIMB PHUGOID
3657 LB @ 35.37% M.A.C.
TRIM AIRSPEED 120 KIAS
CLEAN CONFIGURATION

The power approach short period oscillation was so heavily damped that it was not possible to determine its parameters with the instrumentation installed.

e. LONGITUDINAL CONTROL AND TRIM. Longitudinal trim changes were evaluated for the configurations shown in Table 2 at the most forward and most aft centers of gravity. Two and one half pounds was the maximum stick force experienced for any of these trim changes at either center of gravity position. In other words longitudinal trim changes are almost non-existent, considerably reducing pilot workload.

Longitudinal control was more than adequate for all flight conditions except those at very low airspeed. During performance testing a partial horizontal tail stall was experienced at a calibrated airspeed of 52 knots, with gear down and flaps extended 30°. The power setting was approximately 90% N_1 . This phenomenon had also been experienced during the Ball-Bartoe flight test, but only with greater flap settings.

The problem is caused by the rather thin (8% thick) symmetrical horizontal tail section, which has a small leading edge radius, and the high downwash created by the deflected flaps and the upper surface blowing. As was stated earlier upper surface blowing concepts such as this might be more effective as Canard configurations. If conventional tail configurations are used they should have special treatment such as camber, increased thickness and a large leading edge radius.

10. APPROACH HANDLING QUALITIES EVALUATION. The approach to landing is a time of high pilot workload especially when landing upon the pitching deck of an aircraft carrier. Therefore, if powered lift concepts are to be used aboard ships they must not require a higher pilot workload than do conventional aircraft. As a result, the approach handling qualities while tracking glideslope and deck centerline should be equal to or better than conventional aircraft.

The approach handling qualities for the Jetwing were evaluated on 3° and 6° glideslope approaches with the aircraft loaded to its most aft center of gravity location. Ten approaches were flown on each glideslope using a Visual Approach Slope Indicator (VASI) as a glideslope reference. Approaches were flown in varying levels of atmospheric turbulence and in headwind, tailwind, and windshear conditions to determine the effects of these parameters on the handling qualities and pilot workload.

The evaluation methods consisted of having the pilot assign a Cooper-Harper Rating to each approach and to record time histories of all primary control movements during the approach. The control movement time histories were time sequenced with a 16mm movie camera mounted atop the vertical fin. This movie film showed how well the pilot tracked the glideslope and runway centerline and gave some indication of the reason for the control movements.

Figure 80 shows typical control movement time histories for 3° and 6° approaches. These traces show that the number of control movements during a typical 3° and 6° approach is not large. The number of required movements does increase with an increase in turbulence intensity as would be expected, but this increase appears to be proportional to the turbulence increase and not greater than the turbulence increase.

Pilot ratings for the various approaches are summarized in Table 9.

TABLE 9
APPROACH HANDLING QUALITIES
PILOT RATING SUMMARY

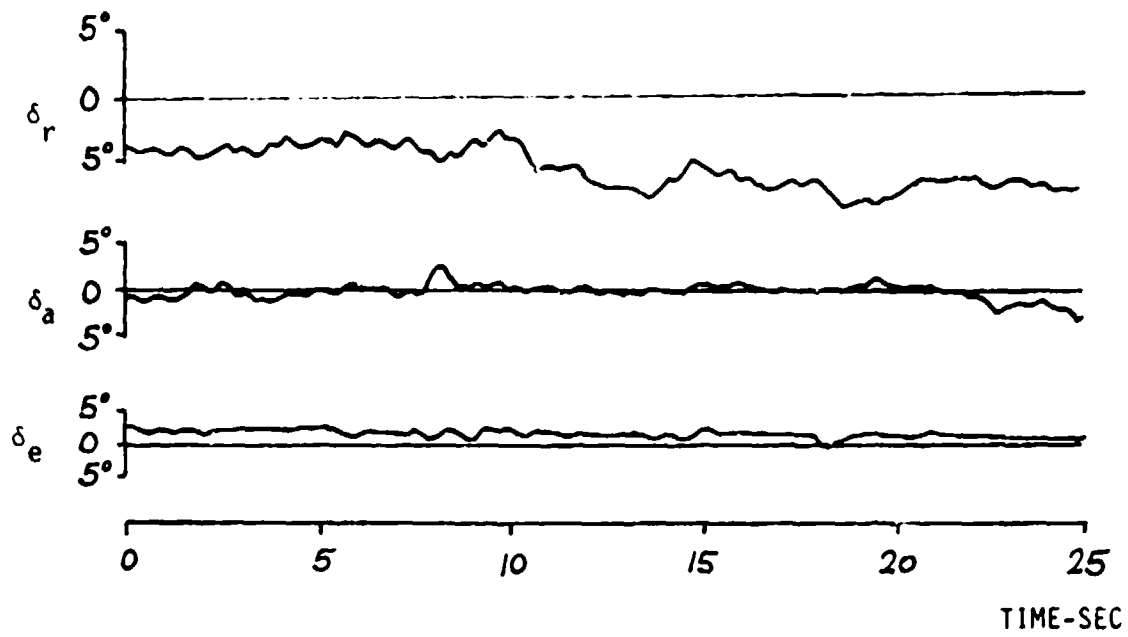
APPROACH SLOPE	TURBULENCE INTENSITY	WIND DIRECTION	WIND SHEAR	PILOT RATING
3°	Calm	None	No	3
3°	Light to Moderate	Headwind	Yes	3.5
3°	Light to Moderate	Tailwind	Yes	5
6°	Calm	None	No	4
6°	Light to Moderate	Headwind	Yes	4.5
6°	Light to Moderate	Tailwind	Yes	6

NOTE: The smaller the pilot rating number the better the rating.

The main factor in degrading the pilot ratings was the poor longitudinal static stability which required the pilot to pay more than usual attention to airspeed control. If the airplane had been stable longitudinally it would have been given Pilot Ratings one to two numbers smaller in each of the cases shown in Table 9.

The conditions of an approach with a tailwind is a more demanding case for a powered lift airplane, and is uncomfortable for the pilot. The tailwind causes the aircraft to overfly the glideslope. In order to correct for this, the pilot must reduce power since power is the primary means for changing flight path angle. However, a reduction in power also means a reduction in C_L MAX capability of the airplane. As a result, the pilot must pay close attention to reductions in power while at approach speeds which are below power off stalling speed. The requirement for paying more attention to power setting further divides the pilot's attention and

3° APPROACH



6° APPROACH

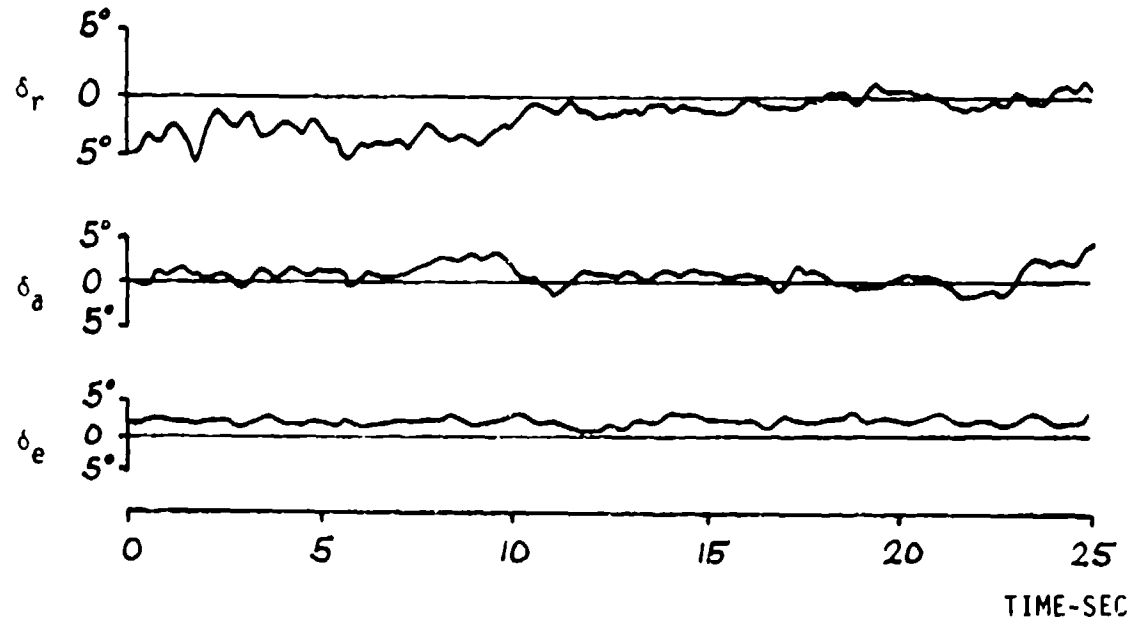


FIGURE 80
TYPICAL CONTROL MOVEMENT
TIME HISTORIES FOR
3° AND 6° APPROACHES

increases his workload. A headwind does not create the same problem since it may be countered by simply increasing the approach speed. As may be seen in figure 44 a large speed increase may be made without significantly changing the flight path angle.

One additional item which reduced the pilot ratings during 6° approaches was forward visibility. In a 6° approach the forward visibility in the Jetwing is poor. This factor caused an increase in pilot rating number of at least one number between the 3° and 6° approaches.

The flight characteristic which decreased the pilot rating numbers over what they might have been was the excellent flight path stability. In all approaches except those with a tailwind it is possible to fly the approach from glideslope capture to landing flare without a throttle movement. This factor considerably reduces pilot workload, and on the Jetwing allowed time to compensate for the longitudinal instability. Other Jetwing flight characteristics which contributed to improved pilot ratings were the small trim changes, the strong directional stability, and the good Dutch Roll characteristics.

In general, if a powered lift aircraft of the Jetwing type can be made longitudinally stable through aerodynamics or a stability augmentation system, its approach handling qualities should exceed those of conventional airplanes.

11. TAKEOFF AND LANDING TESTS. Takeoff and landing tests were conducted with the aircraft loaded to 3686 lbs. at a center of gravity of 35% M.A.C.. Data were recorded on five takeoffs and five landings per the procedures outlined in the test procedures section of this report. Each takeoff and each landing was reduced to no wind, sea level standard conditions at a Gross Weight of 3600 lbs. per the procedures described in Appendix II. The resultant distances from the five takeoffs and landings were averaged to obtain the final distances which are shown in Table 10. The takeoff data reflect a thrust to weight ratio of .497. Thrust reversing was used on all landings.

TABLE 10

JETWING JW-1, SEA LEVEL, STANDARD DAY
NO WIND, TAKEOFF AND LANDING DISTANCES

ITEM	GROUND ROLL	AIR DISTANCE OVER 50 FT	TOTAL DISTANCE OVER 50 FT
TAKEOFF	954 FT	308 FT	1262 FT
LANDING	842 FT	719 FT	1561 FT

The landing distances could have been shortened considerably if the aircraft had a more effective braking system and a landing gear designed for high sink rates.

The effects of a headwind on the above distances are shown in Figures 81 and 82. These figures show that 30 knots of headwind such as might be experienced on a ship at sea would reduce all ground roll distances to under 500 feet.

12. LASER VELOCIMETER THRUST MEASUREMENT. The intent of the laser velocimeter test was to attempt to measure the installed gross thrust of the Jetwing in a static condition, and to evaluate the ambient air mixing of the ejector formed by the upper wing. These tests led to mixed results. First, the attempt to measure gross thrust cannot be considered a success. In the attempt to measure the installed static thrust several problems were encountered. The two primary problems were: 1. the length of time required to obtain individual data points, and 2. the determination of the mass flow rate through the engine. The first problem has considerable impact upon the second. There are three factors which are related to each of these problems. The factors are:

1. Insufficient mechanization and automation of the laser velocimeter.
2. Sunlight reflected from the aircraft surfaces.
3. The small number of particles in the jet exhaust.

A large amount of mechanical design work needs to be accomplished before the laser velocimeter will be practical for use in thrust measurement on as complex a configuration as the Jetwing. The velocimeter used in these tests did not have the capability for rapid movement from one measurement point to the next. The prime reason for this was that little effort has been spent in automating and mechanizing the method for pointing the laser. Previous uses for the laser velocimeter have not required such automation and mechanization. As a result, all pointing adjustments were made by hand. This hand adjustment consumed considerable time and introduced errors into items like mass flow rate which are affected by changes in atmospheric conditions. For this kind of testing the laser velocimeter needs to have the capability for automated, rapid, three dimensional movement.

Reflected sunlight also posed a problem during the test. Reflected sunlight tends to show up as white noise in the data and increases the time required for the velocimeter to determine velocity. Three methods were used during the test to combat this problem. The first method was to move the aircraft and test rig under cover. This change of testing location helped the problem but did not completely solve it. The second method was to paint certain aircraft surfaces flat black. This too was helpful, but was not a complete solution. The third solution, which proved to be fatal for collecting meaningful mass flow data, was to stop taking data when within $1/2$ to one inch of the reflective surface. The problem with this solution will be further discussed later. Probably the best solution for the sunlight problem would be to test in an enclosed structure with indirect light, or to test after dark.

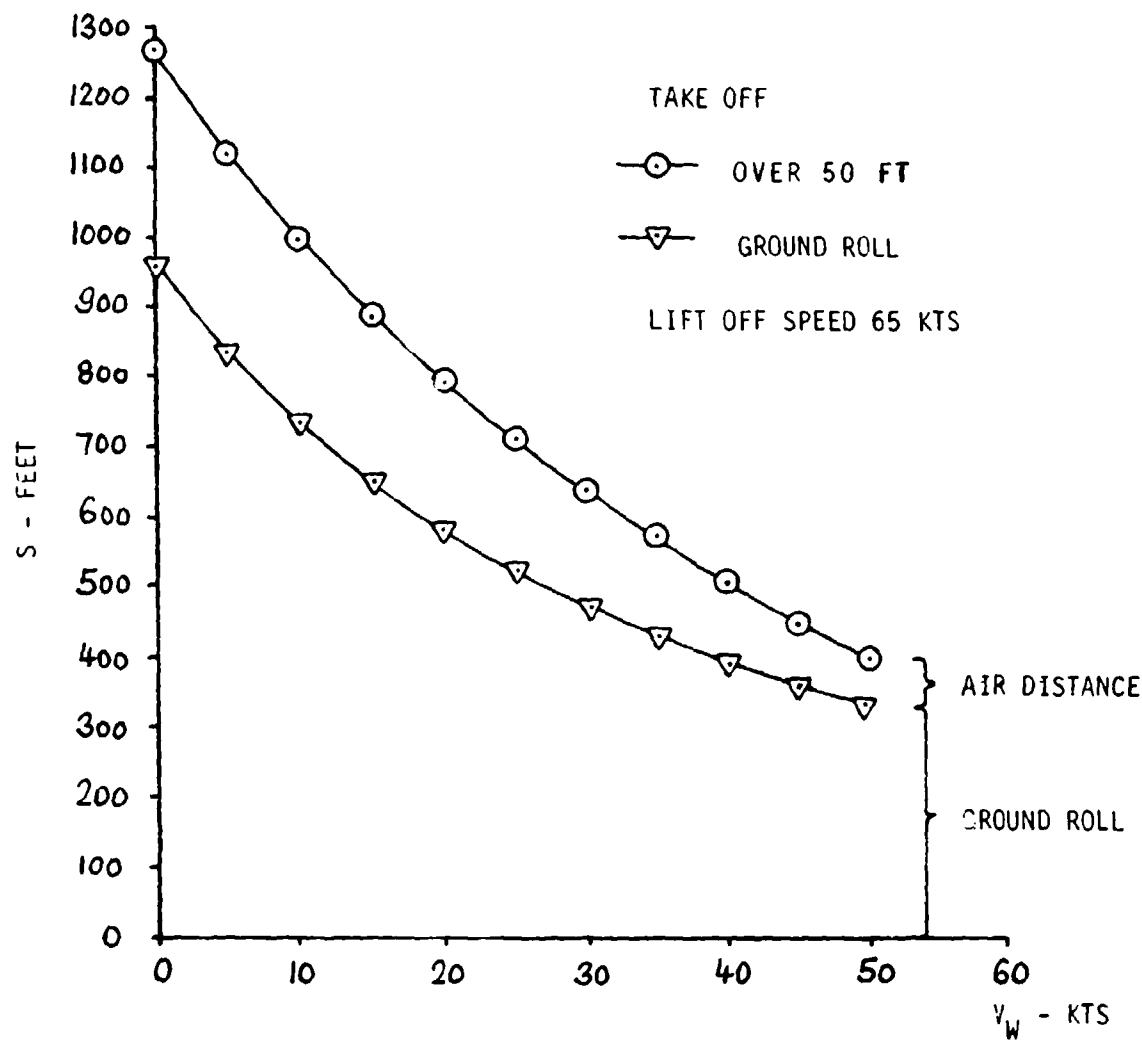


FIGURE 81

JETWING JW-1, N27BB
STANDARD TAKE OFF DISTANCES S AS
FUNCTION OF HEAD WIND VELOCITY V_w

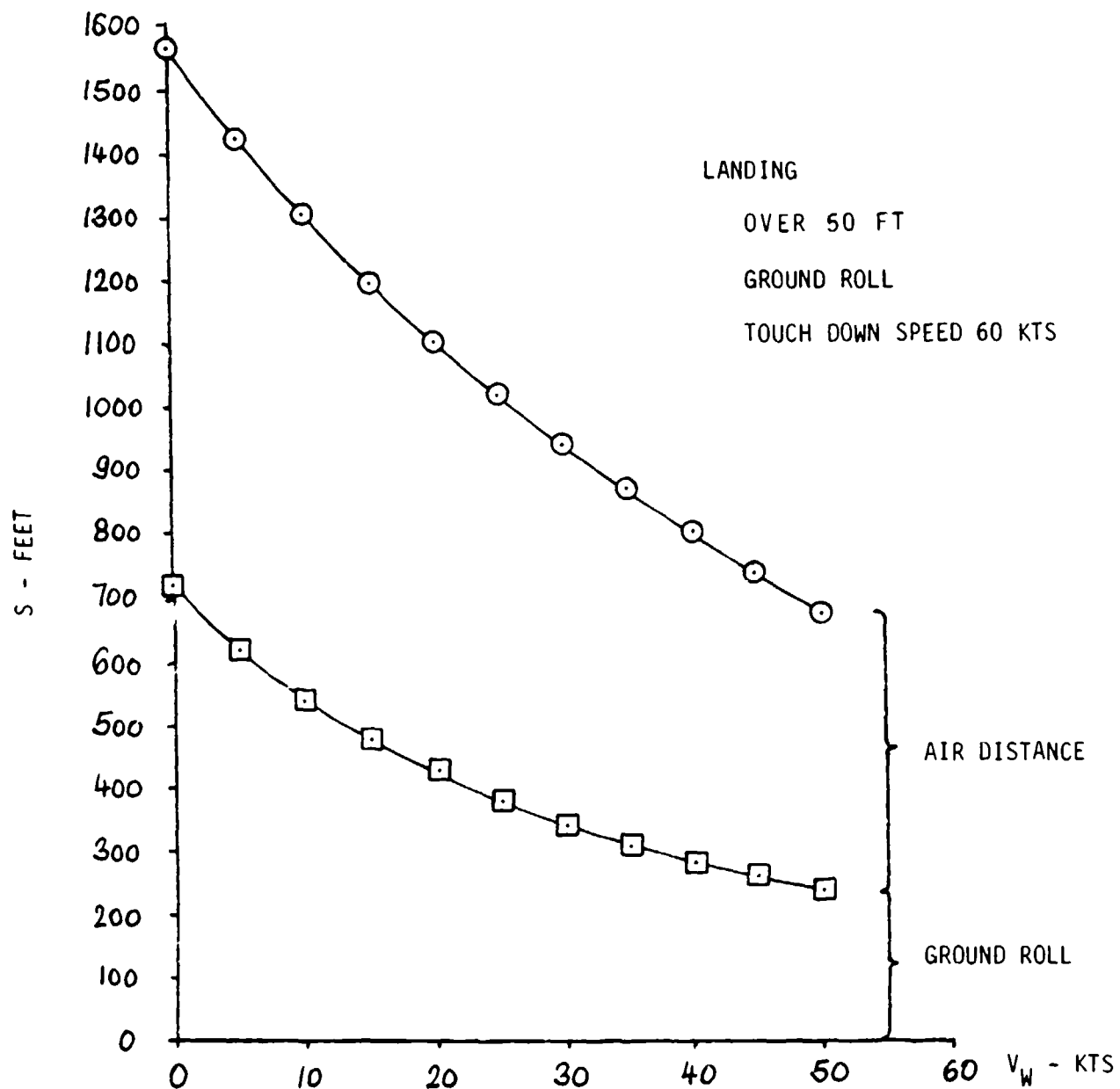


FIGURE 82
JETWING JW-1, N27BB
STANDARD LANDING DISTANCES S AS
FUNCTION OF HEAD WIND VELOCITY V_w

The small number of particles in the jet exhaust was somewhat of a surprise. Prior to the start of testing it was thought that the by-pass air exhaust would present a problem due to a lack of particles. However, when testing began it was found that the hot exhaust presented the largest problem. Since the laser velocimeter works by measuring the doppler phase shift of light reflected from microscopic particles in the flow, the flow must contain sufficient particles to reflect the light, or the laser must have sufficient power to reflect light from fewer and smaller particles. The laser used in these tests only projected from one to one and one half watts of power, and required considerable time to see a large enough sample of particles to calculate the flow velocity. Long periods of time for data collection were particularly true in the hot exhaust where up to 30 seconds were required for each data point. The solution to this problem appears to be a more powerful laser, or the seeding of the flow with some particles which would not be destroyed by the high temperatures and not be harmful to the engine.

To obtain installed static thrust data using the method, the problem of determining mass flow rate through the engine still remains. The initial plan during these tests was to measure the velocities of the flow at the inlet along with the necessary atmospheric parameters, and calculate an inlet mass flow. Then, by obtaining velocities, pressures, and temperatures of the air at the cold duct nozzle the mass flow through the cold duct could be calculated and subtracted from the total mass flow in order to determine the hot exhaust mass flow. However, as mentioned previously, a problem with sunlight reflected from the inlet lip made data collection near the lip very difficult. As a result, the plane where data were taken was moved one inch forward of the inlet lip.

Figures 83 and 84 are representative plots of the velocity profiles taken at the inlet data plane. By use of both horizontal and vertical profiles, a three dimensional average velocity was obtained for the inlet for each power setting tested. These average velocities along with the atmospheric data were used to calculate a mass flow at the inlet.

Table 11 shows the results of these mass flow calculations along with the calculations for the mass flow in the cold and hot ducts as determined by the method previously described.

FIGURE 83
JET WING LASER VELOCIMETER INTAKE VELOCITY MEASUREMENT
VELOCITY PROFILE AT INTAKE (VERTICAL SCAN-55% N_1)

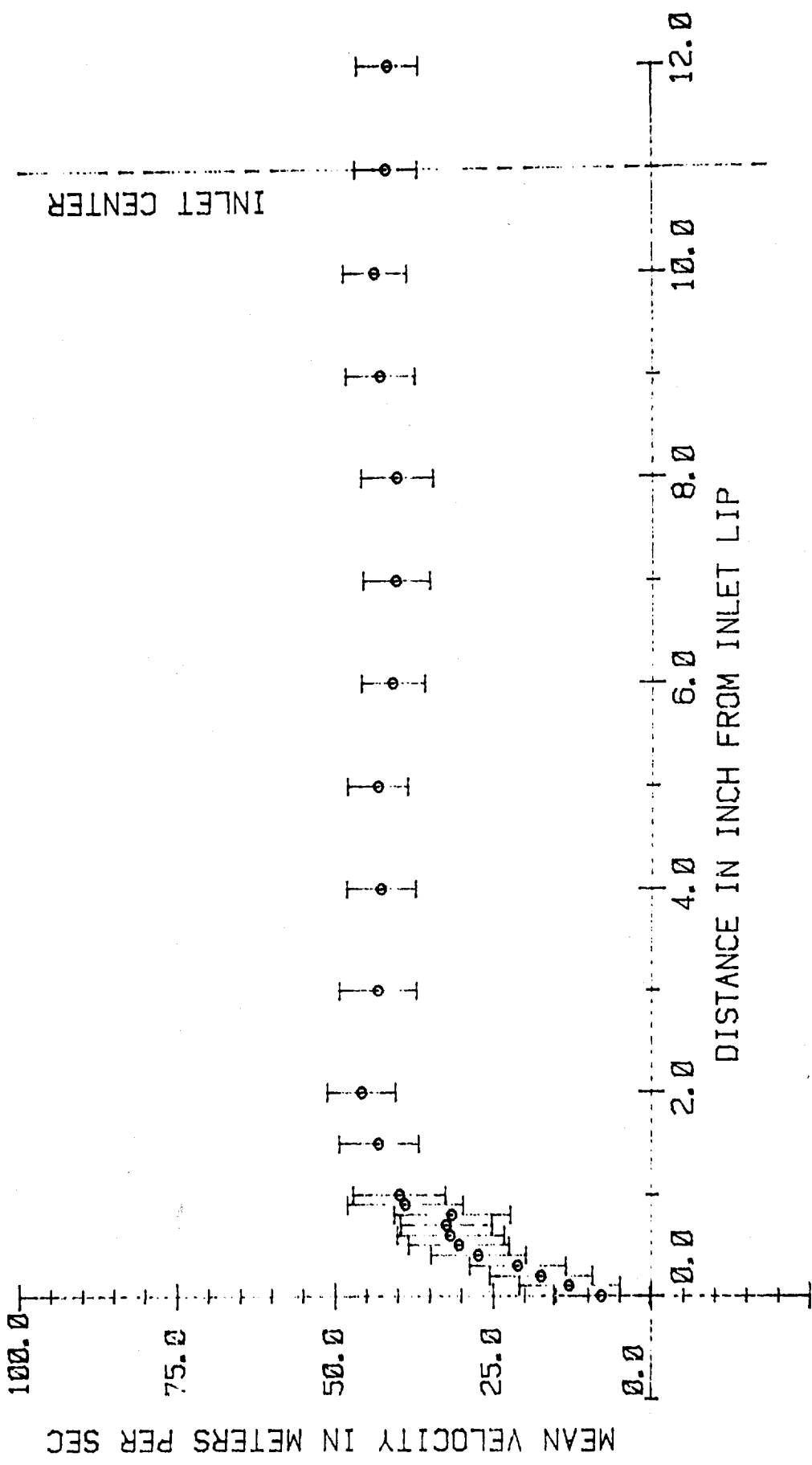


FIGURE 84
JET WING LASER VELOCIMETER INTAKE VELOCITY MEASUREMENT
VELOCITY PROFILE AT INTAKE (HORIZONTAL SCAN-55% N_1)

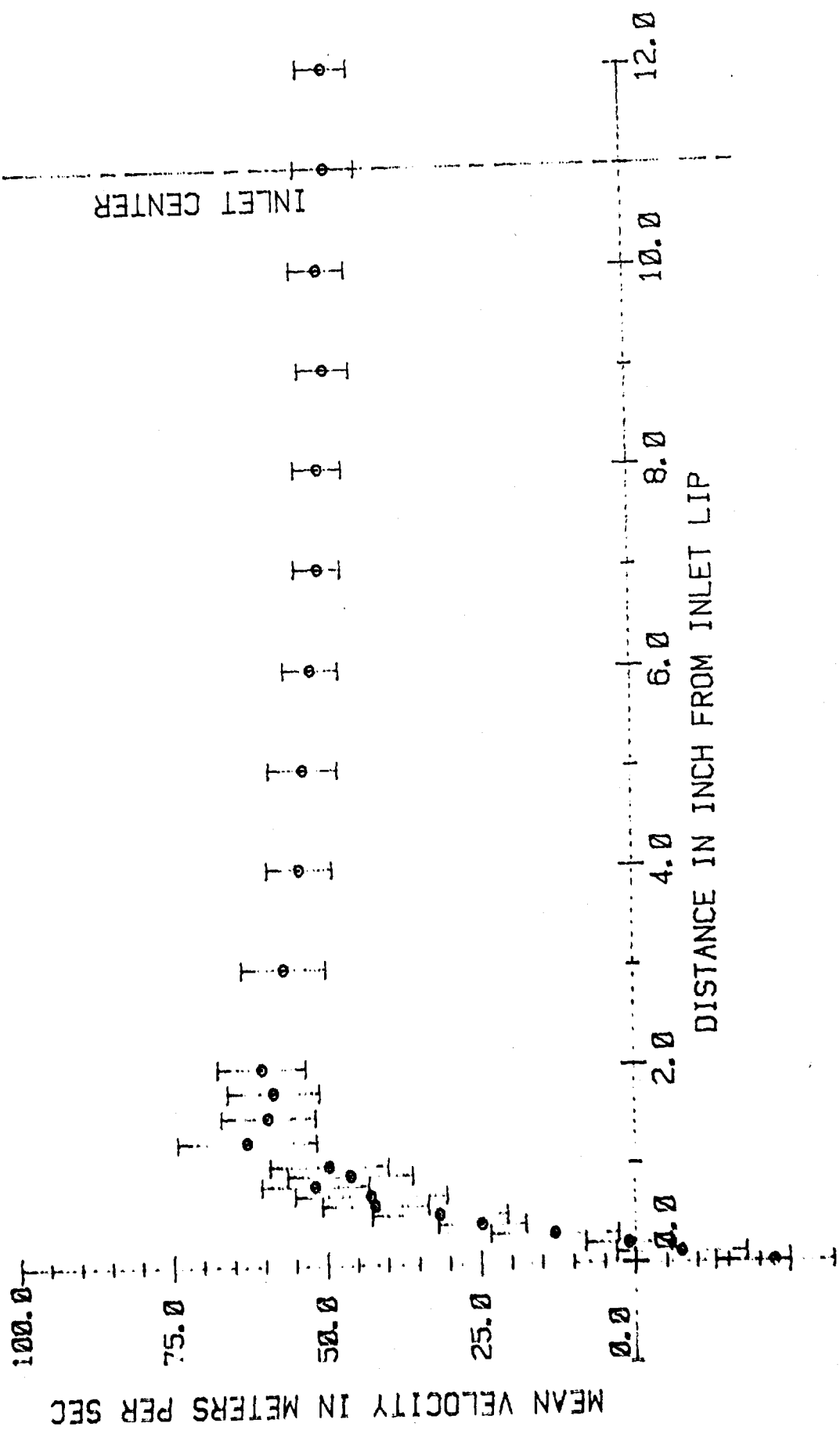


TABLE 11
JETWING ENGINE MASS FLOW
SUMMARY

POWER SETTING	INLET MASS FLOW	COLD DUCT MASS FLOW	HOT DUCT MASS FLOW
40% N_1	19.9 lb/sec	17.6 lb/sec	2.3 lb/sec
55% N_1	28.9 lb/sec	27.4 lb/sec	1.5 lb/sec
70% N_1	31.6 lb/sec	31.2 lb/sec	0.4 lb/sec

The error in locating the data plane one inch ahead of the inlet lip is shown by this table at all power settings, but is more pronounced at the higher power settings. Obviously, at a power setting of 70% N_1 the gas generator requires more than 0.4 lb/sec. of air to operate the engine. The reason for this discrepancy can be understood when one considers that in a static condition a large mass of air is pulled by the engine from behind the inlet plane as well as from in front of it. During the test it was not felt that the error introduced by moving the data plane would be large, and the actual magnitude of the error was not discovered until it was too late to repeat the tests. These errors, along with the time required to collect the velocity data, preclude any meaningful calculation of thrust.

Even though the laser velocimeter in its current state of development has shortcomings as a thrust measuring device, it is quite useful for studying the air flow. Figures 85 through 90 are representative velocity profiles of the cold and hot exhaust ducts taken at a 55% N_1 power setting with the upper wing removed. For comparison Figures 91 and 92 are velocity profiles measured vertically between the main and upper wing at the trailing edge of the upper wing. A comparison of these sets of figures shows that some mixing between the primary and secondary air streams is occurring in the ejector formed by the upper and main wing. However, this mixing is not optimum and would require substantial improvement for effective thrust augmentation. Figures 93, 94 and 95 are vertical profiles measured between the main and upper wing at the leading edge of the upper wing, or at the inlet to the ejector. These profiles also show that there is secondary flow through the ejector, and should be useful data in any attempt to improve the efficiency of the ejector.

In summary, the laser velocimeter has problems as a device for use in thrust measurement, with the major problem being the time required to obtain data. However, as a device for studying air flows it appears to be superior to other techniques since it does not disturb the flow while taking the measurements.

FIGURE 85

JET WING LASER VELOCIMETER EXHAUST VELOCITY MEASUREMENT
VELOCITY AT RIGHT WING HOT DUCT (HORIZONTAL SCAN-55% N_1)

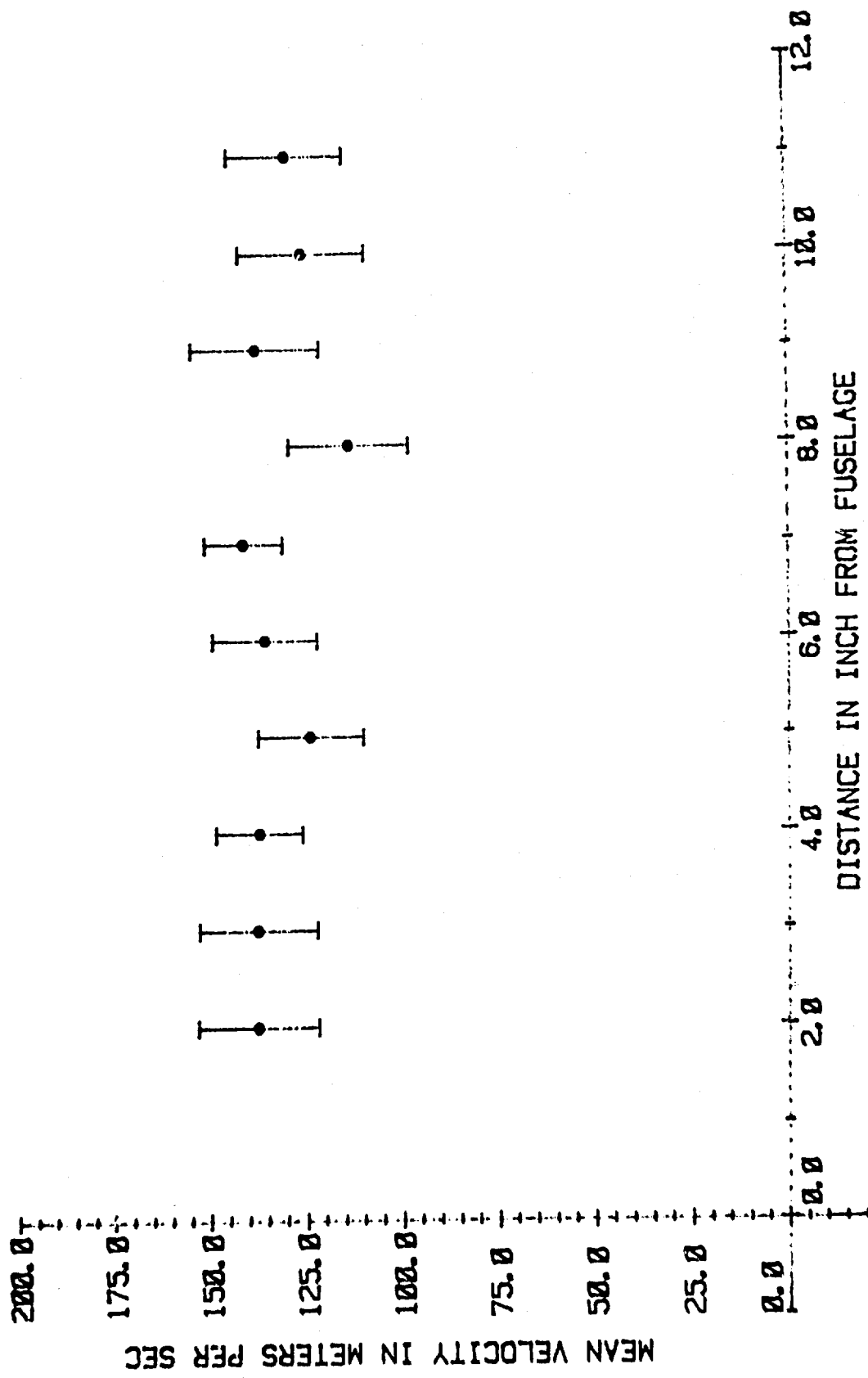


FIGURE 86

JET WING LASER VELOCIMETER EXHAUST VELOCITY MEASUREMENT
 VELOCITY PROFILE AT RIGHT WING HOT DUCT AT 8
 INCHES FROM THE FUSELAGE (VERTICAL SCAN-55% N_1)

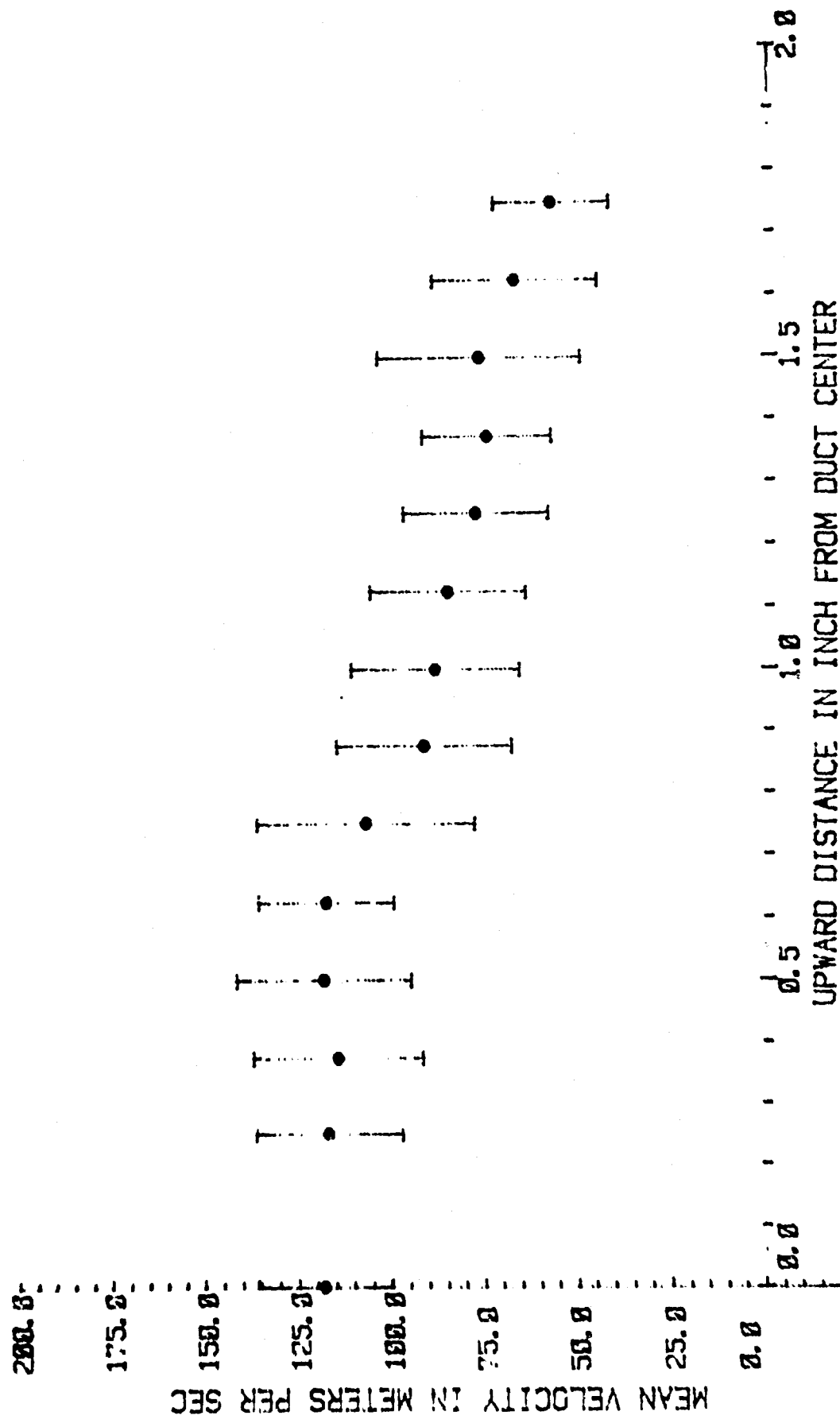


FIGURE 87
JET WING LASER VELOCIMETER EXHAUST VELOCITY MEASUREMENT
VELOCITY AT RIGHT WING INNER COLD DUCT (HORIZONTAL SCAN-55% N_1)

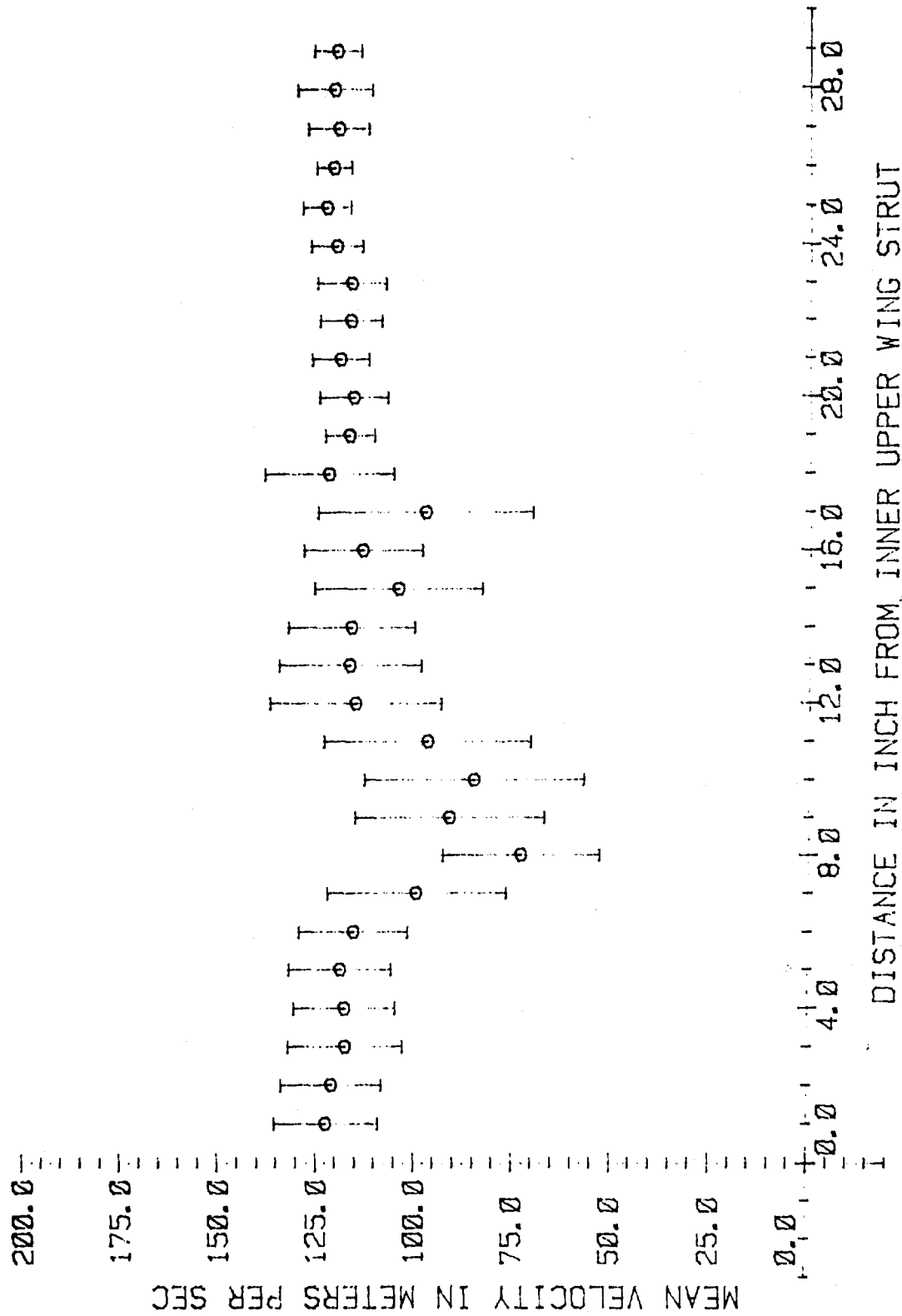


FIGURE 88
 JET WING LASER VELOCIMETER EXHAUST VELOCITY MEASUREMENT
 VELOCITY PROFILE AT RIGHT WING INNER COLD DUCT
 AT 17 INCHES FROM INNER UPPER WING STRUT (VERTICAL SCAN-55% N_1)

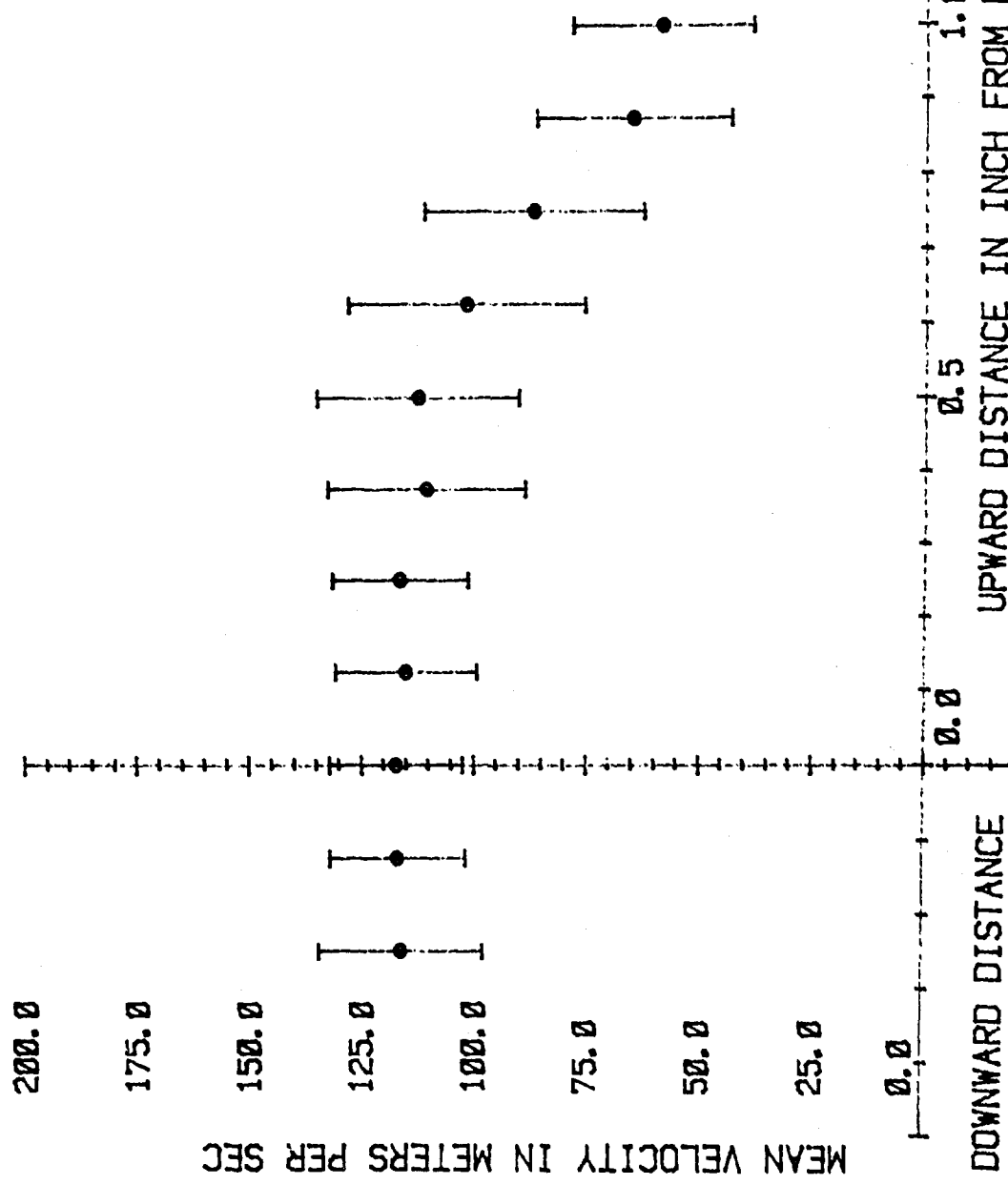


FIGURE 89

JET WING LASER VELOCIMETER EXHAUST VELOCITY MEASUREMENT
VELOCITY AT RIGHT WING OUTER COLD DUCT (HORIZONTAL SCAN-55% N_1)

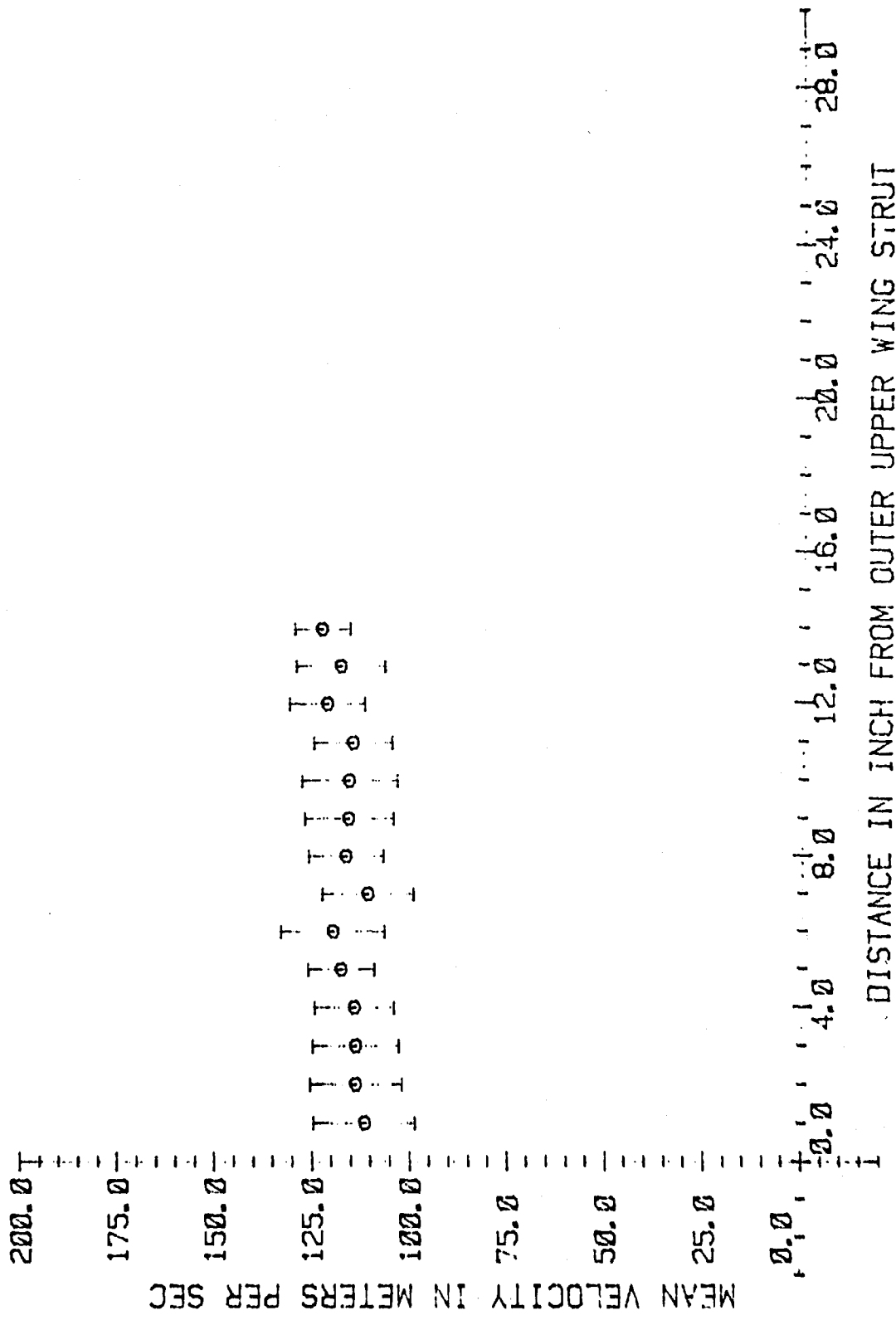


FIGURE 90 JET WING LASER VELOCIMETER EXHAUST VELOCITY MEASUREMENT

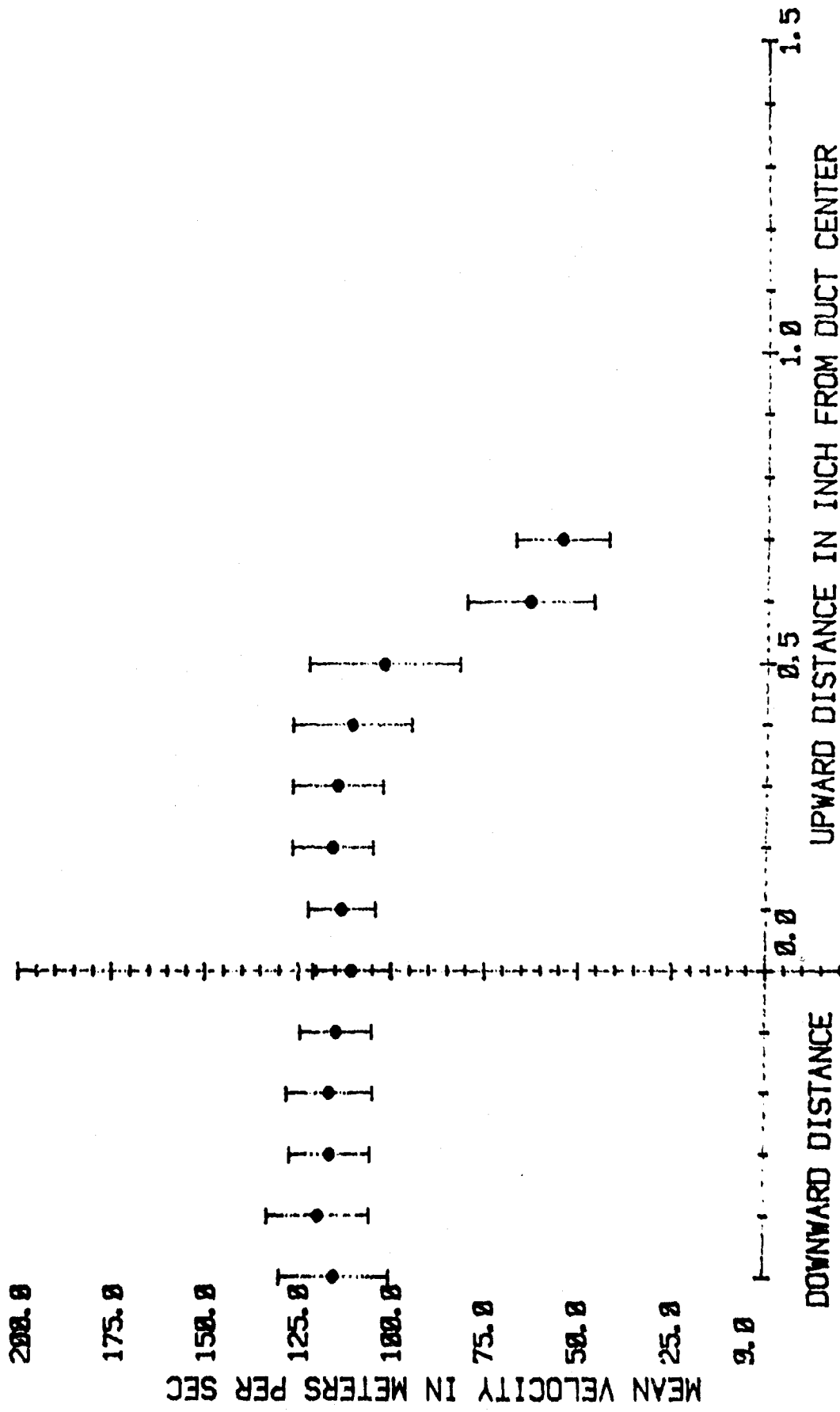


FIGURE 91
 JET WING LASER VELOCIMETER EJECTOR EXHAUST VELOCITY MEASUREMENT
 VELOCITY BEHIND EJECTOR AT RIGHT COLD INNER DUCT
 (VERTICAL SCAN-55% N_1)

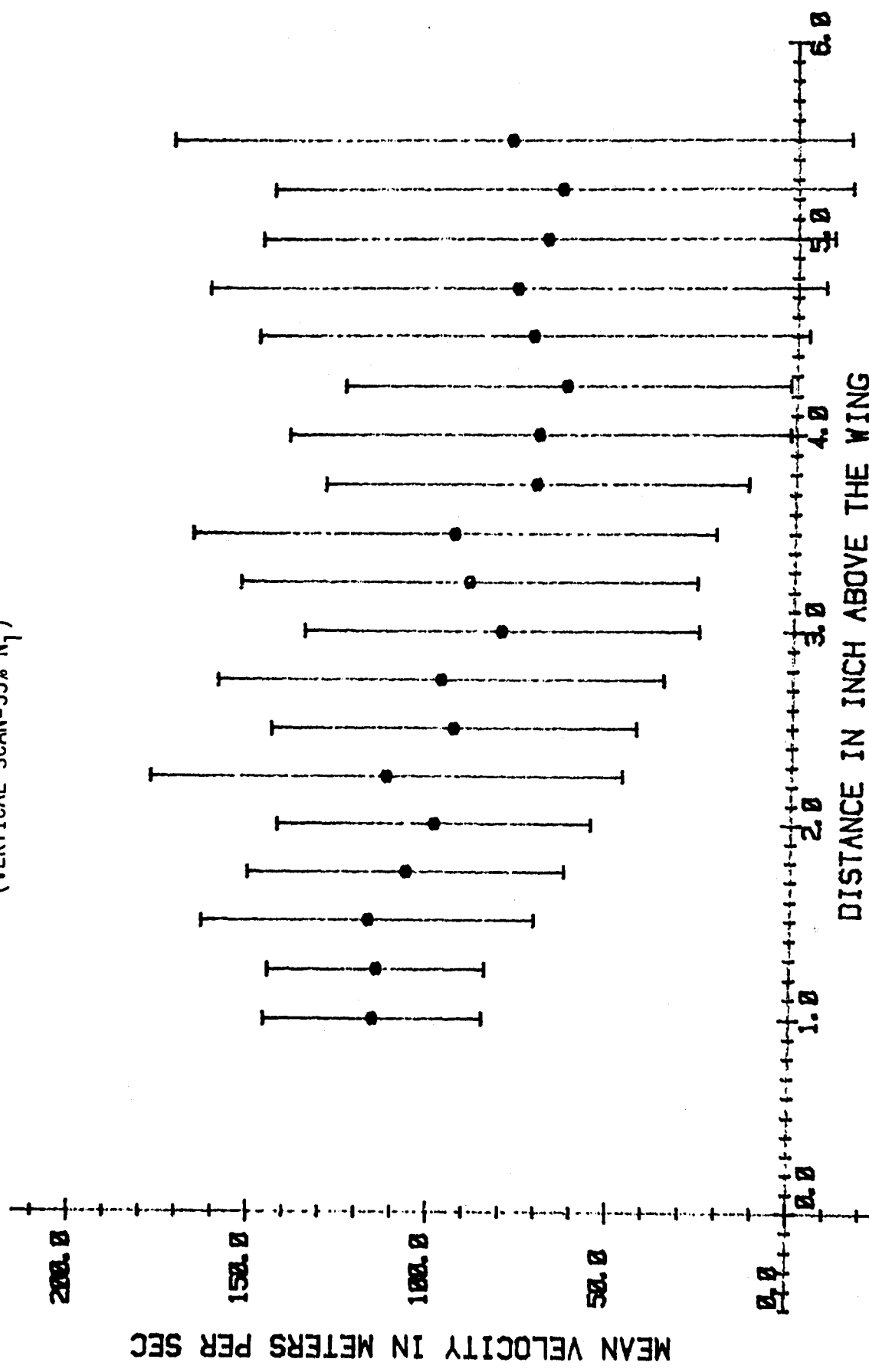


FIGURE 92

JET WING LASER VELOCIMETER EJECTOR EXHAUST VELOCITY MEASUREMENT
VELOCITY BEHIND EJECTOR AT RIGHT COLD OUTER DUCT
(VERTICAL SCAN-55% N_1)

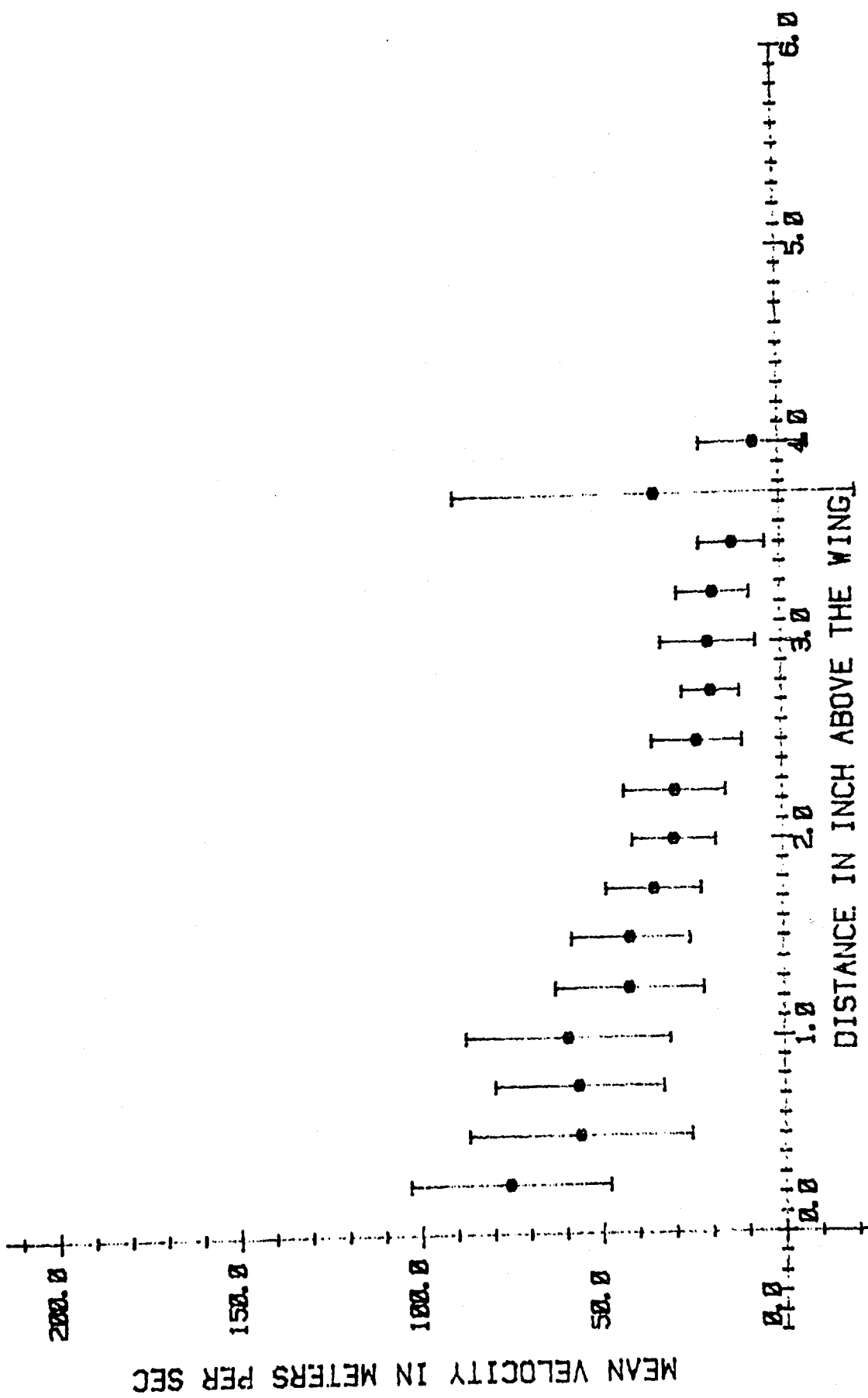


FIGURE 93

JET WING LASER VELOCIMETER EJECTOR INLET VELOCITY MEASUREMENT
VELOCITY AT EJECTOR INLET IN FRONT OF RIGHT HOT DUCT (VERTICAL SCAN-55% N_1)

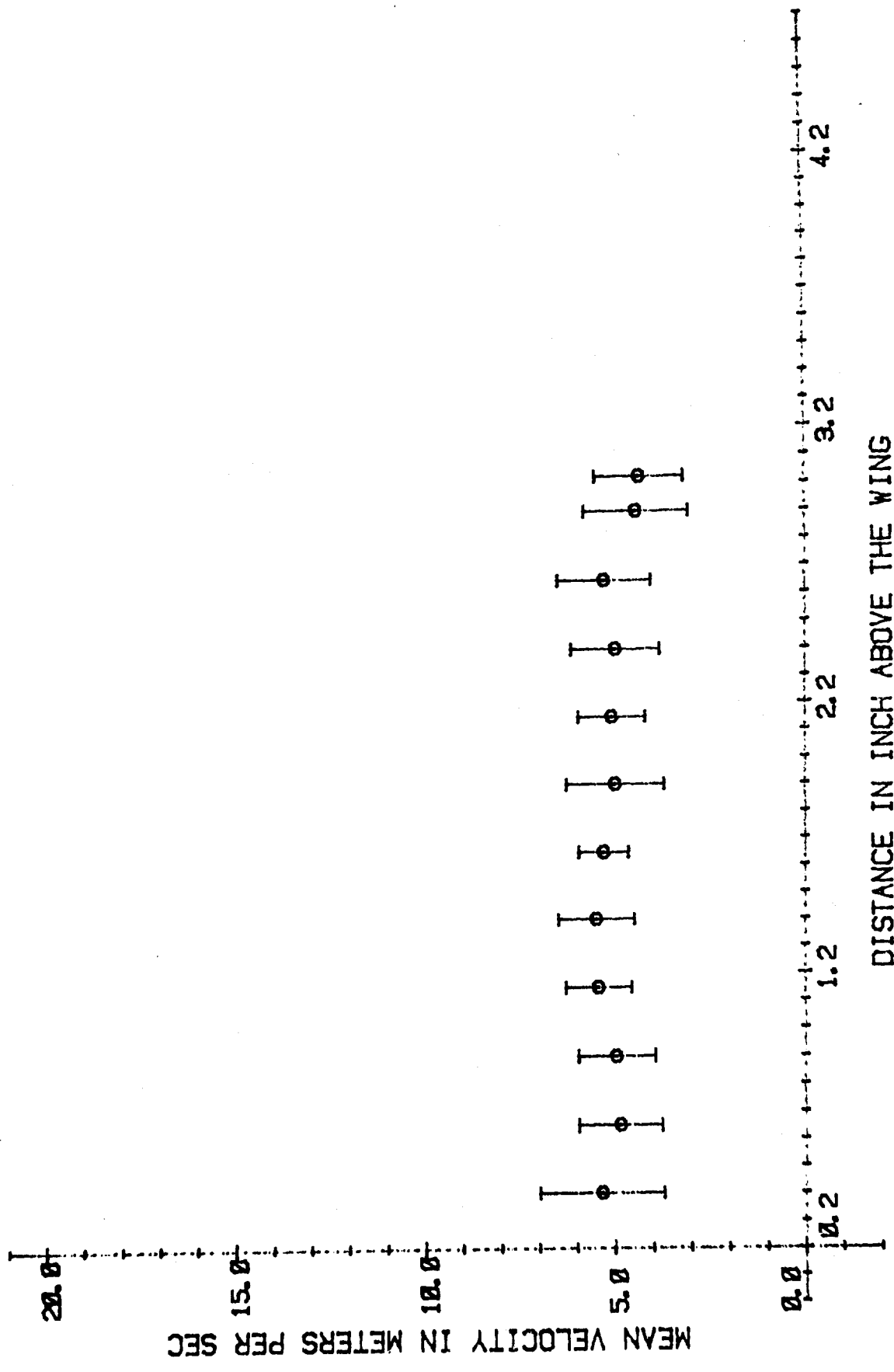


FIGURE 94

JET WING LASER VELOCIMETER EJECTOR INLET VELOCITY MEASUREMENT
 VELOCITY AT EJECTOR INLET IN FRONT OF RIGHT COLD INNER DUCT
 (VERTICAL SCAN-55% N_1)

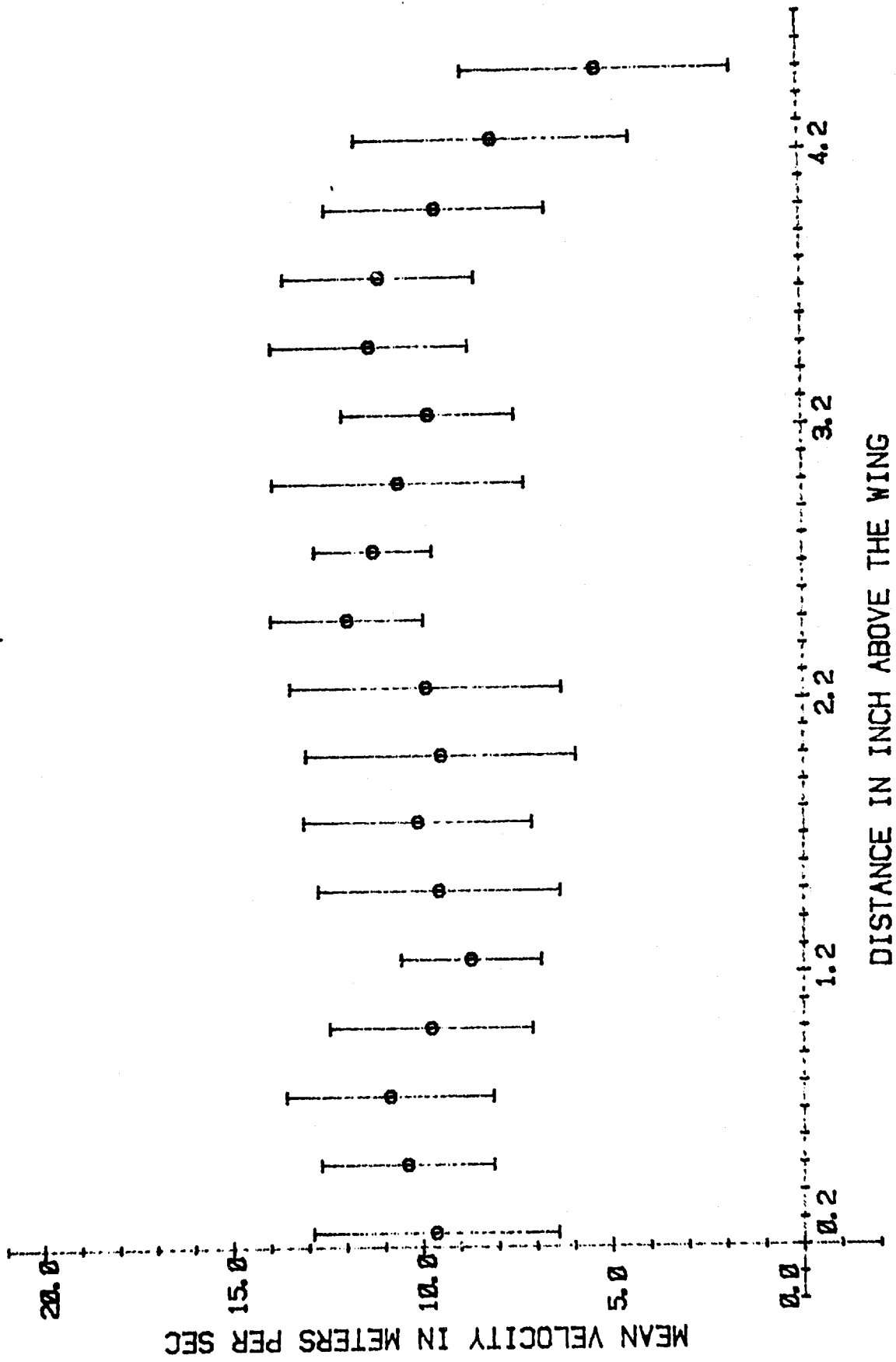


FIGURE 95

JET WING LASER VELOCIMETER EJECTOR INLET VELOCITY MEASUREMENT
 VELOCITY AT EJECTOR INLET IN FRONT OF RIGHT COLD OUTER DUCT
 (VERTICAL SCAN-55% N_1)

MEAN VELOCITY IN METERS PER SEC

15.0

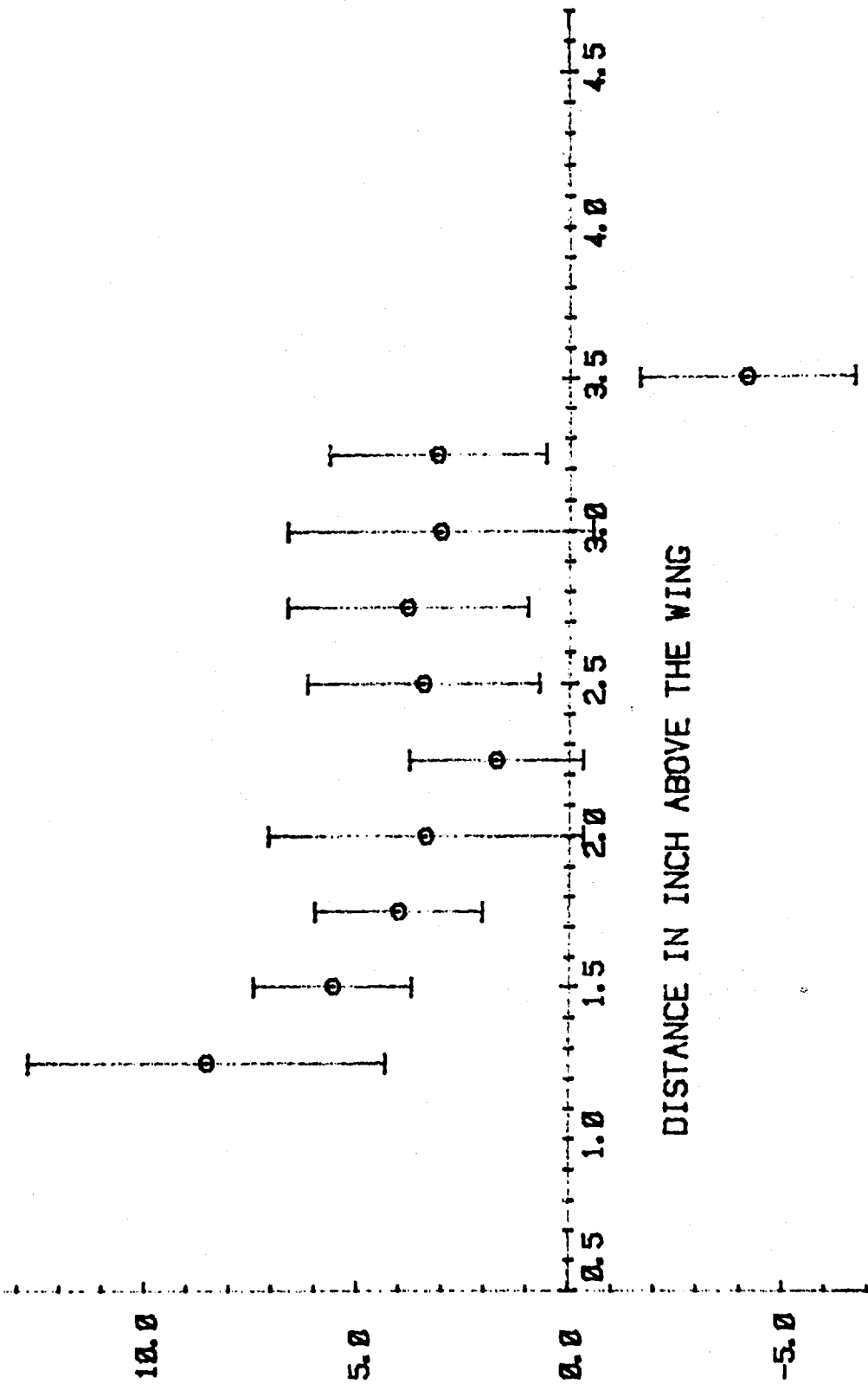
12.0

5.0

0.0

-5.0

DISTANCE IN INCH ABOVE THE WING



REFERENCES

1. "Jetwing from Colorado, Air International, 14 (No. 2): 69-71, Fine Scroll Limited, London, England, February, 1978.
2. Maskell E. C., and Spence, D. A., "A Theory of the Jet Flap in Three Dimensions," Royal Aircraft Establishment, Farnborough, Hants, England, December, 1958.
3. Anon: " Flying Qualities of Piloted Airplanes," MIL-F-8785B(ASG), Department of the Air Force and Naval Air Systems Command, 7 August 1969.
4. Langdon, S. D. "Fixed Wing Stability and Control Theory and Flight Test Techniques," United States Naval Test Pilot School Flight Test Manual No. 103, Naval Air Test Center, Patuxent River, Maryland, August, 1969.
5. Perkins, Courtland D., and Hage, Robert F. Airplane Performance Stability and Control. New York: John Wiley and Sons, Inc., 1963.
6. Cochrane, John A., and Riddle, Dennis W. "Joint Navy/NASA QSRA Flight Research Program Preliminary Summary." Paper presented at the American Institute of Aeronautics and Astronautics--Aircraft Systems and Technology Meeting, August 4, 1980.
7. Parks, E. K. "A Note on Performance Flight Testing of STOL Airplanes and the Application of Inertial Navigation Systems for Performance Testing," Office Memo, Performance and Flying Qualities Branch, Air Force Flight Test Center, Edwards Air Force Base, California, September, 1975.
8. Trimbach, John M. "The V-γ Performance Method as Applied to the Ball-Bartoe Jetwing STOL Aircraft." A Thesis presented for the Master of Science Degree, The University of Tennessee, Knoxville, June, 1981.
9. Williams, J. S. Butler, F. J., and Wood, M. N. "The Aerodynamics of Jet Flaps," Aeronautical Research Council Reports and Memoranda No. 3304, Her Majesty's Stationery Office, London, England, 1963.
10. Herrington, Russel M., et al. "Flight Test Engineering Handbook, "United States Air Force Technical Report No. 6273, Air Force Flight Test Center, Edwards, Air Force Base, California, May, 1961, June 1964, and January 1966.

OTHER REFERENCES NOT SPECIFICALLY CALLED OUT IN THE REPORT OR ITS APPENDICES.

11. Kimberlin, R. D. "Performance Flight Test Evaluation of the Ball-Bartoe JW-1 Jetwing STOL Research Aircraft." Paper presented at the Society of Flight Test Engineers Eleventh Annual Symposium - Flight Testing in the Eighties, Atlanta, Georgia, August, 1980.
12. Rooke, Kenny A. "An Evaluation of Nozzle Pressure Ratio as a Means of Determining In-Flight Gross Thrust of the Ball-Bartoe Jetwing with the Pratt and Whitney JT15D-1 Turbofan Engine Installed." A Thesis presented for the Master of Science Degree, The University of Tennessee, Knoxville, July, 1980.
13. Small, S. M. Prueher, J. W., Williamson, R. C., and Gemmill, A. M. "Fixed Wing Performance Theory and Flight Test Techniques," United States Naval Test Pilot School Flight Test Manual No. 104, Naval Air Test Center, Patuxent River, Maryland, July, 1977.
14. McPherson, R. L. "YC-14 Flight Test Results." presented at the American Institute of Aeronautics and Astronautics - Aircraft Systems and Technology Meeting, Seattle, Washington, August, 1977.
15. Cheney, H. K. "YC-15 STOL Performance Flight Test Methods." Paper presented at the Society of Flight Test Engineers Eighth Annual Symposium - Flight Test Technology, Baltimore, Maryland, August, 1977.
16. Martin, James L. "The Quiet Short-Haul Research Aircraft (QSRA)." SETP Technical Review, 14 (No. 4): 77-93, September, 1979.

SECTION VII

CONCLUSIONS

As a result of the the test program, the following conclusions were reached:

1. The effects of power on the calibration of the Jetwings airspeed system were minimal.
2. The correlation of the results of the simple thrust calibration method used with those of the NASA Ames 40 x 80 foot wind tunnel were excellent. This excellent correlation increased confidence in the method when used for other configurations.
3. The correlation between the flight test results and those of the NASA Ames 40 x 80 foot wind tunnel is sufficient to justify the use of the wind tunnel results for extrapolation to future designs.
4. The Jetwing has excellent rolling performance, comparable to conventional airplanes. This is accomplished without special systems.
5. The lateral-directional stability of the Jetwing is conventional with strong directional stability being exhibited.
6. The static and dynamic longitudinal stabilities of the Jetwing are negative for most of the configurations and centers of gravity tested. This instability appears correctable by proper location of the center of gravity, and the installation of a larger horizontal tail.
7. Pitch damping and maneuvering stability are positive and help make up for the lack of longitudinal stability. The longitudinal short period also helps by being heavily damped.
8. The longitudinal trim changes for configuration and power change are very small and help to improve the longitudinal flying qualities.
9. The Jetwing exhibits a horizontal tail stall at very slow airspeeds with the flaps deflected. This objectional characteristic prohibits a complete evaluation of the low speed performance and handling qualities, but appears to be correctable by an improved horizontal tail design.

10. The handling qualities of the Jetwing in both 3° and 6° glideslope approaches are acceptable in spite of the longitudinal instability. These acceptable handling qualities are primarily due to the excellent flight path stability, the small longitudinal trim changes, and the slow speed of the approaches.
11. The handling characteristics of powered lift airplanes in the landing flare are unusual and may require special consideration in training.
12. The takeoff and landing distances of the Jetwing are very short. This is especially true when strong headwinds exist.
13. The laser velocimeter is an excellent tool for studying air flow. However, as a thrust measuring device it has several shortcomings. The largest of these shortcomings is the amount of time required to take individual data points.
14. As a general conclusion, the Jetwing concept shows promise as a single engine USB, STOL concept for application to several military aircraft categories. The concept has demonstrated the ability to achieve high lift coefficients and resultant performance with a simple and inexpensive approach. All design problems encountered during this program appear to be correctable, and were the result of poor design of the research airplane rather than some inherent flaw in the concept.

SECTION VIII

RECOMMENDATIONS

After an evaluation of the test results, and the conclusions reached from these results, the following items are recommended:

1. That the NASA Ames 40 x 80 foot wind tunnel data, along with the data from this report, be used for extrapolating the Jetwing concept to future aircraft designs.
2. That additional studies be conducted on the Jetwing research aircraft with an enlarged, redesigned horizontal tail. These studies should be done to confirm that such aircraft can be designed without longitudinal stability and control problems, and to further investigate the low speed capabilities of the concept.
3. That strong consideration be given to continued development of such technology for application to future military aircraft.

APPENDIX I

EJECTOR GEOMETRY

The following sketches and dimensions give the geometry and areas of the ejector formed by the upper wing on the Jetwing research aircraft. The areas were measured at the locations shown in Figure I-1.

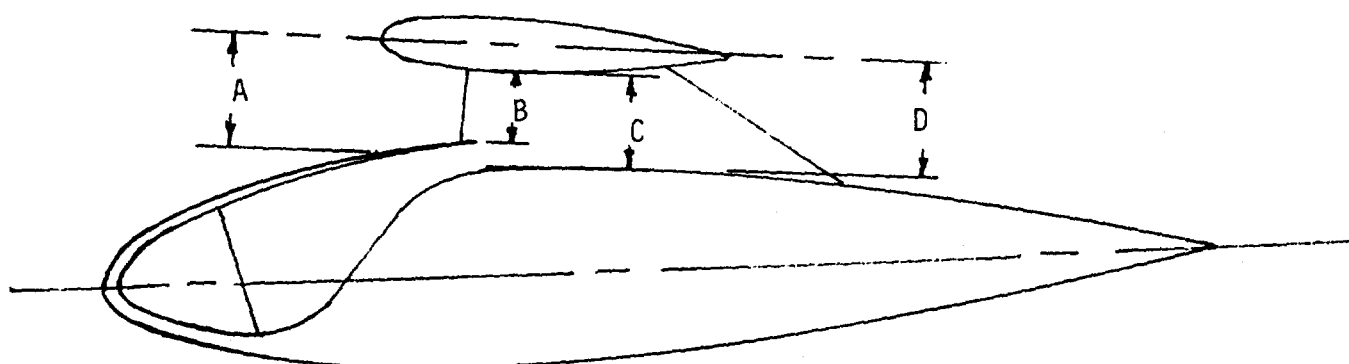
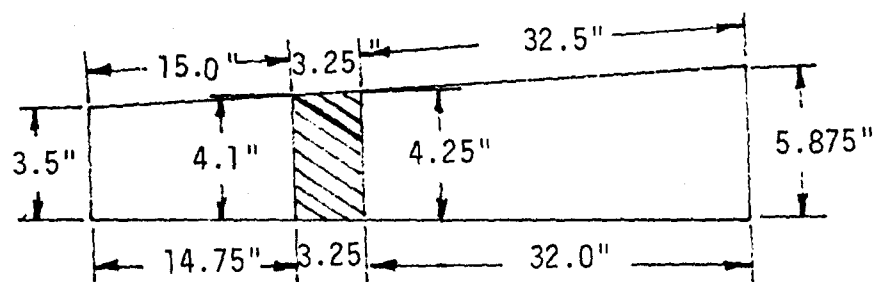


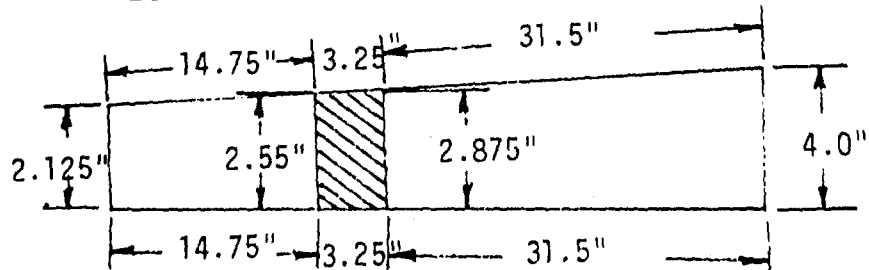
FIGURE I-1

LEFT WING COLD DUCT EJECTOR AREA A



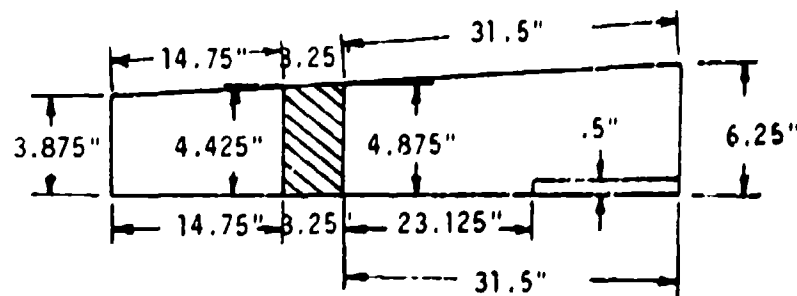
$$\text{TOTAL AREA} = 56.05 + 162.0 = 218.05 \text{ sq. in.}$$

LEFT WING COLD DUCT EJECTOR AREA B



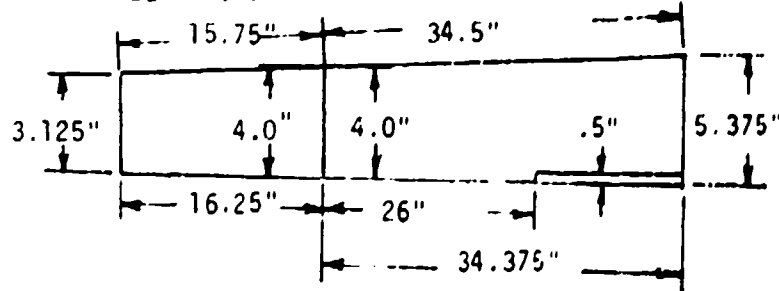
$$\text{TOTAL AREA} = 34.48 + 108.28 = 142.76 \text{ sq. in.}$$

LEFT WING COLD DUCT EJECTOR AREA C



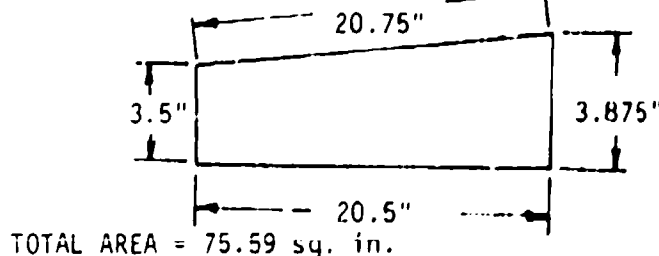
$$\text{TOTAL AREA} = 61.21 + 171.03 = 232.24 \text{ sq. in.}$$

LEFT WING COLD DUCT EJECTOR AREA D



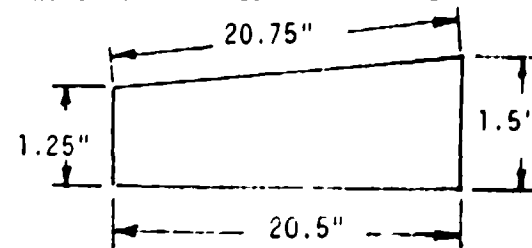
$$\text{TOTAL AREA} = 56.11 + 180.57 = 326.69 \text{ sq. in.}$$

LEFT WING HOT DUCT EJECTOR AREA A

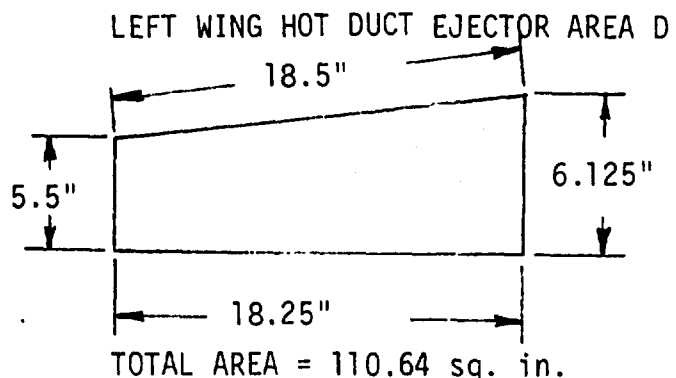
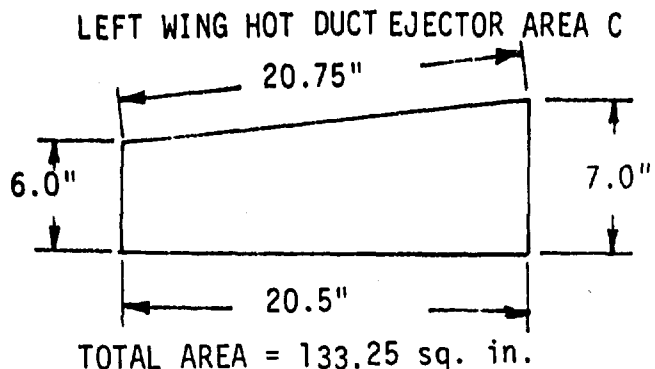


$$\text{TOTAL AREA} = 75.59 \text{ sq. in.}$$

LEFT WING HOT DUCT EJECTOR AREA B



$$\text{TOTAL AREA} = 28.19 \text{ sq. in.}$$



LEFT WING ENGINE NOZZLE AREAS

Cold Duct Area = 76.237 sq. in.

Hot Duct Area = 48.2 sq. in.

LEFT WING EJECTOR AREAS RATIOS

COLD DUCT

$$A/B = 1.53$$

$$\text{Nozzle}/B = 0.53$$

$$\text{Nozzle}/C = 0.33$$

$$D/C = 1.02$$

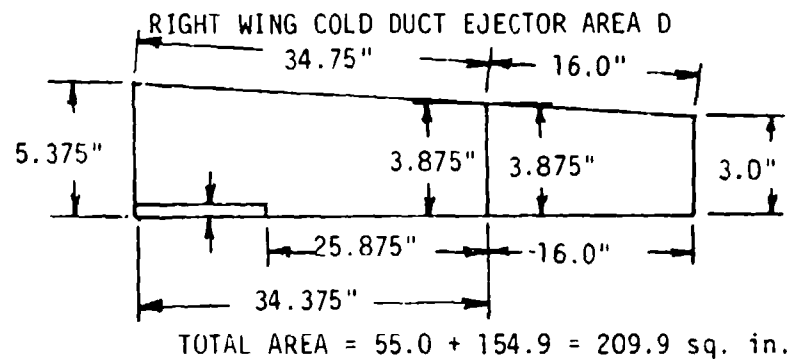
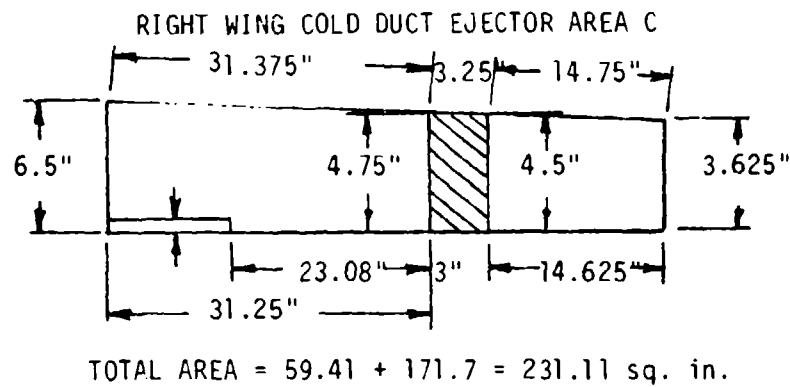
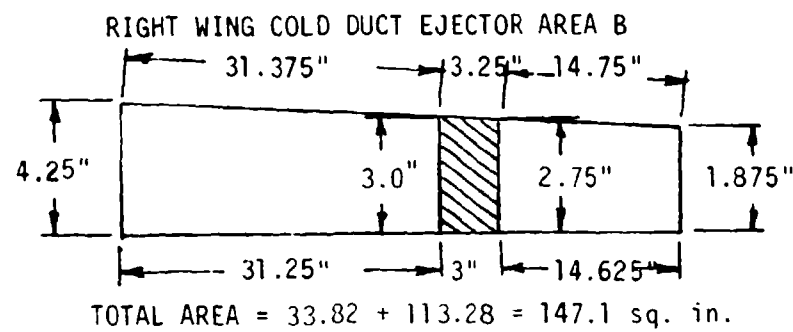
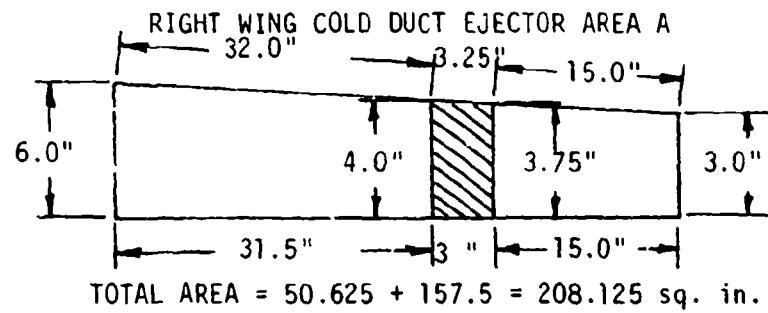
HOT DUCT

$$A/B = 2.68$$

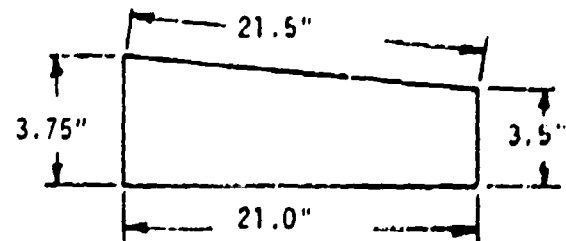
$$\text{Nozzle}/B = 1.71$$

$$\text{Nozzle}/C = 0.36$$

$$D/C = 0.83$$

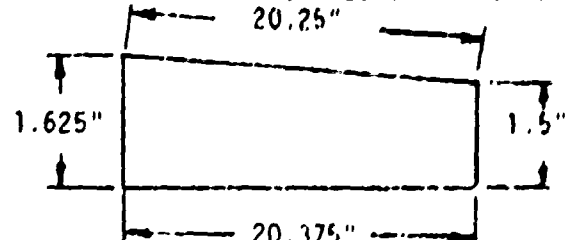


RIGHT WING HOT DUCT EJECTOR AREA A



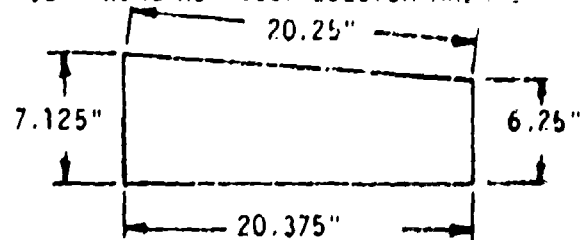
TOTAL AREA = 76.125 sq. in.

RIGHT WING HOT DUCT EJECTOR AREA B



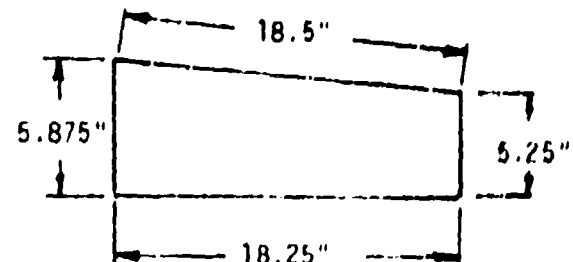
TOTAL AREA = 31.84 sq. in.

RIGHT WING HOT DUCT EJECTOR AREA C



TOTAL AREA = 135.42 sq. in.

RIGHT WING HOT DUCT EJECTOR AREA D



TOTAL AREA = 89.23 sq. in.

RIGHT WING ENGINE NOZZLE AREAS

Cold Duct area = 75.528 sq. in.

Hot Duct area = 48.1 sq. in.

RIGHT WING EJECTOR AREA RATIOS

COLD DUCT

A/B = 1.41

Nozzle/B = 0.51

Nozzle/C = 0.33

D/C = 0.91

HOT DUCT

A/B = 2.39

Nozzle/B = 1.51

Nozzle/C = 0.355

D/C = 0.73

APPENDIX II

PERFORMANCE
DATA REDUCTION
METHODS

INTRODUCTION

For powered lift aircraft both lift and drag are functions of the blowing coefficient (C_J) in addition to the angle of attack. This fact presents certain problems when the conventional speed-power performance techniques are used.

The conventional techniques, such as the constant W/δ techniques, assume that the lift coefficient (C_L) is not a function of thrust. Since this assumption will not hold for a powered lift aircraft, constant W/δ data will no longer normalize into a single curve good for all altitudes and temperatures. The ability to normalize data into a single curve good for all temperatures and altitudes is one of the main reasons for using the W/δ method. Therefore, some other technique must be applied to powered lift aircraft.

V- γ METHOD

The technique most commonly applied to powered lift aircraft is the airspeed (V) versus flight path angle (γ) method. This method is based upon the assumption that, for a given thrust, flight path angle is a function of airspeed. The $V-\gamma$ relationship defines a level of excess thrust for each combination of V and γ . As a result, this excess thrust may be converted into common aircraft performance parameters, such as rate of climb, acceleration in level flight, maximum level flight speed, etc. Since the rate of climb, or acceleration in level flight, is a function of excess thrust, excess thrust may be determined in flight test by using either of these two items as a flight test technique.

For the tests described in this report, the steady climb technique was used. This technique generates a plot of altitude versus time which, when corrected for instrument error, is plotted as shown in Figure II-1. To obtain rate of climb the slope of the H_p versus t line must be taken at a given altitude. This was done using a digital computer which averaged each pair of points and calculated the slope of the resulting line. This slope was then corrected for temperature to obtain the rate of climb (dH/dt).

Once the rate of climb (dH/dt) is obtained the flight path angle (γ) is obtained using the following relationship:

$$\sin \gamma = \frac{dH/dt}{V_T} \quad (II-1)$$

For a steady climb the excess thrust (F_{EX}) can be found from the equation.

$$F_{EX} = F_G - D = W \sin \gamma \quad (II-2)$$

where: D = The total airplane drag including ram drag.

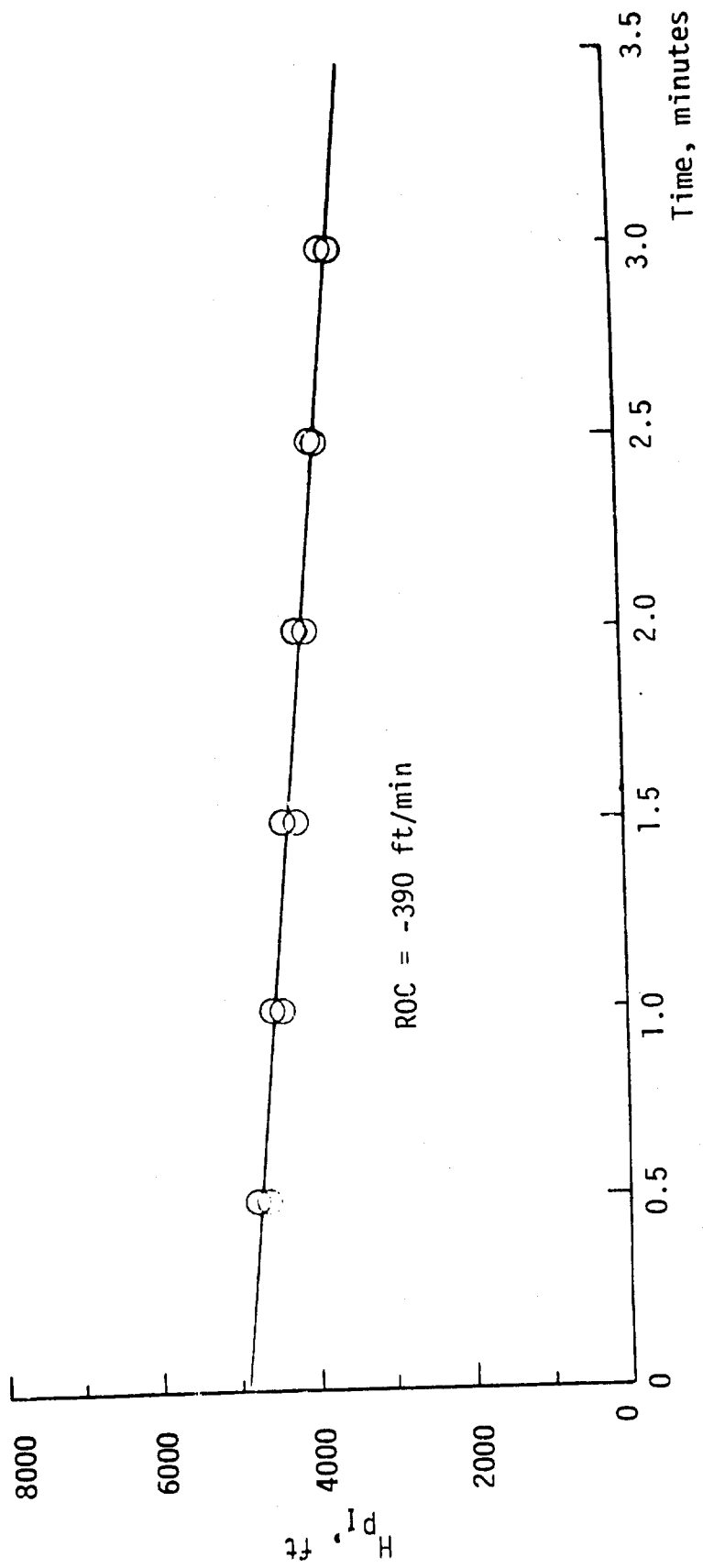


FIGURE II-1 H_{pI} versus time, $V_i = 165$ knots, $N_1 = 80\%$.

From Reference 8

In a steady climb the lift is related to the weight through the following relation:

$$L = W \cos \gamma \quad (\text{II-3})$$

If we solve for the weight in equation II-3 and then substitute for the weight in equation II-2 we have, written in coefficient form:

$$C_{FEX} = C_L \tan \gamma \quad (\text{II-4})$$

Using this equation we may obtain plots of excess thrust coefficient (C_{FEX}) versus lift coefficient (C_L). However, these plots would only be good for the altitude, temperature, and aircraft gross weight conditions where the test data were obtained. What is needed is a method to correct the data to a single plot at sea level standard conditions. Then, by using a reverse technique, the data could be extrapolated to any condition of altitude, temperature or weight. Such a method was developed by Parks in Reference 7 during the YC-14 program.

Parks' method is based upon the assumption that, for a given configuration, the value of $\tan \gamma$ for steady state conditions will not vary if lift coefficient (C_L) and blowing coefficient (C_J) are held constant. Parks arrived at this conclusion by using the relation for excess thrust coefficient (C_{FEX}) developed by Williams in Reference 9.

$$C_{FEX} = C_J - \frac{K C_L^2}{\pi A + 2C_J} - C_{D_0} \quad (\text{II-5})$$

NOTE: The two dimensional blowing coefficient (C_J) of Williams equation has been replaced by the three dimensional blowing coefficient (C_J), and C_{D_0} contains all nonlift dependent drag terms.

If equation II-5 is divided through by C_L it is then possible to see that, for values of constant C_L and C_J , C_{FEX} must also be constant since other variables are fixed. If we then return to equation II-4 we can see that the flight path angle (γ) must also be constant. If γ is constant, then the lift coefficients from two different flight conditions in the same configuration may be set equal. This relation will then allow us to correct data to different conditions such as sea level standard conditions.

If the variables are referenced to a climb or descent at standard weight, the only correction required is that for weight.

For instance the airspeed correction may be derived by equating the lift coefficients for the test and standard conditions and solving for the corrected equivalent airspeed (V_{EW}) as shown below.

$$\frac{W_S \cos \gamma}{1/2 \rho_0 V_{EW}^2 S} = \frac{W_T \cos \gamma}{1/2 \rho_0 V_E^2 S} \quad (II-6)$$

$$V_{EW} = V_E \left(\frac{W_S}{W_T} \right)^{1/2} \quad (II-7)$$

When C_L and C_J are constant as was assumed by Parks then the ratio of C_J/C_L must also be constant for different flight conditions. This equality allows us to correct the observed thrust (F_G) to standard conditions (F_{GS}) through the following relations:

$$\frac{F_{GS}}{W_S \cos \gamma} = \frac{F_G}{W_T \cos \gamma} \quad (II-8)$$

Solving for F_{GS} we have:

$$F_{GS} = F_G \left(\frac{W_S}{W_T} \right)$$

Since the flight path angles (γ) were equated their correction is not required and a plot may be constructed of γ vs V_{EW} for various values of F_{GS} .

For the Jetwing program data were collected by making climbs or descents at a constant airspeed and power setting. Four separate power settings were used at each constant airspeed, and four plots of H_p vs. t , such as is shown in figure II-1, were obtained for each airspeed. Once the slope of H_p vs. t has been obtained from a plot the data were reduced to sea level standard conditions using the reduction sequence shown in Table II-1.

Once corrected the data were plotted on individual plots for each airspeed as shown in Figure II-2. With plots such as this for each airspeed and configuration tested, the combined V - γ maps such as is shown in figures 42, 43, and 44, in the body of the report, were constructed.

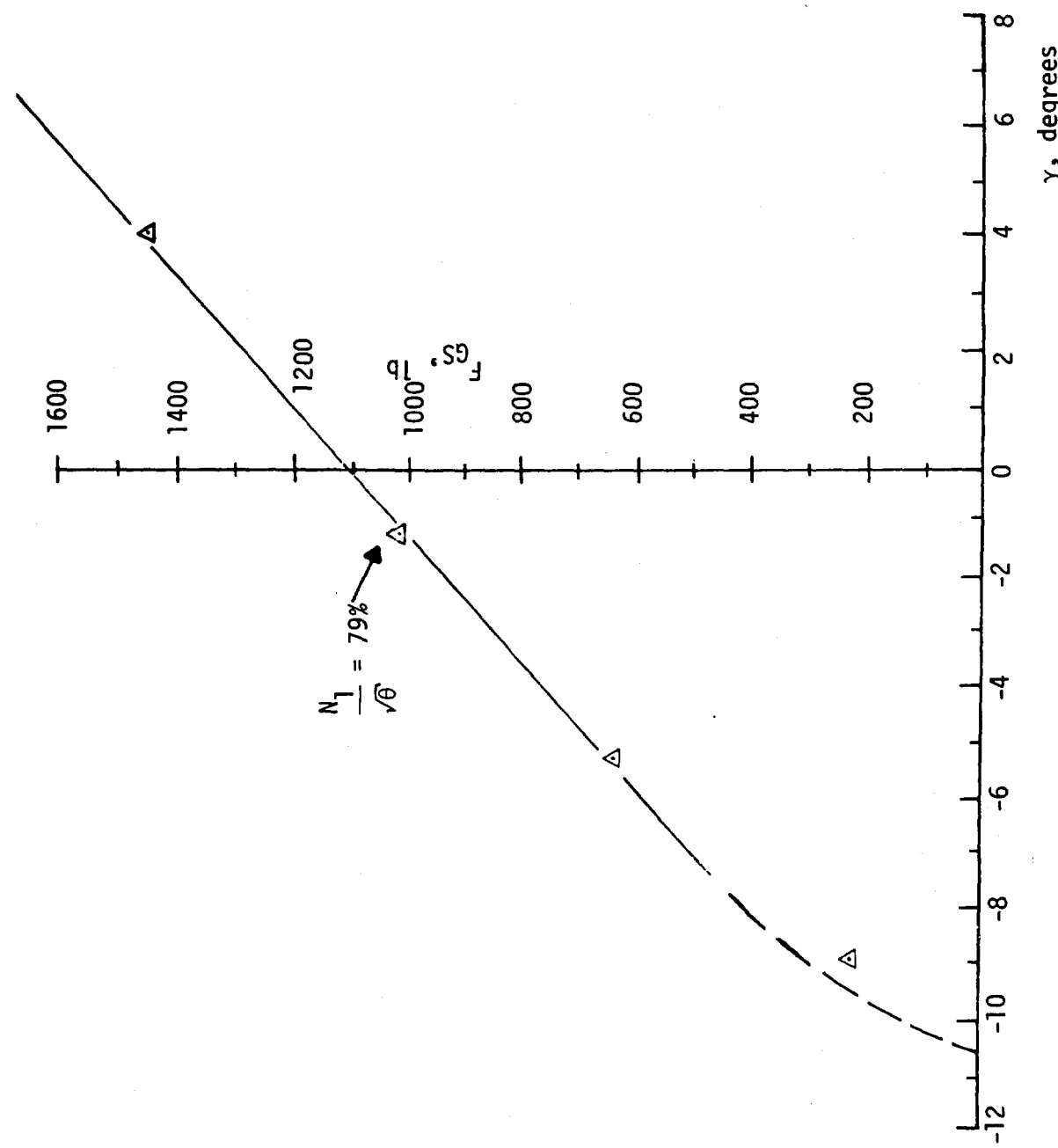


FIGURE II-2 F_{GS} versus γ , sample plot, $V_i = 165$ knot, $V_{EW} = 171.5$ knots, clean configuration.

From Reference 6

Table II - 1 Sample Data Reduction
From Reference 6

No.	Quantity	Reference	Units	Value
1	V_I	Flight Data	Knots	165
2	V_I	Instrument Cal.	Knots	165
3	V_C	Position Corr.	Knots	167.5
4	H_{pi}	Flight Data	Feet	4325
5	H_{pI}	Instrument Cal.	Feet	4305
6	H_{pc}	Position Corr.	Feet	4370
7	δ at H_{pc}	Altitude Tables	N/D	0.8519
8	OAT_I	Flight Data	°F	65.5
9	T_{AI}	Inst. Cal. (8) in °C	°C	22.61
10	T_{AI}	273.16 + (9)	°K	295.77
11	T_S at H_{pc}	Altitude Tables	°K	279.50
12	θ	(10) / 288.16	N/D	1.02641
13	$\sqrt{\theta}$	(12)	N/D	1.01312
14	σ	(7) / (12)	N/D	0.8300
15	$\sqrt{\sigma}$	(14)	N/D	0.9110
16	V_T	(3) / (15)	Knots	183.9
17	ROC (observed)	Flight Data	Ft/Min	-390
18	ROC (temp. corr.)	(17) x (10) / (11)	Ft/Min	-412
19	$\sin Y$	(18) / (16) x 101.34	N/D	-0.02212
20	Y	(19) and Calculator	Degrees	-1.27
21	N_1 at H_{pc}	Flight Data	rpm	80
22	$N_1 / \sqrt{\theta}$	(21) / (13)	rpm	79.0
23	$F_G / 6$	(16), (22) and Fig. 40, p. 67	Lb	11.50
24	F_G	(23) x (7)	Lb	980
25	W_T	Flight Data	Lb	3477.3
26	W_S	Arbitrary	Lb	3600
27	W_T / W_S	(25) / (26)	N/D	0.96592
28	$(W_T / W_S)^{1/2}$	$\sqrt{(27)}$	N/D	0.98281

Table II - 1 (continued)

No.	Quantity	Reference	Units	Value
29	F_{GS}	(24) / (27)	lb	1016
30	V_{EW}	(3) / (28)	Knots	170.4
31 ^a	q	$0.5 \times \rho_0 \times (3) \times 1.689^2$	lb/ft ²	95.12
32 ^b	C_J	(24) / (31) x 8)	N/D	0.0976
33	α'_1	Flight Data	Degrees	0.0
34	α'_I	Instrument Cal.	Degrees	7.0

Note: $V_1 = 165$ kts; $N_1 = 80\%$; Configuration: Clean.

^a $\rho_0 = 0.0023769$ slugs/ft³.

^b $S = 105.6$ ft².

TAKEOFF AND LANDING DATA CORRECTION

To correct the takeoff and landing distances to sea level standard conditions the air distances and ground roll distances were separated for individual correction.

Each takeoff or landing data run was corrected for wind using the following empirical relations from Reference 10.

TAKEOFF GROUND DISTANCE WIND CORRECTION EQUATION.

$$s_{gt} = s_{go} \left(1 + \frac{v_w}{v_{tow}}\right)^{1.85} \quad (II-10)$$

where s_{gt} = the observed ground distance corrected for winds

s_{go} = the observed ground distance

v_w = the wind velocity component along the runway at 6 feet height

v_{tow} = the true ground speed at takeoff

TAKEOFF AIR DISTANCE WIND CORRECTION EQUATION

$$s_{at} = s_{ao} + (v_w)t \quad (II-11)$$

where s_{at} = the observed air distance corrected for winds

s_{ao} = the observed air distance

v_w = the wind velocity component along the runway at a 25 foot height

t = the time of flight from liftoff to the 50 foot height

LANDING AIR DISTANCE WIND CORRECTION EQUATION

$$S_{at} = S_{ao} + (V_w)t \quad (11-12)$$

where S_{at} = the observed landing air distance corrected for winds

S_{ao} = the observed landing air distance

V_w = the wind velocity component along the runway at a 25 foot height

t = the time of flight from the 50 foot height to touchdown

LANDING GROUND DISTANCE WIND CORRECTION EQUATION

$$S_{gt} = S_{go} \left(\frac{V_{TD} + V_w}{V_{TD}} \right)^{1.85} \quad (11-13)$$

where S_{gt} = the observed landing ground distance wind corrected

S_{go} = the observed landing ground distance

V_{TD} = the touchdown airspeed

V_w = the wind velocity component along the runway at 6 foot height

After correction for wind the takeoff ground roll distance was corrected for nonstandard weight, altitude, temperature, and thrust using methods similar to those used for other performance data and the following equation based upon the work of Parks:

$$S_{gs} = S_{gt} \left(\frac{W_s}{W_t} \right)^2 \left(\frac{\sigma_t}{\sigma_s} \right) \left(\frac{F_{gt}}{F_{gs}} \right) \quad (11-14)$$

where S_{gs} = the sea level standard ground distance

T = the test density ratio

S = the standard density ratio at test field elevation

In like manner the takeoff air distance was corrected to standard conditions using the following equation:

$$S_{as} = S_{aT} \left(\frac{W_S}{W_T} \right)^2 \left(\frac{\sigma_T}{\sigma_S} \right) \left(\frac{F}{F_{gT}} \right) \quad (II-15)$$

where S_{as} = the standard takeoff air distance

Once each takeoff segment has been corrected the five runs were averaged to obtain the average standard distance for each segment. These average segments were then added together to obtain the standard takeoff distance over 50 feet.

The landing distance corrections are somewhat simpler since a correction for air distance is generally not considered. The ground distance correction is also simpler since the thrust terms are eliminated. These differences result in the following equation:

$$S_{gs} = S_{gT} \left(\frac{W_S}{W_T} \right)^2 \left(\frac{\sigma_T}{\sigma_S} \right) \quad (II-16)$$

where S_{gs} = the standard landing ground distance.

Once each of the five segments are corrected the landing data were averaged in the same manner as the takeoff data and average standard landing distances obtained.

The takeoff and landing data reduction methods discussed here are semi-empirical and are not exact. However, the error introduced in takeoff and landing test data by pilot technique tends to make all takeoff and landing data obtained by testing a rough approximation.

APPENDIX III

ESTIMATED WEIGHTS

AND

MOMENTS OF INERTIA

FOR

JETWING JW-1

Table III-1 lists the estimated weights, centers of gravity, and moments of inertia for components of the Jetwing research airplane as it was flown for this test program. The estimates are based upon actual complete aircraft weights obtained during the test program, design weight and center of gravity estimates from the Ball-Bartoe Aircraft Company data, and major component weight estimates from partial disassembly of the aircraft.

Also included in Table III-1 are weight, center of gravity, and moments of inertia for the total aircraft based upon the estimated component values.

TABLE III-1

JETWING JW-1
COMPONENT WEIGHT AND MOMENT
OF INERTIA SUMMARY
(ESTIMATED)

Item	C.G. Coordinates			Weight (LB)	Mass Moments of Inertia			Products of Inertia		
	*X (inches)	Y	Z		I_{xx} (slug-ft ²)	I_{yy}	I_{zz}	I_{xy} (slug ft ²)	I_{yz}	I_{xz}
Fuselage	68.6	0	12.5	1083	89.2	1839.0	1829.4	0	0	79.4
Engine	-50.6	0	4.6	633	28.1	357.3	364.4	0	0	-39.0
Pilot and Equipment	70.0	0	16.0	200	17.7	230.1	214.5	0	0	41.1
Fuel	17.5	0	19.0	672	72.8	120.3	70.2	0	0	49.6
Ballast	-75.8	0	13.3	412	6.5	507.1	507.1	0	0	-81.7
Wings	2.8	0	4.7	600	677.4	33.7	609.2	0	0	1.7
Total Aircraft	10.7	0	11.3	3600	892	3088	3595	0	0	-51

*Center of gravity coordinates are up positive in "/" direction, aft positive in "x" direction and taken with respect to the following references:

1. In the longitudinal or "X" direction - The aircraft datum located at the firewall just forward of the fuel tank (see figure 3)
2. In the spanwise or "Y" direction - The aircraft centerline
3. In the vertical or "Z" direction - Water line zero which is located at the lower main longitudinal in the cockpit area (see figure 3)

DISTRIBUTION LIST FOR
JETWING FLIGHT TEST EVALUATION FINAL REPORT

Department of the Navy
Naval Air Systems Command
Washington, D.C. 20361

<u>CODE</u>	<u>COPIES</u>
AIR-00D4	14
AIR-03E	1
AIR-03PA3	2
AIR-03P3A	1
AIR-310	1
AIR-320D	1
AIR-320F	1
AIR-330	1
AIR-528	2
AIR-5301	1
AIR-536	1

Office of Naval Research
800 N. Quincy Street
Arlington, VA 22217

Attn: CAPT M. A. Howard, Code 210	1
Attn: Dr. R.E. Whitehead, Code 438	1

David Taylor Naval Ship Research
& Development Center
Bethesda, MD 20084

Attn: Dr. H. R. Chaplin, Code 16	3
----------------------------------	---

Naval Air Development Center
Warminster, PA 18974

Code 60	2
Code 605C	1

Naval Air Propulsion Center
Trenton, N. J. 08628

Attn: Mr. A. A. Martino, Code P64	2
-----------------------------------	---

Naval Weapons Center
China Lake, CA 93555

Code 324	1
----------	---

COPIES

Department of Aeronautics
Naval Postgraduate School
Monterey, CA 93940

Attn: Professor Max Platzer, Code 67 P1

2

Air Force Wright Aeronautical Laboratories
Wright-Patterson AFB
Dayton, OH 45433

Attn: Col. Butkewicz; AFWAL/FIM

1

Attn: Mr. R. Jeffries; AFWAL/FIMM

3

Attn: Mr. V. Hoehne; AFWAL/FIGC

1

NASA Ames Research Center
Moffett Field, CA 94035

Attn: Mr. John Cochrane; Code FHQ
Mail Stop 237-10

1

Attn: Mr. David Koenig; Code FHA
Mail Stop 247-1

2

NASA Headquarters
Washington, D.C. 20546

Attn: Mr. G. C. Kayten; Code RJ-2

1

Mr. C. William Clay
Mail Stop 9H-41
Boeing Commerical Airplane Company
P.O. Box 3707
Seattle, WA 98124

1

Dr. Frank Aschenbrenner
Vice President for Research & Development
The Ball Corporation
345 South High Street
Muncie, Indiana 47302

1

TOTAL

50

SUPPLEMENTARY

INFORMATION

ERRATA UTSI REPORT 81-1
 A FLIGHT TEST EVALUATION OF THE
 BALL-BARTOE JETWING PROPULSIVE
 LIFT CONCEPT

AD-A103579

<u>PAGE #</u>	<u>PARA.</u>	<u>LINE</u>	<u>CORRECTION</u>
i	3	4	trubofan - should be - turbofan
ii	3	1	add comma after - In conclusion,
iii	-	Figure 12	Supercirtical - should be - Supercritical
iv	-	Figure 25	Miliampmeter - should be - Milliammeter
xvii	-	$\alpha'I$	insturment - should be - instrument
26	2	1	this tests - should be - these tests
26	3	16	valves - should be - values
28	1	1	add comma after - conditions,
28	1	3	delete comma after - data
28	3	4	add symbol - ,Y,
29	3	2	add comma after - testing,
30	2	4	intended - should be - intended
30	2	7	add period after - 90° and delete - roll.
32	3	9	poitions - should be - positions
32	3	10	locations - should be - location
38	1	4	pilots - should be - pilot's
39	5	2	"technique, sufficient" should be "technique, a sufficient"
40	4	7	delete comma after - "the nozzle,"
40	5	6	delete s on "speeds"
43	1	7	accuracy - should be - accuracy - and - instrumentaton - should be - instrumentation
45	4	1	add comma after - instrumentation,

45	4	3	add comma after - Dynamometer,
47	all	-	replace with new p. 47 attached
48	Figure 25		Miliampmeter - should be - Milliammeter
62	2	23	has - should be - had
62	3	2	too - should be - to and - pilots - should be - pilot's
62	5	5	aircrafts - should be - aircraft's
66	1	4	Whitneys - should be - Whitney's
66	1	6	Jetwings - should be - Jetwing's
66	1	8	add comma after - approach,
70			replace with attached - p. 70
72			replace with attached - p. 72
73			replace with attached - p. 73
74			replace with attached - p. 74
75			replace with attached - p. 75
76			add - Wind Tunnel Run # 31
77			add - Wind Tunnel Run # 25
78			add - Wind Tunnel Run #18
79	2	1	add comma after - In summary,
79	3	16	pltos - should be - plots
79	3	22	add comma after - upwash,
82 - 83			add new page 82-1 attached
86	2	11	add comma after - friction,
90	Table 3		"R" at top of right hand column should be - τ_R
90	1	7	1.0 seconds - should be - 1.0 second
90	2	4	add comma after - sideslip,
91	4	5	"achieve a 20° of bank"- should be "achieve 20° of bank".
91	4	7	will - should be - would

91	5	3	airplanes - should be - airplane's
104	1	1	longtudinal - should be - longitudinal
104	2	5	tails - should be - tail's
118		6	add comma after - words,
119	4	11	pilots - should be pilot's
125	2	7	add comma after - nozzle,
125	2	11	collec-tion should be - collection
140		Reference 1	add quotation marks after Colorado,"
142		Conclusion #1	Jetwings - should be - Jetwing's
143		Conclusion #14	delete period after - inexpensive
144	1	3	recomended: should be - recommended:
I-3			Leftwing Cold Duct Ejector Area D, Total Area should be 236.68 sq.in.
II-5	1	1	add comma after - instance,
II-5	3	1	add comma after - equated,
II-7		Table II-1	"From Reference 6" should be From Reference 8"
II-11	2	1	add comma after - corrected,

Aileron and elevator control forces were obtained by use of a hand held force gauge (AMES GAUGE). Rudder forces were obtained from load cells mounted on the rudder pedals. These load cells were connected electrically, through a rotary switch, to a milliammeter which could be read by the pilot (See Figure 25). Control force instruments were calibrated by measuring the force created by standard weights of various sizes.

Control surface position information was obtained by attaching linear potentiometers to the control surface or control pushrods as shown in Figure 26a, b, c and d. These potentiometers were also connected to the milliammeter of Figure 25. Calibration of these instruments was accomplished by measuring control surface deflection angles and obtaining corresponding milliammeter readings.

Angle of attack and angle of sideslip information was obtained from the sensors shown in Figure 27. The angle of attack and sideslip vanes drive rotary potentiometers which are also connected electrically through the 12 position rotary switch to the milliammeter of Figure 25. Calibration was accomplished in a manner similar to the control surface position instrumentation. Zero reference was the aircraft waterline for angle of attack and the aircraft centerline for angle of sideslip.

An accelerometer with a range of 0-5G was installed so as to be located at a nominal aircraft center of gravity. The output of this accelerometer could also be read out on the milliammeter. In addition, the pilot also had available a panel mounted accelerometer which could be used as a reference.

A vertical gyro mounted near the center of gravity, above the exhaust ducting, as shown in Figure 28, was used to determine pitch and bank angles. Prior to installation this device was calibrated with the instrumentation package on a calibration bench. This device was also wired to provide a visual readout through the milliammeter.

Rate gyros for the determination of pitch, roll, and yaw rates were mounted at the aircraft's nominal center of gravity position in the manner shown in Figure 29. These gyros were also bench calibrated with the instrumentation package. Readout of the output of these instruments was also through the milliammeter.

All instrument readings which could be displayed on the milliammeter could also be recorded, three at a time versus a time base, on a cassette magnetic tape recorder. These data could then be played back on an oscilloscope or strip recorder after the flight. The cassette recorder was located just aft of the pilot's seat.

Before being displayed on the milliammeter or recorded on the cassette recorder, all data signals were amplified and conditioned in an instrumentation amplifier and signal conditioner, located near the vertical gyro, as is shown in Figure 30. Power for the electrical instrumentation was controlled through an instrumentation master switch located next to the rotary selector switch.

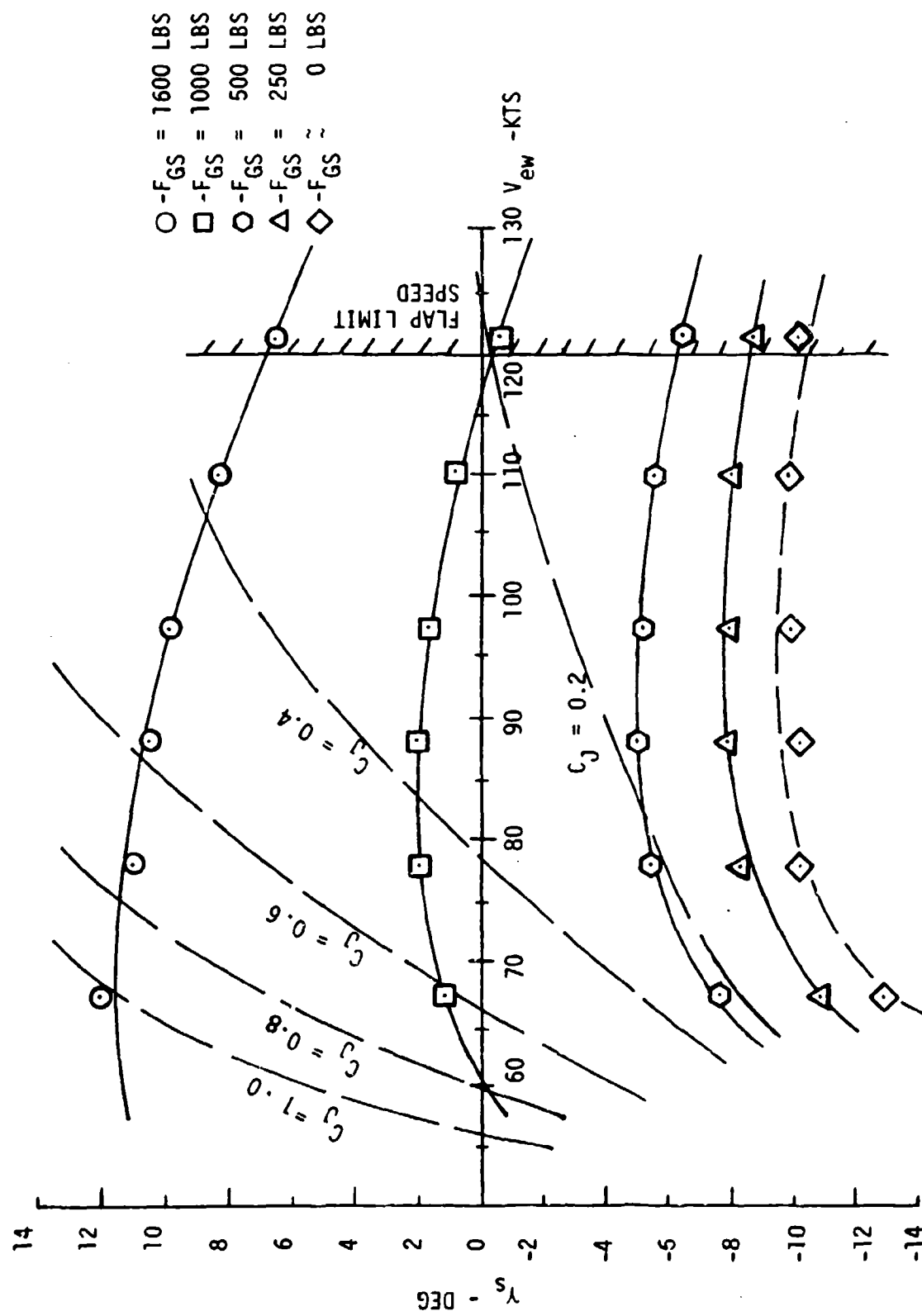
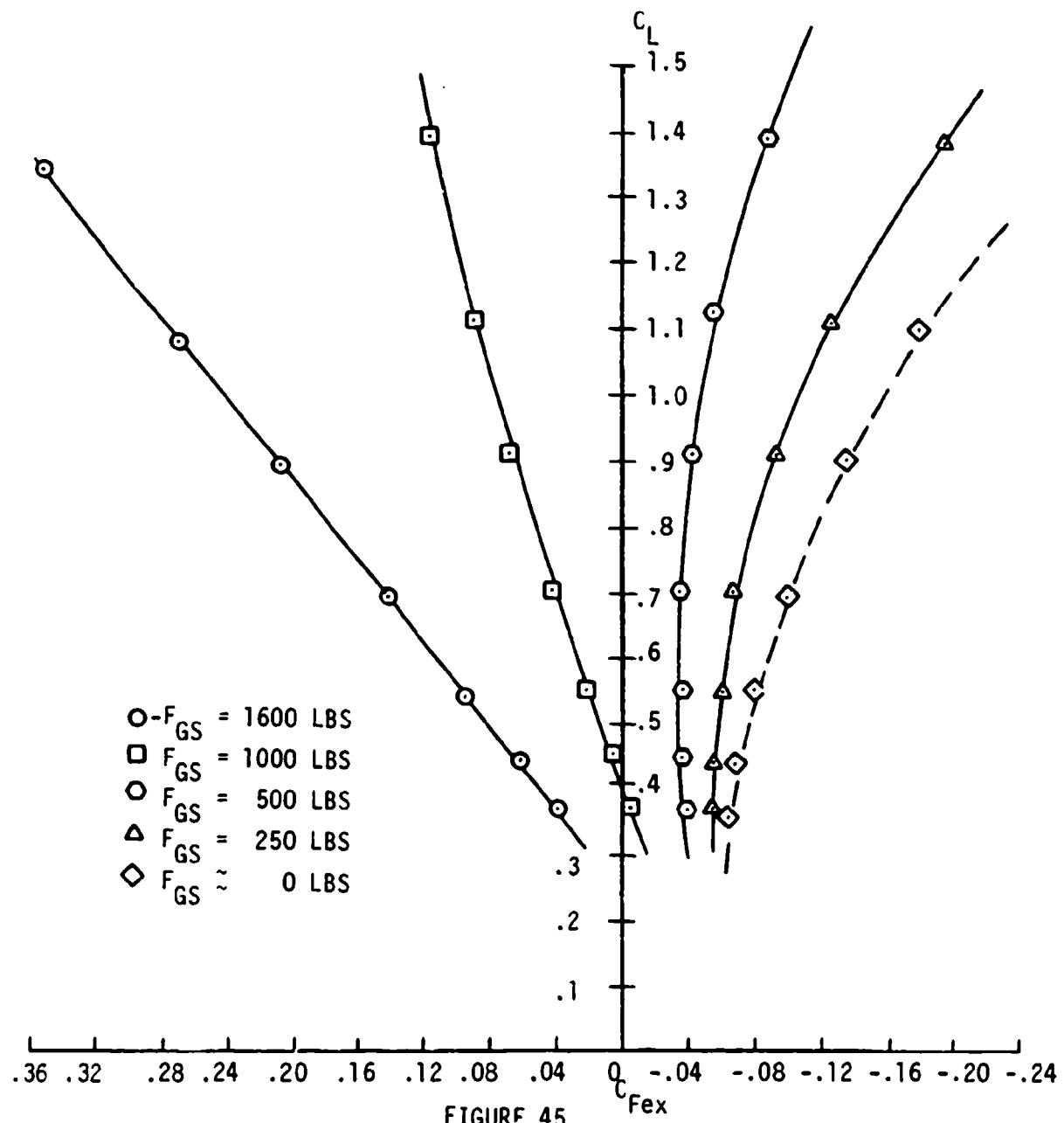


FIGURE 43
JETWING JW-1
 C_L vs V_{ew} , FLAPS 15°
 $W_S = 3600$ LBS



JETWING JW-1
 C_L vs C_{Fex}
 Clean Configuration
 $W_s = 3600$ LBS

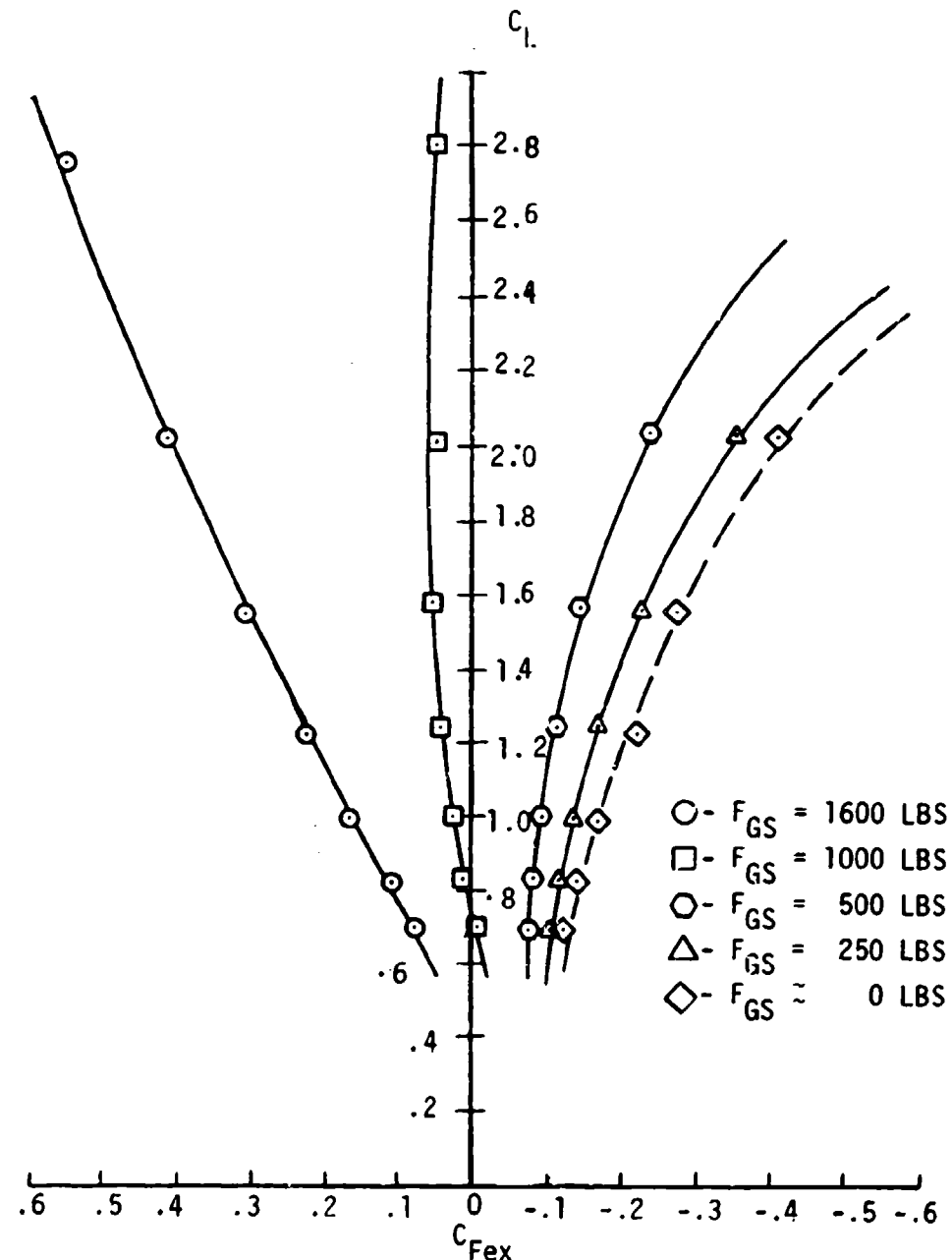


FIGURE 46

JETWING JW-1
 C_L VS C_{Fex}
 GEAR DOWN, FLAPS 15°
 $W_S = 3600$ LBS

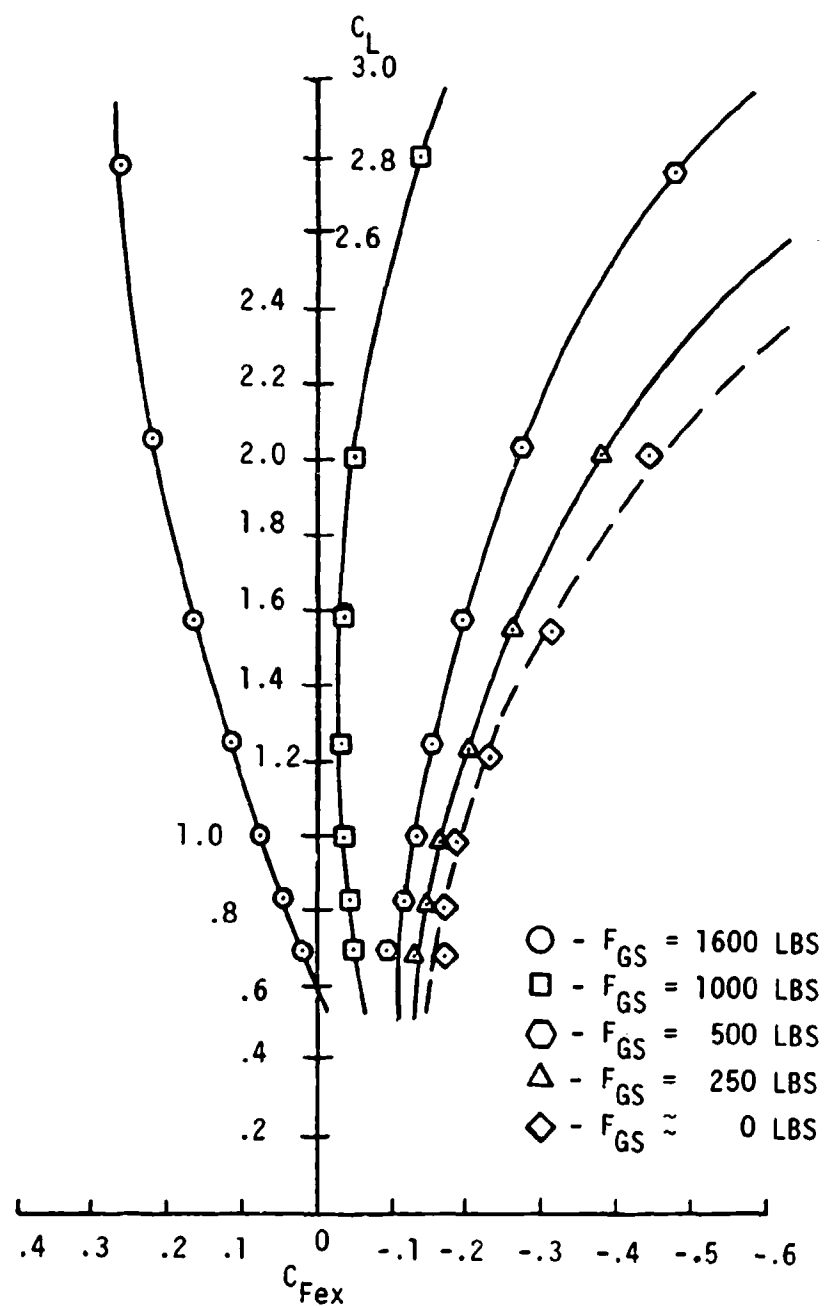


FIGURE 47

JETWING JW-1
 C_L VS C_{Fex}
 GEAR DOWN, FLAPS 30^0
 $W_s = 3600$ LBS

Figures 45, 46, and 47 demonstrate graphically why drag coefficient is no longer a meaningful variable when applied to powered lift airplanes. The right hand curve ($C_J = 0$) in each of these figures would be the same as a conventional drag polar. However, when thrust is applied to the airplane ($C_J > 0$), the polar shifts to the left. If enough thrust (blowing) is applied, the curves become negative. It is interesting to note that this shift to the left only occurs for lift coefficients in excess of zero ($C_L > 0$). The reason for these unusual characteristics is easily seen when one examines the drag equation for a powered lift airplane.

$$C_D = C_{D0} + \frac{K C_L^2}{\pi A + 2C_J} \quad (1)$$

This equation developed by Maskell and Spence in Reference 2 for jet flapped airfoils shows that the induced drag term of the drag equation contains the thrust related term C_J . C_J , the blowing coefficient, may be defined for the Jetwing airplane as:

$$C_J = \frac{F_a}{qS} \quad (2)$$

Since this intermingling of thrust with drag invalidates the conventional meaning of drag, equation 1 is generally expressed as the excess thrust coefficient C_{FEX} .

$$C_{FEX} = rC_J - C_{D0} - \frac{K C_L^2}{\pi A + 2C_J} \quad (3)$$

It may be seen from equation 3 that for the special case of zero thrust ($C_J = 0$), the equation reduces to:

$$C_{FEX} = -C_D \quad (4)$$

Therefore, when comparing performance of powered lift airplanes one must always be sure to compare at equal values of C_J .

Sufficient performance data were obtained to make comparisons with the NASA-Ames Research Center 40' x 80' wind tunnel data at blowing coefficients of $C_J = 0.43$ for the gear and flaps up configuration, and at $C_J = 0.75$ for the other two configurations. These comparisons are shown in Figures 48, 49, and 50. These figures show good correlation between the flight test and wind tunnel data. The correlation should be even better if an accounting is made of the trim drag difference between the flight and wind tunnel tests. The reason for the trim drag

To make an approximate correction of the flight test data in figures 54 thru 56 to geometric angle of attack the following correction factors should be used:

Figure 54: Gear Up, Flaps Up

Correction: -5° at $\alpha' = 20^\circ$

-2° at $\alpha' = 5^\circ$

with linear variation between given values

Figure 55: Gear Down, Flaps 15°

Correction: -6.5° at $\alpha' = 20^\circ$

-2° at $\alpha' = 5^\circ$

with linear variation between given values

Figure 56: Gear Down, Flaps 30°

Correction: -5° at $\alpha' = 20^\circ$

-2° at $\alpha' = 5^\circ$

with linear variation between given values